Technical University
of Leoben

Chair of Materials Science and Testing of Polymers

Doctoral Thesis

Development and testing of encapsulation concepts for integrated PV modules

Nikolina Pervan, mag. ing. cheming.

May 2026

The PhD researcher and the UHasselt supervisor hereby formally declare that the research conducted for the purpose of this PhD thesis was executed in accordance with the principles of good scientific conduct, as stipulated in the UHasselt Integrity charter, the UHasselt charter supervisor – PhD Researcher, the UHasselt Integrity Policy and the UHasselt guidelines for the use of (generative) AI in research.

The author asserts that this PhD thesis is made Open Access immediately upon submission. The full text is publicly available without restrictions.

AFFIDAVIT

I declare on oath that I wrote this thesis independently, did not use any sources and aids other than those specified, have fully and truthfully reported the use of generative methods and models of artificial intelligence, and did not otherwise use any other unauthorized aids.

I declare that I have read, understood and complied with the "Preamble on Integrity in Academic Study, Teaching, and Research Operations" of the Montanuniversität Leoben.

Furthermore, I declare that the electronic and printed versions of the submitted thesis are identical in form and content.

This work is a cumulative dissertation:

(●) Yes
( ) No

Date: 19. May 2026.

_____

Signature

Doctoral thesis

Development and testing of encapsulation concepts for integrated PV modules

Authored by

Nikolina Pervan, mag. ing. cheming.

Submitted to

Montanuniversität Leoben
Leoben, Austria

Doktor der montanistischen Wissenschaften, Dr.mont

&

University of Hasselt
Hasselt, Belgium

Doctor of Engineering Technology

Academic Supervisor
Priv.-Doz. Dr. Gernot Oreski
Chair of Materials Science and Testing of Polymers
Montanuniversität Leoben

Academic Supervisor
Prof. Dr. Ir. Michaël Daenen
Institute for Materials Research (IUMAT)
University of Hasselt

Conducted at
Polymer Competence Center Leoben GmbH
Leoben, Austria

Supported by
EURECA-PRO Doctoral School
Montanuniversität Leoben

"Deja que Dios sea tu fuerza y tu guía, y todo lo demás caerá en su lugar."

Santa Clara de Asís

Acknowledgments

Firstly, I would like to thank my supervisor, Gernot Oreski, for the many engaging, interactive, and never dull moments throughout this PhD. Thank you for your constant support, encouragement, and for being the wind at my back, for helping me believe in myself and teaching me to create more than just experimental results.

I would like to thank the PCCL for the opportunity and for providing such a rich, interdisciplinary infrastructure that supported both my professional and personal development. My gratitude also goes to the Technical University of Leoben, particularly the EURECA-PRO and International Office team, who supported all of my international runaways within the EURECA-PRO Doctoral School. I would also like to extend my thanks to the University of Hasselt, imec, EnergyVille, and TNO for hosting me and helping me grow in research areas that were not available at PCCL. I am deeply grateful to my mentor, Prof. Michael Daenen, for his mentorship, guidance, and support, as well as to Nikoleta, who was both a wonderful friend and colleague during my stay in Belgium. My thanks also go to all the colleagues at imec and TNO for the time shared in the lab and during our lunch breaks.

This research would not have been possible without the generous provision of materials and the technical expertise shared by all collaborating institutions within the DELIGHT, SOPHOKLES, and PV Industriefassade projects. Beyond the logistical support, I am deeply grateful for the guidance and the inspiring working atmosphere provided throughout these collaborations. The opportunity to exchange ideas with such a diverse group of experts was key to connecting this research with real industrial applications and was truly a rewarding aspect of my PhD.

This PhD would be far from finished without the army of friends and colleagues supporting me. Thank you, Sonja Feldbacher, for all your help and for brainstorming solutions for those stubborn CIGS cells. Chiara, Jutta, Brahim, and Marko, there are no words to properly thank you for the help, advice, and the many venting sessions. You helped me keep the faith in myself, and for that, I am eternally grateful. Even though the team at PCCL changed from year to year, all of you enriched my journey and made every day of lab work and data plotting fun and memorable.

Having a friend during a PhD journey is not a simple thing, but finding a friend like Magdalena along the way is something special. Thank you for your friendship during this challenging time, for every Sunday coffee and Tapas Friday. Congratulations to both of us for surviving these years and hunting our PhD titles together!

My thanks extend to all my friends across this spot under the Sun who stayed patient with me and encouraged me to never lose my spark.

Najveća hvala ide mojoj obitelji, mojoj Marici, braći Ivanu i Tomislavu, te nevjesti Regini. Unatoč tome što smo daleko jedni od drugih i tome što vam moj doktorat i nije najjasniji, hvala vam za svu ljubav, podršku, riječi ohrabrenja i što ste uvijek uz mene i za mene. Mojim bakama i djedu, hvala za svu mudrost, molitve i ljubav koju ste mi pružili. Mama i Tata, hvala vam na korijenima koji su me držali čvrsto na zemlji i krilima kojima ste me pustili da poletim. Ovaj doktorat je koliko moj, toliko i vaš. <3

Lastly, I thank the God, my Creator and Saviour, for making this achievement possible. Thank You for the calling of the Camino and for providing me the tools to walk firmly on this journey.

Ovaj doktorski rad posvećujem svim generacijama koje su tu bile prije mene i stvorile mi put, inat i hrabrost da ostvarim san mnogih.

Funding

This thesis was performed at the Polymer Competence Center Leoben GmbH (PCCL, Austria).

The "*Characterization of Lightweight Polymeric Honeycomb Structures for Use as Backsides in Glass-Free PV Modules*" and "*Is EPE the future of PV encapsulation? A comprehensive material-level assessment*" were done as part of the Solar Era Net Project "DELIGHT," which is supported under the umbrella of SOLAR-ERA. NET co-fund by the Austrian Research Promotion Agency (FFG, contract number FO999897443) and the Swiss Federal Office of Energy (SFOE, contract number SI/502501-01). SOLAR-ERA. NET is supported by the European Commission within the EU Framework Programme for Research and Innovation HORIZON 2020 (co-fund ERA-NET Action, No. 691664).

The "*Backsheet-Galvanized Steel Adhesion Approaches for Integrated Photovoltaic Façades: A Comparative Study*" and "*Effects of Manufacturing Process History and the Lamination Duration on Thermomechanical Properties of PV Encapsulants*" were conducted as part of the Austrian "e!MISSION.at – Energy Mission Austria" project "PV Industriefassade" (FFG No. FO999915062) funded by the Austrian Climate and Energy Fund and the Austrian Research Promotion Agency (FFG).

The "*Systematic study of barrier layer coatings for encapsulation of flexible CIGS PV modules*" was conducted as a part of the project "SOPHOKLES", which is supported under the umbrella of "Stadt der Zukunft" funded by Austrian Research Promotion Agency (FFG) [43693964].

Abstract

The global expansion of photovoltaics (PV) is increasingly confronted with limitations in specific geographic contexts, such as densely populated urban centres and mountainous regions, where land availability constrains large-scale field-deployed installations. This has driven the need for integrated PV (IPV) in the built environment. However, conventional glass-glass modules are often too heavy or rigid for lightweight infrastructures. Transitioning to glass-free, polymer-based architectures is essential for enabling flexible, lightweight designs, yet this shift fundamentally redefines the requirements for the polymeric stack, which must now provide the structural integrity and environmental protection formerly offered by glass.

This thesis establishes a scientific framework for application-specific, glass-free PV designs by characterizing the physical, chemical, and thermomechanical behaviour of polymeric materials. Through five systematic studies, the research investigates diverse pathways, ranging from structural reinforcements to specialized thin-film coatings, and evaluates their performance under accelerated aging and varying processing conditions.

The research first addresses the loss of structural rigidity resulting from the removal of the glass layer by evaluating thermoplastic honeycomb sandwich composites (HSCs). Polypropylene-based HSCs were identified as viable glass substitutes due to a coefficient of thermal expansion (CTE) comparable to solar glass, maintaining stable material properties after accelerated aging exposure. In the context of building-integrated steel façades, the study identifies that while adhesion to building elements can be achieved via various bonding approaches, moisture-driven interfacial weakening remains a critical failure mode. The results indicate that further optimization, including the transition toward monolithic backsheets, is necessary to ensure a 25-year service life.

For flexible CIGS and thin-film applications, a screening methodology revealed that polyurethane (PU) formulations provide the optimal balance of adhesion and optical clarity. Crucially, the work demonstrates that standard industrial aging tests (e.g., 1000h damp heat) often over-stress these materials, leading to costly over-engineering for shorter-lived consumer products. Finally, an in-depth analysis of encapsulants revealed that manufacturing history and lamination duration significantly impact thermomechanical stability. These findings exposed inconsistent behaviours in co-extruded materials, which led to a systematic characterization of commercially available ethylene vinyl acetate-polyolefin-ethylene vinyl acetate (EPE) encapsulants. This investigation revealed that EPE encapsulants are highly variable in their properties, with ethylene vinyl acetate (EVA) still comprising up to 64% of the volume, thereby challenging the industry assumption that these multi-layer stacks offer inherently enhanced protection compared to single-layer EVA encapsulants.

This work proves that glass-free PV is not a "plug-and-play" transition. Success depends on a three-stage integration strategy: fundamental material characterization, lamination process adaptation, and targeted optimization of hydrolysis resistance. By matching the material stack to the specific operational environment rather than relying on generalized industrial labels, this thesis provides the scientific foundation necessary for the next generation of adaptable, high-reliability photovoltaic systems.

Kurzfassung

Die weltweite Verbreitung der Photovoltaik (PV) stößt in bestimmten geografischen Kontexten zunehmend an Grenzen, beispielsweise in dicht besiedelten Ballungsräumen und Bergregionen, wo die Verfügbarkeit von Flächen den Bau großer PV Anlagen einschränkt. Dies hat den Bedarf an integrierter Photovoltaik (IPV) im Bauwesen vorangetrieben. Herkömmliche Glas-Glas-Module sind jedoch oft zu schwer oder zu starr für bestehende Infrastrukturen. Der Übergang zu glasfreien, polymerbasierten Architekturen ist unerlässlich, um flexible, leichte Konstruktionen zu ermöglichen. Dieser Wandel definiert jedoch die Anforderungen an den Polymerverbund grundlegend neu, da dieser nun die strukturelle Integrität und den Schutz gegenüber Umwelteinflüssen gewährleisten muss, die zuvor durch Glas geboten wurden.

Diese Arbeit schafft einen wissenschaftlichen Rahmen für anwendungsspezifische, glasfreie PV-Konstruktionen, indem sie das physikalische, chemische und thermomechanische Verhalten von Polymermaterialien charakterisiert. Anhand von fünf systematischen Studien untersucht die Forschung verschiedene Ansätze, die von strukturellen Verstärkungen bis hin zu speziellen Dünnschichtbeschichtungen reichen, und bewertet deren Leistung unter beschleunigten Alterungsbedingungen und unterschiedlichen Verarbeitungsbedingungen.

Die Studie befasst sich zunächst mit dem Verlust der strukturellen Steifigkeit, der durch das Entfernen der Glasschicht entsteht, und untersucht dazu thermoplastische Wabensandwichverbundwerkstoffe (HSCs). HSCs auf Polypropylenbasis wurden als geeignete Glasersatzmaterialien identifiziert, da sie einen mit Solarglas vergleichbaren Wärmeausdehnungskoeffizienten (CTE) aufweisen und ihre Materialeigenschaften auch nach beschleunigter Alterung stabil bleiben. Im Zusammenhang mit gebäudeintegrierten Stahlfassaden stellt die Studie fest, dass zwar die Haftung an Bauelementen durch verschiedene Verklebungsverfahren erreicht werden kann, feuchtigkeitsbedingte Schwächung der Grenzfläche jedoch weiterhin ein kritischer Versagensmodus bleibt. Die Ergebnisse deuten darauf hin, dass eine weitere Optimierung, einschließlich des Übergangs zu monolithischen Rückseitenfolien, erforderlich ist, um eine Lebensdauer von 25 Jahren zu gewährleisten.

Für flexible CIGS- und Dünnschichtanwendungen ergab eine Screening-Methodik, dass Polyurethan (PU)-Formulierungen das optimale Gleichgewicht zwischen Haftung und optischer Klarheit bieten. Die Arbeit zeigt, dass standardmäßige industrielle Alterungstests (z. B. 1000 Stunden feuchte Hitze) diese Materialien oft überbeanspruchen, was zu kostspieliger Überdimensionierung bei kurzlebigen Konsumgütern führt. Schließlich ergab eine eingehende Analyse der Verkapselungsmaterialien, dass die Herstellungsgeschichte und die Laminierungsdauer einen erheblichen Einfluss auf die thermomechanische Stabilität haben.

Diese Erkenntnisse deckten uneinheitliche Verhaltensweisen bei coextrudierten Materialien auf, was zu einer systematischen Charakterisierung handelsüblicher Ethylen-Vinylacetat-Polyolefin-Ethylen-Vinylacetat (EPE)-Verkapselungsmaterialien führte. Diese Untersuchung ergab, dass EPE-Verkapselungsmaterialien in ihren Eigenschaften sehr variabel sind, wobei Ethylen-Vinylacetat (EVA) immer noch bis zu 64 % des Volumens ausmacht, was die in der Branche verbreitete Annahme in Frage stellt, dass diese mehrschichtigen Verbundstoffe im Vergleich zu einlagigen EVA-Verkapselungsmaterialien von Natur aus einen besseren Schutz bieten.

Diese Arbeit belegt, dass glasfreie PV keine „Plug-and-Play“-Umstellung ist. Der Erfolg hängt von einer dreistufigen Integrationsstrategie ab: grundlegende Materialcharakterisierung, Anpassung des Laminierungsprozesses und gezielte Optimierung der Hydrolysebeständigkeit. Indem der Materialstapel an die spezifische Betriebsumgebung angepasst wird, anstatt sich auf verallgemeinerte industrielle Bezeichnungen zu verlassen, liefert diese Arbeit die wissenschaftliche Grundlage für die nächste Generation anpassungsfähiger, hochzuverlässiger Photovoltaiksysteme.

Samenvatting

De wereldwijde uitbreiding van fotovoltaïsche systemen (PV) stuit in bepaalde geografische contexten steeds vaker op beperkingen, zoals in dichtbevolkte stedelijke centra en bergachtige gebieden, waar de beschikbare ruimte grootschalige installaties in het veld in de weg staat. Dit heeft geleid tot een toenemende behoefte aan geïntegreerde PV (IPV) in de gebouwde omgeving. Conventionele glas-glasmodules zijn echter vaak te zwaar of te stijf voor lichtgewichtconstructies. De overgang naar glasvrije, op polymeren gebaseerde architecturen is essentieel om flexibele, lichtgewicht ontwerpen mogelijk te maken, maar deze verschuiving herdefinieert fundamenteel de eisen die aan de polymeerstapel worden gesteld, die nu de structurele integriteit en milieubescherming moet bieden die voorheen door glas werd geboden.

Dit proefschrift biedt een wetenschappelijk kader voor toepassingsspecifieke, glasvrije PV-ontwerpen door het fysische, chemische en thermomechanische gedrag van polymeermaterialen te karakteriseren. Aan de hand van vijf systematische studies onderzoekt het onderzoek diverse benaderingen, variërend van structurele versterkingen tot gespecialiseerde dunne-filmcoatings, en evalueert het de prestaties ervan onder versnelde veroudering en variërende verwerkingsomstandigheden.

Het onderzoek richt zich in eerste instantie op het verlies aan structurele stijfheid als gevolg van het verwijderen van de glaslaag, door thermoplastische honingraatsandwichcomposieten (HSC's) te evalueren. HSC's op basis van polypropyleen werden aangemerkt als geschikte vervangingsmaterialen voor glas, omdat ze een thermische uitzettingscoëfficiënt (CTE) hebben die vergelijkbaar is met die van zonneglas en hun materiaaleigenschappen stabiel blijven na blootstelling aan versnelde veroudering. In de context van in gebouwen geïntegreerde stalen gevels stelt de studie vast dat, hoewel hechting aan bouwelementen via verschillende verlijmingsmethoden kan worden bereikt, vochtgedreven verzwakking van het grensvlak een kritieke faalmodus blijft. De resultaten wijzen erop dat verdere optimalisatie, waaronder de overgang naar monolithische achterplaten, noodzakelijk is om een levensduur van 25 jaar te garanderen.

Voor flexibele CIGS- en dunnefilmtoepassingen bleek uit een screeningmethode dat polyurethaan (PU)-formuleringen de optimale balans bieden tussen hechting en optische helderheid. Cruciaal is dat het onderzoek aantoont dat standaard industriële verouderingstests (bijv. 1000 uur vochtige warmte) deze materialen vaak te zwaar belasten, wat leidt tot kostbare overengineering voor consumentenproducten met een kortere levensduur. Ten slotte bleek uit een diepgaande analyse van inkapselingsmaterialen dat de productiegeschiedenis en de laminatieduur een aanzienlijke invloed hebben op de

thermomechanische stabiliteit. Deze bevindingen brachten inconsistent gedrag in co-geëxtrudeerde materialen aan het licht, wat leidde tot een systematische karakterisering van in de handel verkrijgbare ethyleenvinylacetaat-polyolefine-ethyleenvinylacetaat (EPE) inkapselingsmaterialen. Dit onderzoek bracht aan het licht dat EPE-inkapselingsmaterialen zeer variabel zijn in hun eigenschappen, waarbij ethyleenvinylacetaat (EVA) nog steeds tot 64% van het volume uitmaakt, wat de aanname van de industrie in twijfel trekt dat deze meerlaagse stapels inherent betere bescherming bieden in vergelijking met enkellaagse EVA-inkapselingsmaterialen.

Dit onderzoek toont aan dat de overgang naar glasloze PV geen kwestie is van ‘plug-and-play’. Het welslagen hangt af van een integratiestrategie in drie fasen: fundamentele materiaalkarakterisering, aanpassing van het lamineerproces en gerichte optimalisatie van de hydrolysebestendigheid. Door de materiaalopbouw af te stemmen op de specifieke gebruiksomgeving in plaats van uit te gaan van algemene industriële classificaties, legt dit proefschrift de wetenschappelijke basis die nodig is voor de volgende generatie aanpasbare, uiterst betrouwbare fotovoltaïsche systemen.

List of abbreviations

BAPV	building attached photovoltaics
BIPV	building integrated photovoltaics
BoM	bill of material
CIGS	copper indium gallium (di)selenide
CTE	coefficient of thermal expansion
DH	damp heat
DIC	digital image correlation
DMA	dynamic mechanical analysis
DSC	differential scanning calorimetry
EPE	EVA-POE-EVA
ETFE	ethylene tetrafluoroethylene
EVA	ethylene vinyl acetate
FEM	finite element method
FTIR	Fourier-Transform Infrared Spectroscopy
G_e	degree of crosslinking according to residual enthalpy
GFRP	glass fibre reinforced polymer
GHFM	guarded heat flow meter
G_{MF}	degree of crosslinking according to melt/freeze
HDGS	hot dip galvanised steel
HJT	heterojunction
HSC	honeycomb sandwich composite
IEC	International Electrotechnical Commission
IPV	integrated photovoltaics
NIR	near-infrared
PC	polycarbonate
PCA	principal component analysis
PCT	pressure cooker test
PERC	passivated emitter and rear cell

PET	polyethylene terephthalate
PID	potential-induced degradation
POE	polyolefin
PP	polypropylene
PSC	perovskite solar cell
PU	polyurethane
PV	photovoltaic
TC	thermal cycling
T_c	crystallization temperature
TGA	thermogravimetric analysis
T_m	melting temperature
TOPCon	tunnel oxide passivated contact
TPO	thermoplastic polyolefin
UV	ultraviolet
UVID	ultraviolet-induced degradation
VIPV	vehicle-integrated photovoltaics
WVTR	water vapor transmission rate

Content

1 Introduction

The solar energy had a shy start in 1839 with the observation of the photovoltaic (PV) effect by Alexandre Edmond Becquerel [1]. However, practical progress remained limited for more than a century. In 1954, researchers at Bell Laboratories developed the first modern silicon solar cell, achieving an efficiency of approximately 4% [2]. Initially, these cells were primarily used in space applications due to their high cost [1,2]. Over the following decades, advances in device design steadily increased conversion efficiencies, with laboratory silicon cells now approaching 28% [3] and gradually nearing the theoretical maximum of 33% for single-junction devices [4].

In the early 1970s, PV installations began to appear in remote and off-grid applications such as offshore platforms and isolated buildings [5]. Since the 1990s, the global deployment of solar technologies has expanded dramatically, growing from a few megawatts to hundreds of gigawatts annually [1]. Rising manufacturing volumes and declining module costs enabled PV modules to penetrate a wide range of markets beyond space and remote terrestrial applications [1,5]. Alongside crystalline and amorphous silicon technologies, several thin-film approaches emerged, including gallium arsenide (GaAs), cadmium telluride (CdTe), copper indium gallium (di)selenide (CIGS), organic photovoltaics (OPV), and perovskite solar cells (PSC) [6]. While some of these technologies achieved high laboratory efficiencies, others, like OPV, faced challenges in scaling and long-term stability due to environmental sensitivities such as moisture exposure [7]. Today, the industry remains dominated by crystalline silicon technologies based on p-type and n-type cell technology [8]. The global installed capacity has surpassed 2 TW, with projections indicating continued growth as PVs play an increasingly important role in the global energy transition [8–10].

The rapid expansion of PV modules has also come upon land availability limitations, particularly in densely populated or mountainous regions where large field-deployed installations are constrained [11–13]. This has driven the development of alternative deployment strategies that generate electricity without competing with conventional land use. Examples include agrivoltaics [14], floating PV systems [15], and various integrated photovoltaics (IPV), such as building-integrated photovoltaics (BIPV) [16], vehicle-integrated photovoltaics (VIPV) [17], and small consumer products.

Early IPVs were largely limited to simple two-dimensional modules in building envelopes, with roof attachment being the preferred strategy due to ease of installation and maximum solar exposure. Recent technological advances and increase in module efficiency, together with supportive policies and climate regulations, have accelerated their adoption in diverse urban and industrial environments [18]. Many countries now encourage or mandate

renewable energy generation at the building design stage, supporting the transition toward net-zero-energy buildings [19,20]. However, limitations remain: PV modules can be heavy and may not be suitable for lightweight structures, industrial complexes, or historical buildings, and aesthetic considerations often require custom designs [18,21].

Recent developments illustrate how IPVs are expanding beyond conventional module formats into specialized and application-specific designs, as illustrated by selected examples in Figure 1. Lightweight and flexible module concepts, pavement-integrated modules, glass-free PV systems, and portable solar devices enable integration into surfaces and structures previously unsuitable for conventional PV technologies. Many of these designs rely on advanced polymer-based materials that enable lightweight structures, flexible geometries, and adaptable module architectures [22–25].

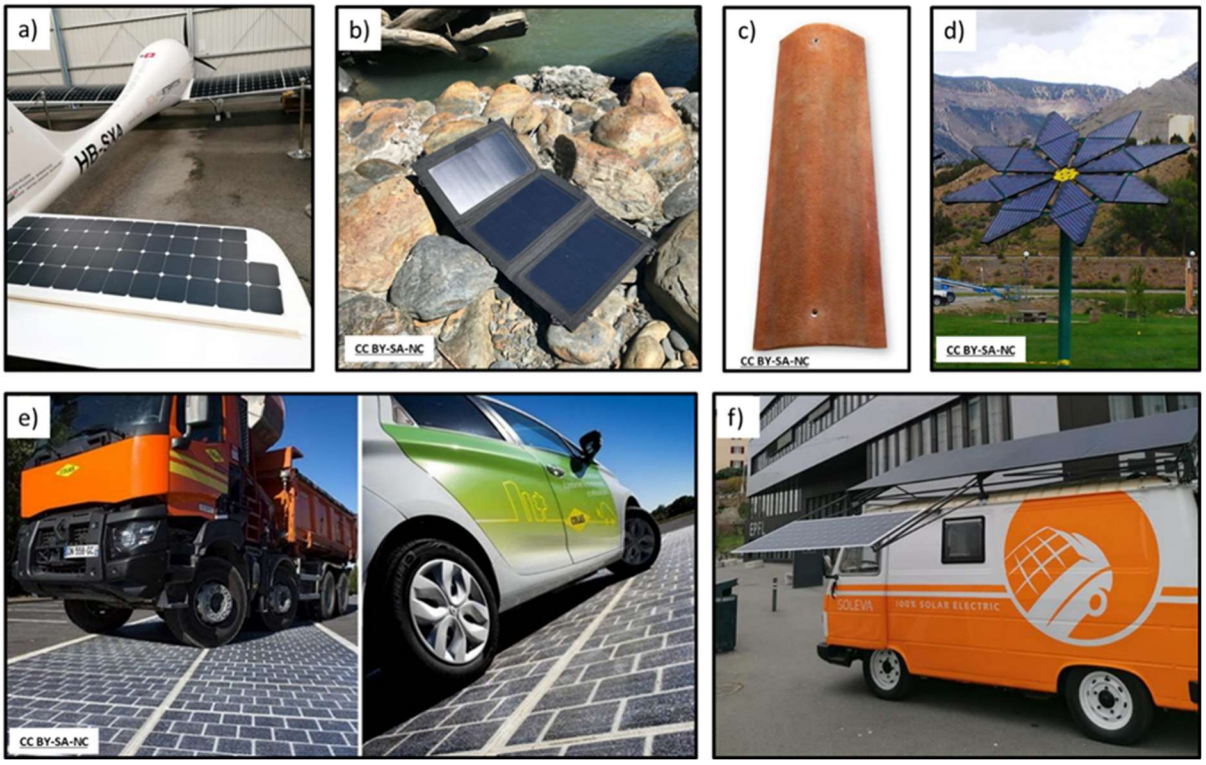

Figure 1. Examples of IPV: a) Solarstratos - stratospheric solar-electric airplane [23], b) portable charging station, c) invisible IPV terracotta rooftile for heritage building [22], d) IPV decorative sculptural installation, e) Wattway project - solar road [24], and f) Soleva - refurbished van with light weight PV attached to the roof [25].

By providing mechanical support and flexibility together with optical coupling and environmental protection functions, polymer components play a central role in expanding the practical deployment of IPVs across diverse applications. Despite these advantages, many polymer-enabled solutions remain niche products with limited large-scale deployment. Operational lifetimes can differ significantly from conventional field-deployed PV systems,

which are typically designed for service exceeding 25 years. While shorter lifetimes may be acceptable for portable or temporary applications, BIPV systems often require durability comparable to conventional construction materials. Consequently, the current industrial BIPV standard for crystalline silicon modules is the glass-glass architecture, which provides enhanced mechanical stability, environmental protection, and compliance with building fire regulations [26].

A central objective of this thesis therefore is to investigate material strategies for the development of durable lightweight IPV module concepts, with a particular focus on polymeric components. In addition, the suitability of alternative polymeric materials for structural and protective functions in glass-free module designs is examined through the characterization of commercially available construction and coating materials. Since IPV modules are often integrated directly onto building envelope substrates, such as metal façade plates, integration strategies based on different adhesion approaches are also studied from both a material and module perspective. Furthermore, this work aims to help bridge the “innovation gap” created by the rapid adoption of new materials by the photovoltaic industry. A primary example of this gap is the transition toward co-extruded encapsulants, which have recently gained significant market share despite limited publicly available scientific data on their material properties. Consequently, the material properties of co-extruded encapsulants are investigated and compared with those of established materials such as ethylene vinyl acetate (EVA), with particular emphasis on their thermomechanical behavior.

In the Chapter 2, the individual module components are discussed in detail. Followed by Chapter 3 on the functional roles of PV components, their material requirements, and the characterization and degradation modes of polymer materials. Finally, Chapter 4 addresses the development of material strategies and polymer-based solutions for lightweight, glass-free IPV module designs.

2 PV module components

A PV module is a multilayer system in which several materials with distinct functions are combined to ensure efficient energy conversion and long-term durability [27]. A typical PV module is a laminate which, amongst others, consists of a front protective layer, encapsulant materials, solar cells with their electrical interconnections, and a rear protective layer. Each component fulfils specific functional roles, including optical transmission, electrical insulation, mechanical support, and protection of the solar cells from environmental stressors [27].

The performance and durability of PV modules therefore depend strongly on the properties of the individual materials and their interactions within the laminate structure [27]. Over the past decades, both module architectures and the materials used for individual components have evolved significantly. Changes in solar cell technology, the emergence of bifacial module designs, and increasing lifetime expectations have continuously driven the development of new polymeric components, especially of encapsulants and backsheets [28].

Currently, the standard industrial architecture is a glass-glass module configuration, in which glass is used on both the front and rear sides of the laminate. In this design, the encapsulant represents the only polymeric material within the module stack. A schematic representation of a standard PV module stack is shown in Figure 2. On the other hand, in IPV modules, even though glass-glass modules are the dominant category, there is no standard architecture [18]. A wide variety of designs exist and polymers play an important role in all protective layers of the module stack [29].

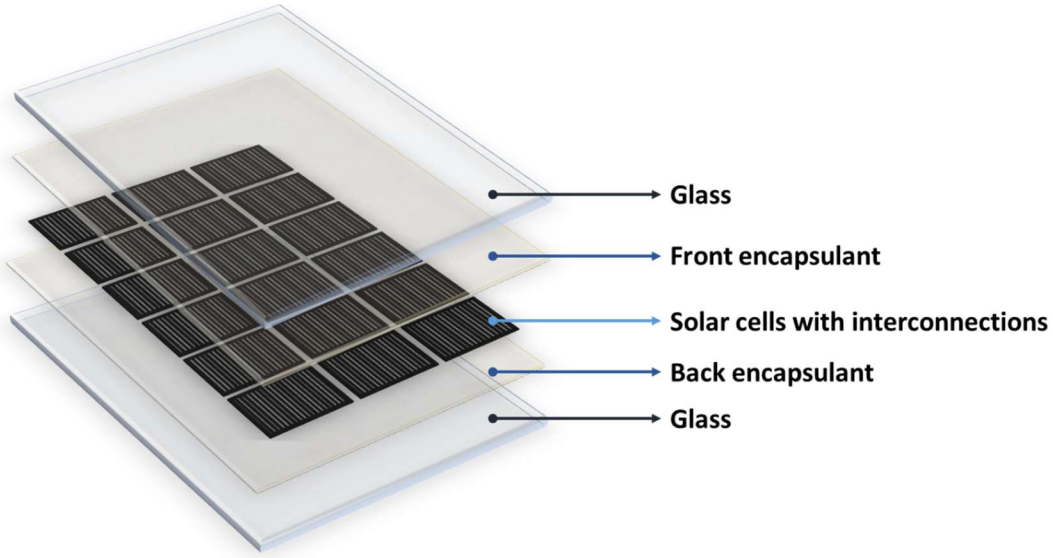

Figure 2. The components of the standard glass-glass PV module.

2.1 Frontsheet

The frontsheet serves as the interface between the solar cell and the environment, necessitating a balance between high optical transmittance and mechanical resilience [27]. While various polymeric alternative materials [27], such as ethylene tetrafluoroethylene (ETFE) [30], coated polyethylene terephthalate (PET) [31] and polycarbonate (PC) [32,33], have surfaced over the last years, tempered low-iron glass remains the dominant frontsheet material due to its unmatched balance of optical clarity, electrical insulation and environmental resistance [27]. The primary role of the frontsheet is to provide mechanical sturdiness, shielding the fragile solar cells from kinetic impacts, such as hail protection, wind and snow loads, while maintaining high solar transmittance to maximize energy conversion and keeping the moisture and oxygen out of the system. Historically, 3.2 mm glass was the industry standard; however, the state of the art has transitioned toward thinner glass profiles (typically 2.0 mm) [27]. This reduction in thickness is a critical trend driven by the need for lightweight modules and the rise of bifacial glass-glass architectures, where weight reduction is essential for structural integrity and ease of installation without compromising the module's reliability [26].

2.2 Backsheet

The backsheet serves as a multi-functional barrier, providing electrical insulation for high-voltage safety and environmental protection against moisture ingress, dirt and ultraviolet (UV) degradation [27]. Mechanically, it offers the structural rigidity necessary to shield fragile cells from wind and snow loads, while in BIPV applications, it can evolve into a primary construction element such as a structural facade or a roofing tile [26]. Additionally, it plays a key role in thermal and optical management, either reflecting light (white backsheet) to boost efficiency or facilitating bifacial gain through transparency [34].

The historical evolution of backsheet technology oscillated between glass and polymeric materials in response to cost and weight constraints [27]. While the early industry relied on glass-glass configurations, the market eventually transitioned to polymeric backsheets. Firstly, to multi-layer fluoropolymer laminated backsheets, then the laminated fluorine-free PET and co-extruded polyolefin based backsheets, to double coated (CPC) backsheets [35,36]. The reason for this transition was to achieve significant weight reductions and lower material prices, while following newly imposed governmental regulations, such as PFAS reduction [36]. However, the current state of the art has witnessed a return to glass backsheet modules [8]. This shift is motivated by the superior moisture barrier properties of glass, which provide better protection for advanced n-type cells [37,38], as well as improved mechanical rigidity and fire safety [26]. Although glass-glass modules are heavier than their polymer-backed

counterparts, the transition to thinner glass (e.g., 2.0 mm) and the resulting increase in energy yield (bifacial gain) have made them the most economically competitive choice for long-term reliability [8].

2.3 Solar cell

The technological heart of the PV module, the one converting solar energy to electricity, is currently undergoing its most significant transition since the commercialization of silicon. While p-type, passivated emitter rear cell (PERC) dominated the previous decade, the current state of the art is defined by the rapid adoption of higher-efficiency n-type technologies, specifically tunnel oxide passivated contact (TOPCon) and heterojunction (HJT) solar cells [6]. As of 2026, mass-produced n-type cells have pushed commercial module efficiencies beyond 23 - 25%, significantly outperforming the 21% ceiling of older p-type products [39].

The current "hot topic" in contemporary PV research are the perovskite and the perovskite-silicon tandem cells. By layering a perovskite as a top-cell over a silicon bottom-cell, these devices have shattered the single-junction Shockley-Queisser limit, with laboratory records surpassing 35% efficiency [40].

Beyond silicon, thin-film technologies, particularly CIGS remain present in BIPV sector. CIGS is favored for its flexibility, lightweight properties, and performance under low-light or shaded conditions, making it suitable for solar facades and flexible roofing membranes where rigid glass panels are impractical [41,42].

2.4 Encapsulant

The encapsulant layer serves as the internal binder of the PV module, and while the chemical compositions have evolved, its fundamental functional roles remain constant: providing mechanical embedding, optical coupling, electrical insulation, and structural adhesion (gluing) between the cells and the outer layers [27].

For decades, EVA was considered the "golden cow" of the industry due to its low cost and ease of processing. However, as the industry is moving toward high-efficiency n-type and perovskite cells, and with the tendency of EVA to degrade in presence of humidity and release acetic acid as by-product that can corrode interconnection and increase occurrence of the potential induced degradation (PID) effect, it is no longer number one choice [43–46]. This has led to the rise of polyolefin (POE) encapsulants [47], which offer superior moisture resistance and chemical neutrality and development of the co-extruded EVA-polyolefin-EVA (EPE) encapsulant (see Figure 3.). This co-extruded material combines the fast processability (crosslinking) of EVA with the high-performance barrier properties of a polyolefin core, with reduced costs compared to POE encapsulants [8,35].

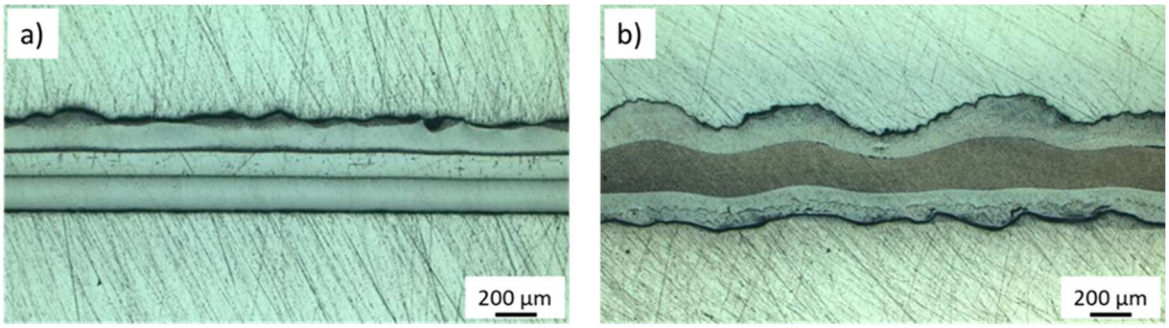

Figure 3. Microscope images of the cross-sections of two different a) and b) EPE encapsulant types [48].

Other encapsulating materials have been used and studied as alternative to EVA, such as ionomers, thermoplastic polyurethane (TPU), silicones and thermoplastic polyolefin (TPO) [27,49,50]. Some of them continue to be researched and monitored but have yet to see widespread commercial adoption compared to the dominant EVA, EPE and POE solutions.

2.5 Other components

Besides the primary components of the PV module stack, PV modules also include several additional elements that contribute to their functionality and durability. These range from essential components such as electrical interconnections to design-dependent elements including junction boxes, edge seals, aluminum or steel frames, and anti-soiling coatings. Although not part of the main stack structure, these components play important roles in ensuring electrical connectivity (junction box), environmental protection (edge seal), mechanical support (frame) and improved productivity (anti-soiling coatings) [27]. Recent developments include efforts to reduce silver content in interconnections [51], eliminate lead from soldering materials [52], and develop improved coatings to mitigate soiling and enhance module performance [53]. However, as these components are not the focus of this thesis, they will not be discussed further.

3 Functional Roles of PV components

The development of the lightweight IPV designs necessitates a fundamental re-evaluation of the bill of materials (BoM). While glass-free architectures offer significant advantages in terms of weight reduction and design versatility, they remove the protection provided by the glass layer, placing unprecedented demands on polymeric components. This chapter moves beyond a simple categorization of layers to a detailed investigation of their multi-functional roles. Regardless of their chemical composition, the polymers explored in this thesis must satisfy a rigorous set of optical, thermal, and mechanical criteria to ensure the suitability for BIPV, optimal performance and reliability of the modules.

3.1 Optical properties

Transparency is a fundamental property in PV modules, as it directly impacts the overall module efficiency. Most of the layers of the module stack contribute to light transmission to some extent.

The frontsheet, in conventional PV modules, glass, provides excellent transparency, high durability, and minimal degradation over time. When glass is replaced with polymeric frontsheet materials, these optical properties must be closely matched to maintain module performance. As previously mentioned, several polymer-based materials have been explored for frontsheet applications. PC has been researched by various, it provides good optical clarity, but it is prone to yellowing over time, however with right additives this can be delayed and there are reported cases with PC used as the frontsheet in VIPV [33,54]. ETFE also offers high optical transmittance and durability, with lower susceptibility to color change, but following the recent EU incentives to reduce PFAS this type of frontsheet is less desirable [30]. Transparent coated PET films are also available on the market [55], though they are less reported in the literature. In addition, for thin-film flexible PV modules advanced organic–inorganic hybrid coatings have been explored as potential front layers [56].

The encapsulant layer ensures optical coupling between the frontsheet and the solar cells. The optical properties of the encapsulant are directly influenced by the polymer type. EVA generally exhibits higher transmittance than POE or EPE, due to lower polymer crystallinity and higher crosslinking degree [47]. The optical properties can further be influenced by the additives, such as UV absorbers or newly emerged UV-downshifting additives that convert UV light into visible light [57,58]. Furthermore, optical properties of encapsulants are impacted by processing conditions, particularly lamination parameters and cooling rates, for instance, optimized cooling steps during vacuum lamination can reduce haze in POE, improving transmittance [59].

The backsheet layer plays a significant role in the optical behavior of the module, particularly for bifacial or semi-transparent designs. Backsheet transmittance affects the amount of light transmitted to the cells in bifacial modules and influence daylight transmission in IPV applications [60]. Semi-transparent modules can provide shading or natural lighting in buildings, or meet specific requirements in agrivoltaic systems, while opaque or colored backsheets may be selected for visual integration or functional purposes. As with the frontsheet and encapsulant, the optical performance of the backsheet is affected by polymer type [61,62], additives and fillers (e.g. TiO2 for UV protection) [63] various protective coatings (e.g. anti-scratch), and long-term material stability [64,65].

For seamless integration, besides backsheets, colored encapsulants, printed patterns, matted or textured glass or frontsheet surfaces are often applied to improve aesthetic integration into buildings, vehicles, or consumer products [66]. These modifications can reduce direct light transmittance and therefore efficiency, but they enable architectural flexibility and visual blending with the surroundings, for which lower generated energy is often acceptable [66].

Optical properties of photovoltaic module materials are typically characterized using UV-vis-NIR spectroscopy, covering the UV, visible (vis), and near-infrared (NIR) regions of the solar spectrum [67–69]. This spectral range corresponds to the wavelengths relevant for common PV cells; crystalline silicon and CIGS solar cells absorb photons roughly between 300 and 1200 nm, while perovskite absorbers primarily utilize the visible region up to approximately 800 nm [70,71]. Beyond the initial optical performance, spectral measurements also enable the evaluation of changes occurring during service life. Degradation mechanisms such as yellowing, haze formation, and additive consumption can be monitored through spectral analysis [68], providing valuable insights for material selection and long-term module reliability.

While light transmission is essential for photovoltaic energy conversion, exposure to solar radiation and other environmental factors can also initiate degradation processes in both polymeric materials and photovoltaic devices. The influence of environmental stressors on module materials is therefore discussed in the following section.

3.2 Environmental protection

PV modules are exposed to a wide range of environmental stressors, and in the glass-free IPV modules polymeric components must serve a dual protective role. On one hand, they provide electrical insulation, preventing current leakage to surrounding structures, humans, and animals (e.g. birds) from the solar cells. On the other hand, they protect fragile solar cells and their interconnections from various stressors that can compromise performance [26].

Effective environmental protection ensures safe module operation while maintaining efficiency and long-term reliability.

While optical properties determine how much sunlight can get to the solar cells, the same solar radiation that enables energy generation can also degrade module materials over time. UV photons can initiate various degradation processes in the PV module components, including the solar cells and polymeric layers. The degradation in solar cells is known as the UV induced degradation (UVID) and it is recognized as one of the causes for the performance loss in n-type solar cells [43,72]. Furthermore, polymer layers themselves are prone to photooxidation which leads to chain scission that can cause material embrittlement and yellowing or browning (see Figure 4. for backsheet yellowing) [73–75]. To mitigate UVID, and photooxidation of polymer chains, polymer matrix formulations often incorporate stabilizing additives such as UV absorbers and antioxidants (e.g. radical scavengers) [57].

Moisture ingress represents a critical environmental challenge for the reliability of PV modules. Water vapor is in the gas form and can penetrate polymer layers, accumulate within the module stack, and initiate a variety of degradation processes, including delamination, corrosion, and cell degradation [76–78]. Therefore, maintaining strong barrier properties is essential for both electrical safety and long-term module performance.

The barrier properties of polymeric materials are commonly evaluated using the water vapor transmission rate (WVTR), which quantifies the amount of water vapor passing through a defined surface area per day (g m^{-2} day^{-1}) [79]. Lower WVTR values of PV module components indicate improved resistance to moisture-induced degradation. Encapsulants, polymeric frontsheets and backsheets must provide effective moisture barriers. In a study by M. Babin et al. [79], various polymeric materials were evaluated and compared. The results showed that the WVTR of backsheets is one to two orders of magnitude lower than that of encapsulants, that polar polymers exhibit significantly higher WVTRs than nonpolar polymers, and that edge sealing plays a crucial role in limiting moisture ingress, even in glass-glass PV modules.

For sensitive thin-film solar cells, the WVTR should be lower than 1×10^{-6} g m^{-2} day^{-1}, which is difficult to achieve using polymer layers alone if long-term performance is required [80,81]. However, for products with limited service lifetimes, polymer-based encapsulation can be an appropriate choice when considering the trade-off between cost and durability.

In addition to radiation and moisture exposure, PV modules are also subject to surface contamination from environmental sources. While outer layers protect the inner from environmental stressors, dust, pollen, bird droppings, and other organic deposits may accumulate on module surfaces during operation (see Figure 4.). In some cases, biological

growth such as moss or mold may also develop on the surface of modules in humid environments (see Figure 5. in subsection 3.3 Mechanical, thermomechanical and thermal properties). Such contamination can reduce optical transmittance, create local shading effects, and lead to the formation of hot spots that negatively affect power generation [82–85]. To mitigate these effects, regular cleaning, and surface treatments of outer layers such as anti-soiling or self-cleaning coatings are increasingly employed to reduce the accumulation of contaminants and maintain optical performance [53].

Figure 4. The presence of the yellowing of the backsheet and the soiling layer on the PV module [27].

While UV radiation, moisture ingress, and biological contamination represent important environmental stressors, PV modules are also subjected to additional external loads during operation. Mechanical stresses such as wind or snow loads, as well as thermal stresses arising from temperature fluctuations and thermal cycling, can further influence the performance and durability of the PV module. These mechanical and thermomechanical aspects are discussed in the following section.

3.3 Mechanical, thermomechanical and thermal properties

PV modules are exposed to a wide range of mechanical loads throughout their manufacturing processes and service life, including lamination [86,87], stresses during transportation and installation [88], wind pressure [89], snow accumulation [90,91], hail impact [92,93], etc. In conventional PV modules, the glass layers provide most of the structural rigidity, protecting the brittle solar cells from excessive bending and deformation, while the encapsulant, as the soft component, cushions the solar cells by absorbing mechanical loads.

Even tempered glass, however, can fail under extreme conditions. For example, in Figure 5., hail caused breakage of a tempered glass layer, nevertheless, together with the encapsulant layer the mechanical impact was absorbed. The module remains functional and is currently monitored on the roof of the University of Leon, Spain.

When glass layers are replaced with lightweight polymeric materials in integrated PV designs, the structural role of the module stack changes considerably. The reduced stiffness of polymer-based architectures requires alternative design strategies to maintain mechanical stability and protect the solar cells. Approaches explored in recent years include reinforcing the back and front of the module with fiber reinforced composites, and integrating metallic substrates or sandwich structures such as polymeric honeycomb cores on the backside of the module [92,94–99]. Such designs leverage high stiffness-to-weight ratios, widely used in engineering applications, to provide mechanical support while significantly reducing module weight. Various testing methods exists for investigation of the mechanical properties of the PV module, however, in dependence on how the PV module is integrated or attached to the substrate, not all tests are needed nor compatible [100–102]. Regardless, hail tests, static and cyclic loads, 4-point bending tests, amongst others should be included for the characterization of any new components considered for the IPV module stack.

Figure 5. The glass breakage due to hail impact and the moss growing in the corner, the PV module is still producing electricity under monitored conditions.

In addition to mechanical loads, PV modules are subjected to thermomechanical stresses arising from differences in the coefficient of thermal expansion (CTE) under diurnal and

seasonal temperature fluctuations [103–105]. As PV modules consist of a multilayer stack of different materials, each with distinct CTE values, thermal expansion mismatches are inevitable. The resulting cyclic expansion and contraction generate internal stresses that can lead to various degradation mechanisms, such as interlaminar delamination, cell displacement, and cracking [106–110].

Compared to glass and silicon, polymeric materials generally exhibit significantly higher CTE values, as confirmed by several studies [111–113]. However, by reinforcing the polymer matrix with glass fibers to form glass fiber reinforced polymer (GFRP) layers, the CTE can be reduced substantially [114]. In addition, the CTE of polymers can be further reduced through approaches such as biaxial chain orientation (e.g., in PET), annealing processes, or reinforcement of the polymer matrix with fillers other than glass fibers [115,116]. The encapsulant layer plays a central role in mitigating mechanical and thermomechanical stresses, as it mechanically bonds the module layers and reduces stress transmission to the solar cells [117]. Therefore, it is of utmost importance to accurately determine CTE values and to predict material interactions and potential degradation mechanisms using finite element modelling (FEM) [118].

Various measurement techniques, such as dynamic mechanical analysis (DMA), thermomechanical analysis (TMA), and digital image correlation (DIC), have been employed to characterize the thermomechanical behavior of encapsulants [111,119,120]. However, in the literature, encapsulant CTE values used in FEM simulations are often simplified. Common assumptions include linear elastic material behavior and a constant CTE of approximately 270 ppm over broad temperature ranges, frequently based on EVA as a reference material [103,121–123].

Integration of PV modules into structural elements, such as steel façades, further complicates the thermomechanical environment. In these applications, the module must accommodate the thermal expansion of the supporting structure, which could differ from that of the PV layers. For instance, solar glass typically exhibits a CTE of approximately 9 ppm [124], while the stainless-steel substrate (e.g. ferritic grade) has a CTE of roughly 10–11 ppm [125,126]. In contrast, the CTE of polymeric backsheets, depending on chemistry, temperature, and layer configuration, ranges from 50 to 200 ppm [111]. When these materials are bonded, the high-modulus glass or steel layers act as a mechanical restraint, severely limiting the natural expansion and shrinkage of the polymer layers. This restrained movement generates significant interlaminar shear stresses at the interfaces, particularly during thermal cycling, which can lead to micro-cracking or adhesive failure [127]. Careful selection of materials and design of interfaces are therefore essential to ensure mechanical compatibility and prevent these stress-induced failures.

Temperature interactions extend beyond the impact on the thermomechanical behavior of PV module components. During the lamination process, all materials in the stack, beyond the encapsulants, must withstand lamination temperatures while maintaining their functionality, without undergoing any material changes such as melting or degradation. During operation, solar cells can reach elevated temperatures and require efficient heat dissipation to maintain optimal performance [128,129]. Materials in direct contact with the cells and outer layers should therefore provide sufficient heat conductivity. Heat conductivity of polymer materials is often limited and can be further challenged in insulated configurations typical for IPV modules. Heat conductivity of BoM can impact the lamination process (e.g. duration [94]) and module´s efficiency in IPV design [128].

Accurate characterization of thermal properties, including thermal transitions (glass transition, melting and crystallization temperature), thermal degradation, and heat conductivity, is necessary to prevent early power losses. Common measurement techniques include differential scanning calorimetry (DSC) [68], thermogravimetric analysis (TGA) [68], and guarded heat flow meters (GHFM) [130], while methods such as laser flash analysis (LFA) [131] and infrared thermography [132] are also used to evaluate heat transport and distribution within PV materials.

3.4 Structural integrity

The structural integrity of PV modules relies heavily on the adhesion between their constituent layers. In conventional, integrated, and emerging PV module designs all components are interconnected primarily through encapsulants. Encapsulants serve as the main adhesive layer, bonding the solar cells to the front and back layers while simultaneously distributing mechanical and thermal stresses across the module [27].

Beyond encapsulants, several other elements contribute to adhesion within the PV stack. For instance, soldering flux enables adhesion between the interconnection ribbons and the solar cells, ensuring stable electrical and mechanical connection [27]. In multilayer laminated backsheets, polyurethane (PU) based adhesives are commonly employed to bond PET and polyethylene (PE) or EVA layers, as well as other polymeric layers such as polyvinyl fluoride (PVF), polyvinylidene fluoride (PVDF), and polypropylene (PP) [133]. Moreover, direct integration of the PV stack on the construction elements such as aluminum or steel façade element can be achieved through adhesion via PV encapsulant or other adhesive layers [134,135]. Strong and durable adhesion at this interface should be maintained throughout the entire life time of the building element.

Adhesion within the PV laminate is governed by a combination of mechanical and chemical mechanisms, ranging from micro-scale physical interlocking to molecular-level interactions

such as covalent, hydrogen, and van der Waals bonding [136,137]. To optimize the interface between dissimilar materials, adhesion can be significantly enhanced through chemical promoters like silane coupling agents in the encapsulant [138], as well as surface functionalization via plasma treatment [139] or mechanical profiling to increase effective surface area [135]. Furthermore, the final bond strength is intrinsically linked to the material's thermal history, as the degree of crosslinking achieved during lamination impacts adhesion strength [140].

Each component in the PV stack thus plays a functional role in maintaining adhesion, which is crucial for long-term module performance. Delamination of any layer can lead to a wide range of degradation mechanisms, including optical decoupling (see Figure 6.), reduced efficiency, short-circuiting in interconnections, and accelerated moisture ingress [141].

Figure 6. Delamination between the front layers in the PV stack.

Quantifying adhesion strength is essential, yet standardized thresholds are limited to certain measurement techniques, such as cantilever beam methods [142]. While these methods have been developed to test the adhesion strength, producers of encapsulant and backsheet materials, as well as researchers in lack of suitable equipment, often rely on alternative techniques such as 90° or 180° peel tests, T-peel tests, lap shear tests, or other mechanical characterization methods which produce different and hard to intercompare results [143–145]. Furthermore, adhesion to construction components in IPV applications still requires systematic determination and verification.

It is important to note that environmental stressors, including thermal cycling, moisture ingress, mechanical loads, and UV exposure, can degrade adhesion over time [144,145]. These factors can compromise the structural and functional integrity of PV modules and will be discussed further in the concluding section of this chapter. Maintaining reliable adhesion under diverse service conditions is therefore a central consideration in PV module design, from conventional to integrated and glass-free architectures.

3.5 Fire retardance

Fire behavior is an important consideration for IPV modules, with additional regulatory and occupant-safety requirements applying specifically to BIPV systems integrated into building envelopes [26]. BIPV modules are subject not only to electrical safety standards but also to building regulations, including fire safety requirements [26]. Compliance with these standards is essential to ensure that BIPV modules do not pose additional hazards to occupants, rescue personnel, or adjacent structures during fire incidents [146,147].

While polymers enable novel module designs, they also introduce fire-related hazards that must be carefully managed [148]. Polymer-containing PV modules can ignite under electrical faults such as hotspots or arcing, or when exposed to external flame sources [149]. Combustion may produce flaming droplets, contribute to fire propagation, release toxic gases and create toxic residues, all of which can increase danger to building occupants, spread of fire and complicate firefighting operations [148,149]. The specific fire behavior depends on the polymer type, composition, and position within the module stack.

In glass-glass PV modules, the glass layers can provide effective protection against external fire exposure, allowing such modules to achieve the required fire classification for roof systems (e.g., BROOF(t1)) [150]. However, in façade applications, the assessment criteria differ, as the fire performance depends not only on the PV module itself but also on the entire façade system [151]. Additional components, such as mounting structures, insulation, and ventilated cavities, play a significant role in meeting fire classification requirements.

When glass is replaced and polymeric materials form the outer layers, their fire behaviour becomes critical. In a study by U. Desai et al. [152], the fire behaviour of a honeycomb sandwich composite backside was investigated according to ISO 11925-2, targeting a minimum classification of Class E under EN 13501-1 fire classification. To achieve this classification, the flame spread (Fs) must remain below 150 mm within the specified test duration. The results (Figure 7.) indicate that, with the exception of PPGF6, all samples exhibited an Fs below 150 mm [152]. However, flaming droplets were observed for all samples within the 2 s test period. This and other reported studies have a consistent observation: polymer-based materials are combustible and may contribute to fire spread, particularly when used as exposed outer layers, thereby posing an increased fire risk in façade applications.

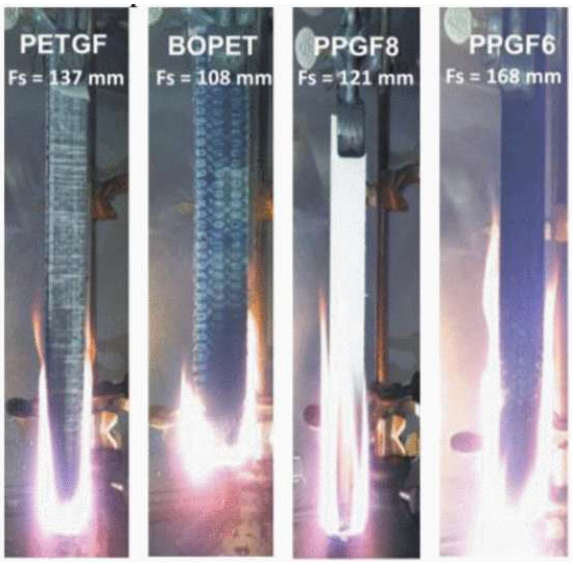

Figure 7. Flammability test on four different honeycomb composite backsides with measured Fs [152].

To mitigate these risks, several technological strategies can be employed. Flame-retardant additives can be incorporated into polymer matrix during material processing, improving resistance to ignition and slowing flame spread. The use of halogen-free flame-retardant additives, including mineral, phosphorus-, nitrogen-, organosilicon-, and bio-based compounds, which reduce environmental and health hazards compared to traditional halogenated flame retardants is emphasized [148,149]. Additionally, intumescent coatings can be applied to polymeric backsheets or other module surfaces. When exposed to heat, these coatings expand and form an insulating char layer that limits heat and oxygen transfer and helps prevent fire propagation [148,149]. Such coatings can be applied both during production and, in some cases, to already installed modules. Challenges remain and yet have to be investigated, regarding long-term durability, compatibility with lamination processes, possible interlayer additive interaction or migration, and most of all the maintenance of optical properties in the transparent components [148].

It should be noted that, while fire behavior represents an important consideration for polymer-based BIPV, this thesis primarily focuses on material characterization and integration strategies. Comprehensive fire testing and the optimization of fire-retardant systems remain outside the scope of this work and are recognized as important directions for future research.

3.6 Degradation modes

While each component surrounding the solar cells fulfils a specific functional role, their long-term durability and reliability under operational conditions cannot be assumed and must be critically evaluated. As mentioned, PV modules are continuously exposed to a range of environmental stressors that can affect their performance [141]. If the BoM and material

combinations are not properly selected and tested, these stressors can induce degradation processes that ultimately lead to power loss or even module failure [141]. While individual stressors may trigger specific degradation modes, their combined action often accelerates failure mechanisms and can result in severe or irreversible damage [153].

Reliability in PV modules is commonly described using the “bathtub curve,” which distinguishes between early-life failures, a steady operational phase, and wear-out failures [153]. Degradation mechanisms may occur at any stage of the module lifetime, from initial deployment to end-of-life. Early identification of potential degradation pathways, material interactions, and weaknesses in BoM combinations is therefore crucial for ensuring long-term performance [153].

A wide range of degradation modes has been observed in field-deployed PV modules. Historically, one of the most observed issues in early commercial modules was the yellowing of EVA encapsulants, which reduced optical transmittance and with that module’s efficiency [153]. Although material formulations have since been improved, similar degradation phenomena still occur from time to time in modern modules. The most commonly observed degradation modes include delamination, discoloration of encapsulants and backsheets, corrosion of metallic components, cell cracking, glass breakage, and electrical degradation effects such as PID, UVID, and light-induced degradation (LID) [153].

These degradation modes are driven by key environmental stressors, primarily moisture, UV radiation, temperature, and mechanical loads as shown in Figure 8 [153,154]. Moisture ingress, in particular, plays a critical role, as it can penetrate polymeric layers, weaken interfacial adhesion, and initiate corrosion of metallization and interconnects [155]. In the presence of moisture, hydrolysis reactions may occur in susceptible polymers such as EVA and PET, leading to chain scission, formation of degradation by-products, and embrittlement [141,153]. For EVA, this includes the generation of acetic acid, which can further accelerate corrosion processes in metallic components and degradation of surface layers in TOPCon cells [43,45]. Moisture is considered as the mayor degradation factor in thin-film solar cells (e.g. CIGS [156]) and in the emerging cell technologies (e.g. tandem silicone-perovskite solar cells [157,158]) where the cell layers (e.g. absorber materials) are highly sensitive to water exposure.

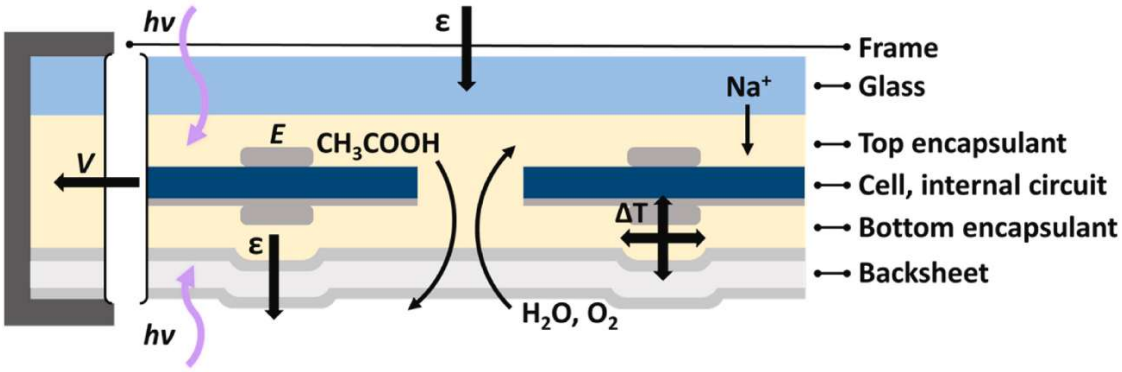

Figure 8. Schematic representation of typical environmental stressors on the glass-backsheet PV module including: light (hv), strain (ε), voltage bias (V), chemical diffusion, ingress and egress (CH3COOH, H2O, O2, Na+), electric field (E), and thermomechanical strain (ΔT) [153].

UV radiation is another major degradation driver, particularly for polymeric materials. Although the UV portion of the solar spectrum (280–400 nm) represents only a small fraction of the total irradiance, it carries sufficient energy to break chemical bonds (e.g., C–C and C–O bonds) in polymer chains. This leads to photooxidation, resulting in chain scission, embrittlement, and the formation of chromophores that cause yellowing or browning, thereby reducing optical transparency [153]. Even though polymer matrix formulations often incorporate stabilizing additives such as UV absorbers and antioxidants, these can be consumed and their protective effect can terminate [159]. Maintaining not only high initial transmittance but also long-term optical stability is therefore essential for module performance.

Temperature further accelerates degradation processes by enhancing chemical reaction rates and diffusion. Additionally, mismatches in CTE among module components induce thermomechanical stresses during temperature fluctuations. These stresses, combined with cyclic diurnal and seasonal variations, can lead to fatigue-related failures such as interfacial delamination, deformation and breakage of the interconnections, and cell cracking [104,123]. Mechanical loads from environmental factors such as wind, snow, hail, or improper installation can further exacerbate these effects, contributing to structural damage including glass breakage.

Based on field observations and expected behavior in emerging module concepts, the most relevant degradation modes can be summarized as follows [153]:

- Delamination: driven by moisture ingress, thermomechanical stress, and mechanical loading; often linked to degradation of adhered interfaces.
- Discoloration (yellowing/browning): primarily caused by UV radiation and moisture-induced chemical changes in polymers.

- Corrosion: induced by moisture and corrosive by-products (e.g., acetic acid), affecting metallic interconnections and solar cell absorber layers.
- Cell cracking: caused by mechanical loads (hail, wind, snow, handling) and thermomechanical stress.
- Cell degradation: resulting from combined effects of moisture, temperature, UV exposure, and electrical stress (e.g., PID, LID, UVID), with additional sensitivity in emerging technologies such as perovskites.
- Glass breakage: mainly due to mechanical stress.
- Backsheet/frontsheet embrittlement and cracking: driven by UV exposure, moisture, thermal aging, and hydrolysis of susceptible polymers such as PET.

To ensure adequate durability, a comprehensive set of international testing standards has been developed, primarily within the International Electrotechnical Commission (IEC) framework [102,160–165]. Commonly applied tests include damp heat (DH) exposure, thermal cycling (TC), UV exposure, and sequential testing that combines multiple stress factors [102]. However, it remains challenging to replicate all relevant field conditions in laboratory environments, and outdoor testing, while essential, is time-consuming. This discrepancy is particularly critical given the rapid development of new PV technologies and materials, including IPV products. Consequently, ongoing research efforts aim to refine existing test protocols and develop new methodologies to better capture real-world degradation behavior.

Ultimately, no single test or material property can fully predict long-term module behavior, as the most reliable assessments require a combination of indoor accelerated testing and outdoor exposure studies. Bridging this gap remains a significant research challenge, tackled by institutions like National Laboratory of the Rockies (NLR) through the use of Combined-Accelerated Stress Testing (C-AST) to mimic the complex interactions of real-world environments [166]. Therefore, a thorough characterization of any new material is essential prior to integration, ensuring that potential degradation mechanisms are identified and long-term performance limitations are fully understood.

The following chapter builds on these considerations by examining novel module designs, their associated constraints and opportunities, and introducing the approaches explored in this thesis to address the identified challenges.

4 Design paths for IPV modules

The selection and validation of the BoM remains a critical step in PV module design and cannot be directly transferred between different module architectures [167]. While the PV industry has historically relied on a limited number of polymer material families, these materials are rarely used in their pure form, but rather as complex formulations containing various additives. These additives may evolve or interact differently under operational conditions, meaning that materials under the same label name, which have previously demonstrated adequate performance, cannot be assumed to remain the same and reliable in new system configurations. This limitation is exemplified by the interaction between POE encapsulants and TOPCon cells, where the degradation of specific additives into acidic by-products resulted in cell corrosion and performance losses [168]. Furthermore, materials that performed well in conventional glass-glass or glass-backsheet modules may not exhibit the same reliability when implemented in glass-free IPV designs. Therefore, material compatibility and long-term behavior must be reassessed for each specific BoM combination.

Based on these considerations, several key challenges (see Figure 9.) arise in the design of glass-free IPV modules, which are addressed in this thesis through targeted material and design approaches.

First, the removal of glass eliminates the primary structural support within the module, requiring alternative solutions to ensure mechanical stability under installation and environmental loads such as wind, hail, and snow. This introduces challenges not only in achieving sufficient stiffness and strength, but also in integrating new structural materials into established PV module architectures. In this context, this thesis investigates glass-free module concepts based on composite-backed structures and the direct integration of modules onto stainless-steel façade elements, aiming to provide mechanically stable and application-relevant design solutions.

Second, structural integrity is closely linked to interfacial performance, as strong and durable adhesion throughout the entire material stack is required. In this context, the thesis investigates adhesion from two distinct perspectives to address different application requirements. On one hand, the research explores adhesion pathways for the direct integration of modules onto façade elements; here, the challenge is maintaining a safety-relevant, load-bearing bond over a 25-year service life under continuous environmental stress. On the other hand, recognizing that not all integrated PV devices are intended for the building envelope, the work also examines the adhesion of protective coatings onto flexible substrates. In this second path, the focus shifts to achieving interfacial quality on prefabricated devices where complex topographies and surface chemistries dictate the bonding success. By

addressing both long-term integration and complex device coating, the thesis seeks to provide a comprehensive understanding of interfacial reliability in glass-free designs.

Third, the introduction of new materials and layer configurations imposes constraints on processing, particularly during vacuum lamination. Polymeric materials must withstand the applied temperature and pressure loads without excessive deformation, which requires prior understanding of their thermal behavior. At the same time, differences in thermal conductivity between materials, ranging from insulating composite structures to conductive metallic substrates, affect heat transfer during lamination and require adaptation of process parameters to ensure proper encapsulant melt-flow and defect-free bonding. Due to these differences, the use of standard industrial parameters for traditional glass modules, presents challenges in achieving uniform heat distribution, therefore optimization is necessary to avoid under-curing or thermal damage to the novel layer configurations. To address these challenges, this thesis involves profiling the thermal behavior of individual materials to propose suitable processing windows for novel BoM configurations. By establishing a scientific logic for material selection, the work seeks to ensure that lamination conditions are aligned with the physical limits of the glass-free design.

Fourth, the transition to glass-free, lightweight architectures significantly shifts the thermomechanical balance of the PV stack. In glass-free designs, the lack of a rigid glass constraint means that even minor variations in the encapsulant’s expansion or contraction can lead to significant warping and mechanical stress. Within this thesis, the challenge is addressed by experimentally investigating the complex thermomechanical behavior of various encapsulants, moving beyond standard industrial simplifications. By examining how processing history and lamination conditions influence the material's dimensional stability, the research aims to establish a more accurate foundation for predicting the reliability of integrated PV assemblies.

Finally, the long-term stability of polymeric materials remains a critical challenge. Polymeric systems are intrinsically susceptible to chemical and physical changes over time, including additive migration, degradation reactions, and the formation of by-products. These processes can progressively alter mechanical, optical, and barrier properties, while also triggering secondary degradation mechanisms at the module level. Importantly, such behavior is governed not only by individual material properties but also by interactions within the multilayer laminate. In this context, this thesis focuses on material characterization and degradation-related behavior under accelerated ageing conditions, providing insights into material stability within complex module configurations.

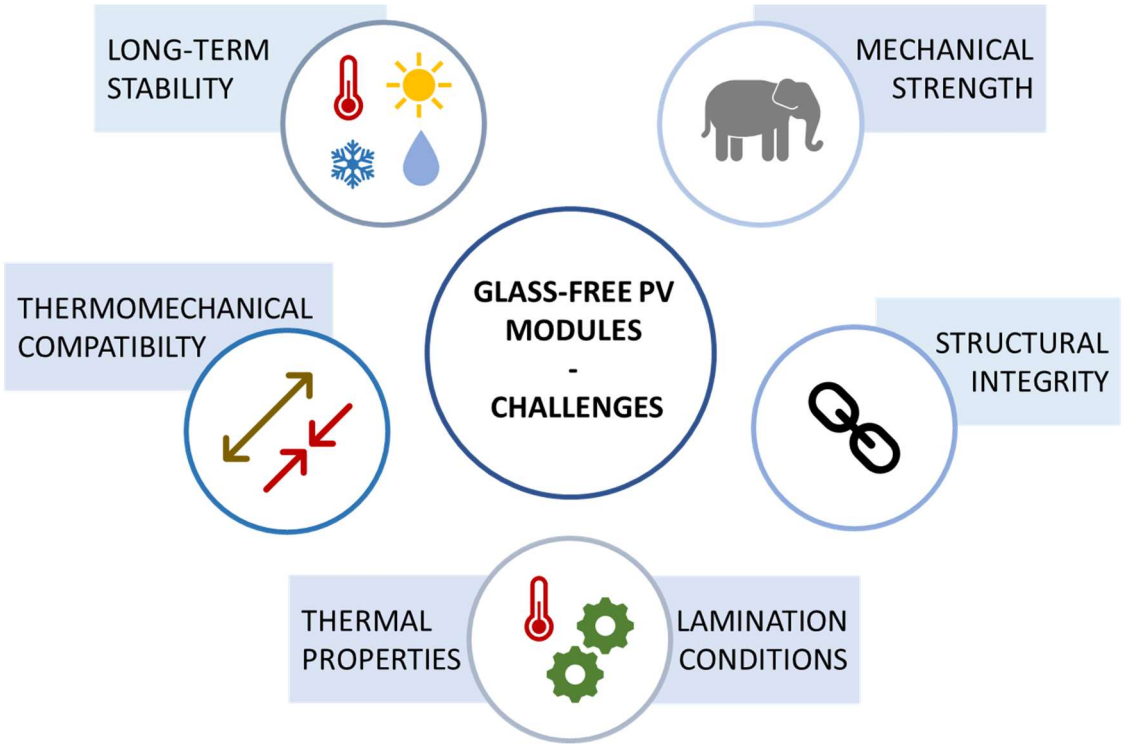

Figure 9. Challenges in design and development of glass-free IPV modules.

Taken together, these challenges highlight the need for a systematic understanding of material behavior, interfacial interactions, and process–structure–property relationships in glass-free IPV modules. Despite extensive developments in polymer-based PV materials, their behavior within glass-free and building-integrated module architectures remains insufficiently understood, particularly with respect to material interactions, processing, and long-term performance. Current approaches often remain largely empirical, focusing on module fabrication and performance testing, while the role and behavior of polymeric materials within multilayer systems are not systematically addressed. As a result, the reliable design of such systems remains limited. This gap motivates the present thesis, which focuses on the role of polymeric materials in enabling and constraining glass-free IPV module concepts.

To address this need, this chapter defines the objectives of this thesis in terms of targeted design approaches for IPV modules, with a specific focus on the enabling and limiting roles of polymeric materials. The first approach investigates glass-free module concepts based on integrated composite backsides that provide mechanical support. The second approach examines adhesion pathways for the direct integration of PV modules onto stainless-steel façade elements. The third approach explores coating-based encapsulation strategies for glass-free thin-film PV modules intended for short-term integrated applications, such as portable products. Finally, the last section addresses the challenges associated with encapsulation materials in glass-free architectures. Without the stiffness of glass to restrain expansion and shrinkage, understanding the thermomechanical properties of standard (EVA

and POE) and novel (co-extruded EPE) encapsulant materials becomes vital. This research correlates the influence of encapsulant processing and the degree of crosslinking with dimensional stability. Furthermore, in addition to investigating the thermomechanical properties of co-extruded EPE encapsulants, a wide spectrum of their optical, chemical, and thermal characteristics is evaluated to identify material differences and predict potential integration challenges within IPV modules.

4.1 Glass-free, lightweight, polymeric composite design

In areas where traditional PV modules are too heavy for integration, particularly in urban [169], industrial infrastructures [170], or heritage buildings [171], removing the glass layers can reduce the weight, but it requires alternative structural components that provide mechanical support, environmental protection, and maintain module functionality. Lightweight composite backsides, including honeycomb sandwich structures [96], have emerged as a promising approach to address these challenges. The properties of these structures and their layers (core material and the reinforced skins) can be tailored to achieve the desired mechanical, thermal, and protective performance while minimizing weight [172]. A schematic representation of the honeycomb backside IPV module stack is shown on Figure 10.

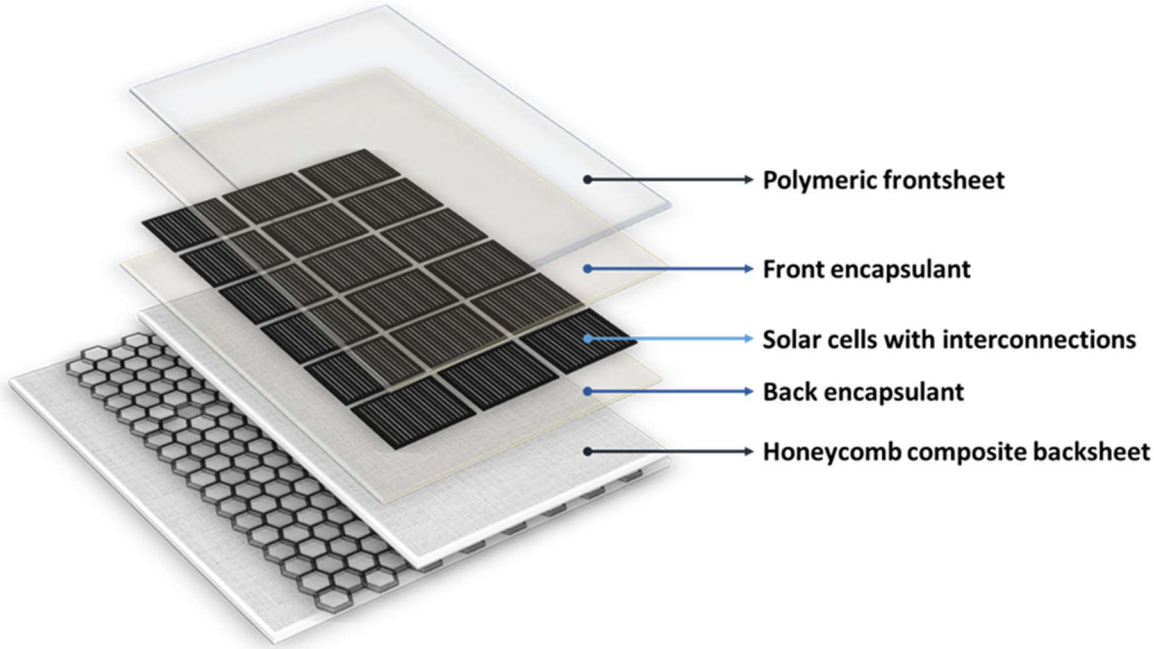

Figure 10. Schematic representation of the honeycomb backside IPV.

Previous studies have demonstrated the potential of PV modules with honeycomb sandwich composite (HSC) backsides, often using aluminum or Nomex® cores with GFRP skins [92,96,173]. These solutions reduced weight while maintaining structural stability under

thermal and damp heat stresses. Furthermore, a rigid and torsion-resistant sandwich composite composed of polyurethane foam as the core and GFRP skins was explored for VIPV integration [174,175]. Overall, honeycomb backed PV modules appeared to be the most promising approach for lightweight integration, but the high cost of Nomex® and the potential for poor electrical insulation of aluminum cores motivated the exploration of thermoplastic HSC as an alternative backside material for lightweight PV modules.

The approach was to test commercially available composites already used in the building and automotive sectors and evaluate their suitability as backsides for PV modules, to bridge the gap between niche and large-scale deployment. Material selection focused on composites that are free of fluorinated compounds, cost-effective, and potentially recyclable. The objective was to determine whether these materials could be integrated into standard lamination processes, assess their ability to protect internal components from environmental stressors such as UV, temperature, and humidity, and analyze their condition after exposure. Within the project, fully functional PV modules were fabricated and tested according to IEC standards.

4.2 Stainless-steel façade integration - polymer as electrical insulation layer

The use of stainless-steel façade elements as the structural rear side of the PV module was investigated within a second integration concept. In this case, the PV module is directly integrated into the façade system, where it together with the metal substrate becomes the part of the building envelope (see Figure 11). Since stainless-steel is electrically conductive, electrical insulation between the active PV components and the façade structure is required [134]. For this purpose, the polymeric backsheet used in standard PV module architectures represents a suitable solution, as it is already designed to provide long-term electrical insulation within conventional module stacks.

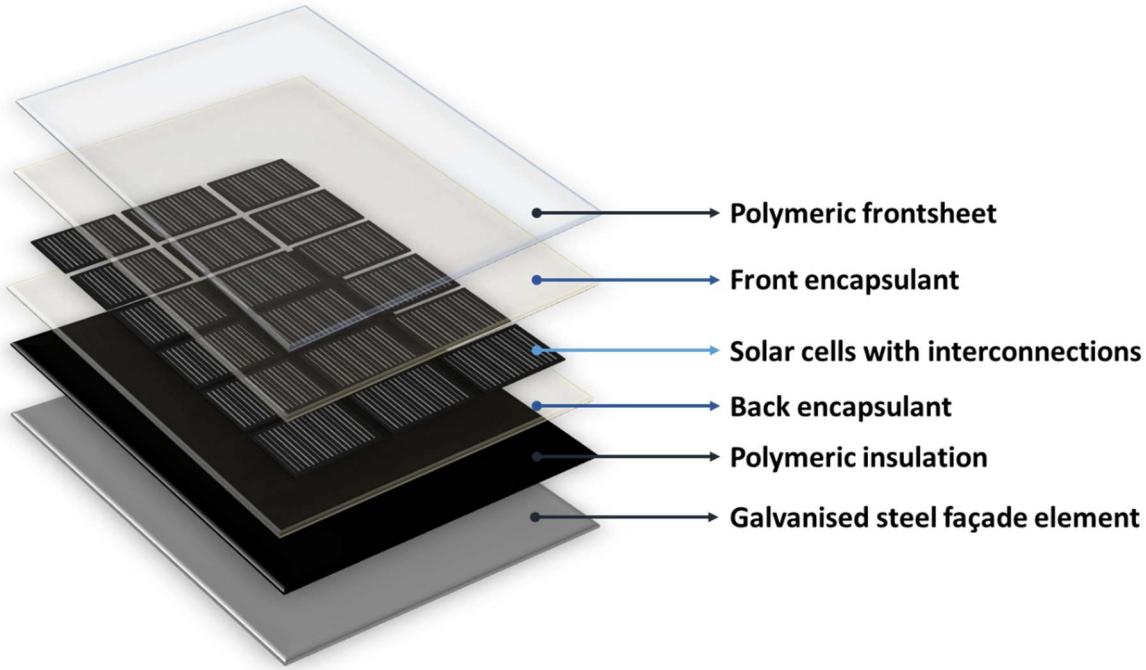

Figure 11. Schematic representation of the galvanised steel façade IPV.

The introduction of a direct polymer–steel interface introduces additional requirements compared to conventional PV modules. In particular, a reliable and durable bond between the backsheet and the metallic substrate is required to ensure mechanical integrity over the module lifetime, especially under environmental loading. Related studies on aluminum-based façade integration have demonstrated that PV stacks can be bonded to metallic substrates using standard encapsulant materials such as EVA or POE [134,176,177]. These studies mainly addressed manufacturing feasibility and electrical performance of PV modules with glass at the front, without a detailed investigation of adhesion durability. Similarly, an investigation on stainless-steel substrates has focused on the influence of surface properties and lamination conditions on the adhesion strength between the stainless-steel substrate and the backsheet, using EVA or POE as adhesive layers [135]. However, the study was limited to initial adhesion measurements and did not address long-term behavior under ageing conditions [135].

As a result, a knowledge gap remains regarding the suitability of encapsulant-based bonding strategies for long-term adhesion stability in steel-integrated PV modules, and whether alternative interfacial concepts are more suitable. This motivated the investigation of different adhesion approaches between the polymeric backsheet and hot dip galvanized steel (HDGS) substrate, with a focus on both initial adhesion performance and durability under environmental stress conditions.

4.3 Glass-free, flexible coating encapsulation

Thin-film photovoltaic technologies, particularly CIGS cells, are well-suited for IPV due to their inherent flexibility, lightweight form factor, and adaptability to complex shapes [42,178,179]. However, encapsulation remains a key challenge for flexible photovoltaic devices, as it requires balancing effective barrier performance with mechanical flexibility and compatibility with scalable manufacturing. Conventional solutions rely on rigid, glass-based designs to prevent moisture ingress [180], but these inherently limit flexibility, restrict shape customization, and are not suitable for continuous roll-to-roll processes.

This limitation is particularly relevant for CIGS cells, which, despite a lower market share compared to silicon [8], offer distinct advantages in terms of form factor. Their compatibility with flexible substrates enables lightweight and conformable modules for applications ranging from portable and IoT devices to BIPV and VIPV [169]. In addition, the technology can be adapted to different application lifetimes through the choice of BoM.

While glass encapsulation provides excellent protection against moisture, its removal in flexible designs exposes CIGS cells to environmental degradation, creating a need for alternative barriers that combine effective protection with mechanical flexibility. To address this challenge, alternative encapsulation strategies, such as coating-based approaches, have been explored [56,181–184]. Polymer-based coatings, such as polyurethane (PU), epoxy, acrylates, and UV-curable systems, provide tunable material properties and are compatible with scalable roll-to-roll deposition methods. Inorganic and hybrid barrier concepts, including AlO_x-based layers, have demonstrated improved resistance to moisture and oxygen ingress, but are often limited by processing complexity, cost, and limited industrial adoption [56].

Despite these advances, scalable and cost-effective encapsulation solutions compatible with flexible device architectures are still lacking. In this context, coating-based encapsulation of flexible CIGS prefabricates on stainless-steel foils was investigated (see figure 12.), focusing on commercially available and specially developed polymer coatings based on silicone, PU, acrylate, and epoxy systems.

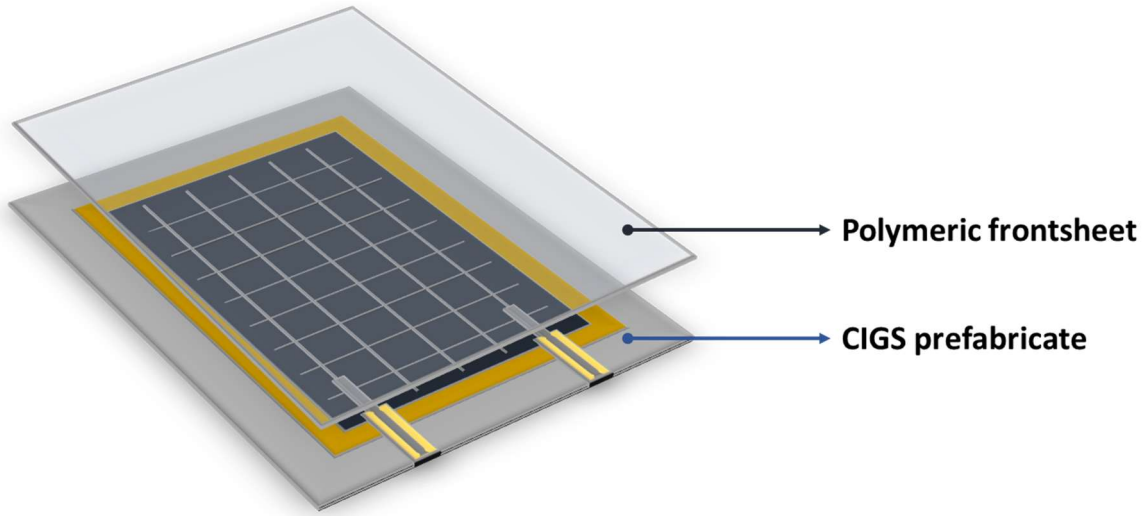

Figure 12. Schematic representation of the coated flexible CIGS IPV.

4.4 Following the encapsulant footsteps

The design of the BoM for PV modules is far from simple. While the encapsulant is the layer that binds the entire stack together, its thermomechanical behavior is often overlooked or oversimplified in design stage and FEM simulation, even though it remains a significant factor in module failure [103,118,185–187]. In conventional glass-glass modules, the rigid glass layers constrain the dimensional changes of the encapsulant; however, the resulting CTE mismatches lead to internal stress accumulation. In contrast, in flexible, lightweight, and glass-free IPV designs, the encapsulant is less constrained, and even relatively small expansion or contraction of the polymer layers can lead to significant module warping or deformation. If not properly managed, these stresses, in both glass-glass and IPV modules, can contribute to failure modes such as solar cell cracking, solder joint fatigue, and delamination, particularly in mechanically sensitive technologies like perovskites, where layer delamination leads to device failure [108–110,188].

A thorough understanding of these failure mechanisms requires an analysis of the encapsulant's thermomechanical behavior across various manufacturing stages, as its final response is not defined by a single event. In other industries, such as automotive and microelectronics, the processing conditions of polymeric parts are known to require optimization to reduce warping and deforming [189–193]; however, this perspective is currently underexplored in PV research.

Therefore, the objective of this part of the thesis is to move beyond simplified assumptions by experimentally characterizing the thermomechanical behavior of various encapsulants. By investigating the impact of processing history and lamination conditions on the CTE values of

six material, including crosslinking EVA, POE and co-extruded EPE, and non-crosslinking TPO, this research seeks to provide an understanding of material behavior and build a foundation for ensuring the mechanical stability of both conventional glass-glass and lightweight IPV designs.

In addition to the BoM design paths for IPV and thermomechanical behavior of the encapsulants, over the course of this PhD thesis research, it became clear that the industry's rapid technological shift was outpacing the scientific knowledge regarding the co-extruded EPE encapsulant. This was driven by the need to protect n-type cells, which exhibit a higher sensitivity to humidity than their p-type predecessors [194]. While EPE is marketed as a “best of both solution” [55], combining the cost-effective EVA with the superior moisture-barrier performance polyolefin core, it remains a relatively "black box" material in terms of its holistic properties, creating a significant knowledge gap for all PV configurations.

Consequently, the final part of this thesis focuses on a systematic characterization of four commercially available EPE films, by examining their chemical, optical, thermal, thermomechanical, and barrier properties, to assess whether these emerging materials truly fulfil their promise.

Together, these studies provide a comprehensive, material-level understanding of standard and emerging encapsulation technologies, bridging the gap between fundamental polymer science and the structural reliability of next-generation IPV.

5 Publications

5.1 List of Included Publications

I **N. Pervan**, U. Desai, G. C. Eder, J. Govaerts, A. Derluyn, W. Winant, A. Faes, C. Ballif, G. Oreski, *Characterization of Lightweight Polymeric Honeycomb Structures for Use as Backsides in Glass-Free PV Modules*, Journal of Applied Polymer Science 142, no. 48 (2025): e57892, https://doi.org/10.1002/app.57892.

II **N. Pervan**, L. Geymayer, M. Fleischanderl, H. Kurz, G. Kitzberger, F. Füreder-Kitzmüller, G. Oreski, *Backsheet-Galvanized Steel Adhesion Approaches for Integrated Photovoltaic Façades: A Comparative Study*, 2026 IEEE 54th Photovoltaic Specialists Conference (PVSC), New Orleans, LA, USA, 2026 (accepted)

III **N. Pervan**, S. Feldbacher, M. Harnisch, A. Zimmermann, G. Oreski, *Systematic study of barrier layer coatings for encapsulation of flexible CIGS PV modules*, Results in Engineering, 2026 (under revision, RINENG-D-26-06508)

IV **N. Pervan**, J. Geier, M. Daenen, G. Oreski, *Effects of Manufacturing Process History and the Lamination Duration on Thermomechanical Properties of PV Encapsulants*, Advanced Energy and Sustainability Research, 2026 (submitted)

V **N. Pervan**, G. Eder, Y. Voronko, A. Macher, K. Novotny, K. Resch-Fauster, G. Oreski, *Is EPE the future of PV encapsulation? A comprehensive material-level assessment*, Solar Energy Materials and Solar Cells, Volume 300, 2026, 114258, ISSN 0927-0248, https://doi.org/10.1016/j.solmat.2026.114258.

5.2 Publication I

Title: Characterization of Lightweight Polymeric Honeycomb Structures for Use as Backsides in Glass-Free PV Modules

Journal: Journal of Applied Polymer Science, https://doi.org/10.1002/app.57892

Date of publication: 27th of August 2025

	Share in %									Total
	Author	Co-authors								
	PhD Student	1	2	3	4	5	6	7	8	
Conceptualization	70	10	10						10	100
Methodology	90	10								100
Formal analysis	90	10								100
Investigation	90	10								100
Visualization	95	5								100
Data curation	90	10								100
Writing - original draft	80	10	10							100
Writing - review & editing		10	20	20	10	10	5	5	20	100
Resources		10		15	30	30			15	100
Supervision									100	100
Project administration									100	100
Funding acquisition									100	100

Author, PhD Student: Nikolina Pervan

Co-author 1: Umang Desai

Co-author 2: Gabriele C. Eder

Co-author 3: Jonathan Govaerts

Co-author 4: Arne Derluyn

Co-author 5: Wouter Winant

Co-author 6: Antonin Faes

Co-author 7: Christophe Ballif

Co-author 8: Gernot Oreski

Journal of Applied Polymer Science

WILEY

Applied Polymer SCIENCE

RESEARCH ARTICLE OPEN ACCESS

Characterization of Lightweight Polymeric Honeycomb Structures for Use as Backsides in Glass-Free PV Modules

Nikolina Pervan[1,2] | Umang Desai[3] | Gabriele C. Eder[4] | Jonathan Govaerts[5] | Arne Derluyn[6] | Wouter Winant[6] | Antonin Faes[3] | Christophe Ballif[3] | Gernot Oreski[1,2]

[1]Polymer Competence Center Leoben GmbH (PCCL), Leoben, Austria | [2]Montanuniversität Leoben, Leoben, Austria | [3]École Polytechnique Fédérale de Lausanne (EPFL), Lausanne, Switzerland | [4]Österreichisches Forschungsinstitut für Chemie und Technik (OFI), Vienna, Austria | [5]Interuniversity Microelectronics Centre (imec), Genk, Belgium | [6]EconCore N.V, Leuven, Belgium

Correspondence: Nikolina Pervan (nikolina.pervan@unileoben.ac.at; nikolina.pervan@pccl.at) | Gernot Oreski (gernot.oreski@unileoben.ac.at)

Received: 19 May 2025 | **Revised:** 14 August 2025 | **Accepted:** 18 August 2025

Funding: Solar Era Net Project "DELIGHT," co-fund by Austrian Research Promotion Agency (FFG, contract number FO999897443) and Swiss Federal Office of Energy (SFOE, contract number SI/502501-01).

Keywords: aging | backsheets | building applied photovoltaic modules | composites | glass-free | lightweight | material characterization | optical and photovoltaic applications | thermal properties | thermoplastics

ABSTRACT

In densely populated or mountainous countries where installation of large-scale solar plants is challenging, photovoltaic (PV) modules in building applications offer a solution by transforming passive surfaces into energy-generating systems. The need for flexible, lightweight, and "invisible" PV modules, with a life-time of over 20 years, comparable performance to the standard modules, and enabled recyclability resulted in various designs on the market. This research focuses on thermoplastic honeycomb sandwich composites (HSCs) with glass fiber-reinforced polymer skins as potential lightweight backsides for PV modules. Through material characterization and damp heat testing, their optical, mechanical, and thermal performance, compatibility with lamination processes, and ability to protect internal components from UV radiation and humidity were evaluated. Results show that proper glass fiber embedment improves mechanical properties and reduces water vapor transmission rates. Semitransparent skins could enable bifacial PV modules but require UV absorbers for long-term stability. HSCs exhibit glass-like thermomechanical behavior but low thermal conductivity, which could affect module temperature regulation. Damp heat exposure caused minor degradation in PP-based materials, while PET materials experienced polymer chain-scission and significant material embrittlement, which indicates the need for improved hydrolysis resistance.

1 | Introduction

The European Green Deal incentivizes increasing the share of renewable energy in the energy mix by at least 40% by 2030 [1]. With this goal, Europe is setting a path for becoming the first carbon-neutral continent by 2050. Although solar power is one of the highest energy-dense renewable sources, its energy density remains low compared to fossil fuels [2]. As a result, large areas must be covered with photovoltaic (PV) modules to generate sufficient energy and meet carbon neutrality [3]. Countries that are either densely populated or have mountainous terrains, such as the Netherlands, Switzerland, and Austria, face challenges in increasing their share of renewable energy produced by solar power due to limited available land for large-scale PV plants.

Building-integrated and building-attached PV (BIPV and BAPV) installations offer a solution by converting "passive" building areas into active renewable energy sources and CO_2

neutral areas [4]. However, PV module integration is not without obstacles; despite the numerous benefits it offers, it also presents challenges.

Current standard PV modules, which consist of a glass backsheet, encapsulant, solar cells with interconnections, glass frontsheet, junction box, and frame, are not a one-size-fits-all solution. Based on technical data sheets from various PV module producers, these modules can weigh up to 20 kg m^{-2}, and with racking systems potentially up to 40 kg m^{-2}. BIPV modules must comply with both PV and building standards/codes, as they have to fulfill a dual role as a building element and an electrotechnical energy generator, where IEC 63092 combines both aspects [4]. Mechanical stability and fire safety are of utmost importance for both BIPV and BAPV systems [5, 6], and standard 3.2 mm glass/glass PV modules typically pass certification with ease.

However, industrial and commercial buildings, as well as historical or heritage buildings may not be able to bear the structural load of these relatively heavy modules. In addition, the predominantly flat geometry, the lack of flexibility, and the "typical" dark, boxed, and rectangular appearance of standard PV modules often do not meet the aesthetic requirements of modern and historical architecture [7], where the aim is to integrate PV modules seamlessly with the building's design, often concealing them within the structure [4]. This can be achieved by hiding solar cells with colored encapsulant and frontsheet foils [8], by opting for thin film solar cell technology or c-Si cell technology for flexible designs [9].

Growing demand for innovative PV module designs specifically tailored for BIPV and BAPV applications is still on the rise. The need for flexible, lightweight, and "invisible" PV modules has opened doors for creativity in the PV industry [10], emphasizing the importance of ensuring that new designs still achieve a service life exceeding 20 years, maintain the performance of standard modules, prioritize recyclability and circularity while remaining cost-effective [5].

In an effort to reduce the weight of integrated/attached PV modules while maintaining or even enhancing mechanical stability, various "sandwich" composite solutions have been tested and integrated as backsides of PV modules [11–16]. Martins et al. investigated the use of honeycomb composite structures as backsides for PV modules. The lamination of these composite structures was done using EVA, ionomer, and thermoplastic polyolefin (TPO) encapsulants, which served as the adhesion layer between the Nomex or aluminum core and the glass fiber reinforced polymer (GFRP) skins. The honeycomb structures showed good mechanical stability even after undergoing thermal cycling and damp heat (DH) tests. PV modules incorporating these backsides exhibited favorable electrical performance, with a power loss of 2%–3% after undergoing artificial aging tests [12]. Kutter et al. introduced a rigid and torsion-resistant sandwich composite composed of polyurethane foam as the core and GFRP skins, aimed as a backside for lightweight PV modules. Their modules were subjected to artificial aging, and the degradation effect was observed following the DH exposure. This resulted in the embrittlement of the GFRP skin, allowing water ingress that led to corrosion of the interconnections. In contrast, thermal cycling and ultraviolet (UV) weathering had no observable impact on the backsheet [16]. Additionally, Alanis et al. conducted simulations to assess the thermal effects of integrating lightweight PV modules with sandwich composites as backside into the box body of refrigerated cargo trucks, confirming their findings through a mini-PV module experimental setup. Their research indicates that, in addition to providing good mechanical properties, sandwich composite structures can help insulate substrates (such as roofs and walls) to which PV modules are attached from the heat generated by the solar cells [17].

As previously mentioned, reducing weight and costs, along with introducing design flexibility, is a key driving factor in the development of glass-free PV modules. While enabling new designs through versatile backsheets, it is important not to neglect the functional role of the backsheet in PV modules. New designs must still protect the internal components from external factors such as gases, humidity, and UV radiation, while providing mechanical stability and electrical insulation of the active part of the PV module [18–20].

Even though sandwich structures with GFRP skins and aluminum or Nomex core materials fulfill the role of a structural backside [12], the high costs of Nomex and the potential for poor electrical insulation of the aluminum core have motivated the investigation of thermoplastic honeycomb sandwich composite (HSC) as a potential substitute for backside material in lightweight PV modules. In this study, commercially available polymeric HSC, already used in building and automotive industries, have been selected and evaluated for their suitability as backsides for PV modules. During material selection, it was ensured that the composites were free of fluorinated compounds, cost-effective, and potentially recyclable. Material characterization was conducted at the component level in accordance with PV standards, including Series IEC 62788 and IEC Technical Specification and the fire tests described in IEC 61730-2 [4], to assess the general, optical, mechanical, and thermal properties of the materials. The objective of this assessment was to determine whether the composites could be integrated into the standard lamination process for the PV module production, evaluate their effectiveness in protecting internal components from environmental influences, for example, UV, temperature, humidity, and analyze the material state after exposure.

Inadequate or improper testing may result in unsuitable materials entering the market and lead to PV failures, which may cause economic losses as well as adverse environmental and health impacts (release of F-reach gasses in case of PV module burning). Testing protocols are not infallible, as it is difficult to predict every environmental stressor and potential interaction that could influence material performance, aging, and degradation. While long-term outdoor testing can provide definitive information on material performance [21], it is time-consuming. Therefore, indoor artificial aging tests and material characterization [22] can sufficiently define material properties to either approve or disqualify specific materials for PV applications.

TABLE 1 | Composition and dimensional properties of HSC with polypropylene (PP) and recycled polyethylene terephthalate (rPET) cores; glass fiber reinforced (GFR) PP, GFR polyethylene terephthalate glycol (PETg), and biaxially oriented (BO)PET skins.

Sample (core_skin)	Core material	Skin material	Areal weight ($kg\,m^{-2}$)	Thickness sandwich (mm)	Thickness skin (mm)
PP80_PP1	PP	GFR PP	2.30	12.00	0.40
PP120_PP2	PP	GFR PP	2.97	11.80	0.47
PP120_PP3	PP	GFR PP	3.37	12.00	0.55
PET80_PET1	rPET	GFR PETg	2.51	10.30	0.48
PET80_PET2	rPET	BOPET	1.82	10.50	0.25

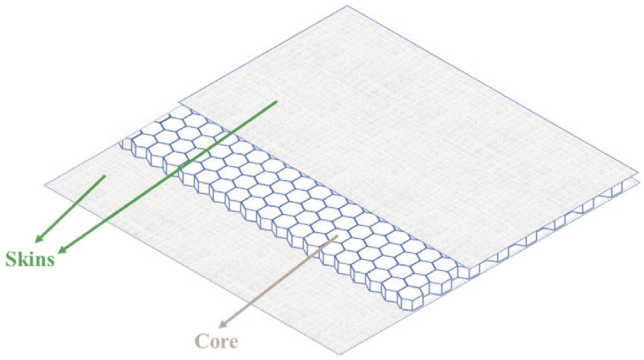

FIGURE 1 | Scheme of a honeycomb sandwich composite structure. [Color figure can be viewed at wileyonlinelibrary.com]

2 | Experimental Section

2.1 | Materials

Five different polymeric HSCs provided by EconCore N.V., Belgium, have been selected as potential PV backsides; details on their composition are given in Table 1, and the structure is shown in Figure 1. The materials were characterized both prior to and post accelerated aging exposure, with all tests conducted in three repetitions to minimize experimental errors.

2.2 | Accelerated Aging

2.2.1 | DH

Series of PV module laminates with PP and PET based HSC as backsides were prepared as described in [23] and exposed to DH conditions of 85°C and 85% humidity for 1000 h, following IEC 61215 MGT 13 [23, 24]. After accelerated aging, samples were taken from both the skin and the core of the HSC for thermal characterization and determination of material durability towards DH conditions.

2.2.2 | Water Condensation

To investigate water condensation within the hollow cell space of the core layer, HSC panels were cut into $10 \times 10\,cm^2$ samples. Aluminum adhesive tape was applied on the edges and rear side of the panels to mimic realistic conditions in a PV module, where the inner side of the backsheet is sealed with the encapsulant and frontsheet, and the edges are sealed with either a frame or an edge seal. The samples were dried at 40°C for 48 h to obtain the initial weight and then placed in a Weiss WLK 64-40 climate chamber. Continuous heating and cooling cycles from 85°C to 5°C and 85% humidity were maintained for 30 days. Samples were kept at 85°C for 18 h and at 5°C for 5 h. The weight of the samples was measured at the end of the cooling cycle. After 30 days, the samples were dried again at 40°C for 48 h and the weight was measured post-drying.

2.3 | Material Characterization

2.3.1 | Microscope Imaging

Light microscopic images of the skin material embedded in epoxy resin were taken with a Light Microscope MAT 7 from Carl Zeiss GmbH, in the bright field mode.

2.3.2 | UV–vis–NIR

Hemispherical transmittance of the independent skins was recorded over the wavelength range between 250 and 2500 nm with a Lambda 950 Ultra Violet-Visible–Near Infrared (UV–vis–NIR) Spectrophotometer (PerkinElmer Inc.).

2.3.3 | Differential Scanning Calorimetry (DSC)

DSC was performed using a DSC 6000 from PerkinElmer Inc. to measure thermograms of each polymeric component material, core and skin, separately. Approximately 10 mg of each material was placed in an aluminum pan with a perforated lid and subjected to a first heating run from −60°C to 300°C, followed by a cooling run from 300°C to −60°C and a second heating run from −60°C to 300°C. The heating rates were set to $10\,K\,min^{-1}$ and a nitrogen flow of $50\,mL\,min^{-1}$ was imposed.

2.3.4 | Heat Conductivity

The heat flow through the HSC samples was measured using a Guarder Heat Flow (GHF) Meter DTC-300 from TA Instruments (thermal conductivity tester). For this purpose,

the samples were cut into round specimens with a diameter of ∅50 mm. The sample was placed between an upper "hot" and a lower "cold" plate. The upper plate is heated to a temperature 15°C higher, and the lower plate is cooled to a temperature 15°C lower than the temperature at which material's heat conductivity is to be determined. Heat flows through the sample from the hot to the cold plate until thermal equilibrium is reached. The heat conductivity is calculated using Fourier's law:

$$\lambda = \frac{\dot{Q}\, d}{A \Delta T} \tag{1}$$

where Q is the heat flow throughout the specimen in W, d is the thickness in m, A is the area in m^2, and ΔT is the temperature difference across the sample in K [25].

2.3.5 | Coefficient of Thermal Expansion (CTE)

The CTE was measured using a Dantec Q400 TCT (Dantec Dynamics) Digital Image Correlation (DIC) system. The device consists of two cameras and a heating/cooling concealed chamber equipped with a thermal plate. Time series of images of the measured sample are taken during the thermal stages, which are then compared to the initial picture. During analysis, the evaluation software Istra 4D (Dantec Dynamics) calculates the relative displacement between the reference and each image of the acquired time series. Sample preparation is important as the software follows a speckle pattern that is applied on the surface of the rectangular sample of $3 \times 3\,cm^2$. The speckle pattern was applied on the skin of the HSC in two layers; the first white coating serves as a primer and substrate cover and is followed by a second layer that is a black coating which is creating the speckle pattern. Achieving good contrast and independent speckles is necessary to guarantee a measurable surface area. The CTE of the honeycomb composites was measured in the temperature range from −50°C to 120°C, with a heating rate of $2\,K\,min^{-1}$.

2.3.6 | Thermogravimetric Analysis (TGA)

TGA was done using a Thermogravimetric System TGA/DSC 1 of Mettler Toledo GmbH. The weight loss of approximately 10 mg of material was monitored while heating the sample in nitrogen atmosphere ($50\,mL\,min^{-1}$) from 35°C to 700°C, with a heating rate of $10°C\,min^{-1}$. The temperature at which the weight loss is equal to 5% with respect to the initial value ($=T_{5\%}$) is considered an indicator for the beginning of the material's decomposition process.

2.3.7 | Mechanical Properties

Zwick Universal Testing Machine (Z020) was used, with a load cell of 1 kN capacity, to perform 4-point bending tests at room temperature on the HSC samples to compare the mode of failure and the flexural rigidity. The tests were performed on the samples of 220 mm length and 25 mm width with a $20\,\mu m\,s^{-1}$ loading rate, 190 mm outer span length, and 90 mm inner span length, in the transversal direction to the core cells, as described in [26].

3 | Results and Discussion

Optimal qualification of the HSCs as a suitable "backsheet" option for PV modules can be achieved by comparing its properties to those of the most commonly used polymer composite backsheet Tedlar-PET-Tedlar (TPT) and the glass backsheet. Summary of all results is presented in Table 2.

3.1 | Physical Properties

The quality of embedment of the glass fibers (GFs) within the skin-sheets was investigated first, as the importance of proper impregnation of GFs within the polymer matrix and its influence on material properties, such as mechanical strength, water vapor, and gas permeation, has been emphasized multiple times in the literature [29, 34–36]. Common processing defects within GFRPs include voids in the form of entrapped air bubbles, insufficient wetting of the GFs with polymer, cracking of the polymer matrix in areas with fiber bundles, and delamination of the layer stack [36] Such defects might negatively impact the mechanical strength and increase the permeation of humidity, oxygen, or other gases in the skins of the HSCs under study. Thus, the water vapor transmission rate (WVTR) of all skin materials was measured and compared to standard PV backsheet materials [36] as it is known to be critical when selecting components for PV modules. Ingress of humidity into the module can lead to degradation of internal components including delamination, yellowing, and hazing of encapsulants, power loss in solar cells, corrosion of interconnection, and ultimately, PV module failure [37–40].

Microscopic images of the cross-sections of the GFR PP skins PP1–PP3 and the PET1 skin are shown in Figure 2. Differences in the GF distribution, for example, formation of fiber bundles, voids, and microcracks in the matrix of the skins are visible. The increase in thickness from PP1 to PP3 is due to the higher content of both GFs and the polymer matrix. With the increase in the amount of polymer in the composite, a decrease in WVTR is expected. The WVTR of these HSC skins was measured by Babin et al. [34]; the results confirm that lower WVTRs were observed for GFRP sheets with a thicker outer polymer layer covering the GFs (Sample PP3), see Figure 3. In contrast, higher WVTRs were measured for samples where the GFs were poorly covered with a thin polymer layer (Sample PP1). The type of polymer matrix also affects the WVTR of GFRP. This becomes evident when comparing the WVTRs of the skin sheets with the PET polymer matrix (Sample PET1, value WVTR) and that with the PP polymer matrix (Sample PP2, value WVTR), despite the samples having the same thickness and GF distribution (see Table 1 and Figure 4) [29]. In addition to increasing the thickness of the outer polymer layer and providing better coverage/embedment of the GFs, a gel coat can be applied to the outer GFRP skin layer to further decrease the water vapor permeability, enhance UV resistance, and, in special formulation, increase fire resistance [41–43].

The light transmittance of PV module backsides, for example, blocking of UV light is particularly important, as it can lead to degradation of internal components, thereby reducing the efficiency and lifetime performance of PV modules [18]. On the

TABLE 2 | Summary of the PP and PET HSC, TPT, and glass backsheet properties, including the effect which HSC could bring onto the PV module.

Property	Backsheet[a]	Glass	PP HSC	PET HSC	Effect of the HSC as a backsheet to the PV module
Thickness (mm)	0.2–0.4 [20]	3.2	11.8–12	10.3–10.5	Thicker PV module—need for new frame design.
Areal weight ($kg\,m^{-2}$)	~0.5[b] [27]	8 [28]	2.3–3.4	1.8–2.5	Significant reduction of weight compared to glass backsheet.
Mechanical strength	weak	strong	GFR skin dependent	Brittle	Replacement of the glass frontsheet as well as the removal of the aluminum frame feasible for PP based HSC.
WVTR ($g\,day^{-1}\,m^{-2}$)	< 1 [20]	$<10^{-6}$	2–8 [29]	0.7–1.2 [29]	WVTR are high and could lead to degradation of the inner components (corrosion, solar cell degradation, encapsulant degradation—delamination).
UV transmission (250–380 nm)	Cut off	90%	< 40%	Cut off at 310 nm	UV absorbers must be added in the polymer matrix to protect backsheet and inner components from photooxidation.
Degradation onset T ($T_{5\%}$—°C)	> 380[c]	—	> 430	> 400	Some backsheets have fire-retardant properties in comparison to the pure PP and PET, on the other hand they can generate toxic gas and toxic residues [30].
Melting temperature (°C)	195 [31]	—	145–175	> 230	PP HSC unsuitable for standard lamination process at 160°C, suitable for noncrosslinking encapsulants such as TPO.
CTE at 25°C (ppm)	> 30[d]	7[c]	6–12[d]	10–17[d]	Similar to the glass, should not result in delamination.
Heat conductivity ($W\,m^{-1}\,K^{-1}$)	0.15 [32]	1 [33]	~0.15	~0.15	Benefit: insulation towards the building Challenge: Potential slower cooling of the PV module—decrease in efficiency.
Accelerated aging	Weak impact	No impact	Material dependent	Material dependent	Chain scission in PET material led to material embrittlement—antihydrolysis additive for polymer matrix necessary.

[a]Standard laminated backsheet with PET core layer.
[b]Calculated from density for 0.34 mm thickness.
[c]Measured at PCCL.
[d]T dependent.

contrary, the transmittance of UV and visible light through the backsheets is beneficial for the yield of bifacial PV modules, as light can be absorbed by the rear side of the cells, converted into electricity, and increase power generation.

PP2, a dark black skin with unspecified additives (most likely carbon black), effectively blocks both visible and UV light. In contrast, PP1, PP3, PET1, and PET2 are semitransparent skins, with visible light transmittance ranging from 38% to 88% (see Figure 4), offering potential for bifacial PV modules. The disadvantage of these semitransparent skins, however, is that the transmitted UV radiation can cause photo-oxidative degradation of the HSC skins and the core. To block or minimize UV transmission, these materials would need to be adapted or supported with additional layers. This can be achieved through the addition of UV absorbers to the polymer

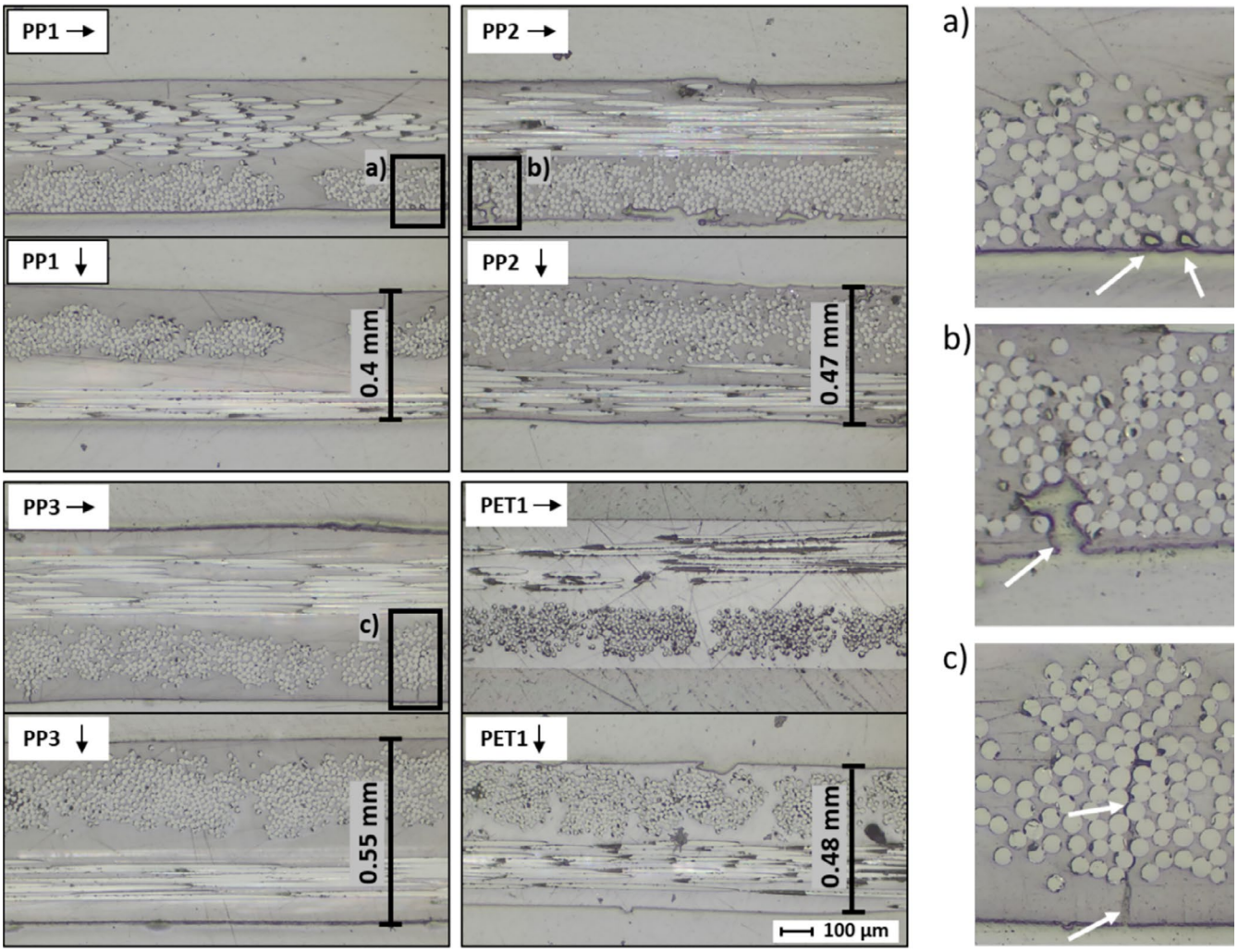

FIGURE 2 | Microscope images of the GFR honeycomb skin cross-sections and polymer matrix defects (a) small air bubble entrapment, (b) large air bubble entrapment, and (c) crack due to the fiber bundle. [Color figure can be viewed at wileyonlinelibrary.com]

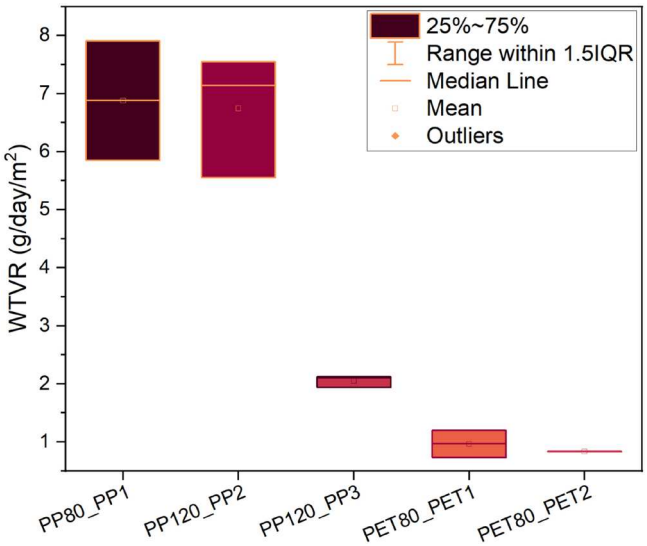

FIGURE 3 | WVTR of HSC skins (recalculated from [29] for the exact thickness of material, instead of WVTR values per 100 µm). [Color figure can be viewed at wileyonlinelibrary.com]

matrix or by applying an external UV-blocking coating to the outer skin layer in combination with a UV-blocking encapsulant on the cell backside.

3.2 | Thermal Properties

Thermal properties of polymer materials are of great significance when designing PV modules. First, during the lamination process of PV module production, which occurs at high temperatures (~150°C) and vacuum pressure (up to 1 bar), all components, besides encapsulating material, must remain dimensionally intact (minimal shrinkage, compression, deformation). Second, throughout the lifetime of a PV module, it will undergo thermal fluctuations (day—night and summer—winter).

The glass transition/softening (T_g) and melting (T_m) temperatures of the HSC components are of special interest to determine the optimal PV module lamination temperatures to avoid structural and dimensional changes of the backsheet material. The first heating thermograms (see Figure 5) show

the thermal behavior of the material before it undergoes the lamination process. The PP HSC components melt in the range from 145°C to 175°C, while the PET core and PET2 skin components have T_m above 230°C. PET1 skin is an amorphous polymer; therefore, it does not melt but only softens at elevated temperatures (T_g above 75°C). Considering the standard lamination conditions developed for the production of glass-based PV modules with EVA encapsulants and polymeric backsheets, the melting temperatures of PP are relatively low. Hence, PP HSC would require an adaptation of the lamination temperature and the careful selection of encapsulants that can be processed at temperatures below 140°C, such as TPOs. However, PET HSC have none or high melting temperatures and should be compatible with commonly used encapsulants, like EVA and crosslinking polyolefins (POEs) or combinations thereof (EPE).

Results of the heat conductivity (λ) measurements show that HSCs are insulating materials, with values below 0.2 $W m^{-1} K^{-1}$ for all material combinations investigated, as shown in Figure 6.

Furthermore, HSCs exhibit λ values up to five times lower than glass ($\lambda = 1 W m^{-1} K^{-1}$) [44]. As c-Si solar cells convert only a portion (~20%–23%) of the absorbed light into electricity and the rest into heat, thermally conductive materials surrounding solar cells are preferred to enhance heat dissipation. Low heat conductivity of insulating materials leads to increased operational temperatures of the PV module, negatively impacting the efficiency of solar cells, as well as the reliability and durability of both the module and its components, especially polymers [4, 45]. Research by Özkalay et al. [46] determined the maximum operating temperatures (T_{max}) for identical modules in open-rack and BIPV systems and evaluated their impact on module efficiency and long-term performance. T_{max} measured for open-rack PV modules in both glass/glass and glass/backsheet configurations was approximately 60°C during the operational hours. In contrast, ventilated and insulated BIPV modules exhibited higher T_{max}, slightly above 80°C and 90°C, respectively [46].

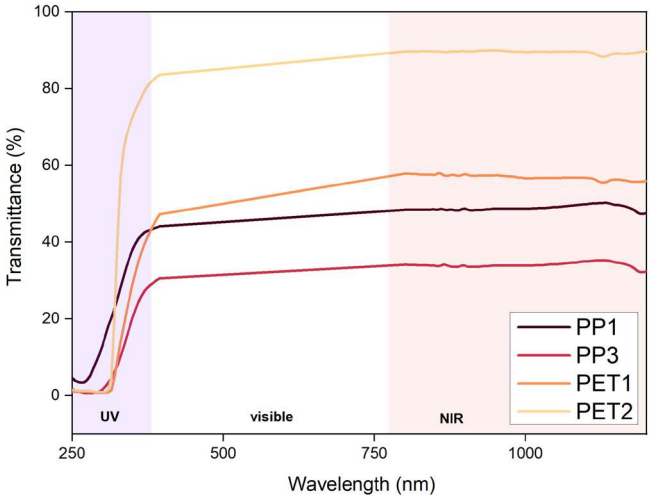

FIGURE 4 | UV—vis—NIR spectra of honeycomb skins. [Color figure can be viewed at wileyonlinelibrary.com]

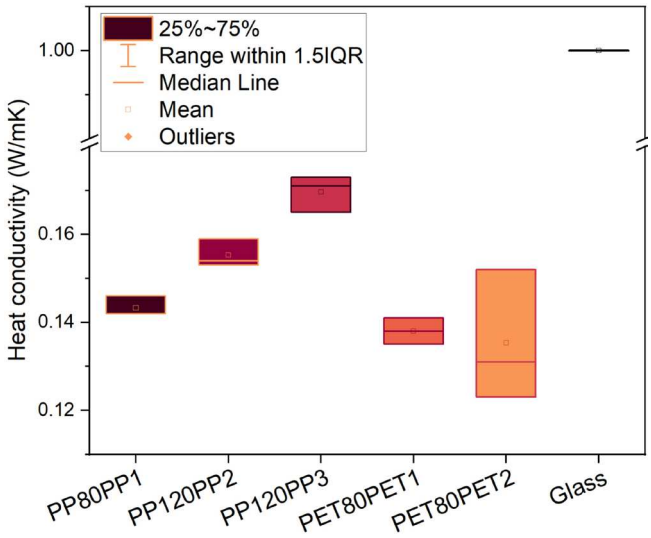

FIGURE 6 | Heat conductivity of the honeycomb sandwich composites and glass. [Color figure can be viewed at wileyonlinelibrary.com]

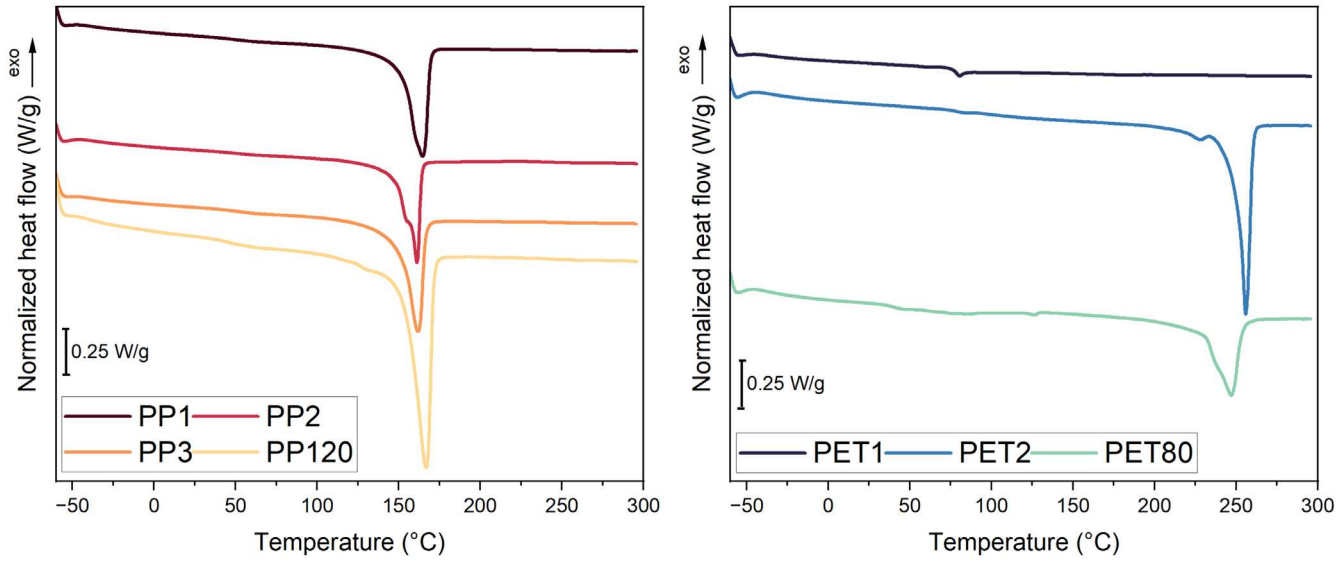

FIGURE 5 | DSC first heating curves of honeycomb components. [Color figure can be viewed at wileyonlinelibrary.com]

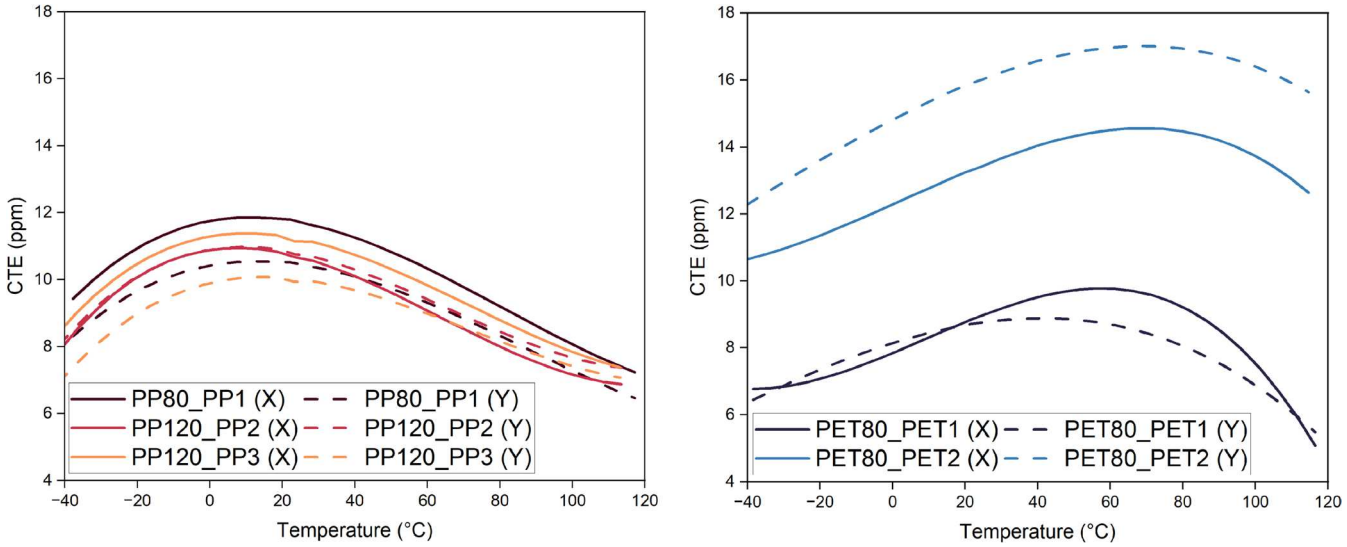

FIGURE 7 | CTE graphs of honeycomb skins (left side PP- and right side PET-based HSC). [Color figure can be viewed at wileyonlinelibrary.com]

Based on these data, similar behavior could be expected when HSCs are integrated as the backsides in lightweight PV modules. Additionally, a challenge can arise during the lamination process as heat conduction and distribution within the PV module can take longer, unless the lamination process is performed by placing the front side of the module on the hot plate. On the positive side, this reduced heat conductivity could provide a benefit in terms of thermal insulation for the building interior to which these PV modules are attached, such as façades or roofing elements [47].

In addition to differences in T_{max} of the modules installed in the open-rack and BIPV configuration, significant day–night temperature variations exceeding 75°C for insulated BIPV modules were measured [46]. These daily temperature fluctuations impact the thermomechanical material behavior of the materials within the module stack, and an inherent mismatch in the CTE between the individual material layers can create internal stresses resulting in interlayer delamination, failures of solder joints, and solar cell cracking [4, 48]. Therefore, careful consideration of the bill of materials (BoM) is essential when selecting components for lightweight PV modules.

The dimensional stability and mechanical behavior of the HSC materials at different temperatures, in terms of CTE, are presented in Figure 7. The HSC skins PP1, PP2, PP3, and PET1 with GFR exhibit comparable behavior in the *x*- and *y*-directions due to the presence of the GFs in 0°–90° ply orientation. These materials show numerical CTE values between 6 and 12 ppm within the temperature range from −40°C to 120°C. The PET2 skin, a biaxially oriented PET material, shows slightly higher CTE values, 10–17 ppm, in the same temperature range, but with a somewhat greater anisotropy in the *x*- and *y*-directions compared to the GFR skins. All HSC skins investigated exhibit low anisotropy and lower CTE values than those of commonly used commercial polymer backsheets (e.g., TPT, coated PET [CPC], coextruded PP, triple polyamide [AAA]) [49, 50]. Additionally, CTE values of GFR HSCs can be compared to those of glass reported in the literature [51] and measured in-house (see Table 2). Given this similar thermomechanical behavior, GFR HSCs are expected to exhibit comparable performance to glass when integrated as a backsheet in a PV module.

3.3 | Mechanical Properties

Upon visual observation, HSC are a thicker product (10.3–12 mm, see Table 1), particularly when compared to standard polymeric backsheets (0.5 mm) or glass backsheets (3.2 mm). On the other hand, the honeycomb-metamaterial core significantly reduces the weight of the composite while enhancing its mechanical strength. When HSC (areal density = 1.82 kg m^{-2}) are implemented as backsheets, the need for a solar glass frontsheet (areal density = 8 kg m^{-2} [52]) can be eliminated, resulting in a reduction of the PV module's weight by up to a factor of four [26].

Load vs. displacement diagrams of the four-point bending tests are shown in Figure 8. The PP80_PP1 HSC was excluded from the test due to the high WVTR and thin wall of the core's cell. The PET-based HSC failed under the compression stress upon reaching its maximum load carrying capacity. On the other hand, the PP-based HSC yielded above the maximum carrying load. This behavior could be due to the fact that at room temperature PET remains in a glassy state (T_g = 80°C, Figure 5), which can restrict the mobility of the chains; hence, resulting in a brittle-like failure. When comparing the mechanical behavior of the PP-based HSC, PP120_PP3 shows greater stiffness (as indicated by the steeper slope in the load-line displacement diagram in the elastic region) and greater load carrying capacity compared to PP120_PP2. This could be connected with the better embedment of the GF in the polymer matrix in PP3 skin when compared to PP2 (see Figure 2).

3.4 | Accelerated Aging Influence on Properties

The longevity of the electricity generation of PV modules is directly linked to the performance of the envelope materials. To ensure a long lifetime, reliability, and maintained efficiency of PV modules, the durability of the materials used in the PV modules needs to be characterized. Material behavior/degradation is best understood

through outdoor testing; this is time-consuming, in particular considering targeted lifetimes of 25 years and beyond. Therefore, indoor artificial aging tests and material characterization methods are typically used to determine reliability and material properties post aging. In this study, a DH test was performed according to IEC 61215, and DSC and TGA characterization methods were done to characterize material state and changes that occurred during the exposure period. Additionally, to investigate water condensation within the hollow cell space of the core layer, HSC were placed in the climate chamber under continuous heating and cooling cycles (from 85°C to 5°C, with 85% humidity) for 30 days.

Upon the accelerated aging, yellowing of the PP HSC was observed, similar to the observation by other studies [5]. Thermal aging affects the stability of additives in the PP matrix, which then change color; however, the effect is reversible after photobleaching [53]. The cooling thermograms from DSC for PP core and PP3 skin material in Figure 9 show no significant changes in the crystallization temperature (T_c), meaning that DH aging left no apparent impact on the polymer matrix. This was similarly observed for commercially available PP backsheets [28, 53–54]. However, a shift to higher T_c values was observed for the PP2 skin, rPET core, and PET2 skin, from 118°C to 124°C, 206°C to 218°C, and 176°C to 186°C, respectively. This shift, indicating an earlier onset of crystallization, occurs due to the chain scission in both PP and PET polymer [55, 56]. This phenomenon has already been reported by Oreski et al., where the authors determined that critical crystallization temperatures between 208°C and 211°C correspond to a reduction in molar mass and severe embrittlement of PET [56]. Lamentably, DH aging resulted in a shift of T_c above the critical values for rPET, and consequently in the loss of mechanical properties, making the rPET core prone to cracking and structural failure under an external mechanical load. Anti-hydrolysis additives can be added to the PET polymer matrix to mitigate the chain-scission process and ensure mechanical strength [57].

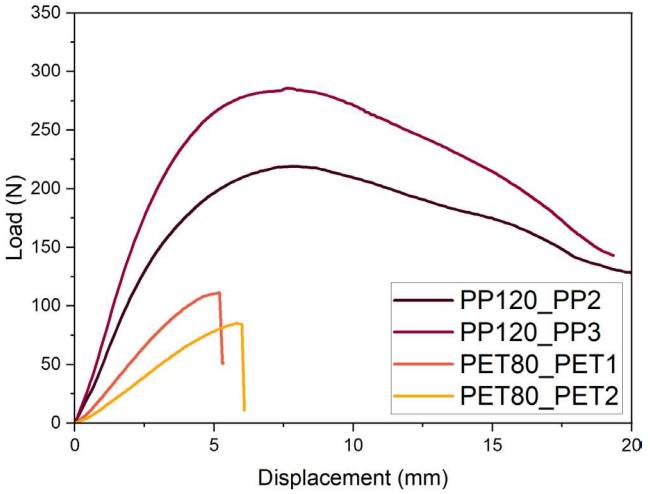

FIGURE 8 | Load versus displacement diagram of PP and PET based HSC under flexural loading. [Color figure can be viewed at wileyonlinelibrary.com]

Aging under the DH conditions also resulted in the earlier material decomposition of both PP and rPET core materials, evident for both materials in Figure 10. The change in the onset decomposition temperature marked by the temperature at which 5% of weight loss ($T_{5\%}$) occurs is more pronounced for the rPET core, where the $T_{5\%}$ shifted from 394°C before aging to 385°C after aging. In contrast, for the PP material, $T_{5\%}$ shifted from 430°C to 428°C after aging. Of all skin materials, only PP2 skin showed earlier decomposition onset, which shifted by 5°C compared to the unaged sample. The polymer chain scission created smaller molecules that are decomposing into volatile products faster; therefore, $T_{5\%}$ shifted toward the lower temperatures.

The water condensation test resulted in a weight gain of less than 0.2 wt% for all HSC samples. Since no established standard could be found for it, an in-house created test procedure was followed. The relatively low weight gain of these materials may be attributed to the "breathability" of the composite's outer skins, which allow moisture vapor transmission and thus prevent water condensation within the closed hexagonal cells of the core. Alternatively, it

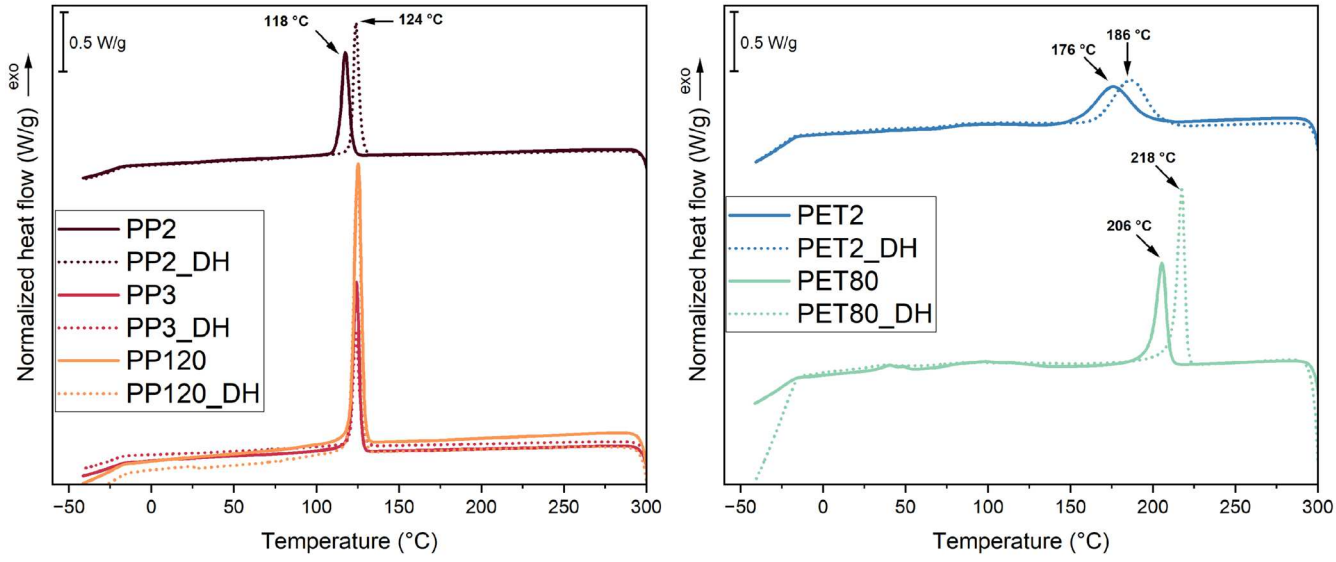

FIGURE 9 | DSC cooling curves of unaged and aged PP and PET. [Color figure can be viewed at wileyonlinelibrary.com]

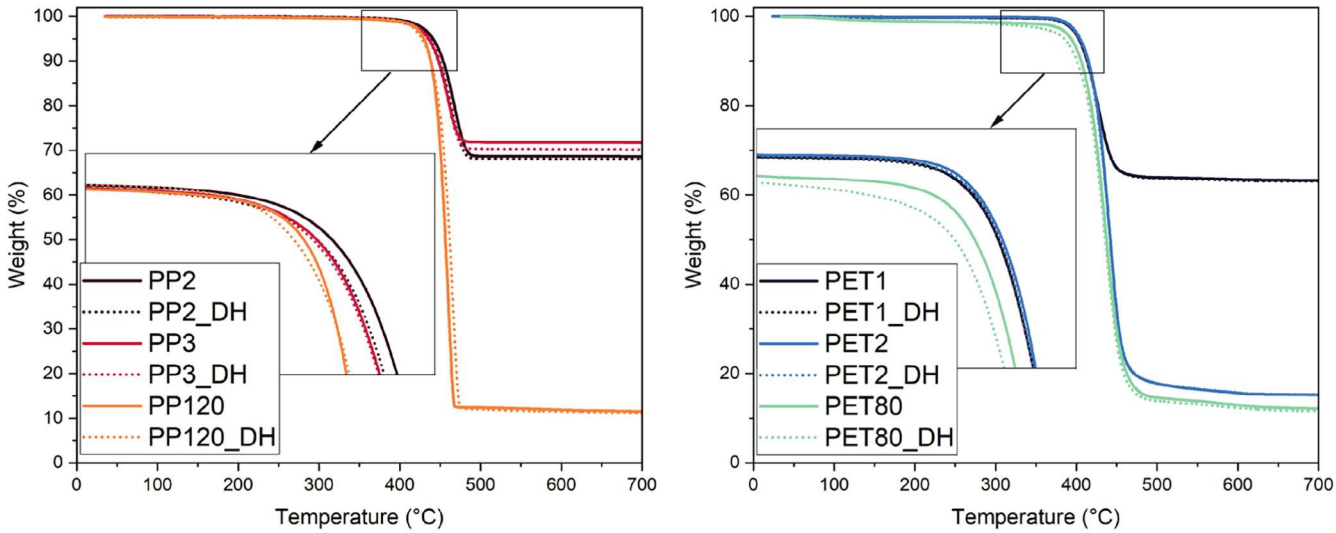

FIGURE 10 | TGA curves of core material before and after aging. [Color figure can be viewed at wileyonlinelibrary.com]

is possible that the test procedure itself needs further adaptation to create better conditions for water condensation. Nevertheless, it can be concluded that no significant weight gain is expected for BAPV and BIPV modules with HSC backsheets under the heating and cooling conditions typically encountered during outdoor exposure. This property brings a positive impact, as water will not accumulate in the hollow areas and impact overall weight, material durability, and mold growth [4].

4 | Conclusions

The selected, commercially available PP and PET HSC, already used in building and automotive industries, proved to be promising materials for the backside integration into the lightweight PV modules. Results have shown that proper GF embedment within the polymer matrix, in the GFRP skin material, improves the mechanical properties of entire sandwich composites and reduces WVTRs. Semitransparent skins with transmission in the NIR and visible light spectra could enable bifacial PV modules but require the addition of the UV absorbers to ensure long-term stability of HSC components and of the internal module components (encapsulants and solar cells). HSCs exhibit glass-like thermomechanical behavior but low thermal conductivity, which could affect module temperature regulation and negatively impact efficiency. DH exposure caused minor degradation in PP-based materials, which resulted in yellowing, while PET materials experienced more prominent polymer chain scission and significant material embrittlement, which indicates the need for improved hydrolysis resistance. Further investigation is required to assess mechanical reliability. Replacing the glass front-sheet and removing the aluminum frame are considered feasible, though evaluation is still ongoing.

Author Contributions

Nikolina Pervan: conceptualization (equal), data curation (lead), formal analysis (lead), investigation (lead), methodology (equal), visualization (lead), writing – original draft (lead). **Umang Desai:** conceptualization (equal), data curation (supporting), formal analysis (supporting), investigation (supporting), methodology (supporting), visualization (supporting), writing – original draft (supporting). **Gabriele C. Eder:** conceptualization (equal), writing – review and editing (equal). **Jonathan Govaerts:** conceptualization (equal), writing – review and editing (equal). **Arne Derluyn:** resources (equal). **Wouter Winant:** resources (equal), writing – review and editing (equal). **Antonin Faes:** writing – review and editing (supporting). **Christophe Ballif:** writing – review and editing (supporting). **Gernot Oreski:** conceptualization (equal), funding acquisition (lead), project administration (lead), resources (equal), supervision (lead), writing – review and editing (lead).

Acknowledgments

The research work of this paper was performed at the Polymer Competence Center Leoben GmbH (PCCL, Austria) as part of the Solar Era Net Project "DELIGHT," which is supported under the umbrella of SOLAR-ERA.NET co-fund by the Austrian Research Promotion Agency (FFG, contract number FO999897443) and the Swiss Federal Office of Energy (SFOE, contract number SI/502501-01). SOLAR-ERA.NET is supported by the European Commission within the EU Framework Programme for Research and Innovation HORIZON 2020 (co-fund ERA-NET Action, No. 691664). N/A

Conflicts of Interest

The authors declare no conflicts of interest.

Data Availability Statement

The data that support the findings of this study are available on request from the corresponding author. The data are not publicly available due to privacy or ethical restrictions.

References

1. The European Parliament and the Council of the European Union, "Directive (EU) 2023/2413 of the European Parliament and of the Council of 18 October 2023 Amending Directive (EU) 2018/2001, Regulation (EU) 2018/1999 and Directive 98/70/EC as Regards THE Promotion of Energy From Renewable Sources, and Repealing Council Directive (EU) 2015/652," *Official Journal of the European Union* L series (2023).

2. J. K. Nøland, J. Auxepaules, A. Rousset, B. Perney, and G. Falleti, "Spatial Energy Density of Large-Scale Electricity Generation From Power Sources Worldwide," *Scientific Reports* 12 (2022): 21280.

3. M. Deshaies, "Problèmes géographiques des transitions énergétiques quelles perspectives pour l'évolution du système énergétique ?," *Mondes En Développement* 192 (2020): 25–44.

4. N. M. Chivelet, C. Kapsis, and F. Frontini, *Building-Integrated Photovoltaics: A Technical Guidebook*, 1st ed. (Routledge, 2024).

5. G. Oreski, J. S. Stein, G. C. Eder, et al., "Motivation, Benefits, and Challenges for New Photovoltaic Material & Module Developments," *Progress in Energy* 4 (2022): 32003, https://doi.org/10.1088/2516-1083/ac6f3f.

6. IEA PVPS, "Fire Safety of BIPV: International Mapping of Accredited and R&D Facilities in the Context of Codes and Standards 2023," Report (IEA PVPS, 2023).

7. National Heritage Institute, *Photovoltaic Systems in Heritage Protection* (National Heritage Institute, 2022).

8. G. Eder, G. Peharz, R. Trattnig, et al., "COLOURED BIPV—Market, Research and Development," 2019 Report IEA-PVPS T15-07: 2019 (IEA-PVPS, 2019).

9. N. Pervan, S. Feldbacher, M. Harnisch, T. Tettenborn, A. Zimmermann, and G. Oreski, eds., *Ultra-Thin Flexible Glass as Environmental Shield for CIGS Photovoltaic Modules*, EU PVSEC 2024, ISBN 3-936338-90-6, 2024.

10. IEA PVPS, *Successful Building Integration of Photovoltaics—A Collection of International Projects* (IEA PVPS, 2021).

11. A. C. Martins, V. Chapuis, F. Sculati-Meillaud, A. Virtuani, and C. Ballif, "Light and Durable: Composite Structures for Building-Integrated Photovoltaic Modules," *Progress in Photovoltaics: Research and Applications* 26 (2018): 718–729, https://doi.org/10.1002/pip.3009.

12. A. C. Oliveira Martins, V. Chapuis, A. Virtuani, L.-E. Perret-Aebi, and C. Ballif, "Hail Resistance of Composite-Based Glass-Free Lightweight Modules for Building Integrated Photovoltaics Applications," in *Proceedings of the 33rd European Photovoltaic Solar Energy Conference and Exhibition* (EPFL, 2017), 2604–2608.

13. A. C. Martins, V. Chapuis, A. Virtuani, and C. Ballif, "Robust Glass-Free Lightweight Photovoltaic Modules With Improved Resistance to Mechanical Loads and Impact," *IEEE Journal of Photovoltaics* 9 (2019): 245–251, https://doi.org/10.1109/JPHOTOV.2018.2876934.

14. A. C. Martins, V. Chapuis, A. Virtuani, H.-Y. Li, L.-E. Perret-Aebi, and C. Ballif, "Thermo-Mechanical Stability of Lightweight Glass-Free Photovoltaic Modules Based on a Composite Substrate," *Solar Energy Materials & Solar Cells* 187 (2018): 82–90, https://doi.org/10.1016/j.solmat.2018.07.015.

15. P. Grygiel, J. Tarłowski, M. Prześniak-Welenc, et al., "Prototype Design and Development of Low-Load-Roof Photovoltaic Modules for Applications in On-Grid Systems: Solar Energy Materials and Solar Cells," *Solar Energy Materials and Solar Cells* 233 (2021): 111384.

16. C. Kutter, F. Basler, L. E. Alanis, J. Markert, M. Heinrich, and D. H. Neuhaus, eds., "Integrated Lightweight, Glass-Free PV Module Technology for Box Bodies of Commercial Trucks," in *37th European Photovoltaic Solar Energy Conference and Exhibition, EU PVSEC 2020* (Fraunhofer-Gesellschaft, 2020), 1711–1718.

17. L. E. Alanis, A. Velte-Schäfer, N. Jajoo, et al., "Thermal Effect of VIPV Modules in Refrigerated Trucks," *Solar Energy Materials and Solar Cells* 275 (2024): 113000.

18. A. Omazic, G. Oreski, M. Halwachs, et al., "Relation Between Degradation of Polymeric Components in Crystalline Silicon PV Module and Climatic Conditions: A Literature Review," *Solar Energy Materials & Solar Cells* 192 (2019): 123–133, https://doi.org/10.1016/j.solmat.2018.12.027.

19. G. Oreski, C. Barretta, L. Castillon, P. Christöfl, and M. Köntges, "Importance of Bill of Material (BOM) Control and IEC 61215 Scope of Application," in *37th European Photovoltaic Solar Energy Conference and Exhibition* (EU PVSEC, 2020).

20. G. Oreski, A. Mihaljevic, Y. Voronko, and G. C. Eder, "Acetic Acid Permeation Through Photovoltaic Backsheets: Influence of the Composition on the Permeation Rate," *Polymer Testing* 60 (2017): 374–380, https://doi.org/10.1016/j.polymertesting.2017.04.025.

21. DuPont Photovoltaic Solutions, *DuPont Global PV Reliability: 2020 Field Analysis* (DuPont Photovoltaic Solutions, 2020).

22. S. Uličná, R. L. Arnold, J. M. Newkirk, et al., "Material Characterization of Seven Photovoltaic Backsheets Using Seven Accelerated Test Conditions," *Solar Energy Materials and Solar Cells* 267 (2024): 112726.

23. J. Govaerts, P. Dufke, B. Luo, et al., eds., "Light as Heaven, Strong as Hell(?): Testing Honeycomb-Based Laminates for Light-Weight c-Si PV Applications," in *Proceedings of the 40th European Photovoltaic Solar Energy Conference and Exhibition* (EU PVSEC, 2023).

24. IEC, "IEC 61215-1:2021, Terrestrial Photovoltaic (PV) Modules—Design Qualification and Type Approval—Part 1: Test Requirements," 2021.

25. ASTM International, "Standard Test Method for Evaluating the Resistance to Thermal Transmission of Materials by Guarded Heat Flow Meter Technique," 2019.

26. U. Desai, M. Courtant, G. Eder, G. Oreski, A. Faes, and C. Ballif, "Novel Mechanically Robust and Environmentally Stable Light-Weight Colored Photovoltaic Modules Based on Composite Polymer Backsheets," *Solar RRL* 9 (2025): 2500177.

27. DuPont, "DuPont Tedlar Polyvinyl Fluoride (PVF) Films," 2014, https://www.dupont.com/content/dam/dupont/amer/us/en/photovoltaic/public/documents/DEC_Tedlar_GeneralProperties1.pdf.

28. A. Omazic, G. Oreski, M. Edler, et al., "Increased Reliability of Modified Polyolefin Backsheet Over Commonly Used Polyester Backsheets for Crystalline PV Modules," *Journal of Applied Polymer Science* 137 (2020): 48899, https://doi.org/10.1002/app.48899.

29. M. Babin, G. C. Eder, Y. Voronko, and G. Oreski, "Water Vapor Permeability of Polymeric Packaging Materials for Novel Glass-Free Photovoltaic Applications," *Journal of Applied Polymer Science* 141 (2024): e55733, https://doi.org/10.1002/app.55733.

30. Fraunhofer UMSICHT, "End-of-Life Pathways for Photovoltaic Backsheets: End-of-Life Treatment—Experiments, Germany," Report (Fraunhofer UMSICHT, 2017).

31. M. Knausz, G. Oreski, G. C. Eder, et al., "Degradation of Photovoltaic Backsheets: Comparison of the Aging Induced Changes on Module and Component Level," *Journal of Applied Polymer Science* 132 (2015): 1–8, https://doi.org/10.1002/app.42093.

32. J. Zhou, Z. Zhang, H. Liu, and Q. Yi, "Temperature Distribution and Back Sheet Role of Polycrystalline Silicon Photovoltaic Modules," *Applied Thermal Engineering* 111 (2017): 1296–1303.

33. B. Luo, J. Govaerts, F. Lisco, et al., "Encapsulation Strategies for Mechanical Impact and Damp Heat Reliability Improvement of Lightweight Photovoltaic Modules Towards Vehicle-Integrated Applications," *Solar Energy Materials and Solar Cells* 273 (2024): 112932.

34. C. Tselios, D. Bikiaris, P. Savidis, C. Panayiotou, and A. Larena, "Glass-Fiber Reinforcement of In Situ Compatibilized Polypropylene/Polyethylene Blends," *Journal of Materials Science* 34 (1999): 385–394.

35. A. Baker, S. Dutton, and D. Kelly, *Composite Materials for Aircraft Structures* (American Institute of Aeronautics and Astronautics, 2004).

36. Y. Fu and X. Yao, "A Review on Manufacturing Defects and Their Detection of Fiber Reinforced Resin Matrix Composites," *Composites Part C: Open Access* 8 (2022): 100276.

37. O. K. Segbefia, A. G. Imenes, and T. O. Sætre, "Moisture Ingress in Photovoltaic Modules: A Review," *Solar Energy* 224 (2021): 889–906.

38. H. E. Yang, R. H. French, and L. S. Bruckman, eds., *Durability and Reliability of Polymers and Other Materials in Photovoltaic Modules* (William Andrew Publishing, 2019).

39. Y. Voronko, G. C. Eder, M. Knausz, G. Oreski, T. Koch, and K. A. Berger, "Correlation of the Loss in Photovoltaic Module Performance With the Ageing Behaviour of the Backsheets Used," *Progress in Photovoltaics Research and Applications* 23 (2015): 1501–1515, https://doi.org/10.1002/pip.2580.

40. S. Uličná, A. Sinha, D. C. Miller, B. M. Habersberger, L. T. Schelhas, and M. Owen-Bellini, "PV Encapsulant Formulations and Stress Test Conditions Influence Dominant Degradation Mechanisms," *Solar Energy Materials & Solar Cells* 255 (2023): 112319, https://doi.org/10.1016/j.solmat.2023.112319.

41. J. Smoleń, K. Bechcińska, W. Smok, P. Olesik, and K. Stępień, "Assessment of the Effectiveness of Selected Coatings for Protection Against UV Radiation in Glass Fiber Reinforced Composites (GFRP)," *Composites Theory and Practice* 24 (2024): 65–71.

42. G. Demircan, M. Kisa, M. Ozen, A. Acikgoz, Y. Işıker, and E. Aytar, "Nano-Gelcoat Application of Glass Fiber Reinforced Polymer Composites for Marine Application: Structural, Mechanical, and Thermal Analysis," *Marine Pollution Bulletin* 194 (2023): 115412.

43. R. E. Fyfe, "Fire Protection Coating for FRP-Reinforced Structure", Patent "US20090075051A1," 2009.

44. Schott AG, "TIE-31: Mechanical and Thermal Properties of Optical Glass," 2004, https://www.schott.com/shop/medias/schott-tie-31-mechanical-and-thermal-properties-of-optical-eng.pdf?context=bWFzdGVyfHJvb3R8MjIxODU3fGFwcGxpY2F0aW9uL3BkZnxoYjkvaGI0Lzg4MjAyMzc5MjY0MzAucGRmfGJmMzI4ZjE5ZTEyNzdiMjRkYWQ5Y2QyOWFiNmU1MTU5ZDdmMWJjZDFlODEwZTllMjlkMjk1ZWEzN2JlNjY5MjI.

45. E. Özkalay, A. Virtuani, G. Eder, et al., "Correlating Long-Term Performance and Aging Behaviour of Building Integrated PV Modules," *Energy and Buildings* 316 (2024): 114252, https://doi.org/10.1016/j.enbuild.2024.114252.

46. E. Özkalay, G. Friesen, M. Caccivio, et al., "Operating Temperatures and Diurnal Temperature Operating Temperatures and Diurnal Temperature Variations of Modules Installed in Open-Rack and Typical BIPV Configurations," *IEEE Journal of Photovoltacis* 12 pages: 133–140, 2022.

47. H. P. Ebert, "Functional Materials for Energy-Efficient Buildings," *EPJ Web of Conferences* 68 (2015): 08001.

48. G. C. Eder, Y. Voronko, G. Oreski, et al., "Error Analysis of Aged Modules With Cracked Polyamide Backsheets," *Solar Energy Materials and Solar Cells* 203 (2019): 110194.

49. P. Romer, G. Oreski, A. J. Beinert, H. Neuhaus, and M. Mittag, "More Realistic Considerations of Backsheets Coefficient of Thermal Expansion on Thermomechanics of PV Modules," in *37th European Photovoltaic Solar Energy Conference and Exhibition* (EUPVSEC, 2020), 772–776.

50. P. Fuchs, A. Halm, and M. Klenk, eds., "FEM Simulation of Influence of Different Polymeric Module Materials and Layouts on Thermomechanical Deformations in Strings of Shingled Solar Cells," in *2023 24th International Conference on Thermal, Mechanical and Multi-Physics Simulation and Experiments in Microelectronics and Microsystems (EuroSimE)* (IEEE, 2023).

51. M. Knausz, G. Oreski, M. Schmidt, et al., "Thermal Expansion Behavior of Solar Cell Encapsulation Materials," *Polymer Testing* 44 (2015): 160–167, https://doi.org/10.1016/j.polymertesting.2015.04.009.

52. Glass Technology Services, "Glass Weight Calculator," accessed March 28, 2025, https://www.glass-ts.com/resources/glass-weight-calculator/results.

53. G. Oreski, C. Barretta, A. Macher, et al., "Investigation of the Crack Propensity of Co-Extruded Polypropylene Backsheet Films for Photovoltaic Modules," *Solar Energy Materials and Solar Cells* 259 (2023): 112438.

54. A. Aiello, S. Mitterhofer, J. Obrzut, et al., "A Spatially Resolved Evaluation of Accelerated Environmental Aging on Emerging Polypropylene-Based Photovoltaic Backsheets Using Raman Spectroscopy," *Progress in Photovoltaics: Research and Applications* 33 (2025): 652–662.

55. W. Camacho and S. Karlsson, "Assessment of Thermal and Thermo-Oxidative Stability of Multiextruded Recycled PP, HDPE and a Blend Thereof," *Polymer Degradation and Stability* 78 (2002): 385–391.

56. G. Oreski, B. Ottersböck, C. Barretta, P. Christöfl, S. Radl, and G. Pinter, "Degradation of PET—Quantitative Estimation of Changes in Molar Mass Using Mechanical and Thermal Characterization Methods," *Polymer Testing* 125 (2023): 108130.

57. B. Ottersböck, G. Oreski, and G. Pinter, "Correlation Study of Damp Heat and Pressure Cooker Testing on Backsheets," *Journal of Applied Polymer Science* 133 (2016): 44230, https://doi.org/10.1002/app.44230.

5.3 Publication II

Title: Backsheet-Galvanized Steel Adhesion Approaches for Integrated Photovoltaic Façades: A Comparative Study

Journal: IEEE Xplore digital library (IEEE PVSEC 54 Conference proceedings)

Date of submission: 15th of May 2026 (accepted)

	Share in %							Total
	Author	Co-authors						
	PhD Student	1	2	3	4	5	6	
Conceptualization	70	10	10				10	100
Methodology	90						10	100
Formal analysis	100							100
Investigation	70		30					100
Visualization	100							100
Data curation	100							100
Writing - original draft	100							100
Writing - review & editing		10	10	10	10	10	50	100
Resources		5	60	5	5	5	20	100
Supervision							100	100
Project administration							100	100
Funding acquisition							100	100

Author, PhD Student: Nikolina Pervan

Co-author 1: Lukas Geymayer

Co-author 2: Martin Fleischanderl

Co-author 3: Hannes Kurz

Co-author 4: Gregor Kitzberger

Co-author 5: Friedrich Füreder-Kitzmüller

Co-author 6: Gernot Oreski

Backsheet-Galvanized Steel Adhesion Approaches for Integrated Photovoltaic Façades: A Comparative Study

Nikolina Pervan[1,2,3], Lukas Geymayer[4], Martin Fleischanderl[4], Hannes Kurz[4], Gregor Kitzberger[4], Friedrich Füreder-Kitzmüller[4], Gernot Oreski[1,2]

[1] Polymer Competence Center Leoben GmbH (PCCL), 8700 Leoben, Austria; [2] Chair of Materials Science and Testing of Polymers, Technical University of Leoben, 8700 Leoben, Austria; [3] UHasselt, Institute for Materials Research (IUMAT), B-3600 Hasselt, Belgium, [4] voestalpine Stahl GmbH, 4020 Linz, Austria

Abstract — **The integration of photovoltaics (PV) into building façades enables the expansion of renewable energy generation without additional land use. This work investigates a lightweight PV module concept designed for integration into large-scale steel façade elements. The proposed architecture omits front glass, using a transparent polymeric film as a frontsheet, while the structural steel façade sheet is integrated at the rear of the module during manufacturing. A key challenge for this concept is achieving durable adhesion between the polymeric backsheet and the hot-dip galvanized steel (HDGS) substrate. Three different adhesion approaches were investigated and comparatively evaluated. Approach A (conventional) relies on bonding the backsheet to the HDGS using an encapsulant layer, while approach B (modified) uses a thin adhesive layer at the interface. Approach C (proprietary) on the other hand, eliminates intermediate layer, and employs an alternative interfacial design developed in collaboration with industrial partner. Adhesion strength was assessed using 180° peel test, and durability was studied under accelerated aging conditions, including damp heat exposure (85 °C / 85% relative humidity) and thermal cycling (−40 to 85 °C). Peel tests were conducted before and after aging. Results demonstrate that while all three approaches achieved robust initial adhesion to HDGS, exposure to damp heat led to significant degradation at the POE-PET interface in approach A and the cohesive failure of the adhesive layer in approach B after 1000 hours. Approach C emerged as the most durable solution, maintaining superior interfacial integrity and mechanical performance across all accelerated aging tests.**

I. Introduction

As part of the European Green Deal, Europe aims to increase the share of renewable energy in its energy mix to at least 40% by 2030 [1], while progressing toward climate neutrality. A major constraint in this transition is the limited availability of free space for large-scale photovoltaic (PV) installations, particularly in densely populated regions such as Belgium and the Netherlands and in geographically constrained areas such as Austria and Switzerland [2]. Since the energy density of solar power is significantly lower than that of fossil fuels, large installation areas are required to meet decarbonization targets [3].

As a result, integrating PV systems into existing infrastructure has become an important strategy to expand deployment without additional land use. However, conventional PV modules are often unsuitable for direct structural integration due to their weight and mechanical limitations [4]. This has driven the development of lightweight, glass-free PV concepts where structural rigidity is provided by the building element itself.

Recent studies have investigated integrating PV module stacks into metal façade systems, such as aluminum and stainless steel [5]-[8]. In the explored integrated architectures on metal substrates, the backsheet serves as a dielectric barrier. Because the metal substrate acts as a large, conductive ground, the electrical insulation provided by the backsheet is the most critical safety factor for building integrated PV (BIPV) compliance.

S. Jahreis et al. [5] have bonded PV stack to aluminum façade substrates using ethylene-vinyl acetate (EVA) and polyolefin (POE) encapsulant materials, with one variant employing a non-specified adhesive interlayer. The study primarily addressed manufacturing feasibility and post-process performance after accelerated aging, while the underlying interfacial adhesion behavior was not systematically analyzed [5].

A study by Y. Kim et al. [7] examined adhesion between PV backsheet, EVA and POE encapsulants, and stainless-steel substrates, focusing on the influence of surface roughness and lamination parameters on initial adhesion strength. However, the absence of accelerated aging limited any conclusions regarding long-term stability. Besides fundamental research, there are already companies promoting roof or façade elements with metal-substrate integrated PV, including Roofit Solar [9], ArcelorMittal [10], Ernst Schweizer AG [11], BIMsolar PIM [12] and Kalzip GmbH [13].

Despite progress in integrating PV stacks onto metallic substrates, the long-term reliability of polymer-metal interfaces remains insufficiently understood. While such interfaces are central to industries ranging from food packaging laminates [14] to encapsulated microelectronics [15], BIPV components face unique extremes: they must maintain structural integrity over vast surface areas, up to 12 m in length (as planned in the PVfaçade project), while enduring decades of direct weathering. This makes the durability of the steel-polymer bond a distinct engineering hurdle compared to shorter-lived or

protected consumer applications. To address this gap, this study systematically investigates the interfacial integrity of a polymeric backsheet adhered to hot-dip galvanized steel (HDGS) under damp heat and thermal cycling exposure.

II. BIPV Façade Technology

A. Module configuration

As a building element, PV module must meet requirements for mechanical stability and rigidity [16]. The design concept behind the lightweight BIPV module in PVfaçade Project involves replacing the front glass cover of conventional PV modules with a transparent polymeric film as a frontsheet. To compensate for the resulting loss of structural integrity, mechanical stability is reintroduced through the integration of the HDGS sheet as a back-side component (see Fig. 1).

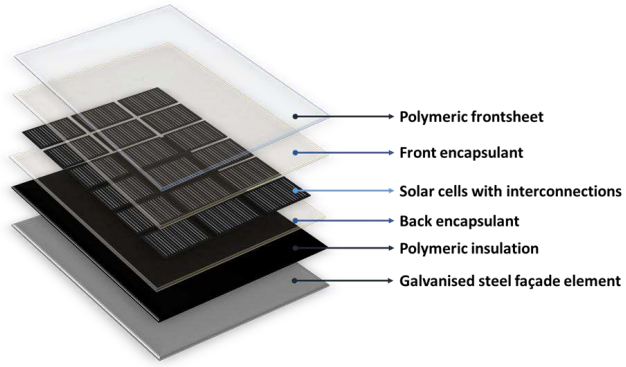

Fig. 1. Material lay-up of BIPV module structure.

HDGS sheets are already commonly used in the construction of industrial buildings, and serve as an ideal structural base for BIPV modules. Given that the BIPV module is a complex multi-layer product, establishing a durable bill of materials (BOM) is essential. In this research, material selection was guided by four key criteria: availability, sustainability, processability, and long-term performance.

Regarding availability, the study prioritizes commercially available products manufactured in Europe. From a sustainability perspective, the selection aims for halogen-free and recyclable materials wherever feasible. Ultimately, the module components must ensure minimal performance degradation over a service life exceeding 30 years.

Based on the material screening from the previous work [17], EVA was identified as incompatible with galvanized substrates in BIPV applications. Under damp heat aging, the deacetylation of EVA caused release of acetic acid, which promoted corrosion of the galvanized layer. This chemical interaction resulted in interfacial separation of the backsheet [17]. Consequently, any polymeric materials, including encapsulants or backsheets containing EVA, were excluded from the present study. Therefore, POE-based encapsulants, which were proved to provide good adhesion between the backsheet and frontsheet layers [18], were selected to promote adhesion between the HDGS and the backsheet.

Two commercially available polyethylene terephthalate (PET)-based backsheets were selected as the electrical insulation layer, consisting of one (BS-1) or two PET layers (BS-2). Both backsheets feature an integrated polyethylene (PE) adhesion-promoting layer oriented toward the cell side. The internal layers of the backsheets (PET/PE and PET/PET/PE) are bonded with a thin adhesive layer. Although the specific chemistry of this adhesive was not disclosed by the supplier, internal analysis showed a close spectral match to the polyurethane (PU) family, suggesting a PU-based system or a related copolymer blend.

The integration of the HDGS sheet as a structural back component introduces a critical interface within the BIPV module, namely the adhesion between the polymeric backsheet and the HDGS substrate. This interface must maintain mechanical integrity during manufacturing, installation, and throughout its service life under environmental exposure. To address this challenge, three distinct approaches for adhering the backsheet to the HDGS sheet were investigated. These strategies differ in their interfacial design and bonding mechanisms while remaining compatible with standard industrial lamination processes.

B. Adhesion approaches

Three distinct approaches were investigated to achieve durable adhesion between the two different polymeric backsheets and the HDGS substrate, the resulting multi-layer stack configurations for all investigated material combinations are summarized in Table I.

TABLE I
Material combinations in the Sample Lay-up

Substrate	Adhesion approach	Electrical insulation layer	Accelerated aging
hot-dip galvanized steel (HDGS)	A (POE layer)	BS-1 (PET/PE)	100, 250, 500 and 1000 h at 85 °C and 85% rh & 50, 100 and 200 thermal cycles from -40 to 85 °C
	B (adhesive layer)	BS-1 (PET/PE)	
	B (adhesive layer)	BS-2 (PET/PET/PE)	
	C (proprietary)	BS-1 (PET/PE)	
	C (proprietary)	BS-2 (PET/PET/PE)	

Approach A (conventional) relies on bonding the backsheet to the HDGS using an encapsulant layer, while approach B (modified) uses a thin adhesive layer at the interface. Approach A is implemented in a single-step lamination process for all module components, whereas approach B requires a two-step process. Beyond the processing difference, the increased stack thickness and the additional encapsulant layer in approach A introduce an extra combustible component, which may increase the flammability of the PV module.

Approach C (proprietary) on the other hand, eliminates intermediate layer, and employs an alternative interfacial design developed in collaboration with the industrial partner. The adhesive layer in approach B and the details of approach C are proprietary and will not be disclosed here; however, the resulting adhesion and comparison among all three approaches are presented.

The preparation of the sample coupons followed a collaborative manufacturing workflow. Samples utilizing approaches B and C were prepared at voestalpine Stahl GmbH, leveraging industrial-scale processing capabilities. Samples using approach A were laminated using a single-sided heated vacuum laminator. For the latter, lamination parameters were based on the encapsulant supplier's recommendations, with specific modifications to the vacuum and heating profiles to account for the single-sided heating configuration.

C. 180° peel test and accelerated aging

Adhesion performance was quantified through 180° peel testing in accordance with ASTM D3330. Tests were performed at room temperature using a Zwick/Roell Zwicki (2.5 kN) universal testing machine equipped with a 1 kN load cell and operated at a constant test speed of 5 mm s^{-1}.

To evaluate the long-term reliability of the polymer-metal interfaces, all sample groups were subjected to accelerated aging in damp heat (DH): 85 °C / 85% relative humidity) and thermal cycling (TC): − 40 to 85 °C in accordance with IEC 61215-2:2021 [19]. Adherence to these protocols ensured the samples met the rigorous durability requirements for PV module qualification criteria [20]. Peel tests were performed at specific intervals to track degradation kinetics, with measurements taken after 100, 250, 500, and 1000 hours of DH exposure, and after 50, 100, and 200 TC. These stressors were prioritized as moisture ingress and thermo-mechanical fatigue, driven by the mismatch in coefficients of thermal expansion (CTE) between the steel and polymer, are the potential drivers of interfacial degradation. To ensure statistical significance, a minimum of five specimens were measured for each combination of material and aging duration.

Following the peel tests, the delaminated interfaces were analysed using a Perkin Elmer Fourier Transform Infrared (FTIR) spectrometer. This analysis was instrumental in determining the specific failure mode, allowing for a clear distinction between cohesive and adhesive failure type.

III. Results and Discussion

A. BS-1: approach A

For the evaluation of bonding with the approach A, only the BS-1 backsheet was used. The combination of a POE encapsulant layer with the thicker BS-2 backsheet was excluded to minimize the total polymer volume, thereby optimizing the module for weight, stack thickness, and fire safety behavior.

The unaged samples demonstrated high initial adhesion, with an average adhesion strength of 104 N/10 mm. Although delamination initiated as an adhesive failure between the POE and the HDGS substrate, the failure path quickly transitioned. Visually, the delaminated POE surface appeared transparent, which suggested a clean adhesive separation from the white PET backsheet. However, FTIR spectroscopy (Fig. 2) revealed the presence of characteristic PET peaks in the fingerprint region below 2000 cm^{-1} (most notably the C=O stretch at ~1715 cm^{-1} and C-O stretching at ~1240 cm^{-1} [21]) combined with POE peaks in the 2900–2800 cm^{-1} range (corresponding to CH_2 symmetric and asymmetric stretching [22]). This confirms that the failure was actually cohesive within the backsheet, leaving a thin, translucent layer of the PET outer skin bonded to the POE encapsulant. Therefore, the average peel strength was calculated specifically across this cohesive region, as the initial metal-interface separation represented a negligible portion of the total peel area.

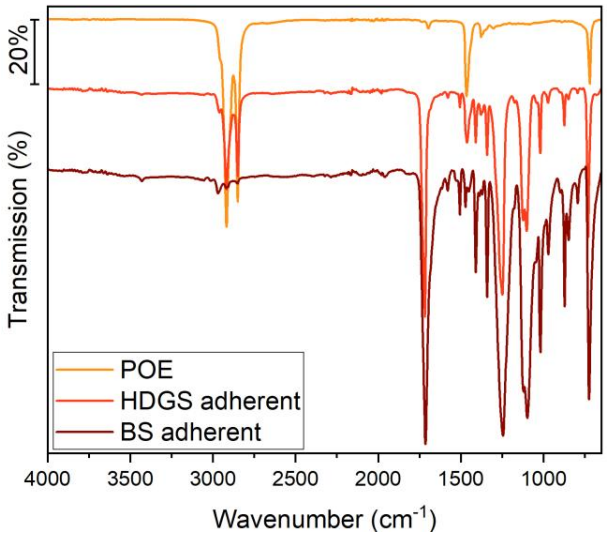

Fig. 2. FTIR-ATR spectra of the HDGS and BS interface surfaces after delamination (adhesion approach A), together with a POE encapsulant reference spectrum.

As observable from the Fig. 3. the introduction of environmental stress via DH exposure significantly compromised adhesion strength. After 100 h of DH, the adhesion strength decreased to 20 N/10 mm. At this stage, the failure mode shifted to a primarily adhesive separation between the POE and the PET-air layer, though certain regions remained

well-adhered and continued to exhibit cohesive failure. By 1000 h of DH, the adhesion strength reached a minimum of 5.5 N/10 mm, with the adhesive failure almost entirely in POE/PET-air interface.

In contrast, the samples showed greater resilience to TC. Even after 200 cycles, the average adhesion strength remained high at 72 N/10 mm, maintaining the same cohesive failure mode observed in the unaged samples. This suggests that while the POE/PET-air interface is highly susceptible to hydrolytic degradation, it remains mechanically stable under thermomechanical fatigue.

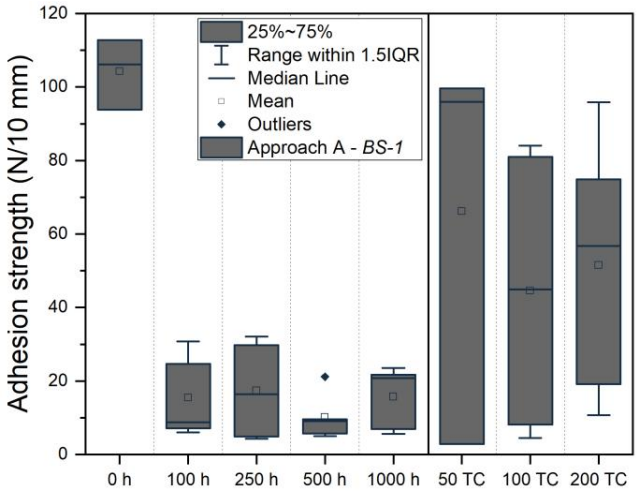

Fig. 3. Adhesion strength values for samples with BS-1 adhered to HDGS with approach A, before and after damp heat and thermal cycle exposure.

B. BS-1: approaches B and C

Samples prepared using approach B with the BS-1 backsheet demonstrated a markedly different failure mechanism than those observed in approach A. While initial visual inspection suggested cohesive failure within the PET, subsequent microscopic analysis (Fig. 4) revealed that the mono PET-air layer was actually a coextruded PET/PET laminate. Therefore, delamination primarily occurred at this internal coextruded interface, as the interlaminar adhesion within the backsheet was weaker than the bonds between the other interfaces. Consequently, the initial average adhesion strength of 4.2 N/10 mm represents the internal structural integrity of the backsheet rather than the adhesion between the HDGS and the polymer stack.

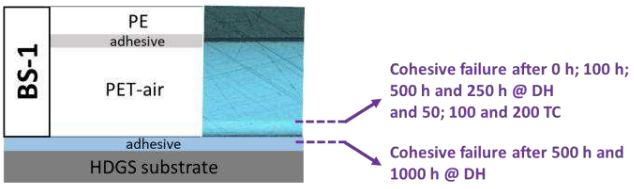

Fig. 4. Schematic cross-section of the layer stack for samples prepared using approach B with backsheet BS-1 (integrated microscopic image), and the corresponding delamination interfaces after accelerated aging. Arrows indicate the locations of delamination before and after damp heat and thermal cycling, the layers are not to scale.

Exposure to DH led to a significant reduction in adhesion strength, which remained stable at approximately 3 N/10 mm throughout the 100 h, 250 h, and 500 h intervals, as shown in Fig. 5. For the samples aged for 500 h in DH, a hybrid failure mode emerged; while two out of five samples maintained the internal backsheet delamination observed in unaged samples, three out of five samples (60%) exhibited a shift to cohesive failure within the adhesive layer between the HDGS and the backsheet. This transition signals the onset of hydrolytic degradation within the primary adhesive layer. By 1000 h of DH, this cohesive failure within the adhesive was observed across all specimens, with the adhesion strength dropping to a critical value of 0.2 N/10 mm.

Interestingly, TC did not impact the integrity of the steel-adhesive-backsheet bond. Instead, it had a far more pronounced impact on the PET/PET coextruded interface than moisture exposure did. After only 50 cycles, the adhesion strength was halved to 1.9 N/10 mm, eventually reaching 0.7 N/10 mm after 200 cycles. This indicates that while the primary adhesive remains stable, the coextruded interface within the backsheet is particularly vulnerable to the thermomechanical stresses induced by cyclic loading.

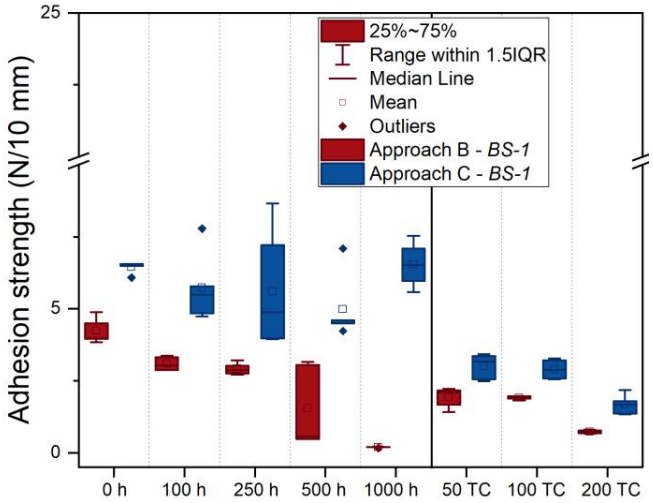

Fig. 5. Adhesion strength values for samples with BS-1 adhered to HDGS with approach B (red) and C (blue), before and after damp heat and thermal cycle exposure.

For samples laminated using approach C, the failure interfaces mirrored those of approach B, with delamination localized within the coextruded PET/PET interface. However, approach C consistently yielded adhesion values 1–3 N/10 mm higher than approach B across all tested conditions. This improvement may be attributed to the specific lamination parameters used in approach C, suggesting a

beneficial effect on the interlaminar adhesion within the backsheet layers.

A unique phenomenon was observed after 1000 h of DH exposure: delamination occurred across multiple interfaces, progressing from the coextruded PET/PET interface into the interlaminar adhesive/PE layer. This complex failure caused significant plastic deformation of the PE layer during the peel test. This resulted in a localized, false increase in the average peel strength due to the force required to plastically deform (stretch) the PE [23]. Consistent with the findings for approach B, TC proved to be the more detrimental stressor for the interlaminar adhesion of the backsheet, further highlighting the sensitivity of these coextruded interfaces to thermomechanical fatigue.

C. BS-2: approaches B and C

Samples prepared using approach B with the BS-2 backsheet exhibited cohesive delamination within the backsheet both before aging and after most accelerated aging conditions. The only exception was the sample group subjected to 1000 h of DH, where failure occurred cohesively within the adhesive layer between the HDGS and the backsheet. Accelerated aging influenced the overall adhesion strength; therefore, delamination within the backsheet was analysed in detail to assess changes in adhesion strength and failure behaviour.

Within the backsheet, the adhesion strength initially increased from 9.8 N/10 mm to 18.8 N/10 mm after 100 h of DH exposure, likely due to heat- and/or humidity-induced post-curing of the adhesive layers. With continued aging, the adhesion strength decreased, reaching 2.6 N/10 mm after 500 h of DH exposure, which is attributed to progressive degradation of the adhesive layer in the BS. In parallel, the delamination interface within the backsheet changed as shown in Fig 6. Initially, adhesive failure occurred at the PET-air/adhesive interface; however, after 500 h of DH exposure, the failure mode shifted to cohesive failure within the adhesive layer between the PET-air and PET-core layers. In contrast, TC did not alter the failure interface compared to unaged samples, though it slightly reduced the average adhesion to 8.5 N/10 mm after 200 cycles.

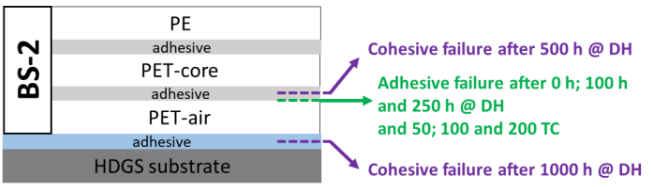

Fig. 6. Schematic cross-section of the layer stack for samples prepared using approach B with backsheet BS-2 (PET/PET/PE), and the corresponding delamination interfaces after accelerated aging. Arrows indicate the locations of delamination before and after damp heat and thermal cycling, the layers are not to scale.

For samples prepared using approach C and BS-2, delamination also occurred cohesively within the backsheet both before and after all accelerated aging conditions. The measured adhesion strength was consistently higher than that of samples from approach B by approximately 1–3 N/10 mm across all DH conditions (Fig. 7), aligning with the trend observed for BS-1. This once again suggests that the lamination parameters of approach C have a beneficial effect on the interlaminar adhesion within the backsheet layers. The evolution of the failure interfaces within the backsheet followed a similar trajectory to approach B, with samples aged for 1000 h in DH exhibiting cohesive failure within the internal adhesive layer between the PET-air and PET-core. Notably, TC impacted the average interlaminar adhesion of approach C samples more significantly than in approach B, ultimately reducing the adhesion strength to values similar to those observed in the approach B group.

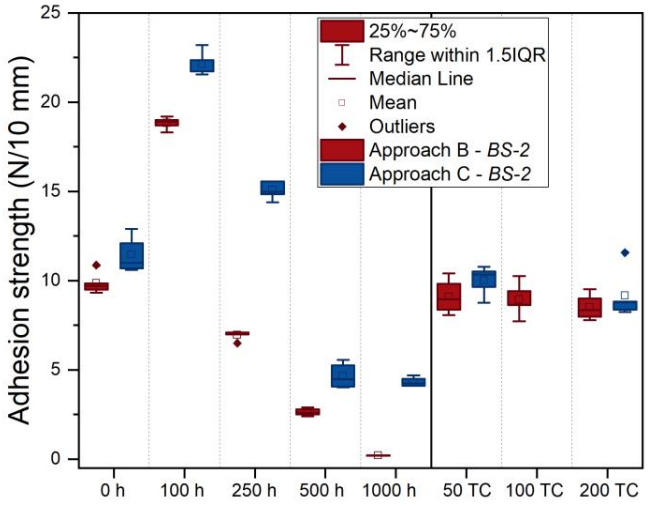

Fig. 7. Adhesion strength values for samples with BS-2 adhered to HDGS with approach B (red) and C (blue), before and after damp heat and thermal cycle exposure.

D. Adhesion strength – degradation paths

The observed decline in POE–PET adhesion under DH exposure from approach A, despite stability during TC, points to a chemical rather than mechanical failure path. In this interface, moisture acts as a primary degradant through several simultaneous mechanisms: the disruption of secondary Van der Waals forces via interfacial water accumulation and the potential hydrolysis of silane coupling agents commonly used in POE formulations to promote adhesion to solar cell and solar glass [24]. To mitigate this, surface functionalization of the PET, such as corona treatment, plasma activation, or the application of specialized primers, could be employed to enhance chemical coupling with the POE, potentially delaying moisture-induced debonding.

In the multi-layer backsheets, such as BS-1 and BS-2, the interlaminar adhesion behaviour is largely governed by the chemistry of the incorporated adhesives. The initial increase in strength during DH exposure is consistent with the behaviour

of moisture-curable adhesives, such as certain PU-based systems, where residual reactive groups (e.g., isocyanates) react with diffused water to increase cross-linked density [25]. However, this reinforcement is temporary, continued moisture ingress likely triggered hydrolytic chain scission, leading to the chemical breakdown and embrittlement of the adhesive backbone, as observed for BS-2 after prolonged DH exposure [26]. Similar observations were made by several other research institutes on both laboratory and field aged backsheets [27]-[33].

Moisture also acted as a degrading mechanism for the adhesive used to bond the HDGS to the backsheet in approach B. The cohesive failure within the adhesive after 1000 h of DH exposure revealed that this formulation was not adapted for prolonged hydrothermal stress. Although moisture penetration will be significantly reduced in a complete PV module stack, the susceptibility of this adhesive to hydrolysis poses a critical risk for edge delamination. To ensure long-term reliability against moisture, it is essential to reformulate adhesive with improved hydrolysis resistance.

Ultimately, the mechanical vulnerability of the stack was exposed during TC. Because the rigid HDGS substrate acts as a significant mechanical constraint with a substantially lower CTE than the polymers, it restricts the natural expansion and contraction of the backsheet. This constraint generates high internal stresses, particularly at the interlaminar interfaces. In multi-layer PET backsheets, layers often possess different processing histories, leading to localized CTE mismatches within the backsheet itself. When locked to the HDGS, these internal layers pull against one another, causing the interfaces to fatigue and eventually fail.

The impact of this internal interfacial weakness on long-term module reliability cannot be overstated, especially when considering the scale of envisioned BIPV applications. For large-scale façade components reaching length size of up to 12 m, these CTE mismatches will play an even more dominant role, as the cumulative thermal strain over such lengths can lead to catastrophic delamination. Since all three approaches achieved robust bonding to the HDGS, the internal backsheet structure remains the primary weak link in the system. Therefore, while adhesive reformulation is necessary for the chemical stability of Approach B, transitioning toward a monolithic (single-layer) backsheet is strongly recommended to minimize the number of interfaces susceptible to thermal-mechanical degradation.

In interpreting the adhesion data, it must be noted that the 180° peel test provides a comparative rather than an absolute measure of interfacial adhesion strength. Because a portion of the applied force is inevitably consumed by the plastic deformation of the polymeric peel arm, the recorded values do not correspond directly to pure interfacial adhesion energy. While methods like the width-tapered single cantilever beam and the compressive shear tests provide a more precise adhesion strength values, they are significantly more time-consuming [30], [34]-[36].

For the requirements of this study, the 180° peel test was the most practical choice to allow for a consistent, comparative evaluation across a large number of samples. Using this method as an efficient screening tool allowed for the identification of clear performance trends within a reasonable timeframe. Once the most optimal backsheet and adhesion approach is defined, more precise testing will be conducted in the final phase of the project to characterize the absolute adhesion strength.

IV. Summary and Outlook

In this work, PV modules were laminated onto HDGS façade components, forming a multi-layer system in which the polymeric backsheet provides electrical insulation while the adhesive strategy governs the mechanical coupling to the HDGS substrate. Three different adhesion strategies were systematically compared with respect to their initial adhesion strength and durability under DH and TC: approach A (conventional) using a POE encapsulant as the adhesive layer, approach B (modified) with a thin adhesive layer, and approach C (proprietary) featuring an alternative interfacial design.

The investigation confirmed that while all approaches provide robust initial bonding, long-term durability is dictated by the chemical and mechanical stability of the internal layers. Results for approach A revealed that the POE–PET interface is highly susceptible to moisture-driven weakening. In the case of approach B, the cohesive failure observed after 1000 hours of DH exposure confirms that the adhesive formulation was not adapted for prolonged hydrothermal stress. Although moisture penetration is naturally reduced in a full PV module stack, the vulnerability of this layer remains a critical risk for edge delamination, necessitating a reformulation of the adhesive to enhance its hydrolysis resistance. In contrast, approach C emerged as the most durable solution, maintaining superior interfacial integrity throughout all accelerated aging tests.

Future work is underway to further quantify these degradation mechanisms and refine the module architecture for large-scale application. Cross-sections of aged samples will be examined using nanoindentation to map mechanical changes within the individual layers and quantify the degree of polymer degradation. Additionally, full-stack mini-modules have been installed for outdoor monitoring to correlate laboratory data with natural weathering performance. Further durability testing, including UV accelerated aging, will be conducted to define adhesion performance under the full spectrum of environmental conditions. Ultimately, the results suggest that while adhesive reformulation is necessary for specific designs, transitioning toward monolithic backsheets and employing PET surface treatments are the most effective strategies to eliminate internal failure planes and ensure the 25-year service life required for steel-integrated BIPV.

Acknowledgments

This work was conducted as part of the Austrian “e!MISSION.at – Energy Mission Austria” project “PV

Industriefassade" (FFG No. FO999915062) funded by the Austrian Climate and Energy Fund and the Austrian Research Promotion Agency (FFG).

This research project (grant number: 911658) was funded by COMET – Competence Centers for Excellent Technologies – through BMIMI, BMWET, and the co-financing federal provinces (Styria through SFG, Upper Austria, Vorarlberg) and carried out with the participation of scientific and company partners. The COMET program is managed by FFG.

The authors would like to acknowledge Maja Knezović for her contribution to sample preparation and mechanical characterization, as well as Christian Veas and Marissa Maier for their assistance with the spectroscopic measurements.

REFERENCES

[1] "DIRECTIVE (EU) 2023/2413 OF THE EUROPEAN PARLIAMENT AND OF THE COUNCIL of 18 October 2023 amending Directive (EU) 2018/2001, Regulation (EU) 2018/1999 and Directive 98/70/EC as regards the promotion of energy from renewable sources, and repealing Council Directive (EU) 2015/652: 2023/2413," in *Official Journal of the European Union*, 2023.

[2] M. Deshaies, "Problèmes géographiques des transitions énergétiques : quelles perspectives pour l'évolution du système énergétique ?," *Transition énergétique et développement*, no. 192, pp. 25–44, https://shs.cairn.info/revue-mondes-en-developpement-2020-4-page-25?lang=fr, 2020.

[3] J. K. Nøland, J. Auxepaules, A. Rousset, B. Perney, and G. Falleti, "Spatial energy density of large-scale electricity generation from power sources worldwide," *Scientific Reports*, vol. 12, https://doi.org/10.1038/s41598-022-25341-9, 2022.

[4] Maeve Campbell, *Thinner than a pencil, these solar panels are set to revolutionise solar power.* [Online] Available: https://www.euronews.com/2021/10/29/thinner-than-a-pencil-these-solar-panels-are-set-to-revolutionise-solar-power. Accessed on: May 04 2026.

[5] S. Jahreis, B. Jaeckel, R. Koepge, J. Fröbel, P. Schenk, M. Pander, and R. Castro, "Design, manufacturing, and performance of innovative aluminium-backed BIPV facade modules: a case-study in Germany," *Energy and Buildings*, vol. 344, p. 116047, 2025.

[6] Fraunhofer CSP, *Modular aluminum elements with integrated photovoltaic modules for solar facades.* [Online] Available: https://www.imws.fraunhofer.de/en/presse/pressemitteilungen/2024/solar-facade-building-integrated-module-aluminum.html. Accessed on: May 04 2026.

[7] Y.-S. Kim, A.-R. Kim, S. J. Tark, C.-B. Mo, S. Hwang, and Y. Kang, "Analysis of adhesion characteristics of steel back plates and encapsulants for fire-proof BIPV modules," *Results Eng.*, vol. 21, p. 101649, 2024.

[8] S. Jahreis, B. Jaeckel, R. Koepge, J. Froebel, P. Schenk, and M. Pander, "Design, Manufacturing and Analysis of Aluminium-backed BIPV Facade Modules: Electrical Performance and Outdoor Tests," (en), *42nd European Photovoltaic Solar Energy Conference and Exhibition*, 2025.

[9] Roofit.Solar, *The Perfect Solar Roof: 2-in-1 Solar Powered Roofing Material.* [Online] Available: https://roofit.solar/solar-roof/?_gl=1*1ep1auc*_up*MQ.*_ga*MTQxOTA0MDgzMS4xNzc3ODg1NTI5*_ga_R5CE5G0LBG*czE3Nzc4ODU1MjgkbzEkZzAkdDE3Nzc4ODU1MjgkajYwJGwwJGgw. Accessed on: May 04 2026.

[10] ArcelorMittal Building Solutions, *Helioroof: Prefabricated insulated solar roof panel.* [Online] Available: https://buildingsolutions.arcelormittal.com/en/generic/helioroof-prefabricated-insulated-solar-roof-panel. Accessed on: May 04 2026.

[11] Ernst Schweizer AG, *Like a tile, but including a solar system.* [Online] Available: https://ernstschweizer.com/en/solarsystems/solar-roof-tiles-soltile/. Accessed on: May 04 2026.

[12] BIMsolar PIM, *ACTIV'GLASS - BIPV ventilated cladding: COPPER ACTIV'FACADE K7' mounted with SCHWEIZER FSP-H.* [Online] Available: https://pim.bim-solar.com/ecatalog/activglass_sch_copper. Accessed on: May 04 2026.

[13] Kalzip SolarSysteme, *Kalzip® solar systems: Integrated PV roofing solutions for creative solar architecture.* [Online] Available: https://www.kalzip.com/wp-content/uploads/2020/03/Kalzip-Solar-systems_EU.pdf. Accessed on: May 04 2026.

[14] S. Devisme, J.-M. Haudin, J.-F. Agassant, R. Combarieu, D. Rauline, and F. Chopinez, "Adhesion in polypropylene/aluminum laminates made by extrusion coating," *J Appl Polym Sci*, vol. 112, no. 5, pp. 2609–2624, 2009.

[15] K. L. Mittal and T. Ahsan, *Adhesion in Microelectronics*: Wiley, 2014.

[16] N. M. Chivelet, C. Kapsis, and F. Frontini, *Building-Integrated Photovoltaics: A Technical Guidebook,* 1st ed. New York: Routledge, 2024.

[17] N. Pervan, S. Feldbacher, C. Barretta, L. Geymayer, G. Kitzberger, M. Fleischanderl, H. Kurz, F. Fureder-Kitzmüller, and G. Oreski, "Integration of Photovoltaics in Steel Facade Panels," in *2025 IEEE 53rd Photovoltaic Specialists Conference (PVSC)*, Montreal, QC, Canada, 2025, p. 597.

[18] N. Pervan, C. Veas, S. Feldbacher, L. Geymayer, G. Kitzberger, M. Fleischanderl, H. Kurz, F. Füreder-Kitzmüller, G. Oreski, "Transforming Industrial Facades with Integrated Photovoltaics," in *EU PVSEC 2025*.

[19] *Terrestrial photovoltaic (PV) modules - Design qualification and type approval - Part 2: Test procedures*, IEC 61215-2:2016, 2016.

[20] G. Oreski, C. Barretta, L. Castillon, P. Christöfl, and M. Köntges, "Importance of Bill of Material (BOM) Control and IEC 61215 Scope of Application," in *37th European Photovoltaic Solar Energy Conference and Exhibition (EU PVSEC)*.

[21] F. Dubelley, E. Planes, C. Bas, E. Pons, B. Yrieix, and L. Flandin, "The hygrothermal degradation of PET in laminated multilayer," *Eur. Polym. J.*, vol. 87, pp. 1–13, 2017.

[22] G. Oreski, C. Barretta, P. Christöfl, P. Gebhardt, K.-A. Weiß, D. C. Miller, S. Uličná, M. Kempe, L. S. Bruckman, A. Virtuani, H. Li, B. Habersberger, J. Munro, K. Proost, and M. Kühne, "What Is a Polyolefin? A Critical Overview of Ethylene Copolymers Used as Solar Photovoltaic Module Encapsulants," *Prog. Photovolt.*, no. 34, pp. 367–395, 2026.

[23] G. Oreski and G. Pinter, "Peeling of Flexible Laminates-Determination of Interlayer Adhesion of Backsheet Laminates Used for Photovoltaic Modules," (eng), *Materials (Basel, Switzerland)*, vol. 15, no. 9, 2022.

[24] Jishnu Ramachandran Nair *et al., Eds., Formulation Studies of Polyolefin Elastomer Encapsulants with Adhesion Promoters: Impacts on Adhesion Strength and Crosslinking Behavior*, 2025.

[25] H. Moon, J. E. Park, W. Cho, J. Jeon, and J. J. Wie, "Curing Kinetics and Structure-Property Relationship of Moisture-Cured One-Component Polyurethane Adhesives," *Eur. Polym. J.*, vol. 201, p. 112579, 2023.

[26] J. Yu, R. Jiang, and D. Song, "Preparation and performance study of carbodiimide-modified polyurethane-acrylic resin composite coatings with high transparency, strong adhesion, and excellent weathering performance," *Prog. Org. Coat.*, vol. 201, p. 109130, 2025.

[27] F. D. Novoa, D. C. Miller, and R. H. Dauskardt, "Environmental mechanisms of debonding in photovoltaic backsheets," *Sol. Energy Mater. Sol. Cells*, vol. 120, no. PART A, pp. 87–93, 2014.

[28] Chiao-Chi Lin, Peter J. Krommenhoek, Stephanie S. Watson, and Xiaohong Gu, "Depth profiling of degradation of multilayer photovoltaic backsheets after accelerated laboratory weathering: Cross-sectional Raman imaging," (en), *Sol. Energy Mater. Sol. Cells*, vol. 144, pp. 289–299, http://www.sciencedirect.com/science/article/pii/S0927024815004547, 2016.

[29] S. E. Julien, M. D. Kempe, J. J. Eafanti, J. Morse, Y. Wang, A. Fairbrother, S. Napoli, A. W. Hauser, L. Ji, G. S. O'Brien, X. Gu, R. H. French, L. S. Bruckman, K.-T. Wan, and K. P. Boyce, "Characterizing photovoltaic backsheet adhesion degradation using the wedge and single cantilever beam tests, Part I: Field Modules," *Sol. Energy Mater. Sol. Cells*, vol. 215, https://www.scopus.com/inward/record.uri?eid=2-s2.0-85082862885&doi=10.1016%2fj.solmat.2020.110669&partnerID=40&md5=a048558f313d662b6be884c19bb606f0, 2020.

[30] J. Tracy, N. Bosco, F. Novoa, and R. Dauskardt, "Encapsulation and backsheet adhesion metrology for photovoltaic modules," *Prog. Photovoltaics Res. Appl.*, vol. 25, no. 1, pp. 87–96, 2017.

[31] S. E. Julien, J. H. Kim, Y. Lyu, D. C. Miller, X. Gu, and K. Wan, "Cohesive and adhesive degradation in PET-based photovoltaic backsheets subjected to ultraviolet accelerated weathering," *J. Sol. Energy*, vol. 224, pp. 637–649, 2021.

[32] Y. Voronko, G. C. Eder, B. S. Chernev, M. Knausz, G. Oreski, T. Koch, and K. A. Berger, "Analytical Evaluation of the Ageing Induced Changes of the Adhesive within Photovoltaic Backsheets," in *28st European Photovoltaic Solar Energy Conference*, pp. 3037–3042.

[33] G. J. Jorgensen, K. M. Terwilliger, J. A. DelCueto, S. H. Glick, M. D. Kempe, J. W. Pankow, F. J. Pern, and T. J. McMahon, "Moisture transport, adhesion, and corrosion protection of PV module packaging materials," (en), *Sol. Energy Mater. Sol. Cells*, vol. 90, pp. 2739–2775, 2006.

[34] M. Tiefenthaler, G. M. Wallner, and R. Pugstaller, "Effect of global damp heat ageing on debonding of crosslinked EVA- and POE-glass laminates," *Sol. Energy Mater. Sol. Cells*, vol. 264, p. 112602, 2024.

[35] M. Tiefenthaler, G. M. Wallner, and R. Pugstaller, "The Effects of Global Damp Heat Ageing on Debonding of Polyolefin Glass Laminates," in *2023 IEEE 50th Photovoltaic Specialists Conference (PVSC)*, San Juan, PR, USA, 2023, pp. 1–3.

[36] N. Bosco, J. Eafanti, S. Kurtz, J. Tracy, and R. Dauskardt, "Defining Threshold Values of Encapsulant and Backsheet Adhesion for PV Module Reliability," *IEEE J. Photovoltaics*, vol. 7, no. 6, pp. 1536–1540, 2017.

5.4 Publication III

Title: Systematic study of barrier layer coatings for encapsulation of flexible CIGS PV modules

Journal: Results in Engineering

Date of submission: 9th of April 2026 (under review since 24th of April 2026)

	Share in %					Total
	Author	Co-authors				
	PhD Student	1	2	3	4	
Conceptualization	60	10			30	100
Methodology	80	20				100
Formal analysis	100					100
Investigation	70		30			100
Visualization	100					100
Data curation	100					100
Writing - original draft	100					100
Writing - review & editing		20	20	10	50	100
Resources		20	40	40		100
Supervision		50			50	100
Project administration		50			50	100
Funding acquisition		50			50	100

Author, PhD Student: Nikolina Pervan

Co-author 1: Sonja Feldbacher

Co-author 2: Martina Harnisch

Co-author 3: Andreas Zimmermann

Co-author 4: Gernot Oreski

Systematic study of barrier layer coatings for encapsulation of flexible CIGS PV modules

Nikolina Pervan[a,b,c], Sonja Feldbacher[a], Martina Harnisch[d], Andreas Zimmermann[d], Gernot Oreski[a,b]

[a] Polymer Competence Center Leoben (PCCL), Austria, nikolina.pervan@pccl.at, sonja.felbacher@pccl.at, gernot.oreski@pccl.at

[b] Chair of Materials Science and Testing of Polymers, Technical University of Leoben, Austria

[c] Hasselt University, Institute for Materials Research, Belgium

[d] Sunplugged GmbH, Austria, martina.harnisch@sunplugged.at, andreas.zimmermann@sunplugged.at

Abstract

Copper indium gallium (di)selenide (CIGS) solar cells can be deposited onto flexible substrates, enabling their integration into portable devices and complex-shaped modules for building- and vehicle-integrated photovoltaics. However, their sensitivity to humidity has traditionally favored rigid module designs with glass encapsulation, limiting flexible, application specific solutions. This study investigates coating encapsulation of flexible CIGS prefabricates on stainless-steel foils using commercially available and specially developed barrier coatings. Fourteen coating materials were selected and grouped according to their main component: acrylate, epoxy, polyurethane (PU), and silicone. Acrylate coatings exhibited defects or insufficient adhesion under mechanical loading, epoxy coatings showed significant volumetric shrinkage during curing, and silicone coatings were constrained by additional processing steps and thickness limitations, reducing their suitability for scalable industrial applications. PU coatings, despite complex curing behavior, demonstrated good adhesion, uniform coverage, and maintained substrate flexibility, making them the most promising candidates. Accordingly, PU coatings were subjected to accelerated aging tests to evaluate adhesion, optical stability, and overall suitability for flexible CIGS PV modules durability. Coatings with poor initial adhesion delaminated rapidly under pressure cooker test within 1 h. Contrary, under damp heat exposure, degradation progressed more slowly, with wrinkling, delamination and yellowing, developing over several hundred hours, with PU 6 and PU 4 showing the best overall combination of adhesion and optical stability. As a final step, a systematic coating rating scheme was applied to identify the most promising materials for long-term encapsulation performance.

Key words

CIGS, BIPV, flexible PV, encapsulation, barrier coatings

1 Introduction

Copper indium gallium (di)selenide (CIGS) and other thin-film photovoltaic (PV) technologies accounted for less than 2% of the global PV market in 2024 [1]. Despite their lower module efficiencies compared to crystalline silicon (c-Si) technologies (<19% versus >24%), CIGS solar cells continue to maintain a presence in the market [1–3]. This persistence is not driven by peak efficiency, but by form-factor advantages, most notably their compatibility with flexible substrates and cost-effective roll-to-roll manufacturing processes [4–8]. CIGS solar cells can be deposited onto a variety of flexible substrates, including stainless-steel metal foils [7,9], polymer films [10,11], and ultra-thin glass with thicknesses of 100 µm [12,13]. Their mechanical flexibility and ability to be deposited directly onto functional components enable a high degree of customization and integration in diverse applications, ranging from small portable and Internet of Things (IoT) devices to complex-shaped photovoltaic modules for building-integrated photovoltaics (BIPV) and vehicle-integrated photovoltaics (VIPV) [14–18]. Furthermore, depending on the selected bill of materials (BOM), CIGS technology can be tailored for both short-term and long-term applications.

However, these form-factor advantages introduce significant challenges with respect to module reliability and qualification. In particular, CIGS PV modules face difficulties in meeting existing qualification standards, such as IEC testing protocols [19], which are primarily designed to assess long-term outdoor exposure and may not adequately reflect the operational requirements of devices intended for short-duration or application-specific use. In addition, the relatively high sensitivity of CIGS cells to humidity has historically driven module designs toward rigid configurations, typically incorporating glass front encapsulation to limit moisture ingress [20,21]. Such designs enable operational lifetimes of up to 20 years with degradation losses below 20% [22]. However, they inherently constrain mechanical flexibility and are incompatible with continuous roll-to-roll manufacturing.

To overcome these limitations, a transition toward roll-to-roll-compatible encapsulation and lamination processes is underway, although optimization of the BOM remains a critical challenge [23]. While flexible CIGS modules are already commercially available, they often rely on high-cost specialty polymer frontsheets, whose compositions are generally not disclosed by manufacturers [24,25]. Beyond conventional lamination, alternative encapsulation strategies have been explored, including the application of transparent, flexible barrier coatings deposited as single or multilayer systems using additive manufacturing techniques. Prior studies have reported the use of polymer-based coatings such as polyurethane (PU), epoxy, acrylates, and ultraviolet (UV)-curable materials, however, coating application and long-term durability were not systematically investigated [26,27]. Thin ceramic films and multilayer polymer–ceramic barrier structures, most commonly based on atomic layer deposition (ALD) of AlOx, have also been studied [27–30]. Although the presence of AlOx layer has demonstrated enhanced resistance to moisture and oxygen ingress, its adoption in PV module manufacturing appears limited due to high processing costs, complex deposition methods, and limited commercial availability. As a result, vacuum lamination remains to be

the dominant manufacturing approach, despite being suboptimal for flexible and roll-to-roll-compatible modules.

While demand for flexible, application-specific CIGS PV modules continues to increase, scalable and low-cost encapsulation solutions compatible with roll-to-roll manufacturing remain lacking. Addressing this gap is the central motivation of this present study where coating–based encapsulation of flexible CIGS PV prefabricates on stainless-steel foils is systematically investigated. An assessment was performed on a range of commercially available coating materials typically used as barrier layers in stainless-steel construction, transportation, and organic light-emitting diode (OLED) applications to provide protection against moisture and other harsh environmental conditions. These coatings were deposited onto the various substrates present in CIGS PV prefabricates supplied by Sunplugged GmbH using multiple application methods. The objective of this study is to identify coating–process combinations that meet the encapsulation requirements of flexible PV modules intended for BIPV products, with particular emphasis on adhesion performance and compatibility with roll-to-roll manufacturing.

2 Methodology

Coating application was selected as a scalable, low-cost approach for the encapsulation of flexible CIGS PV modules. A variety of deposition techniques are available for coating deposition (see section 2.4 Coating application methods) and this method offers advantages compared to vacuum lamination such as fast processing, design flexibility and reduced material waste [31]. A key requirement for the encapsulation process was that the applied coatings maintain the flexibility of the module after curing. The experimental approach involved defining functional requirements for the encapsulation materials, selecting commercially available candidates, and the optimal deposition process. Coating quality and the effectiveness of drying or curing procedures were assessed visually after each application step and following accelerated aging tests, including exposure to pressure cooker test (120 °C, 100% relative humidity) and damp heat (85 °C, 85% relative humidity).

2.1 CIGS prefabricate

The CIGS PV prefabricate investigated in this study consists of multi-layered thin-film stack on a stainless-steel substrate. The deposition processes of the individual cell layers including the CIGS absorber onto SiOx coated stainless-steel and composition of SiOx are a proprietary knowledge of Sunplugged GmbH and therefore not further addressed here. The surfaces targeted for encapsulation include the stainless-steel edges and corners (frame-like regions), which transition into a thin and narrow SiOx barrier layer that electrically insulates the stainless-steel from the CIGS cell. The front contact layer, i.e. the uppermost material of the solar cell, was Indium Tin Oxide (ITO), along with a copper-based grid used for module interconnection and Kapton® tape applied along the edges of the copper busbars.

Since strong adhesion to the stainless-steel substrate and the SiOx layer (which forms the frame around the cells) is critical to prevent delamination on the sides and water ingress, the study evaluated, complete CIGS prefabricate (configuration 1), self-standing stainless-steel foil (configuration 2), stainless-steel foil with a SiOx layer (configuration 3), and stainless-steel foil with CIGS cell layer stack (configuration 4). A schematic representation of all four configurations is shown in Figure 1.

It should be noted that this study does not investigate the effect of coatings on functioning PV modules. Functional modules were not tested due to limited availability and variations in the CIGS layer stack and module efficiency. Only the prefabricated substrates were examined in this work. The effect of coatings on complete, functioning modules will be addressed in future studies by the company partner, who will test the most promising coating materials identified here.

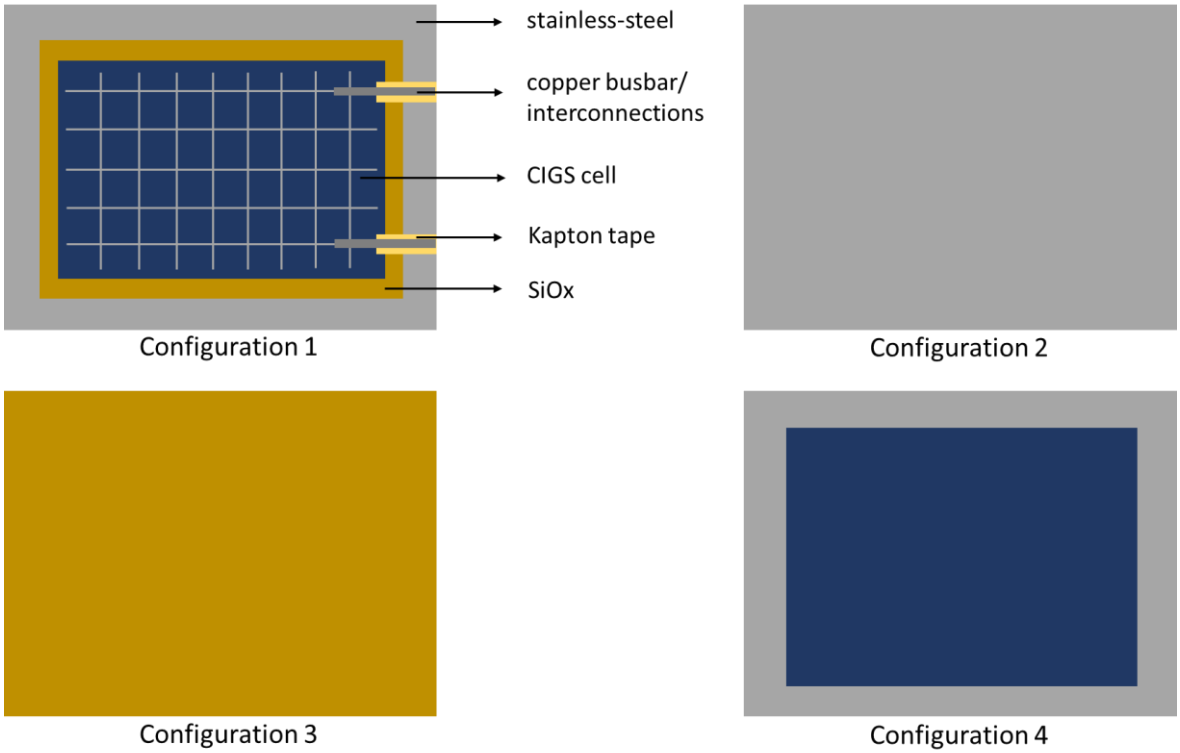

Figure 1. Schematic representation of the four substrate configurations.

2.2 Material requirements

The selection of suitable materials for the encapsulation of flexible CIGS PV modules requires careful consideration of both device performance and process compatibility. As summarized in Table 1. Coating requirements for flexible CIGS encapsulation., the key requirements include specific optical, chemical, mechanical, and processing properties [26].

Optically, the front coating must maintain high transparency and low haze to ensure efficient light transmission towards the CIGS cell layer, while also exhibiting stability under prolonged ultraviolet (UV) exposure. Chemically, encapsulation materials must be inert with respect to all underlying layers, presence of any strong or corroding solvents is not preferred.

Mechanically, coatings must adhere strongly to heterogeneous substrates and maintain flexibility after curing, enabling the final module to withstand bending or minor deformation without cracking or delamination [27].

From a processing standpoint, materials must exhibit viscosities suitable for coating techniques and be compatible with the thermal limits of the substrates during curing. Uniform coverage and layer thickness of less than 500 µm are critical for consistent barrier performance and thin end product. Finally, practical considerations such as commercial availability (European market), cost-effectiveness, and scalability for roll-to-roll processing were incorporated into the selection criteria.

Table 1. Coating requirements for flexible CIGS encapsulation.

Optical transparency	> 90% transmission over visible and NIR range (400 to 1200 nm)
UV stability	No yellowing, hazing or microcracking under UV exposure
Heat resistance	No softening nor degrading up to 100 °C
Viscosity	Between 2000 to 10 000 mPa s
Adhesion	Strong adhesion to all CIGS prefabricate components
Curing	Low temperature curing, without by-product formation
Chemistry	Halogen and acid free systems
Mechanical flexibility	High flexibility post-curing to fit roll-to-roll process
Thickness	< 500 µm

2.3 Coating selection

One of the objectives of this study was to identify commercially available coatings suitable for the encapsulation of flexible CIGS PV modules. Several criteria guided the selection process, covered in previous sub-section. Additionally, cost-effectiveness was important, as economically viable solutions are essential for scalable production of PV modules.

In addition to practical considerations, the selection of the suitable coatings was based on the prior applications in related fields. Coatings originally developed for OLED devices, transportation vehicles (e.g. boats), and other industrial applications where stainless-steel protection is of importance, were considered due to their proven durability under harsh environmental conditions, including moisture, temperature fluctuations, and mechanical stress. These coatings are typically designed to serve as barrier layers, protecting sensitive functional layers while maintaining flexibility and adhesion on heterogeneous substrates. Additionally, silicone coatings developed for PV encapsulation [32], which are not yet widely used and for which limited performance data are available in the literature, were included in the study.

Based on these criteria, candidate materials were identified for further evaluation in terms of compatibility with flexible PV prefabricates, processability, and expected long-term stability.

The selected coatings, experimental testing and their performance are presented in section 3 Results and discussion.

2.4 Coating application methods

Coating techniques with potential compatibility for roll-to-roll processing were selected to enable integration into existing CIGS production lines. In this study, coatings were applied using mold casting, spray coating, doctor blade coating, and gravure coating.

The mold casting, even though unsuitable for the roll-to-roll processing [31,33], was employed as a laboratory-scale reference method, providing controlled film formation under static conditions. Spray coating was selected as best method for low viscosity coatings, and due to its flexibility, possibility of coating complex shape products and demonstrated potential for implementation in roll-to-roll environments [31,34].

Doctor blade coating was included as a technique directly compatible with roll-to-roll processing, offering well defined control over wet film thickness through parameters such as blade gap, coating speed, and coating viscosity [31]. Gravure coating method represents a fully industrialized roll-to-roll process and was investigated as a benchmark for high-throughput, continuous coating under conditions relevant to CIGS prefabricates manufacturing [31,35].

Together, these methods enable assessment of coating performance across deposition techniques with increasing relevance to integration into CIGS production lines.

2.5 Drying and/or curing processes

The coatings selected for this study required different curing strategies depending on their chemistry. UV curing was the preferred method due to its rapid curing kinetics and low thermal load, making it well suited for inline implementation. Thermal curing was the second preferred option, as it can also be relatively fast, is temperature-controlled, and can be applied inline in roll-to-roll processing. Process temperatures were limited to ≤150 °C to preserve CIGS functionality and minimize thermomechanical mismatch. Room temperature curing (drying) was considered the least favorable method due to inherently longer processing times. Nevertheless, this curing condition was required for certain coating systems.

2.6 Material performance

Coatings were initially evaluated immediately after application to assess wetting behavior. After complete curing, the state of both the coating and substrate, as well as adhesion, was assessed using a stepwise procedure. Visual inspection was performed first, followed by manual bending tests (with angles up to 60°) to evaluate whether the coatings could withstand mechanical deformation without delamination or cracking. Samples passing this test were subsequently subjected to accelerated aging using a pressure cooker test (PCT) (120 °C, 100% relative humidity, steam pressure >100 kPa) and damp heat (DH) test (85 °C, 85% relative humidity, 1000 hours, IEC 61215 standard). PCT was conducted in an in-house chamber with a stainless-steel mesh, 1 h exposure time was considered sufficient to identify weakly adhered coatings. After accelerated testing, samples were visually inspected for optical or adhesion

defects, including the state of the substrate and coating, and manual bending was repeated for coatings showing no visible delamination to confirm mechanical integrity.

3 Results and discussion

3.1 Selected coatings, application methods and curing processes

A set of fourteen commercially available coatings was selected as potential candidates for the barrier layer of flexible CIGS PV modules. Two of the coatings were further optimized in close collaboration with industrial partner, following detailed discussions of application-specific requirements from Table 1. and resulting in formulations optimized for the targeted barrier performance. The selected coatings were arranged into four groups according to their main component: acrylate, epoxy, polyurethane (PU) and silicone-based coatings. The complete list of tested coatings is provided in Table 2.

Application methods were selected based on the viscosity of each coating and are listed together with the curing mechanisms and conditions in Table 2. As mentioned previously, UV curing is the preferred method; however, the availability of transparent, UV-curable coatings suitable for outdoor applications is limited, and only two coatings met the requirements for this study. Both UV-curable coatings were acrylate-based and underwent curing through a photopolymerization mechanism. This process was initiated by photo-initiators incorporated into the formulation, which absorbed UV radiation and underwent photochemical cleavage to generate highly reactive free radicals. These radicals initiated the polymerizations of the acrylate functional groups, leading to extensive crosslinking and the formation of a three-dimensional polymer network [36].

Thermally assisted curing was carried out for the silicone, PU, and epoxy-based coatings, although the underlying curing mechanisms differ among these systems. Silicone coatings 1 and 3 cure via a platinum-catalyzed hydrosilylation (addition-cure) reaction, resulting in the formation of a crosslinked poly (dimethyl siloxane) (PDMS) network [37]. PU-based coatings cured through an addition reaction between isocyanate and hydroxyl (polyol) functional groups; in the presence of catalysts and/or elevated temperature, this reaction proceeds via step-growth polymerization, resulting in a crosslinked polymer network [38,39]. In contrast, epoxy-based coatings in general cure through reactions between epoxy monomers and co-monomers (hardeners) and/or initiators. Depending on the formulation, epoxy polymers may be formed via step-growth polymerization, chain polymerization, or a combination of both mechanisms [40]. As the materials used in this study were commercial-grade products and detailed formulation information was not provided by the suppliers, the specific curing mechanism in the epoxy coatings could not be conclusively identified.

Although prolonged room temperature (rT) drying is the least favorable curing approach, some PU coatings and silicone 2 fell into this category. Curing of silicone 2 was assisted by atmospheric humidity via a condensation-cure mechanism [41], however, the detailed curing chemistry was not disclosed by the supplier. The PU coatings here had different formulations, but followed the same curing mechanism as described above, except that curing occurred at

room temperature. Nevertheless, these coatings were applied to all substrate configurations and evaluated for their performance to assess their feasibility, with the understanding that curing parameters could be modified if necessary, for example by increasing the curing temperature, enhancing ventilation to accelerate solvent evaporation, or modifying the curing chemistry to a faster-curing system.

Table 2. Tested coating types, application methods, curing mechanisms and conditions.

Coating type	Number of components	Application methods	Curing mechanism	Curing conditions
acrylate 1	1	spray coating; gravure coating	photopolymerization	UV curing (<1 min)
acrylate 2	1	gravure coating	photopolymerization	UV curing (<1 min)
epoxy 1	2	mold casting	epoxy monomer crosslinking	24 h at rT
epoxy 2	2	mold casting	epoxy monomer crosslinking	12 h at 60 °C
PU 1	2	spray coating; gravure coating	addition polymerization	12 h at rT or 2 h at 60 °C
PU 2	2	spray coating; gravure coating	addition polymerization	10 h at rT or 3 h at 60 °C
PU 3	2	spray coating	addition polymerization	24 h at rT
PU 4	2	spray coating	addition polymerization	24 h at rT
PU 5	1	spray coating	humidity assisted addition	24 h at rT or 3 h at 65 °C
PU 6	3	spray coating; doctor blade	addition polymerization	24 h at rT
PU 7	2	mold casting; doctor blade	addition polymerization	4 h at 70 °C in the vacuum
silicone 1	2	mold casting; doctor blade	addition polymerization	48 h at rT or 35 min at 100 °C
silicone 2	2	mold casting; doctor blade	condensation reaction	48 h at rT
silicone 3	2	mold casting; doctor blade	addition polymerization	48 h at rT or 35 min at 120 °C

3.2 Applied and cured coatings

Visual inspection of the coated substrates was conducted both after coating application and after completion of the curing process. Three substrate configurations were coated with all investigated coatings: self-standing stainless-steel foil (configuration 2), stainless-steel foil with a SiO_x layer (configuration 3), and stainless-steel foil with CIGS cell layer stack (configuration 4). Additionally, to evaluate wetting quality and uniformity, copper busbars were added in configuration 4 to create variation in the surface profile. Prior to coating, all

substrates were cleaned with either ethanol or isopropanol to remove surface contaminants and promote optimal wetting of the coating materials.

Upon inspection, several challenges were observed across the different substrate types, as illustrated in Figure 2. Thorough surface cleaning and minimization of surface profile variations (e.g., through the use of thinner copper busbar tape) were found to be critical for achieving uniform coatings. Height variations across the substrate surface led to localized air entrapment during application, which compromised wetting and resulted in non-uniform coating layers. Maintaining a dust-free environment during coating application was also essential, as even minor particulate contamination disrupted coating continuity and uniformity.

Several coatings exhibited void formation within the layer, which was attributed to two main factors: the skin effect and air entrapment during coating preparation. The skin effect refers to the formation of a thin, partially cured surface layer before the underlying solvent has fully evaporated, thereby trapping solvent and generating microbubbles during curing [42]. Air entrapment, on the other hand, results from insufficient degassing of air bubbles introduced during the mixing of multi-component coatings. In some cases, these entrapped bubbles remained in the applied coating and evolved into voids upon curing. In addition, droplets formation of coating on the substrate surface were observed. These resulted from the mismatches between the surface tension of the substrate (or localized areas of it) and that of the applied coating, a phenomenon commonly referred to as coating dewetting [43]. This effect was particularly pronounced on substrates with SiOx layer (configuration 3) highlighting the sensitivity of the coating process to substrate-coating interactions.

Overall, the visual inspection highlighted the importance of substrate preparation, environmental control, and careful handling of the coating mixture in achieving defect-free, uniform layers. Following these observations, the coatings were evaluated by material group.

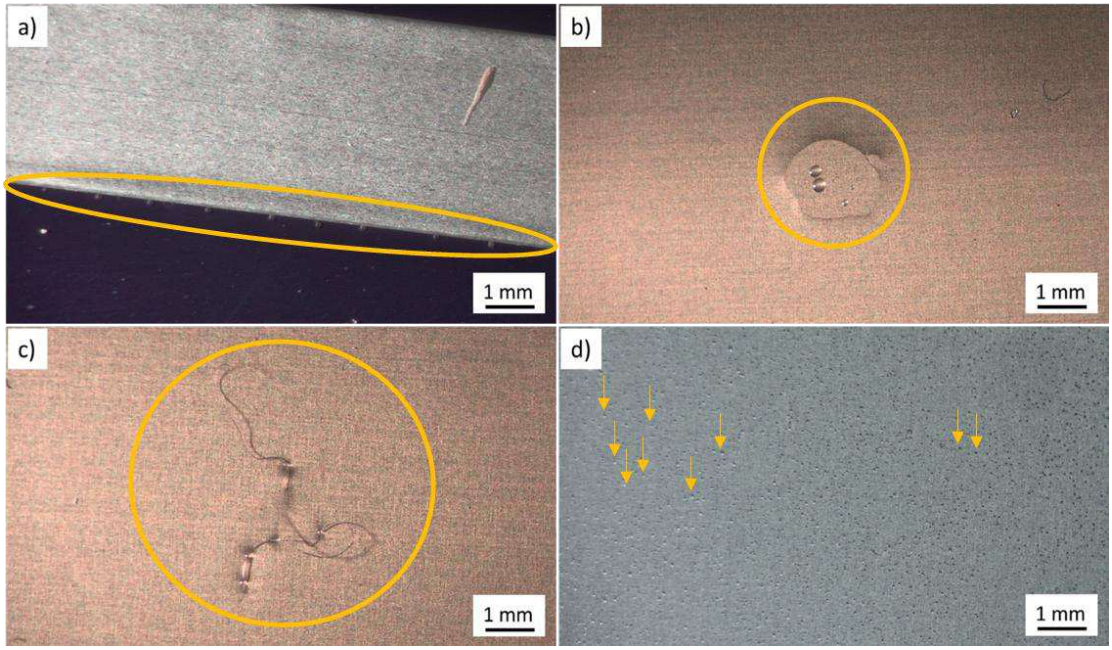

Figure 2. Coating defects after coating application: a) air bubbles near the busbar for spray coated samples (PU 1 and 6), b) dry spot due to improper cleaning (acrylate 1), c) entrapped dust particle, and d) micro voids over entire coating layer due to the skin effect (PU 3).

Acrylate-based coatings

For the UV-curable acrylates, spray coating and gravure coating were identified as the most suitable application methods. Acrylate 1 exhibited poor wetting on the SiOx layer, which is attributed to a mismatch in surface energy between the inorganic oxide surface and the organic acrylate formulation, resulting in pronounced droplet formation. Adequate wetting was observed only on the stainless-steel and ITO layers; however, even minimal surface contamination, resistant to ethanol and isopropanol cleaning, led to localized droplet formation, indicating a narrow and contamination-sensitive processing window. In contrast, acrylate 2 showed good initial wetting on all investigated substrates, but adhesion after UV curing was insufficient. Delamination occurred on all substrates during bending tests designed to simulate the mechanical stresses encountered in flexible PV module applications, suggesting inadequate interfacial bonding strength. Since a uniform and defect-free coating could not be reliably achieved with acrylate 1, and acrylate 2 failed to meet the adhesion requirements under mechanical loading, both materials were excluded from further investigation.

Epoxy-based coatings

Epoxy coatings 1 and 2 could be applied using doctor blade and casting methods. However, pronounced volumetric shrinkage during curing (>10%) generated significant internal stresses, leading to deformation of the substrates. Non-disclosable filler material provided by the supplier were incorporated into the formulations primarily to adjust viscosity and reduce water vapor transmission rates; it was further hypothesized that the presence of inert fillers could also mitigate dimensional change during curing. Despite this, no measurable reduction in shrinkage was observed, and dimensional changes during curing continued to induce substrate deformation. Consequently, both epoxy coatings were excluded from further testing.

PU-based coatings

With the exception of PU 7, the PU coating formulations exhibited lowest viscosity and could be applied by spray coating, doctor blade, or gravure coating, all of which are readily compatible with industrial roll-to-roll processing. In contrast, mold casting was the supplier-recommended application method for PU 7.

PU 2, a water-based formulation, was considered potentially risky due to the sensitivity of CIGS cells to water; nonetheless, it was tested to expand the dataset and to include a wider range of PU formulations. This coating was applied and cured without any defects and exhibited good initial adhesion to all substrates. The optimized PU 3 presented challenges during curing, as a pronounced skin effect led to microbubble entrapment within the coating,

as shown in Figure 2. d. Further optimization yielded PU 4, which could be successfully applied and cured without exhibiting these issues.

Substrate cleaning was critical for successful application of PU 1, 4, and 6, particularly on configurations incorporating a SiO_x layer, where dry spots were frequently observed. A similar sensitivity to substrate cleanliness was noted for PU 6 on bare stainless-steel substrates.

In addition to substrate preparation, the choice of application method strongly influenced coating quality for PU 1, 6, and 7. For PU 1 and 6, spray coating resulted in incomplete wetting and voids near copper busbars; these issues were resolved by implementing gravure or doctor blade coating, with optimized movement to allow the coating to fill surface profile variations. PU 7 proved to be the most challenging formulation to apply. Initial application via mold casting was difficult due to the high viscosity and slow flow behavior of the material, resulting in an uneven layer. As a two-component system, PU 7 required thorough mixing to achieve a homogeneous resin, which inevitably introduced air bubbles. The rapid curing behavior, with a pot life of less than 30 minutes, further limited the time available for bubble release, resulting in air entrapment within the cured layer. In collaboration with the supplier, attempts were made to optimize the viscosity using thinners; however, no alternative formulations were available. Application via doctor blade improved coating uniformity, and curing in a vacuum oven removed the majority of entrapped air, although small and micro-scale bubbles persisted. Despite these limitations, PU 7 was included in accelerated aging tests alongside the other PU coatings.

PU 5 was applied via spray coating onto all substrates without difficulty; however, after curing, an orange peel effect was observed on configuration 3. This defect, likely resulting from surface tension mismatches, could not be resolved for this configuration. Configurations 2 and 4 were nonetheless exposed to accelerated aging to evaluate adhesion on these substrates.

PU coatings with good initial adhesion and uniform coverage were selected for accelerated aging experiments to evaluate their stability under stress conditions. The flexibility of PU 7, along with its prior use in OLED encapsulation, regardless of present micro voids, made it the leading candidate. Therefore, configuration 1 (mini CIGS PV module prefabricate) was coated with PU 7 to assess its performance under accelerated aging.

Silicone-based coatings

Silicone-based coatings showed significant application and performance limitations. Doctor blade deposition was not feasible due to improper curing of the applied layer at low thicknesses and material overflow at higher blade gaps, restricting application to mold casting. Mold casting required extended preparation times and vacuum degassing both before and after application to remove entrapped air. All three silicone formulations exhibited poor initial adhesion, as cured layers could be manually peeled from all substrates. The use of a supplier-recommended primer significantly improved adhesion for silicone 1 and silicone 2, whereas no compatible primer was available for silicone 3, which was excluded from further testing. In addition, complete curing of silicone 1 and 2 was only possible for layer thicknesses exceeding

500 µm. Due to excessive coating thickness, complex processing, and limited applicability, silicone-based coatings were excluded from further evaluation.

3.3 Accelerated aged coatings

PU coated samples passing initial inspection were subjected to accelerated aging using either PCT or DH test. After accelerated aging, samples were visually inspected for optical or adhesion defects, including the state of the substrate and coating, and manual bending was repeated for coatings showing no visible delamination to confirm mechanical integrity.

Delamination of weakly adhered coatings was already evident after 1 h in the PCT; the films began to wrinkle, warp, or detach completely from the substrates. PU 1 and PU 2 coatings delaminated from all substrate types. PU 4 delaminated from configurations 3 and 4, PU 6 delaminated from configuration 3. An example of samples after 1 h in the PCT is shown in Figure 3., where the difference in adhesion of PU 6 on configuration 2 (good adhesion) compared with configuration 3 (weak adhesion) is clearly visible. All other samples retained good adhesion. The only observable change in optical properties occurred for PU 2, which developed a hazy appearance. This effect is most likely attributable to water absorption at the inner side of the coating following loss of adhesion to the substrate, potentially caused by insufficient curing.

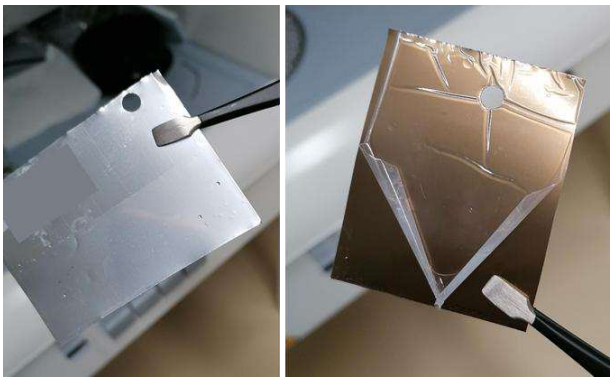

Figure 3. Samples with PU 6 coating on the stainless-steel (left) and SiOx (right) substrates after 1 h in PCT.

Coating-substrate combinations that exhibited weak adhesion after the PCT were excluded from DH exposure, with the exception of PU 4 and 6. PU 4 and 6 were intentionally subjected to DH exposure to determine the time required for a similar degradation behavior to occur. Exposure to 85 °C and 85% relative humidity led to progressive degradation of several PU coatings, with effects varying depending on coating type and substrate. After 250 h, only visual inspection of the samples was performed, revealing initial degradation characterized by spider-web-like wrinkling initiating from the corners for PU 4 on configurations 3 and 4, as well as for PU 6 on configuration 3 (see Figure 4.). This wrinkling resulted from localized coating delamination, which created tunnel-like pathways for humidity ingress and thereby accelerated further delamination propagating deeper along the coating–substrate interface. In addition, pronounced yellowing was observed for PU 5, while all other combinations remained unchanged.

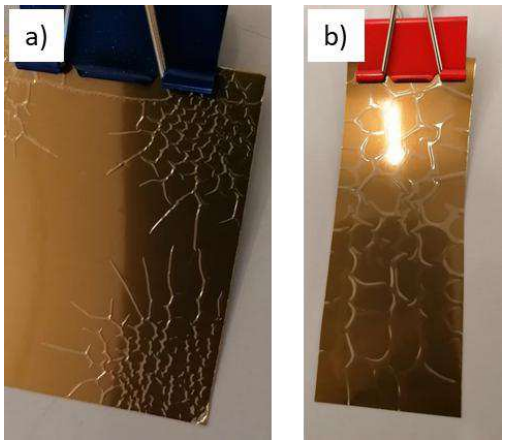

Figure 4. Spider web-like delamination formation on a configuration 3 coated with a) PU4 and b) PU 6 after 250 of DH exposure.

Further exposure to DH resulted in continued expansion of the spider-web-like wrinkling and increased yellowing of the PU 5 coatings, while PU 7 began to show signs of yellowing after approximately 500 h. After 1000 h, the spider-web-like wrinkling had spread across the entire surface of PU 4 on configurations 3 and 4, and PU 6 had completely delaminated from configuration 3 (see Figure 5.). PU 6 demonstrated good adhesion and compatibility with the stainless-steel substrate and the ITO layer of the CIGS stack, showing no signs of yellowing. PU 4 exhibited good adhesion only on stainless-steel and likewise showed no yellowing. In contrast, PU 7 and PU 5 did not delaminate on any substrate but showed yellowing after DH exposure, which was more pronounced for PU 5.

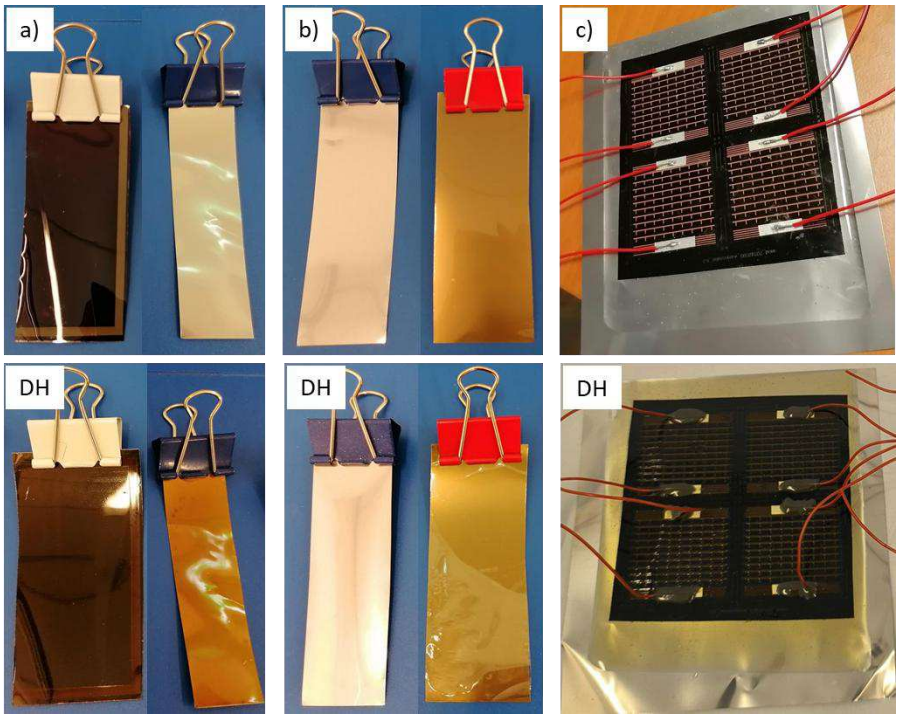

Figure 5. Coated samples before and after 1000 h in DH conditions: a) PU 5 on configuration 2 and 4 (yellowing of the coating); b) PU 6 on configuration 2 (no delamination) and configuration 3 (fully delaminated); c) PU 7 on mini CIGS PV module prefabricate (yellowing of the coating).

Since the coatings investigated in this study were of commercial grade, the exact polymer chemistry, additive content, and stabilizer formulations were not disclosed and are therefore beyond the scope of this work. Consequently, only interpretations based on observations reported in the literature are provided. Yellowing of polyurethane coatings is a well-known phenomenon, typically resulting from polymer oxidation which can be accelerated by UV exposure, elevated temperature, humidity, or a combination of these factors [44]. This effect is commonly mitigated through the inclusion of antioxidants [44]; however, in some of the coatings studied here, a low concentration (PU 7) or absence (PU 5) of such stabilizers likely contributed to the observed yellowing.

Adhesion of PU coatings is strongly influenced by both the polymer chemistry and the substrate. PUs containing a high density of functional groups generally exhibit strong adhesion, whereas non-polar, short-chain PUs tend to adhere less strongly, particularly if they are susceptible to hydrolytic degradation [45]. Selecting PU formulations with a higher density of reactive functional groups, likely the case for the more robust PUs in this study, can therefore enhance adhesion and overall reliability under environmental stressors such as heat and humidity.

3.4 Rating of the coatings

A summary of observations and ranking for all tested coatings with respect to their suitability for flexible CIGS module encapsulation is provided in Table 3. The application column combines results of coating preparation, component mixing, the state of the coating after preparation, wetting behavior, and the suitability of the chosen deposition method. On the other hand, the curing process was graded qualitatively as slow, fast, or relatively slow, with any additional post-curing changes also noted. Initial adhesion was assessed as weak or good, while the impact of accelerated aging was evaluated in terms of optical changes and adhesion degradation. Based on these criteria, a total ranking was assigned, categorizing coatings as either unfit (does not meet minimum requirements) or partially suitable (meets some criteria, but requires further testing). None of the coatings fully met all requirements, reflecting both the stringent testing conditions and the complexity of encapsulation requirements for flexible CIGS. As previously noted, the DH accelerated aging conditions employed here may be overly severe for the materials studied. Observed changes, including loss of adhesion and yellowing, might not occur in products intended for short-term use. Consequently, aging conditions should be adapted to avoid overstressing the coatings and overestimating the real impact of environmental exposure. Furthermore, with additional development and formulation optimization, acrylate 2 may achieve better initial adhesion and the addition of anti-oxidative additives could prevent yellowing in PU 5. Overall, substantial potential remains for adaptation and optimization of the coatings presented here. Encapsulation via coating appears to be a promising approach and should be further investigated.

Table 3. Summary of observations and ranking according to suitability for flexible CIGS encapsulation.

Coating	Application (wetting + R2R fit)	Curing process + observations	Initial adhesion	Aging impact	Ranking
acrylate 1	Droplet formation	-	-	-	unfit
acrylate 2	Uniform wetting + R2R	Fast	Weak	-	unfit
epoxy 1	Uniform wetting + Mold casting	Dimensional change	-	-	unfit
epoxy 2		Dimensional change	-	-	unfit
PU 1	Uniform wetting + R2R	Relatively slow	Good	Adhesion loss	unfit
PU 2		Relatively slow	Good	Adhesion loss	unfit
PU 3		Slow + skin effect	-	-	unfit
PU 4		Slow	Good	Reduced adhesion	Partially suitable
PU 5		Slow + orange peel	Good	Strong yellowing	unfit
PU 6		Slow	Good	Reduced adhesion	Partially suitable
PU 7	Microbubbles + R2R	Relatively slow + vacuum	Good	Yellowing	Partially suitable
silicone 1	Mold casting + thick layer	Relatively slow	Primer needed	-	unfit
silicone 2		Slow	Primer needed	-	unfit
silicone 3		Relatively slow	Weak	-	unfit

4 Conclusions

A set of fourteen commercially available coatings was evaluated as potential barrier layers for flexible CIGS PV modules. The coatings were grouped according to their main component: acrylate, epoxy, PU, and silicone-based materials. Application methods were chosen based on coating viscosity and included mold casting, spray coating, doctor blade, and gravure coating. UV curing was preferred due to its rapid kinetics, followed by thermal curing (≤150 °C), while rT drying was used only when required by specific formulations.

Initial inspections revealed that acrylate, epoxy, and silicone coatings exhibited poor uniformity, adhesion issues, or caused excessive substrate deformation. In contrast, PU coatings showed formulation-dependent differences in application and adhesion. Most PUs could be applied uniformly using doctor blade or gravure coating, whereas PU 7 required careful mixing and vacuum curing to minimize entrapped air resulting from rapid curing and high viscosity. Substrate preparation was critical for achieving good adhesion, particularly for

PU 1, 4, and 6 on SiO_x-containing configurations. Overall, only the PU coatings were found suitable for further evaluation.

Coatings with weak initial adhesion delaminated rapidly under PCT, with delamination observed already after 1 h. Contrary, under DH exposure, degradation developed more gradually, with spider-web-like wrinkling, delamination and yellowing occurring over several hundred hours. PU 6 and PU 4 showed the best overall combination of adhesion and optical stability. These results demonstrate that PCT provides a rapid screening method for coating-substrate compatibility, whereas DH testing is necessary to evaluate slower aging phenomena, including optical changes.

While this study focused solely on damp heat exposure, comprehensive assessment of coating performance will require additional environmental stressors. Future work should include thermal cycling to evaluate thermomechanical effects and UV exposure to assess photochemical stability, providing a more complete understanding of coating durability and optimal coating-substrate combinations. However, aging conditions should be adapted to avoid overstressing the coatings and overestimating the real impact of environmental exposure. As functional modules were not tested due to limited availability and variations in the CIGS layer stack and module efficiency, the effect of coatings on fully operational modules will be addressed in future studies by Sunplugged, who will evaluate the most promising PU materials identified in this study.

Acknowledgement

The authors gratefully acknowledge Elisabeth Reiser and KANSAI HELIOS Austria GmbH (ex Rembrandtin Coatings GmbH) for their contributions to the optimization of coatings and assistance with coating application. The authors also acknowledge the companies that supplied cost-free coatings investigated in this study: Akzo Nobel N.V. (Awlgrip, Poland), bto-epoxy GmbH (Austria), Dow Silicones (Belgium), ROARTIS bvba (Belgium) and Synthene SAS (France).

Funding source

The research work presented in this study was performed at the Polymer Competence Center Leoben, Austria. The study was conducted as a part of the project “SOPHOKLES”, which is supported under the umbrella of “Stadt der Zukunft” funded by Austrian Research Promotion Agency (FFG) [43693964].

This research project (grant number: 911658) was funded by COMET – Competence Centers for Excellent Technologies – through BMIMI, BMWET, and the co-financing federal provinces (Styria through SFG, Upper Austria, Vorarlberg) and carried out with the participation of scientific and company partners. The COMET program is managed by FFG.

References

[1] VDMA e.V. Photovoltaics Equipment (Ed.), International Technology Roadmap for Photovoltaics (ITRPV): 16th Edition 2025, 2025.

[2] J.R. Angulo, A. Berastain, L.A. Conde, A. Carhuavilca, V. Pleshcheva, J. Montes-Romero, M.A. García, V. Campos-Falcon, A. Montoya, W. Gosgot, E. Coaquira, P. Puma, E. Alfaro, R.J. Vidal, N.J. Beltran, L. Chirinos, M. Cataño, R. Condori, E. Palo-Tejada, M. Barrena, C.A. Polo, R. Espinoza, E. Muñoz-Cerón, J. de La Casa, J.A. Töfflinger, Yield and performance analysis of PERC, HIT, and CIGS photovoltaic systems in five Peruvian city-climates, J. Sol. Energy 304 (2026) 114204. https://doi.org/10.1016/j.solener.2025.114204.

[3] M.A. Green, E.D. Dunlop, J. Hohl-Ebinger, M. Yoshita, N. Kopidakis, A.W. Ho-Baillie, Solar cell efficiency tables (Version 55). Progress in Photovoltaics: Research and Applications, 2020. https://onlinelibrary.wiley.com/doi/full/10.1002/pip.3228 (accessed 22 September 2025).

[4] K.R. Kumbhar, R.S. Redekar, A.B. Raule, P.M. Shirage, J.H. Jang, N.L. Tarwal, Predictive modeling and optimization of CIGS thin film solar cells: A machine learning approach, J. Sol. Energy 294 (2025) 113509. https://doi.org/10.1016/j.solener.2025.113509.

[5] Y.-C. Wang, T.-T. Wu, Y.-L. Chueh, A critical review on flexible Cu(In, Ga)Se2 (CIGS) solar cells, Mater. Chem. Phys. 234 (2019) 329–344. https://doi.org/10.1016/j.matchemphys.2019.04.066.

[6] F. Kessler, D. Rudmann, Technological aspects of flexible CIGS solar cells and modules, J. Sol. Energy 77 (2004) 685–695. https://doi.org/10.1016/j.solener.2004.04.010.

[7] M. Powalla, W. Witte, P. Jackson, S. Paetel, E. Lotter, R. Wuerz, F. Kessler, C. Tschamber, W. Hempel, D. Hariskos, R. Menner, A. Bauer, S. Spiering, E. Ahlswede, T.M. Friedlmeier, D. Blazquez-Sanchez, I. Klugius, W. Wischmann, CIGS Cells and Modules With High Efficiency on Glass and Flexible Substrates, IEEE J. Photovoltaics 4 (2014) 440–446. https://doi.org/10.1109/JPHOTOV.2013.2280468.

[8] Mario Pagliaro, Giovanni Palmisano, Rosaria Ciriminna, Flexible Solar Cells, WILEY-VCH, 208.

[9] C. Zhang, T. Qi, W. Wang, C. Zhao, S. Xu, M. Ma, Y. Feng, W. Li, M. Chen, C. Yang, W. Li, High efficiency CIGS solar cells on flexible stainless steel substrate with SiO2 diffusion barrier layer, J. Sol. Energy 230 (2021) 1033–1039. https://doi.org/10.1016/j.solener.2021.11.006.

[10] M.G. Faraj, K. Ibrahim, A. Salhin, Investigation of CIGS Solar Cells on Polyethylene Terephthalate Substrates, Int. J. Polym. Mater. 60 (2011) 817–824. https://doi.org/10.1080/00914037.2010.551363.

[11] T. Nakada, T. Kuraishi, T. Inoue, T. Mise, CIGS thin film solar cells on polyimide foils, in: 2010 35th IEEE Photovoltaic Specialists Conference, Honolulu, HI, USA, IEEE, 20.06.2010 - 25.06.2010, pp. 330–334.

[12] A. Gerthoffer, F. Roux, F. Emieux, P. Faucherand, H. Fournier, L. Grenet, S. Perraud, CIGS solar cells on flexible ultra-thin glass substrates: Characterization and bending test, Thin Solid Films 592 (2015) 99–104. https://doi.org/10.1016/j.tsf.2015.09.006.

[13] A.M. Amare, I. Hwang, I. Jeong, J.H. Park, J.G. An, S. Song, Y.-J. Eo, A. Cho, J.-S. Cho, S.K. Ahn, S. Ahn, J. Gwak, M. Rehan, H. Park, J.H. Yun, K. Kim, D. Shin, High-efficiency cadmium-free Cu(In,Ga)Se2 flexible thin-film solar cells on ultra-thin glass as an emerging substrate, J. Alloys Compd. 1024 (2025) 180187. https://doi.org/10.1016/j.jallcom.2025.180187.

[14] Ankit Singh, Recent Advancements in Thin-Film Solar Modules, 2025. https://www.azocleantech.com/article.aspx?ArticleID=1986 (accessed 12 January 2026.).

[15] A. Ali, K. Singh, D.N. Thalakotuna, K.P. Esselle, A Solar Cell Integrated Antenna for on-the-Move IoT Applications, in: 2025 19th European Conference on Antennas and Propagation (EuCAP), Stockholm, Sweden, IEEE, 2025, pp. 1–5.

[16] B. Li, B. Hou, G.A.J. Amaratunga, Indoor photovoltaics, The Next Big Trend in solution-processed solar cells, InfoMat 3 (2021) 445–459. https://doi.org/10.1002/inf2.12180.

[17] Michael Gumm, The advantages of †exible thin-†lm solar modules, 2016. https://miasole.com/wp-content/uploads/2015/05/The-advantages-of-flexible-thin-film-solar-modules.pdf.
[18] N. Adamovic, A. Zimmermann, A. Caviasca, R. Harboe, F. Ibanez, 2017. Custom designed photovoltaic modules for PIPV and BIPV applications. J. Renewable Sustainable Energy 9, 021202. https://doi.org/10.1063/1.4979820.
[19] H. A Kim, J.H. Baeg, J. Shin, J. Park, S. Lee, Effect of Damp Heat on the Performance Degradation of Flexible CIGS Photovoltaic Modules, Int J Adv Tech 09 (2018). https://doi.org/10.4172/0976-4860.1000200.
[20] J.S. Britt, E. Kanto, S. Lundberg, M. Beck, CIGS Device Stability on Flexible Substrates, in: 2006 IEEE 4th World Conference on Photovoltaic Energy Conference, Waikoloa, HI, IEEE, 2006, pp. 352–355.
[21] C. Han, Analysis of moisture-induced degradation of thin-film photovoltaic module, Sol. Energy Mater. Sol. Cells 210 (2020) 110488. https://doi.org/10.1016/j.solmat.2020.110488.
[22] N. Rin, C. Han, Lifetime prediction method for moisture-induced degradation of glass-to-glass solar cell modules using spatially distributed diode model, Sol. Energy Mater. Sol. Cells 225 (2021) 111052. https://doi.org/10.1016/j.solmat.2021.111052.
[23] P. Christöfl, C.G.M. van Kessel, M.M. Koetse, D. Roosen, G. Rigamonti, G. Oreski, 2026. Evaluation of Polyolefin Encapsulants for Roll-to-Roll Lamination Applications. Progress in Photovoltaics: Research and Applications, under revision.
[24] BougeRV, BougeRV Yuma 200W CIGS Thin-film Flexible Solar Panel with Pre-Punched Holes. https://uk.bougerv.com/products/yuma-200w-cigs-flexible-solar-panel-with-holes (accessed 14 January 2026).
[25] MiaSole, FLEX-N Series. https://miasole.com/products/ (accessed 14 January 2026).
[26] G. Griffini, S. Turri, Polymeric materials for long-term durability of photovoltaic systems, J. Appl. Polym. Sci. 133 (2016). https://doi.org/10.1002/app.43080.
[27] K. Aitola, G. Gava Sonai, M. Markkanen, J. Jaqueline Kaschuk, X. Hou, K. Miettunen, P.D. Lund, Encapsulation of commercial and emerging solar cells with focus on perovskite solar cells, Sol. Energy 237 (2022) 264–283. https://doi.org/10.1016/j.solener.2022.03.060.
[28] E.Y. Choi, J. Kim, S. Lim, E. Han, A.W. Ho-Baillie, N. Park, Enhancing stability for organic-inorganic perovskite solar cells by atomic layer deposited Al2O3 encapsulation, Sol. Energy Mater. Sol. Cells 188 (2018) 37–45. https://doi.org/10.1016/j.solmat.2018.08.016.
[29] S.-T. Zhang, M. Guc, O. Salomon, R. Wuerz, V. Izquierdo-Roca, A. Pérez-Rodríguez, F. Kessler, W. Hempel, T. Hildebrandt, N. Schneider, Effective module level encapsulation of CIGS solar cells with Al2O3 thin film grown by atomic layer deposition, Sol. Energy Mater. Sol. Cells 222 (2021) 110914. https://doi.org/10.1016/j.solmat.2020.110914.
[30] L.C. Olsen, M.E. Gross, G.L. Graff, S.N. Kundu, X. Chu, S. Lin, Approaches to encapsulation of flexible CIGS cells, in: Reliability of Photovoltaic Cells, Modules, Components, and Systems, San Diego, CA, SPIE, 2008, 70480O.
[31] F.C. Krebs, Fabrication and processing of polymer solar cells: A review of printing and coating techniques, Sol. Energy Mater. Sol. Cells 93 (2009) 394–412. https://doi.org/10.1016/j.solmat.2008.10.004.
[32] Shravan Chunduri, New Silicones With High Durability For BIPV: Estimating To Match The Life Of Other Building Components Of 50 Years, Dow Is Promoting New Silicone Based Encapsulation Solution For BIPV, 2022. https://taiyangnews.info/technology/new-silicones-with-high-durability-for-bipv (accessed 12 January 2026).
[33] K. Foroutani, S. Khademi, S. Sharafkhani, A. Enayati-Gerdroodbar, N. Afsarimanesh, A. Zolfagharian, M. Salami-Kalajahi, B. Pourabbas, Conducting Polymer-Based Coatings and Thin

Films: A Review on Film Processing and Deposition Techniques, Polym. Rev. 65 (2025) 1057–1100. https://doi.org/10.1080/15583724.2025.2511828.
[34] F. Aziz, A.F. Ismail, Spray coating methods for polymer solar cells fabrication: A review, Mater. Sci. Semicond. Process. 39 (2015) 416–425. https://doi.org/10.1016/j.mssp.2015.05.019.
[35] S.A. Mauger, K.C. Neyerlin, A.C. Yang-Neyerlin, K.L. More, M. Ulsh, Gravure Coating for Roll-to-Roll Manufacturing of Proton-Exchange-Membrane Fuel Cell Catalyst Layers, J. Electrochem. Soc. 165 (2018) F1012-F1018. https://doi.org/10.1149/2.0091813jes.
[36] E. Rossegger, R. Höller, D. Reisinger, M. Fleisch, J. Strasser, V. Wieser, T. Griesser, S. Schlögl, High resolution additive manufacturing with acrylate based vitrimers using organic phosphates as transesterification catalyst, Polímeros 221 (2021) 123631. https://doi.org/10.1016/j.polymer.2021.123631.
[37] Z. Brounstein, J. Zhao, D. Geller, N. Gupta, A. Labouriau, Long-Term Thermal Aging of Modified Sylgard 184 Formulations, Polymers 13 (2021). https://doi.org/10.3390/polym13183125.
[38] M.F. Sonnenschein, Polyurethanes: Science, technology, markets, and trends, Second edition, Wiley, Hoboken, 2020.
[39] Charles R. Hegedus, Andrew G. Gilicinski, Robert J. Haney, Film Formation Mechanism of Two-Component Waterborne Polyurethane Coatings, Journal of Coatings Technology 68 (1996).
[40] J.-P. Pascault, R.J.J. Williams, General Concepts about Epoxy Polymers, in: J.-P. Pascault, R.J.J. Williams (Eds.), Epoxy Polymers, Wiley, 2010, pp. 1–12.
[41] F. Gubbels, An overview of the chemistry of condensation curing silicone sealants and adhesives, International Journal of Adhesion and Adhesives 132 (2024) 103728. https://doi.org/10.1016/j.ijadhadh.2024.103728.
[42] S. Arai, M. Doi, Skin formation and bubble growth during drying process of polymer solution, Eur. Phys. J. E Soft Matter 35 (2012) 57. https://doi.org/10.1140/epje/i2012-12057-2.
[43] P. Samyn, M. Biesalski, O. Prucker, J. Rühe, 2019. Dewetting and photochemical crosslinking of adhesive pads onto lithographically patterned surfaces. J Appl Polym Sci 136, 47321. https://doi.org/10.1002/app.47321.
[44] P. Scholz, V. Wachtendorf, A.-M. Elert, J. Falkenhagen, R. Becker, K. Hoffmann, U. Resch-Genger, H. Tschiche, S. Reinsch, S. Weidner, Analytical toolset to characterize polyurethanes after exposure to artificial weathering under systematically varied moisture conditions, Polym. Test. 78 (2019) 105996. https://doi.org/10.1016/j.polymertesting.2019.105996.
[45] I. Mantis, K.K. Gupta, R. Ambat, Evaluating polyurethane coatings for corrosion protection of electronics under humidity exposure, Corros. Commun. (2025). https://doi.org/10.1016/j.corcom.2025.03.005.

5.5 Publication IV

Title: Effects of Manufacturing Process History and the Lamination Duration on Thermomechanical Properties of PV Encapsulants

Journal: Advanced Energy and Sustainability Research

Date of submission: 5th of May 2026

	Share in %				Total
	Author	Co-authors			
	PhD Student	1	2	3	
Conceptualization	70	10		20	100
Methodology	70	20		10	100
Formal analysis	90	10			100
Investigation	90	10			100
Visualization	80	20			100
Data curation	80	20			100
Writing - original draft	90	10			100
Writing - review & editing		30	20	50	100
Resources				100	100
Supervision			10	90	100
Project administration				100	100
Funding acquisition				100	100

Author, PhD Student: Nikolina Pervan

Co-author 1: Jutta Geier

Co-author 2: Michael Daenen

Co-author 3: Gernot Oreski

Effects of Manufacturing Process History and the Lamination Duration on Thermomechanical Properties of PV Encapsulants

Nikolina Pervan[1, 2, 3], Jutta Geier[1, 2], Michael Daenen[3, 4, 5], Gernot Oreski[1, 2]

[1] Polymer Competence Center Leoben GmbH (PCCL), Sauraugasse 1, 8700 Leoben, Austria
[2] Chair of Materials Science and Testing of Polymers, Technical University of Leoben, Otto Glöckel-Strasse 2, 8700 Leoben, Austria
[3] UHasselt, Institute for Materials Research (IUMAT), Martelarenlaan 42, B-3500 Hasselt, Belgium
[4] imec, IUMAT, Thor Park 8320, B-3600 Genk, Belgium
[5] EnergyVille, IUMAT, Thor Park 8320, B-3600 Genk, Belgium

Abstract

Encapsulants are vital for the structural integrity and protection of photovoltaic (PV) modules, yet the impact of processing history and crosslinking on their thermomechanical behaviour is often oversimplified in numerical simulations. This study experimentally investigates how lamination conditions affect six encapsulant types, including crosslinking (EVA, POE), non-crosslinking (TPO), and co-extruded (EPE) materials. The degree of crosslinking was characterized using differential scanning calorimetry (DSC) and Fourier transform infrared spectroscopy (FTIR), while thermomechanical properties were assessed via digital image correlation. Results indicate that conventional DSC-based methods, while standard for EVA, have significant limitations when applied to complex or multi-layer encapsulants. Conversely, FTIR-ATR combined with principal component analysis (PCA) proved to be an effective, rapid method for assessing crosslinking. The findings reveal that manufacturing history strongly influences pre-lamination behaviour, even within the same polymer family. Increased lamination duration drives encapsulants toward more isotropic coefficients of thermal expansion (CTE), with non-crosslinking materials reaching stability faster. These results emphasize that using realistic post-lamination properties in finite element modelling is essential, as simplified assumptions can lead to significant errors in predicted stress behaviour. Accurate material characterization is therefore crucial for improving PV module reliability assessments.

Key words

PV encapsulants, EPE, crosslinking degree, thermomechanical behaviour, CTE

1. Introduction

With the continuous rise in photovoltaic (PV) module installations, the decrease of module prices, and the rapid evolution of solar cell technologies, material selection within the PV module stack continues to be a critical factor for its long-term reliability [1–6]. According to ITRPV, performance warranties are extending toward 30 years, while module architectures and bill of materials are undergoing significant transitions [1] without the knowledge on long-term performance of the new module designs. In particular, the industry is moving from glass/backsheet to glass/glass module designs, from p-type to n-type, perovskite and silicone-perovskite tandem solar cells, and from the long-established ethylene vinyl acetate (EVA) encapsulant toward alternative materials such as polyolefin (POE), thermoplastic polyolefin (TPO), and co-extruded EVA-POE-EVA (EPE) encapsulants [1,2,7,8]. These developments place new demands on the performance and stability of polymeric materials used in PV modules. For instance, n-type and perovskite solar cells exhibit sensitivity to moisture, while in glass-free PV designs the moisture barrier often needs to be further supported by the encapsulant layer [9–13]. In addition, perovskite and tandem devices can be prone to delamination during or after lamination due to mismatches in thermomechanical properties [14,15]. Alongside these technical challenges, cost pressure has also driven the development and adoption of alternative encapsulant materials, such as EPE [7].

Encapsulants play a central role in the mechanical and structural integrity of PV modules. Beyond providing optical coupling and electrical insulation, they embed and connect solar cells with the rest of the stack, reduce moisture ingress and minimize transfer of the stresses between module components induced by environmental loading [16,17]. Among all components in a glass/glass PV module, the encapsulant is the only soft, polymeric layer and therefore largely governs how the module responds to thermal and mechanical loads. Daily and seasonal thermal cycling leads to repeated expansion and contraction of the PV stack components, resulting in stresses caused by coefficient of thermal expansion (CTE) mismatches between glass, solar cells, interconnects, and polymer layers [18,19]. While the glass layer in conventional modules helps constrain dimensional changes of the encapsulants in the stack, the situation is different for flexible, lightweight, or glass-free integrated PV module designs. In these cases, even relatively small expansion or contraction of the polymer layers may lead to larger warping or deformation of the module. If not properly managed, these stresses can contribute to failure modes such as solar cell cracking, solder joint fatigue, delamination, and in the case of mechanically sensitive technologies such as perovskites, solar cell layer delamination and device failure [14,15,19–22].

Thermomechanical behaviour of polymers has been extensively studied in other technological fields, including automotive, microelectronics, packaging, and medical applications [23–32]. In contrast, experimental investigations focusing on the thermomechanical properties of PV polymeric components, including encapsulants, remain limited [33–38]. Many studies addressing thermomechanical effects in PV modules rely primarily on numerical simulations, in which encapsulant behaviour is often simplified to facilitate modelling, or sometimes even ignored [39]. Common assumptions include linear elastic material behaviour and often assumed constant CTE at 270 ppm over broad temperature ranges, frequently based on EVA

as a reference material [40–46]. While researchers introduced viscoelastic material descriptions to better capture encapsulants behaviour [36,42,47], constant CTE values are still widely used. As a result, simulated stress states may deviate significantly from experimentally observed behaviour. Furthermore, the influence of manufacturing processing history of encapsulants is fully neglected. In reality, the thermomechanical response of polymer materials is strongly influenced by their processing history [26]. However, systematic experimental studies addressing the impact of encapsulant processing history on thermomechanical properties are scarce [48]. Polymer morphology, crystallinity, and dimensional stability are affected by manufacturing conditions (extrusion temperature and speed, stretching in both machine and transverse direction, speed of cooling down, annealing process) prior to lamination [24,26,33,49]. These factors determine the initial material state entering the PV module and may significantly alter expansion and contraction behaviour during the lamination process.

On the other hand, lamination temperature, pressure, dwell time, and cooling conditions determine the extent to which initial processing history is overwritten and new polymer networks and chain orientations are formed [34]. These parameters are of great importance for minimizing residual stresses which can impact PV module reliability during operation [44,50]. For crosslinking encapsulants, the degree of crosslinking represents an additional impacting parameter on encapsulants properties in the PV module. Previous studies have demonstrated methods for determining the degree of crosslinking [51–62] and the importance of its impact on adhesion, discoloration, corrosion, and potential-induced degradation in PV modules [50,63–67]. In contrast, the influence of the degree of crosslinking on thermomechanical properties, particularly on CTE behaviour, has received little attention [68]. On top of that, for non-crosslinking encapsulants such as TPO, the absence of a defined curing reaction raises fundamental questions regarding how sufficient lamination conditions should be defined to ensure long-term reliability.

This work addresses mentioned gaps by experimentally investigating the effect of processing history and lamination duration on the thermomechanical properties of PV encapsulants. A total of six encapsulant materials, including crosslinking EVA, two crosslinking POE types, a non-crosslinking TPO and two co-extruded EPE, were studied under multiple lamination conditions. The degree of crosslinking was characterized using destructive (differential scanning calorimetry) and non-destructive (Fourier transform infrared spectroscopy) techniques, and thermomechanical behaviour was assessed using digital image correlation. By systematically separating the effects of processing history and lamination conditions, this study provides experimental insight into encapsulant thermomechanical behaviour relevant to current and emerging PV module technologies.

2. Materials and methods

The experimental investigation was carried out on six commercially available PV encapsulant materials, produced by different manufacturers. The encapsulants are referred to anonymously throughout the text to avoid bias or brand-specific interpretation. The study included an industry-standard EVA, followed by two crosslinking POEs, one non-crosslinking

TPO, and two EPE encapsulants. The two EPE encapsulant differed with their polyolefin core type, EPE- 1 had a non-crosslinking and the EPE- 2 crosslinking polyolefin core. For each encapsulant type, a roll of approximately 10 m in length was available. From each roll, two specimens with dimensions of 20 x 20 cm^2 were cut from random positions along the roll length, in order to account for potential in-roll material variability. The degree of crosslinking and thermomechanical properties of all encapsulants were investigated in both unlaminated (uncured) and laminated (cured) states.

Lamination of single encapsulant sheets was performed by placing the material between two 2 mm thick glass plates. A non-stick polytetrafluoroethylene (Teflon®) mat was used between the glass and encapsulant layers to prevent adhesion (see Figure 1). Thickness control spacers were employed to avoid edge pinching effects during lamination. Cooling was performed within the glass stack to limit deformation of the encapsulant during cooling, thereby approximating the material state post-cooling as close as to one within a PV module. An overview of the investigated materials and lamination parameters is provided in Table 1.

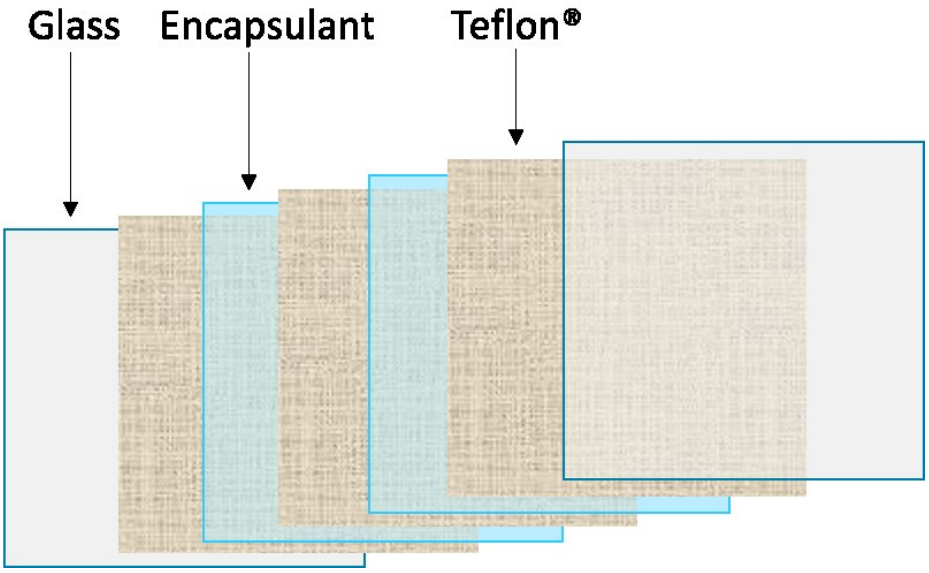

Figure 1. Representative scheme of the laminated layer stack including glass, Teflon® and encapsulant.

Table 1. Encapsulant materials and lamination conditions.

Encapsulant	Polymer type	Crosslinking chemistry	Lamination conditions
EVA	ethylene vinyl acetate	peroxides	**Evacuation step** at 135 °C (110 °C for TPO) for 4 minutes. **Lamination step** at 150 °C (155 °C for EVA; 135 °C for TPO) for 2, 5, 10, 12, 15, 20 and 30 minutes.
POE-1	ethylene α-olefin	peroxides	
POE-2	ethylene α-olefin	peroxides	
TPO	ethylene ethyl acrylate	non-crosslinking	
EPE-1	EVA - ethylene acrylate copolymer - EVA [8]	peroxides for EVA layers	
EPE-2	EVA - ethylene α-olefin - EVA [8]	peroxides	

2.1 Differential Scanning Calorimetry (DSC)

Differential scanning calorimetry (DSC) was performed using a DSC 4000 from PerkinElmer Inc. to measure thermograms of encapsulants. Approximately 7 mg of each material was placed in an aluminium pan with perforated lid. For each material, three measurements were performed, and the average of these measurements was used for the calculations. DSC measurements were carried out in accordance with IEC 62788-1-6:2017 for the combined enthalpy and melt/freeze method [69]. According to this standard, the degree of crosslinking of EVA-based encapsulants can be determined from the residual curing enthalpy and from changes in the crystallization behaviour. In the work of [62] the method was proven to be suitable for determination of crosslinking degrees of POE encapsulants. In the present study, the same methodology was applied to all crosslinking encapsulants investigated.

The initial measurement temperature was set to 25 °C, and the first heating step was performed up to 100 °C in order to melt the specimen and eliminate structure-related thermal history while remaining below the peroxide activation temperature. Subsequently, the sample was cooled to −20 °C to obtain the crystallization peak of both uncured and cured encapsulants. From the first cooling curve, the crystallization onset temperature (T_o), peak temperature (T_c), and peak shape (SF) were evaluated to calculate the degree of crosslinking (G_{MF}). In the second heating step, the sample was heated to 225 °C to allow the peroxide decomposition and the curing reaction to occur. From the second heating curve, the crosslinking reaction enthalpy of the uncured sample and the residual enthalpy of the laminated samples were determined to calculate the degree of crosslinking (G_e). An additional cooling step to −20 °C was then performed to obtain a crystallization peak from a fully cured sample, which was used as a “maximum cured” reference for the degree of curing calculations. No dwell time was applied between the steps; the heating rates were set to 10 °C min^{-1} and a nitrogen flow of 50 mL min^{-1} was maintained.

2.2 Fourier transform infrared spectroscopy (FTIR) and principal component analysis (PCA)

Fourier transform infrared spectroscopy in attenuated total reflexion mode (FTIR-ATR) was applied as a non-destructive method to investigate the crosslinking behaviour of the encapsulant materials. This method was chosen as it enables possible observation of small chemical differences between materials that might have been below limit of detections of the destructive methods studied here. FTIR-ATR measurements were performed using a SpectrumTwo spectrometer (PerkinElmer, Inc., USA) equipped with a Quest ATR unit with diamond crystal (Specac Ltd., United Kingdom). Three spectra per sample were recorded over a wavenumber range of 4000 to 650 cm^{-1} at a resolution of 4 cm^{-1}, with each spectrum representing the average of four scans.

The obtained FTIR-ATR spectra were analysed by principal component analysis (PCA). PCA is an exploratory multivariate statistical method that reduces the dimensionality of complex datasets while preserving most of the original variation [70,71]. In this study, PCA was used as a visualisation tool to reveal spectral trends, sample groupings and changes related to the degree of crosslinking. In general, PCA reduces the dimensionality of the dataset by generating a smaller number of new variables, referred to as principal components (PCs), which retain most of the variation present in the original data. The first principal components account for the largest share of the total variance. In this study, score plots of the first two components (PC1 and PC2) were used to assess possible trends within the sample sets. Prior to PCA, the spectra were pre-processed by Standard normal variate (SNV) normalization and first-derivative transformation using a Savitzky Golay filter with smoothing. In addition, mean centering was applied before PCA. The PCA results were then compared with the findings of the other methods used in this study.

2.3 Digital image correlation (DIC) – Coefficient of thermal expansion (CTE)

The dimensional stability of the unlaminated samples and coefficient of thermal expansion (CTE) of the unlaminated and laminated samples were measured using a Dantec Q400 TCT digital image correlation (DIC) system from Dantec Dynamics. The device consists of two cameras and a temperature-controlled chamber equipped with a heated/cooled thermal plate. During measurement, a time series of images of the sample surface are taken during the thermal stages. The recorded images were evaluated using Istra 4D software (Dantec Dynamics), which calculates the relative surface displacement by correlating each image in the series with the initial reference image.

Samples for DIC measurements were square shaped with dimensions of 4 x 4 cm^2. They were cut from the 20 x 20 cm^2 laminated sheets at positions several centimetres away from the edges to exclude regions affected by thickness reduction due to unavoidable edge pinching during lamination. Sample preparation is an important step as the Istra 4D software follows a speckle pattern that is applied on the surface of the sample. The speckle pattern was applied on the encapsulants in 2 layers; the first white coating serves as a primer and substrate cover and is followed by a second layer, black coating, which creates the speckle pattern. Achieving good contrast and independent speckles is necessary to guarantee a measurable surface area.

The measurements were done in the temperature range from 20 to 120 °C, with a heating rate of 2 °C min^{-1}. For the dimensional stability of the unlaminated encapsulants, the length change in both the machine direction and transverse direction was followed relative to the initial diameter of 20 mm, taken from the centre of each sample.

3. Results

3.1 The behaviour and degree of crosslinking from DSC

As mentioned, according to IEC 62788-1-6:2017, the degree of crosslinking of EVA-based encapsulants can be determined from the residual curing enthalpy and from changes in crystallization behaviour. In this study, the same heating profile was applied to all encapsulants, and the degree of crosslinking was calculated following the equations provided in the standard [69].

The first cooling and second heating curves are particularly important, as they provide the information required for the calculation of the degree of crosslinking. Therefore, these curves were carefully analysed and compared. Calculated values for the degree of crosslinking from enthalpy (G_e) and melt/freeze (G_{MF}) method are presented in Table 2. Due to the large amount of data, Figure 2 and Figure 3 show only the DSC curves for POE- 1, EPE- 1, and EPE- 2; the remaining curves for the other encapsulants are provided in the **Error! Reference source not found.** together with graphs showing the full heating range for all encapsulants at the lamination time of 15 min.

Table 2. Crosslinking degrees calculated according to residual enthalpy (G_e) and melt/freeze method (G_{MF}).

Lamination time (min)	EVA		POE-1		POE-2		EPE-1		EPE-2	
	G_e (%)	G_{MF} (%)	G_e (%)	G_{MF} (%)	G_e (%)	G_{MF} (%)	G_e (%)	G_{MF} (%)	G_e (%)	G_{MF} (%)
2	14.9	7.2	39.5	2.9	0	0*	0	0*	0	Dual peak
5	66.1	79.0	20.9	12.3	2.3	0*	10.5	1.3	34.6	
10	63.6	96.4	63.7	52.5	52.4	46.0	59.2	90.4	94	
12	66.1	99.3	58.2	50.2	64.3	66.1	67.1	110.7¤	94.7	
15	77.7	101.7¤	54.9	69.5	85.7	64.6	96.1	106.0¤	96.2	
20	80.7	100.9¤	67	88.1	85.7	63.8	93.4	103.3¤	99	
30	84	101.7¤	76.9	94.9	85.7	76.7	94.7	101.1¤	97.7	

*false negative value

¤false positive value

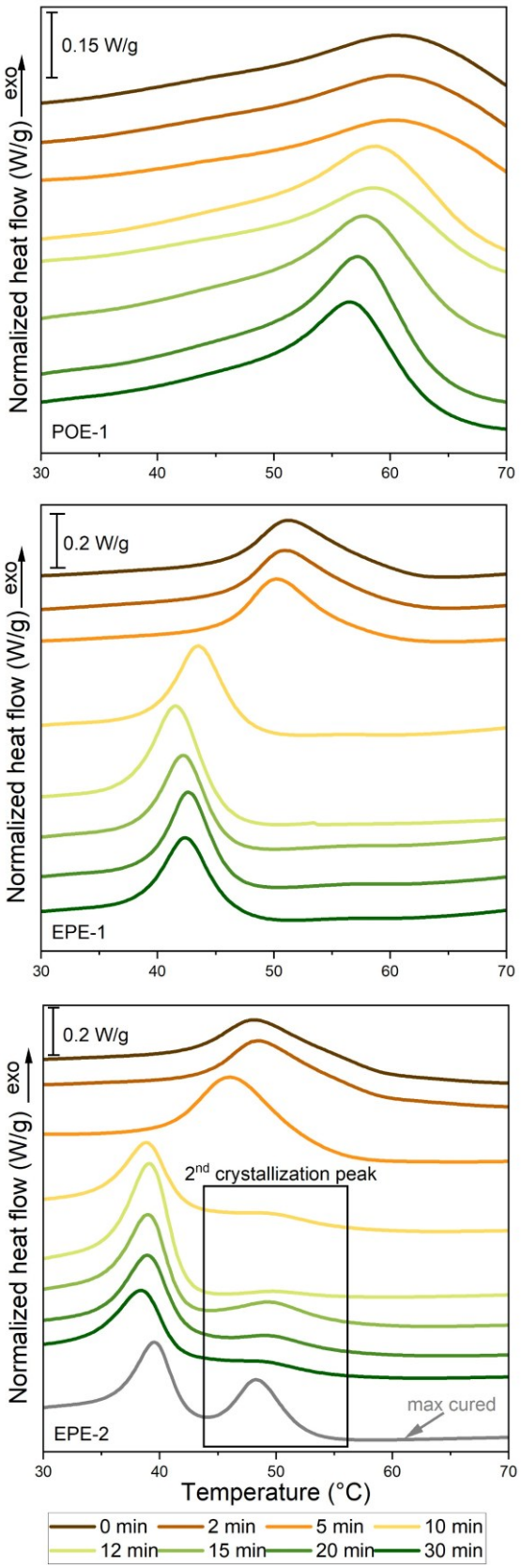

Figure 2. The 1st cooling DSC curves of uncured and laminated POE- 1, EPE- 1 and EPE- 2 in temperature range of 30 - 70 °C, where the crystallization peak is observed.

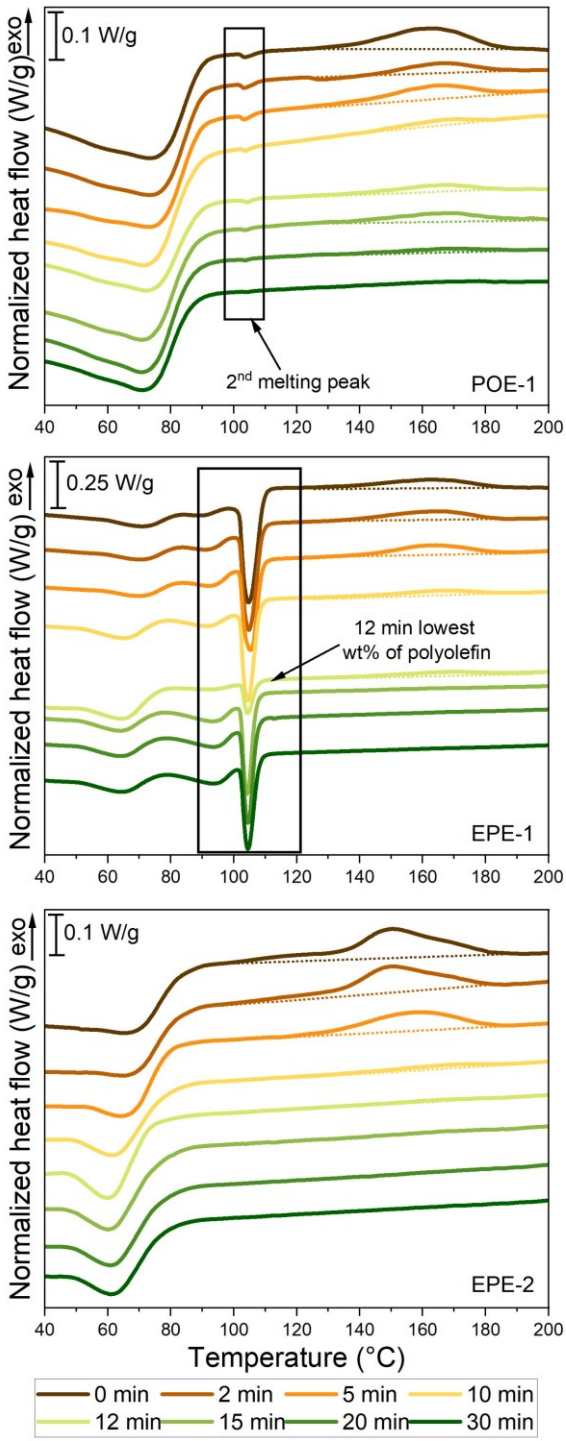

Figure 3. The 2nd heating DSC curves of uncured and laminated POE- 1, EPE- 1 and EPE- 2. The dotted line indicates the thermogram baseline and aids in identifying the exothermic crosslinking peak.

For the EVA encapsulant, according to the change in the crystallization peak from 1st cooling curves, a degree of curing of 96.4% is reached after 10 min of lamination. However, in the 2nd heating curve, an exothermic peak, between 160 °C and 180 °C, is still present at this lamination duration, suggesting that some peroxides remain undecomposed. This may be attributed to incomplete peroxide decomposition or delayed degassing due to the excess

peroxide content commonly added to ensure complete crosslinking, resulting in differences in the calculated degree of crosslinking [62,72]. This observation is confirmed by the calculations, while the degree of curing for the G_{MF} does not change for ≥12 min laminated samples. The apparent increase of G_{MF} above 100% for ≥15 min is likely an artefact resulting from small variations in crystallization behaviour, which are sensitive to the maximum heating temperature used in the DSC cycle. G_e is in steady increase and reaches a maximum value of 84% for 30 min lamination duration.

POE- 1 exhibits the slowest curing behaviour among the studied single layer encapsulants. Furthermore, a second melting peak at approximately 104 °C is observed, likely from the presence of a small amount of the crystalline fraction from low density polyethylene. An exothermic peak in the 2nd heating curve remains visible up to a lamination time of 30 min, and a similar trend is observed in the crystallization peak during the 1st cooling. However, the calculated values of G_e and G_{MF} differ, the degree of crosslinking from the residual enthalpy is lower than the melt/freeze, 76.9% and 94.9%, respectively.

POE- 2 exhibits a relatively slow change in the crosslinking behaviour for lamination times below 10 min. Additionally, the false negative G_{MF} values are observed for 2 and 5 min lamination times. These values are likely related to differences in thermal history between extrusion and lamination of encapsulant, which impact the crystallization behaviour of the semi crystalline polymer network while the degree of crosslinking is still low. A lamination duration of 15 min at 150 °C appears sufficient to ensure complete peroxide decomposition and to reach the maximum degree of curing for this material formulation. For lamination times ≥15 min, the characteristic exothermic peak associated with peroxide-initiated crosslinking is no longer visible. However, a change in the baseline slope of the heat-flow curve within the same temperature interval indicates the presence of residual crosslinking reaction. Based on the residual enthalpy, the calculated degree of crosslinking stabilizes at approximately 85% across all samples. Furthermore, the first cooling thermograms reveal a change of the crystallization peak for all specimens laminated for ≥15 min. This behaviour suggests that residual crosslinking reaction, observed in the 2nd heating, continues beyond the primary peroxide-initiated stage, although at a reduced rate, likely governed by thermally activated radical recombination or gradual network rearrangement processes.

As expected, TPO is a non-crosslinking encapsulant, and therefore its thermal properties are independent of lamination duration.

More complex crosslinking behaviour is observed for the EPE encapsulants. As mentioned previously, EPE- 1 and EPE- 2 differ in the nature of their polyolefin core materials. In EPE- 1, the polyolefin core is a non-crosslinking type, therefore, the peroxides present in the material are intended solely for EVA crosslinking. Consequently, no changes in the melting or crystallization peaks of the polyolefin core are observed. Analysis of the 2nd heating curves revealed an unexpected deviation for the samples laminated for 12 min. All three tested specimens exhibited a lower apparent polyolefin fraction compared to samples laminated for other durations. These specimens were taken from random positions within a single 20 × 20 cm² laminated sample. Additional DSC measurements were performed on several specimens

from the same laminate, and the reduced apparent polyolefin content was consistently observed. This suggests that the effect is not related to measurement variability but rather to a structural inhomogeneity within the laminate. A possible explanation is an uneven distribution of the polyolefin layer within the laminated stack. To verify this assumption, cross-sections of the laminate were examined by optical microscopy. The images confirmed local variations in the polyolefin layer distribution. Representative images are provided in the Supporting Information. For the crosslinking behaviour from the 2nd heating curve, contrary to the single EVA encapsulant, the exothermic peak after 15 min of lamination duration is no longer observable. A similar trend is observed from the 1st cooling curves, where the crystallization peak for samples laminated for ≥15 min is influenced by the amount of polyolefin core present, but no further crosslinking is observed.

EPE- 2 exhibits distinctly different behaviour compared to the EPE-1. In this material formulation, both the EVA and POE components are crosslinking polymers. For uncured and under-cured samples (0, 2 and 5 min lamination time), two exothermic peaks are observed, which could be attributed to the presence of different crosslinking systems [73]. In contrast to the measured single layer EVA and POE samples, no exothermic peak is observed after 12 min of lamination, indicating that the peroxides have fully decomposed, and EPE- 2 has reached an apparent degree of crosslinking of 94.7%. However, analysis of the 1st cooling curves, together with the cooling curve from the 2nd cooling step, referring to the "maximum cured sample" (grey curve in Figure 2) shows that the crosslinking reaction is still ongoing, similar to the behaviour observed for POE- 2. At this stage, heat acts as the main driving factor for further network formation, and the reaction proceeds slowly at 150 °C. This behaviour indicates that, although the peroxides have decomposed, the curing process has not reached its maximum extent. Higher lamination temperatures or longer lamination times are therefore required to achieve a higher degree of curing in the polyolefin core, as visible from the 2nd cooling curve, where the crystallization peak associated with the polyolefin phase appears with higher intensity.

In addition, even though the crosslinking reaction in EPE- 2 proceeds slowly after peroxide decomposition, similar to POE- 2, no baseline slope change is observed in the 2nd heating curve. This low detectability of residual crosslinking reaction is due to the slow reaction rate, combined with the polyolefin fraction representing only about one third of the total mass in a small sample size (≈7 mg). Additionally, the degree of curing could not be determined using the melt/freeze method, which is designed for encapsulants exhibiting a single crystallization peak. Whereas the presence of two crystallization peaks in EPE- 2 prevents reliable calculation using this approach.

3.2 PCA of FTIR-ATR spectra of encapsulants according to lamination duration

PCA of all crosslinking encapsulants revealed distinct clusters corresponding to low, medium, and high degrees of crosslinking, with clear trends in distribution between lamination durations from right (0 min) to the left (30 min) (see Figure 4). Across all materials, 0 and 2 min lamination samples consistently fall in the low-crosslinked cluster, as expected. For POE-1 and EPE-1, 5 min lamination falls in the medium-to-low range, whereas for the other encapsulants

it is closer to medium-to-high. Lamination time of 10 min appears sufficient to reach medium-to-high crosslinking for EVA according to PCA clustering, in agreement with DSC, whereas POE-2 is clustered higher by PCA than indicated by DSC. Lamination times above 12 min generally fall in the high-crosslinked cluster for all encapsulants, in close agreement with DSC calculations. Comparison with DSC data indicates that PCA clusters generally reflect the trends observed in the G_{MF} calculations. For the EPE encapsulants it is important to highlight that the FTIR-ATR is essentially a surface-sensitive method, as the penetration depth of measurement is limited to only a few micrometres. Therefore, in the multilayer encapsulants, the recorded spectra mainly reflect the outermost EVA layer rather than the full multilayer structure.

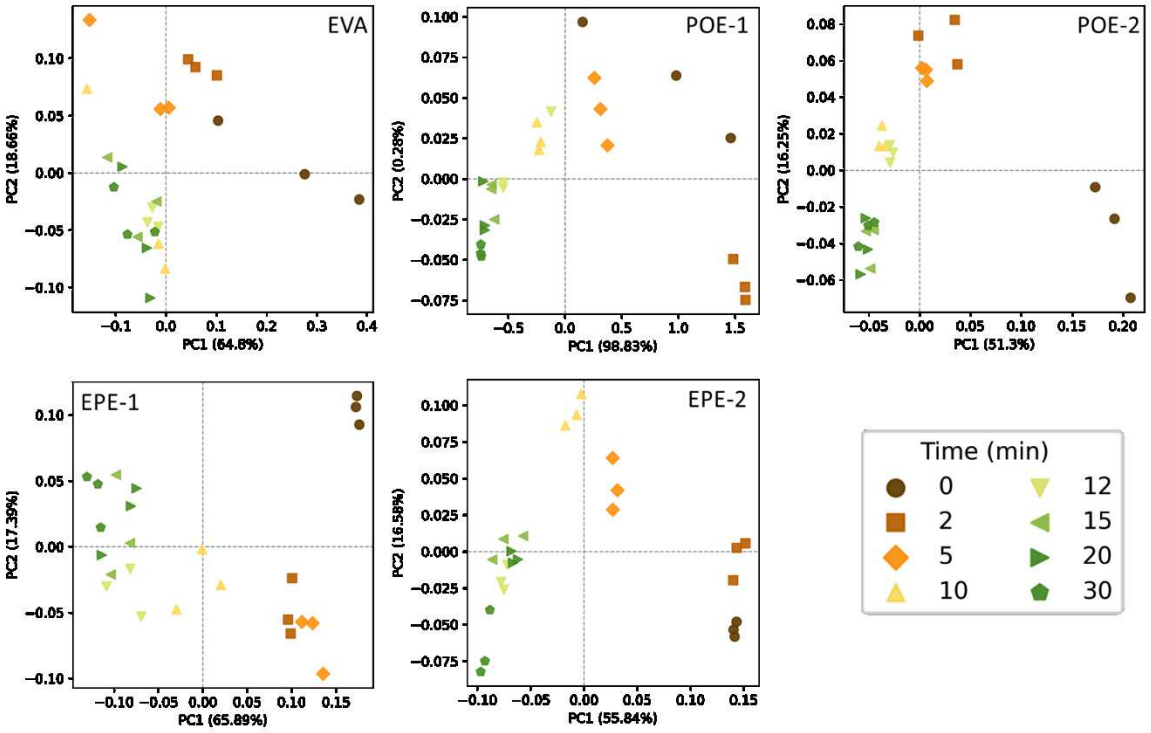

Figure 4. PCA scatter plots of PC1 vs. PC2 for all crosslinking encapsulants at different lamination times.

3.3 Thermomechanical behaviour of unlaminated (uncured) and laminated encapsulants

The coefficient of thermal expansion (CTE) measurements of the unlaminated encapsulants revealed pronounced differences in dimensional stability, reflecting variations in processing history between studied encapsulants. These differences were observed not only between different material classes, but also among encapsulants belonging to the same material group, highlighting the strong influence of processing conditions on dimensional behaviour prior to lamination. Such variations are expected to affect stress development and layer misalignment during PV module lamination.

Figure 5 shows the in-plane dimensional changes, calculated from horizontal and vertical gauge lines taken from the centre of the samples, each with an initial length of 20 mm. Figure

6 presents the CTE evaluated over the central area of the sample, represented by a regular grid (see the red mesh in Figure 7a), in the temperature range from 20 to 120 °C for all investigated unlaminated encapsulants, in both the machine direction (MD) and the transverse direction (TD). Dimensional stability (i.e., shrinkage and expansion) is directly related to the CTE, as the latter is derived from the measured dimensional changes.

EVA encapsulant exhibited shrinkage in both directions over the measured temperature range. As the material contracted in-plane, a corresponding increase of 0.15 mm in thickness was observed, indicating material flow towards the interior. Shrinkage was more pronounced in the MD, while a reduction in shrinkage rate was observed at temperatures around 90 °C.

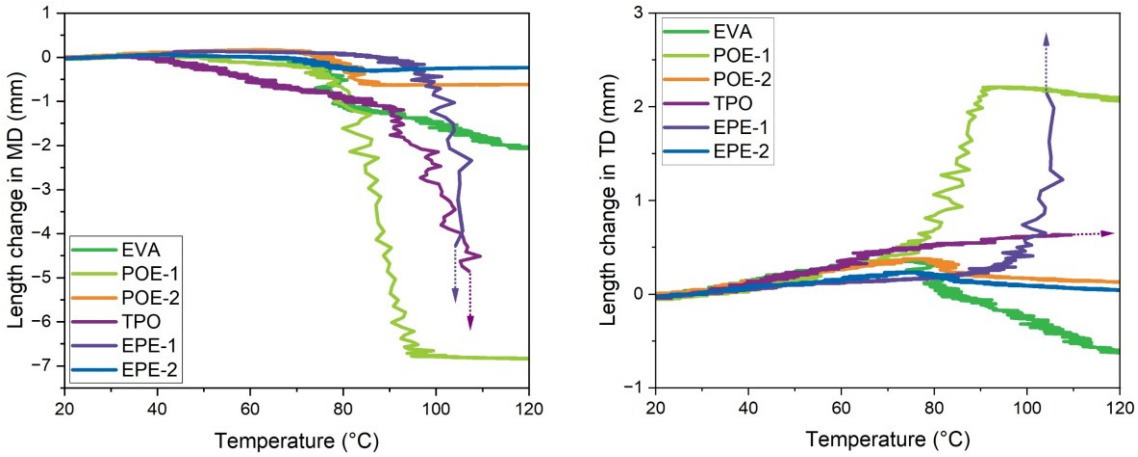

Figure 5. Dimensional (length) change in machine (MD) (left) and transverse (TD) (right) direction for unlaminated encapsulants. Dotted arrows point the visually observed shrinkage or expansion trends for TPO and EPE- 1, beyond the data measured by DIC.

Although POE- 1 and POE- 2 belong to the same material class, significant differences in their dimensional response were observed, indicating differences in processing history. POE- 1 showed strong shrinkage in the MD accompanied by expansion in the TD. The magnitude of shrinkage clearly exceeded the transverse expansion, suggesting a high degree of molecular orientation post manufacturing process, likely introduced during stretching and insufficient relaxation during cooling. Similar to EVA, in-plane shrinkage was accompanied with the specimen thickness increase from 0.45 mm to about 1.0 mm after the complete thermal cycle. In contrast, POE- 2 exhibited substantially lower dimensional changes in both directions, with shrinkage magnitudes approximately eleven times lower than those observed for POE- 1, indicating more optimized processing conditions.

TPO, as the only single-layer thermoplastic encapsulant investigated, experienced pronounced shrinkage in the MD once the melting onset temperature was reached. Above approximately 105 °C, the applied speckle pattern could no longer be tracked by DIC due to excessive deformation caused by encapsulant warping, and no further quantitative data could be obtained. Nevertheless, visual observation confirmed continued shrinkage in the MD. Only minor expansion was observed in the TD.

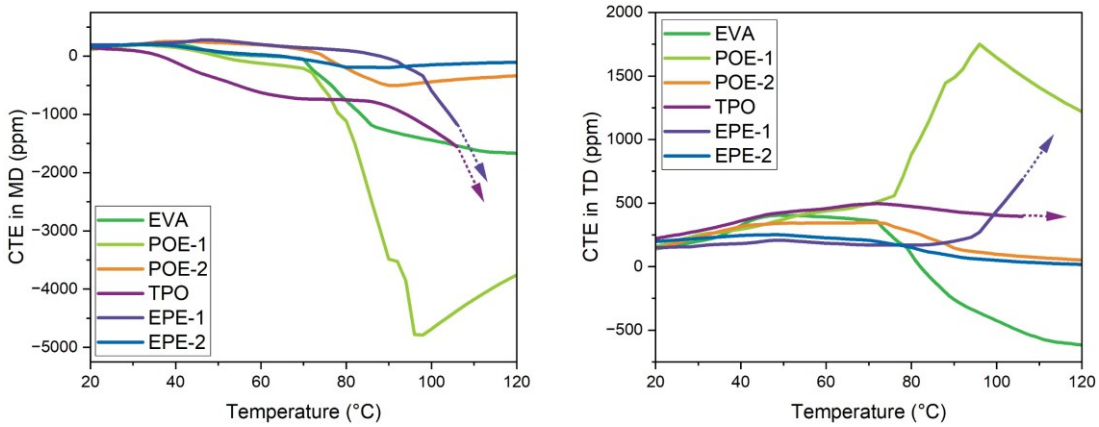

Figure 6. CTE in machine (MD) (left) and transverse direction (TD) (right) for unlaminated encapsulants. Dotted arrows point the CTE behaviour trends for TPO and EPE- 1, beyond the data measured by DIC.

EPE-1, which contains a thermoplastic core layer, exhibited the largest dimensional change among the investigated encapsulants. A pronounced shrinkage was observed in the MD, while expansion in the TD was higher than for the other materials. On Figure 7, the dimensional change of EPE- 1 specimen can be seen after the heating and cooling step, observable shrinkage corresponds to the combined shrinkage occurred during heating and additional shrinkage that took place during the cooling stage. This shrinkage is accompanied by a substantial increase in thickness, from an initial value of 0.45 mm to approximately 1.5 mm.

Among all investigated materials, EPE- 2 demonstrated the highest dimensional stability. Only minor shrinkage was observed in MD directions (-0.23 mm or 1.1%), indicating highly optimized processing conditions relative to the other encapsulants studied.

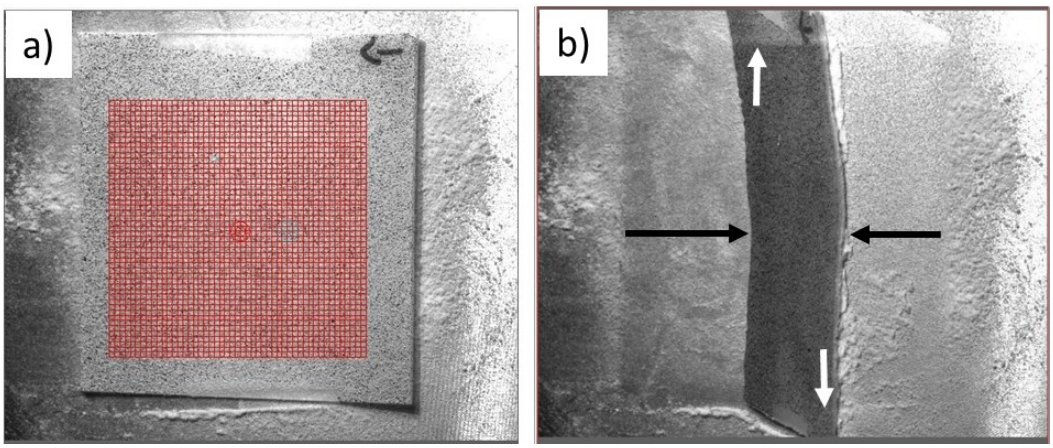

Figure 7. Unlaminated EPE-1 before (a) and after (b) CTE measurements, shrinkage in machine (black arrows) and expansion in transverse direction (white arrows).

A lamination time of 2 min appears sufficient to remove most of the processing history (see Figure 8), however, it is not long enough to allow full relaxation and reorientation of polymer chains in the molten state, nor to enable significant crosslinking to form a crosslinked polymer network, as seen from DSC results. Nevertheless, an impact on dimensional stability is still observed. Lamination applies a unidirectional pressure over the entire surface, which leads to

a transition from the MD-shrinkage/TD-expansion behaviour observed in the unlaminated state to predominantly MD-shrinkage/TD-shrinkage, i.e., material contraction occurring in both directions.

EVA exhibits the strongest shrinkage, likely due to its lower viscosity, which allows greater chain mobility and stretching during lamination. Since crosslinking reaction is still limited at this stage, and the lamination duration is insufficient to fully reorient the polymer chains in new shape, contraction upon reheating occurred. Interestingly, POE- 1, which displayed high shrinkage in the unlaminated state, adopts a more thermomechanical stable configuration after 2 min of lamination. Both EPE-1 and TPO also exhibit reduced shrinkage compared to their unlaminated states, while POE- 2 follows similar trend as POE- 1. Among all materials, EPE- 2 continues to display the highest dimensional stability, maintaining minimal shrinkage in both directions.

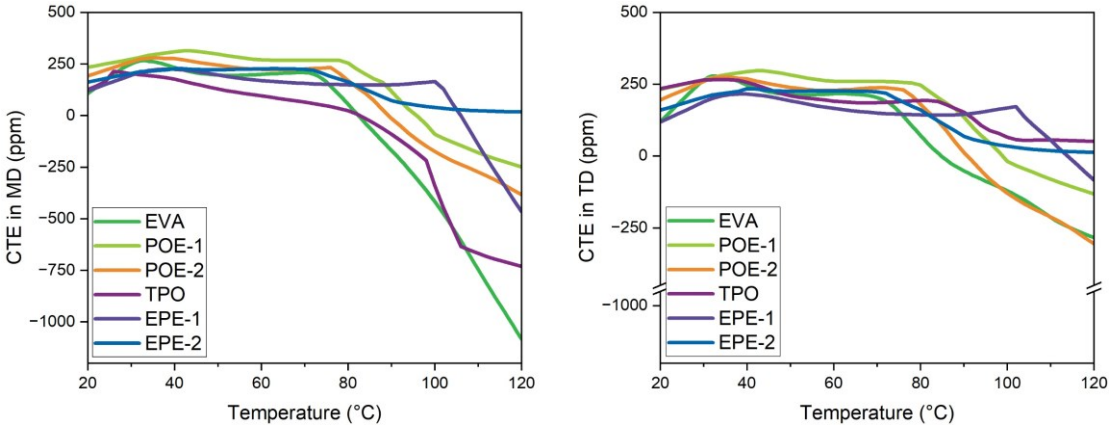

Figure 8. CTE curves in machine (MD) (left) and transverse direction (TD) (right) of 2 min laminated encapsulants.

For longer lamination times (see Figure 9), all encapsulants show a clear reduction in anisotropy, with expansion and contraction becoming increasingly similar in both the machine and transverse directions. This behaviour results from a combination of the uniform lamination pressure applied over the surface, sufficient time for polymer chain relaxation and reorientation, and crosslinking reactions contributing to dimensional stability through the formation of a crosslinked polymer network.

A lamination time of 5 min was insufficient to achieve final dimensional stability for EVA, POE- 1, and POE- 2, nearly sufficient for TPO and EPE-1, and close to sufficient for EPE- 2. POE- 1 exhibited highest shrinkage in both directions, suggesting need for longer lamination times at 150 °C for polymer chain reorientation and higher crosslinking degree. All encapsulants obtained “final” thermomechanical properties for ≥10 min lamination duration.

Interestingly, a small difference in CTE values and curve shape was observed for EPE- 1 laminated for 12 min. DSC analysis indicated that this sample contains a lower fraction of the polyolefin core, suggesting that in coextruded encapsulants the relative layer thickness can additionally influence thermomechanical properties. While the effect is not large, it is noticeable.

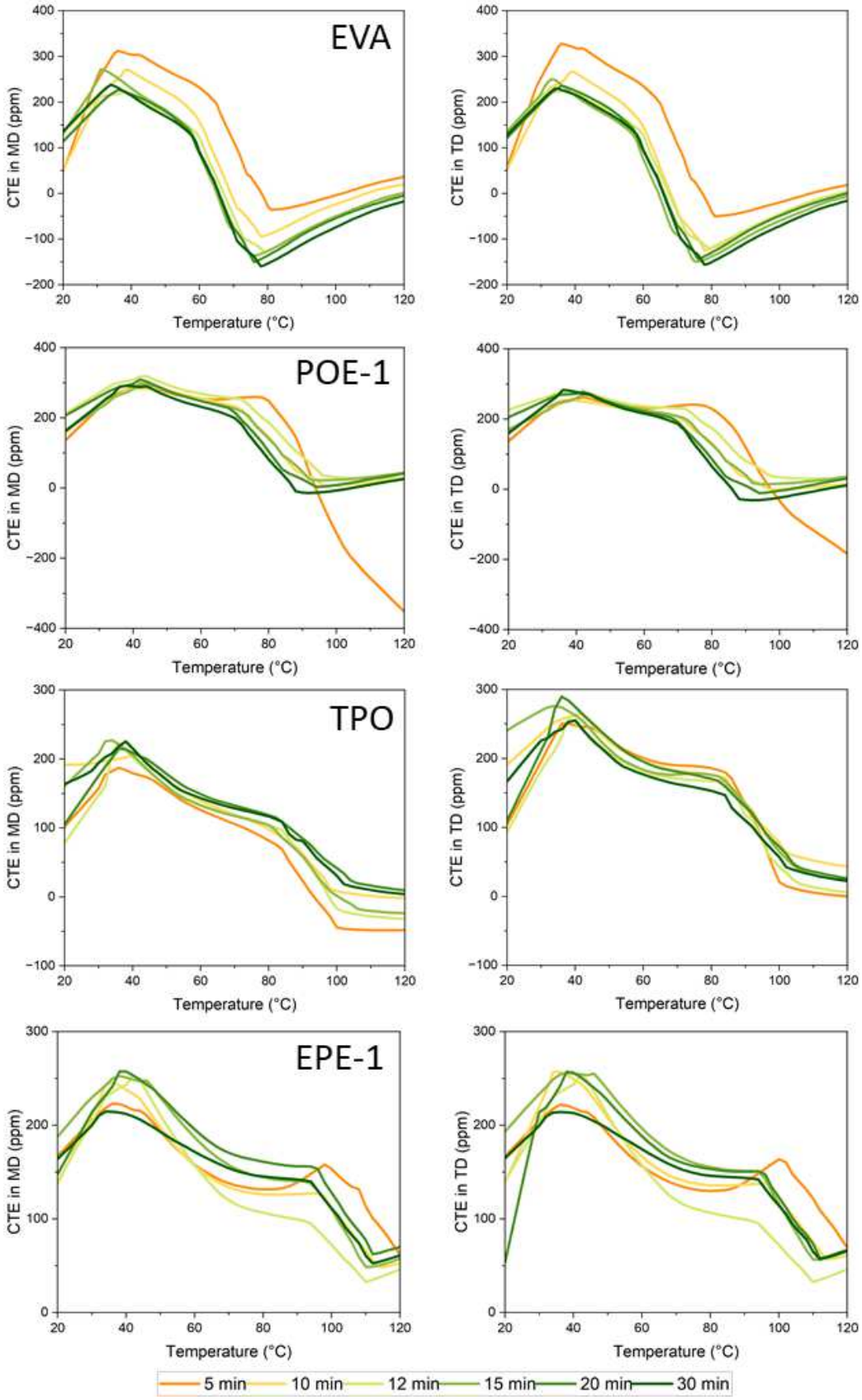

Figure 9. CTE curves in in machine (MD) (left) and transverse (TD) (right) direction of 5 to 30 min laminated EVA, POE- 1, TPO and EPE- 1 samples.

When the thermomechanical behaviour of all six encapsulants laminated for 30 min is compared (see Figure 10), clear differences in CTE values and temperature-dependent dimensional changes are observed. These differences appear not only between different polymer types, but also within the same material groups, as shown by the variation between POE-1 and POE-2 and between EPE-1 and EPE-2. Non-crosslinking TPO and partially crosslinking EPE-1 show the lowest CTE range and only minor contraction above the melting temperature. In contrast, crosslinking materials, EVA, POE-1, POE-2, and EPE-2, exhibit CTE values ranging from approximately 250 ppm to −100 ppm across the measured temperature range, together with noticeable contraction in the melting region, which can be linked to remaining non-crosslinked polymer fractions.

Despite these differences between materials, overlapping the CTE curves measured in machine and transverse directions (Figure 10) shows that all encapsulants individually display nearly isotropic behaviour after 30 min of lamination. Compared to the initial state and shorter lamination times, this indicates that longer lamination improves the uniformity of the thermomechanical response.

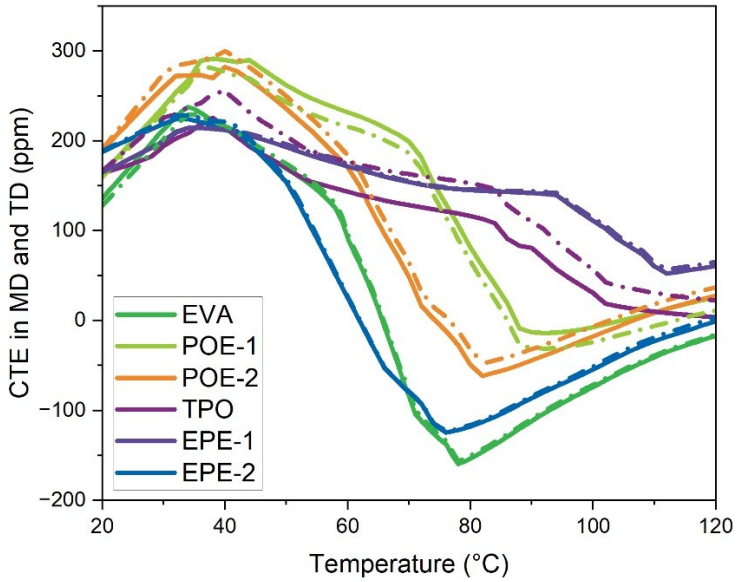

Figure 10. CTE curves in machine (solid line) and transverse direction (dash/dot line) of 30 min laminated encapsulants.

4. Discussion

In practice, the selection of encapsulants often relies on familiarity rather than systematic evaluation. Engineers may choose materials based on previous experience, literature examples, or simply because the polymer type has “worked before” [20]. While convenient, this approach can be misleading, even materials labelled under the same polymer family, such as in case of POE and EPE, often differ in formulation, additive content, or processing history, leading to unexpected variations in material behaviour [2,8]. This inherent variability becomes especially critical when predicting reliability of PV modules.

4.1 Determining degree of crosslinking

Combined enthalpy and melt/freeze DSC methods have been used to evaluate degree of curing for EVA [62,72,74], but applying these methods to POE and coextruded EPE encapsulants reveals their limitations. For EVA, G_e values indicated a lower degree of crosslinking compared to G_{MF}, likely due to excess peroxides in the formulation. Once the maximum degree of curing is reached, additional non-decomposed peroxides remain, contributing to residual enthalpy without affecting the crystallization peak [62,72]. While this may lead to misinterpretation of the crosslinking degree, it poses additional concern. Residual peroxides in combination with other additives can cause encapsulant yellowing and corrosion of PV module components [22,75].

POE- 1 and POE- 2 differed in the speed of their crosslinking, and for both of them, peroxides were decomposed before the maximum degree of curing could be reached, at least according to the G_{MF} calculations. POE is generally considered a slow-curing material with a lower overall degree of crosslinking compared to EVA, suggesting that the available peroxide content was sufficient to reach an optimal cure despite apparent differences in measurement [59].

The limitations of these methods become more apparent for coextruded EPE encapsulants. In EPE- 1, peroxides are present only to crosslink the EVA layer, however it is still unclear if they can diffuse from the EVA layer to the polyolefin core layer and affect overall crosslinking behaviour. For EPE-1, residual enthalpy-based calculations show a clear trend in crosslinking development, while G_{MF} values become unreliable due to the influence of the polyolefin layer on the crystallization peak of EVA, producing apparent “over-curing” or false positive values. EPE- 2 presents a different challenge, both layers are crosslinking polymers, but with distinct curing rates. While G_e indicates high crosslinking and rapid peroxide decomposition, melt/freeze calculations are limited by a second crystallization peak in the 2nd cooling curve. Additional measurement limitations for POE- 2 and EPE- 1 must be considered, as observed from the difference in the crystallization behaviour after lamination compared to the unlaminated sample, that produced false negative G_{MF} values, replace by “0*” in Table 2.

These observations highlight that methods developed for EVA must be reconsidered and adapted for more complex, multilayer encapsulants. Non-destructive FTIR method together with PCA revealed distinct clusters corresponding to low, medium, and high degrees of crosslinking. Even though, comparison with DSC data indicated that PCA clusters generally reflect better the trends observed in the G_{MF} calculations, the uncertainties from the DSC calculations were observed once again from the deviations in results. Even though FTIR-ATR is a surface measurement, in combination with PCA it could serve as a fast method to assess whether encapsulants are sufficiently crosslinked, by correlating cluster positions in the PCA with the degree of crosslinking measured using quantitative methods such as Soxhlet extraction. It should be noted, however, that despite being non-destructive at the measurement level, FTIR cannot be readily implemented for inline monitoring, as the encapsulant still needs to be extracted from the module, similar to DSC and Soxhlet methods.

While gel content determination by Soxhlet extraction has long been regarded as the most reliable technique for assessing the degree of crosslinking in individual EVA or POE layers, its

applicability reaches practical limits in multilayer EPE systems. Accurate determination becomes considerably more challenging, as it requires detailed knowledge of layer composition, relative mass fractions, and individual crosslinking behaviour, particularly when components cure at different rates. Previous studies on Soxhlet extraction in EPE have largely focused on extraction time, which was found to be longer than for the corresponding individual materials [59,60].

4.2 Dimensional stability of unlaminated encapsulants

Results from this study provide direct experimental evidence that manufacturing history decisively governs the thermomechanical response of encapsulants both before and during lamination. Although the influence of extrusion and cooling conditions is well recognized in polymer science, it is often overlooked in encapsulant selection for PV modules. The pronounced differences in dimensional stability observed here confirm that the initial state of the film entering the lamination process is far from uniform, even among materials belonging to the same encapsulant category.

The comparison between POE- 1 and POE- 2 clearly illustrates this effect. Despite their identical material classification and base polymer, POE- 1 exhibited strong shrinkage in the MD accompanied by TD expansion, indicating significant residual molecular orientation introduced during film extrusion and stretching, and insufficient relaxation during cooling. In contrast, POE- 2 showed substantially lower dimensional changes, suggesting more optimized extrusion and post-processing conditions. These differences cannot be attributed to polymer chemistry, but rather reflect the processing history embedded in the material.

Similar behaviour was observed for TPO and EPE-1, both of which demonstrated pronounced shrinkage in the MD upon reaching the melting onset temperature. Such aggressive contraction indicates the release of internal stresses accumulated during manufacturing. Conversely, EPE-2 exhibited the highest dimensional stability among all investigated materials, suggesting effective stress relaxation during or an annealing step after production.

For clarity, Figure 11 schematically illustrates the evolution of polymer chain orientation throughout encapsulant manufacturing and stages of PV module lamination. In the first step, during extruder mixing, the polymer matrix is compounded with additives such as peroxides, antioxidants, and UV stabilizers. At this stage, polymer chains are considered unconstrained. In the second step, during encapsulant sheet extrusion and film shaping and stretching, molecular orientation is introduced as the film is elongated, particularly in the machine direction. The third step involves cooling, during which partial relaxation of the oriented chains should occur, and end of the encapsulant manufacturing process. However, depending on cooling rate and processing conditions, residual imposed orientation may become frozen as the material solidifies below its melting temperature and crystallizes [24,26,76]. This defines the initial state of the encapsulant prior to lamination. The fourth step represents the first stage of lamination, where the module stack is heated without applied pressure. In this unconstrained state, the previously imposed polymer chain orientation can relax freely, leading to in-plane dimensional changes, most commonly shrinkage in the machine direction, as observed in this study. The extent of this relaxation depends strongly on the manufacturing

history of the film and explains the pronounced differences in dimensional stability between materials of the same polymer family. The subsequent lamination stages, which will be discussed in the following section 4.3 Thermomechanical behaviour of laminated encapsulants, further modify polymer orientation and thermomechanical behaviour.

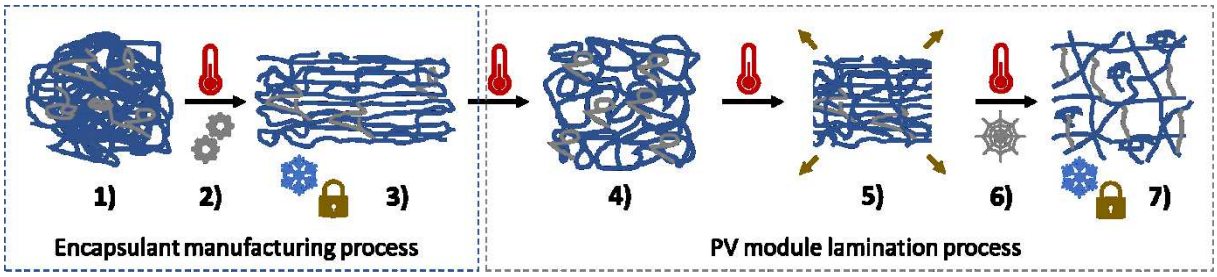

Figure 11. Changes in polymer structure alignment of the encapsulant during its manufacturing process (1–3): (1) polymer matrix compounding, (2) sheet extrusion and stretching, and (3) cooling at the end of the process; and during the PV module lamination process (4–7): (4) evacuation step, (5) heat and pressure application, (6) full pressure (crosslinking), and (7) final cooling of PV module.

The implications of thermally induced encapsulant shrinkage during the unconstrained heating stage extend beyond dimensional stability and may also relate to failure modes reported in the literature, especially for mechanically sensitive photovoltaic technologies such as perovskite solar cells. A recent minimodule encapsulation study has shown that POE can produce shrinkage or warpage severe enough to cause delamination of the perovskite cell stack and PV module failure [14]. Moreover, outdoor and accelerated indoor testing has demonstrated instances of encapsulant induced partial delamination in perovskite solar cells, even among nominally identical devices, underscoring the influence of subtle variations in material behaviour on long term integrity [20]. In mechanically fragile stacks, such as those incorporating perovskite absorbers or transport layers with low fracture toughness, even moderate dimensional changes during early lamination steps could cause interfacial shear and promote partial debonding.

Beyond perovskite solar cells, the impact of encapsulant dimensional changes on the backsheet has been reported in the literature. In one study, backsheet wrinkling was correctly attributed to contraction of the encapsulant during lamination [76], whereas another study attributed the deformation solely to the backsheet's CTE above glass transition temperature (T_g) and did not consider encapsulant effects [77]. The present study analysis suggests that sudden and pronounced shrinkage of the encapsulant at high lamination temperatures is the primary driver of such backsheet wrinkling. Since the backsheet is above its T_g during the first heating stage, it becomes softer and more compliant, allowing the contracting encapsulant to deform it, resulting in permanent wrinkles. The same phenomenon was observed in in-house lamination tests, where the polymer frontsheet was visibly wrinkled (Figure 12a).

The dimensional change effect can also be present in PV modules with different back and front side encapsulants with different processing histories. As illustrated in Figure 12b, when two different encapsulants are laminated together and the backside encapsulant (black colour)

exhibits greater shrinkage than the front encapsulant (orange colour) difference in shrunken area is clearly observable. With the ongoing development of TOPCon module designs, where EVA (including white EVA variation), POE, and EPE combinations can be interchanged between frontside and backside encapsulation, difference in the thermomechanical behaviour can cause residual stresses which may accumulate within the stack, potentially compromising module´s long-term reliability [78–80].

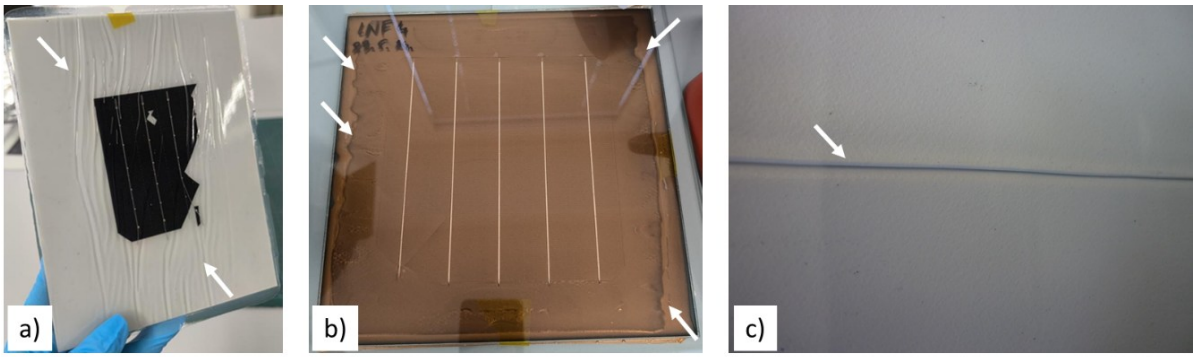

Figure 12. Examples of defects created during the lamination of PV modules caused by high encapsulant shrinkage: a) wrinkles in the frontsheet, b) back encapsulant shrinking, and c) wrinkle in the backsheet [76].

Collectively, these observations reinforce the need to evaluate encapsulant materials not only for nominal polymer type, adhesion or moisture barrier performance but also for their thermomechanical behaviour and dimensional stability prior to lamination. The first heating stage of lamination represents a critical window in which residual orientation, polymer chain relaxation, and material-specific shrinkage interact to define stress development within the module stack, a factor that can have lasting consequences for cell alignment, module reliability, and performance of emerging PV technologies.

4.3 Thermomechanical behaviour of laminated encapsulants

Building on the understanding of how the manufacturing history affects unlaminated encapsulants, this section connects the subsequent lamination stages from the Figure 11. with the resulting thermomechanical behaviour.

In the fifth step in Figure 11 a uniform pressure is applied to the PV module stack, causing the melted encapsulant to flow and cover all areas around the interconnections and solar cells, eliminating voids. Pressure is applied gradually to allow encapsulant to flow and fill areas around the interconnection and cells, while minimizing squeeze-out and ensuring the required encapsulant thickness for both insulating and buffering functions. During the sixth stage, full pressure is applied over the PV module and polymer chains are stretched unidirectionally into their new configuration. In crosslinking encapsulants, this step also initiates the crosslinking reaction, forming a new polymer network [34]. With sufficient lamination time, a higher degree of curing occurs, and the polymer network reaches a more stable state. For the non-crosslinking encapsulants, lamination time should be long enough for polymer chains to reorient and relax in the new configuration.

The final, seventh step is cooling, which locks the encapsulant in its new configuration. It is important to note that polymer chains are never fully crosslinked due to the complex nature of the polymer matrix, limited peroxide availability, and their non-uniform distribution [81]. Once a random crosslinked network forms, chain mobility decreases, but the remaining non-crosslinked fraction retains some freedom of movement once pressure is removed, leading to in-plane contraction during the cooling stage. This phenomenon has been observed in the literature through curving of the PV module laminate, solar cell and interconnection displacement [50,82–86].

Following these lamination stages, the thermomechanical behaviour of the encapsulants begins to reflect both the relaxation of residual chain orientations and the progression of crosslinking reactions. Even short lamination duration partially reduces the effects of prior processing, allowing polymer chains to adopt a new configuration resulting in change in the CTE values, but too short lamination times (2 and 5 min) are not sufficient for full relaxation of the polymer matrix nor to form a crosslinked polymer network. Material-specific differences in the time required to reach “final” CTE values are evident: A lamination time of 5 min was insufficient to achieve final dimensional stability for EVA, POE- 1, and POE- 2, nearly sufficient for TPO and EPE-1, and close to sufficient for EPE- 2. These differences arise from three main factors. First, polymer type: non-crosslinking encapsulants reach their new configuration faster, likely because only heat and in-the plane pressure influence chain orientation. Second, the degree of crosslinking: thermomechanical behaviour of encapsulants with lower crosslinking degrees exhibit higher CTE values and anisotropy. The third and final is the difference in the residual stress from the manufacturing, which was lowest for the EPE- 2.

Interestingly, the encapsulants that showed the largest dimensional changes in unlaminated state, TPO and EPE-1, exhibit the lowest CTE range in measured temperature range, after extended lamination. This behaviour is attributed to the higher degree of structural order within the polymer matrix. These materials possess significantly higher crystallinity, which ultimately dictates the final CTE values [32]. These findings suggest that, through an optimized manufacturing process or controlled post-manufacturing annealing, these materials could offer improved dimensional compatibility for perovskite and tandem solar cells during lamination; however, long-term compatibility and stability still need to be validated.

The contraction that occurs during cooling sets the initial stress state of the laminate. Once in the field, these stresses are combined with additional thermomechanical loads caused by daily and seasonal temperature changes. PV modules experience continuous thermal cycling, and the size of these temperature swings depends strongly on how the module is installed. Field deployed or building attached modules are usually cooled by airflow at the back, keeping temperatures relatively moderate, whereas integrated and insulated PV modules can reach higher temperatures and see larger temperature differences [87]. As a result, the effective expansion and contraction of the layers is greater, meaning that CTE mismatches create larger stresses between the layers over time. These repeated stresses can add up and influence the long-term durability of the module.

As discussed in the introduction, many studies investigating thermomechanical stresses in PV modules rely on finite element modelling, where encapsulant behaviour is often simplified by assuming constant CTE over broad temperature ranges. The results presented in this work demonstrate that the dimensional behaviour of encapsulants is strongly influenced by their processing history and by the lamination process itself. Therefore, the thermomechanical properties of encapsulants after lamination should be considered when using FEM to predict thermomechanical stresses in PV modules.

5. Conclusions

While in practice, the selection of encapsulant materials for a PV module is often based on familiarity rather than systematic characterization, it is important notice that even materials labelled under the same commercial nomenclature, such as POE and EPE, can differ in formulation, additive content, or processing history, leading to unexpected variations in material behaviour, as observed in this study.

When determining crosslinking degree using combined residual enthalpy and melt/freeze methods, several limitations emerged. The peroxide content in the material may be higher than needed, leaving residual peroxides that make the encapsulant appear under-crosslinked, or too low, giving the opposite impression. Therefore, comparing G_e with G_{MF} is necessary, but both methods have limitations, as G_{MF} values can be influenced by thermal history, which is affecting crystallization behaviour and yielding inaccurate results. In this study, combining FTIR-ATR with PCA proved to be a suitable non-destructive technique for qualitatively assessing crosslinking. Both methods, however, face challenges with coextruded encapsulants. DSC results are affected with EVA and polyolefin distribution in the stack and peroxide distribution across layers, as both G_e and G_{MF} calculations are impacted. FTIR-ATR measures the surface, limiting assessment only to the outer EVA layers.

Dimensional stability measurements revealed significant differences among encapsulants and highlighted the strong influence of manufacturing history on thermomechanical behaviour. Unlaminated encapsulants retain stresses and molecular orientation introduced during manufacturing, which can be released as shrinkage during unconstrained heating (the first lamination step). This dimensional change may relate to failure modes reported in the literature, especially for mechanically sensitive photovoltaic technologies such as perovskite solar cells. Surprisingly, literature reports on dimensional stability measurements are scarce, despite existing IEC 62788-1-5 standard for measuring the maximum representative change in linear dimensions of encapsulation sheet material.

An interesting observation came from measurements of the CTE versus lamination duration, showing a clear need for 5–10 min of lamination time for encapsulant to reach final values. Differences in CTE values between encapsulants were observed: encapsulants with non-crosslinking polyolefins, such as TPO and EPE-1, exhibited the strongest shrinkage initially, but after sufficient lamination, they reached the lowest CTE range. This underscores the importance of optimizing extrusion processes or applying post-processing annealing to reduce

processing-induced stresses, enabling non-crosslinking encapsulants to provide better support for minimizing CTE mismatch in the PV stack.

It is important to note that these measurements were performed on unconstrained encapsulants, so reported CTE values will differ from those in a fully stacked module, where movements are constrained. Nonetheless, these measurements capture the intrinsic tendencies of the encapsulants post-lamination and indicate the stresses or CTE mismatches that would be present in a PV stack. Future work will include CTE measurements within individual layers of the stack and track three-dimensional changes in the PV module.

Acknowledgments

This work was conducted as part of the Austrian “e!MISSION.at – Energy Mission Austria” project “PV Industriefassade” (FFG No. FO999915062) funded by the Austrian Climate and Energy Fund and the Austrian Research Promotion Agency (FFG).

This research project (grant number: 911658) was funded by COMET – Competence Centers for Excellent Technologies – through BMIMI, BMWET, and the co-financing federal provinces (Styria through SFG, Upper Austria, Vorarlberg) and carried out with the participation of scientific and company partners. The COMET program is managed by FFG.

The authors would like to acknowledge Ivaylo Mitev for his advices for sample preparation and CTE measurements, and Christian Veas and Lisa Maitz for their assistance with non-destructive spectroscopic measurements.

Data Availability Statement

The data that support the findings of this study are available on request from the corresponding author.

References

[1] VDMA e.V. Photovoltaics Equipment (Ed.), International Technology Roadmap for Photovoltaics (ITRPV): 16th Edition 2025, 2025.

[2] G. Oreski, C. Barretta, P. Christöfl, P. Gebhardt, K.-A. Weiß, D.C. Miller, S. Uličná, M. Kempe, L.S. Bruckman, A. Virtuani, H. Li, B. Habersberger, J. Munro, K. Proost, M. Kühne, What Is a Polyolefin? A Critical Overview of Ethylene Copolymers Used as Solar Photovoltaic Module Encapsulants, Prog. Photovolt. (2026) 367–395. https://doi.org/10.1002/pip.70038.

[3] Jarret Zuboy, Martin Springer, Elizabeth C. Palmiotti, Joseph Karas, Brittany L. Smith, Michael Woodhouse, Teresa M. Barnes, Getting Ahead of the Curve: Assessment of New Photovoltaic Module Reliability Risks Associated With Projected Technological Changes, IEEE Journal of Photovoltacis 14 (2024) 4–22.

[4] Intersolar, Solar Technology is Undergoing Great Changes: Market Trend – January 28, 2025, 2025. https://www.intersolar.de/market-trends/solar-cell-development (accessed 10 December 2025.).

[5] Timothy J. Silverman, Elizabeth C. Palmiotti, Martin Springer, Nick Bosco, Mike Deceglie, Ingrid Repins, Ashley Gaulding, Tough Break: Many Factors Make Glass Breakage More Likely, 2024.

[6] G. Oreski, J.S. Stein, G.C. Eder, K. Berger, L. Bruckman, R. French, J. Vedde, K.A. Weiß, Motivation, benefits, and challenges for new photovoltaic material & module developments, Prog. Energy 4 (2022) 32003. https://doi.org/10.1088/2516-1083/ac6f3f.

[7] Shravan K. Chunduri, Michael Schmela, TaiyangNews Solar Backsheets & Encapsulants Market Survey 2024/25, 2025.

[8] N. Pervan, G. Eder, Y. Voronko, A. Macher, K. Novotny, K. Resch-Fauster, G. Oreski, Is EPE the future of PV encapsulation? A comprehensive material-level assessment, Sol. Energy Mater. Sol. Cells 300 (2026) 114258. https://doi.org/10.1016/j.solmat.2026.114258.

[9] S. Zhang, Z. Liu, W. Zhang, Z. Jiang, W. Chen, R. Chen, Y. Huang, Z. Yang, Y. Zhang, L. Han, W. Chen, Barrier Designs in Perovskite Solar Cells for Long-Term Stability, Advanced Energy Materials 10 (2020) 2001610. https://doi.org/10.1002/aenm.202001610.

[10] P. Subudhi, D. Punetha, Pivotal avenue for hybrid electron transport layer-based perovskite solar cells with improved efficiency, Sci Rep 13 (2023) 19485. https://doi.org/10.1038/s41598-023-33419-1.

[11] M. Babin, G.C. Eder, Y. Voronko, G. Oreski, Water vapor permeability of polymeric packaging materials for novel glass-free photovoltaic applications, J. Appl. Polym. Sci. 141 (2024) e55733. https://doi.org/10.1002/app.55733.

[12] C. Sen, H. Wang, M.U. Khan, J. Fu, X. Wu, X. Wang, B. Hoex, Buyer aware: Three new failure modes in TOPCon modules absent from PERC technology, Sol. Energy Mater. Sol. Cells 272 (2024) 112877. https://doi.org/10.1016/j.solmat.2024.112877.

[13] P. Gebhardt, U. Kräling, E. Fokuhl, I. Hädrich, D. Philipp, 2024. Reliability of Commercial TOPCon PV Modules—An Extensive Comparative Study. Prog. Photovolt., pip.3868. https://doi.org/10.1002/pip.3868.

[14] H. Jiao, M. Hegde, N. Li, M. Owen-Bellini, L. Schelhas, T.J. Dingemans, J. Huang, Metal Halide Perovskite Solar Module Encapsulation Using Polyolefin Elastomers: The Role of Morphology in Preventing Delamination, PRX Energy 3 (2024). https://doi.org/10.1103/PRXEnergy.3.023013.

[15] M. de Bastiani, G. Armaroli, R. Jalmood, L. Ferlauto, X. Li, R. Tao, G.T. Harrison, M.K. Eswaran, R. Azmi, M. Babics, A.S. Subbiah, E. Aydin, T.G. Allen, C. Combe, T. Cramer, D. Baran, U. Schwingenschlögl, G. Lubineau, D. Cavalcoli, S. de Wolf, Mechanical Reliability of Fullerene/Tin

Oxide Interfaces in Monolithic Perovskite/Silicon Tandem Cells, ACS Energy Lett. 7 (2022) 827–833. https://doi.org/10.1021/acsenergylett.1c02148.
[16] C. Peike, I. Häldrich, K.-A. Weiß, I. Dürr, Overview of PV module encapsulation materials, Photovoltaics International (2013) 85–92.
[17] A.W. Czanderna, F.J. Pern, Encapsulation of PV modules using ethylene vinyl acetate copolymer as a pottant: A critical review, Sol. Energy Mater. Sol. Cells 43 (1996) 101–181. https://doi.org/10.1016/0927-0248(95)00150-6.
[18] E. Özkalay, G. Friesen, M. Caccivio, P. Bonomo, A. Fairbrother, C. Ballif, A. Virtuani, Operating Temperatures and Diurnal Temperature Operating Temperatures and Diurnal Temperature Variations of Modules Installed in Open-Rack and Typical BIPV Configurations, IEEE Journal of Photovoltacis 12 (2022) 133–140.
[19] M. Köntges, G. Oreski, U. Jahn, P. Hacke, K. Weiss, G. Razzongles, M. Paggi, D. Parleviet, T. Tanahashi, R. French, M. Richter, A. Morlier, C. Tjengdrawira, H. Li, K.A. Berger, G. Makrides, W. Herrmann, Assessment of Photovoltaic Module Failures in the Field: Report IEA-PVPS T13-09:2017, 2017.
[20] U. Erdil, M. Khenkin, W.M. Bernardes de Araujo, Q. Emery, I. Lauermann, V. Paraskeva, M. Norton, S. Vediappan, D.K. Kumar, R.K. Gupta, I. Visoly-Fisher, M. Hadjipanayi, G.E. Georghiou, R. Schlatmann, A. Abate, E.A. Katz, C. Ulbrich, 2025. Delamination of Perovskite Solar Cells in Thermal Cycling and Outdoor Tests. Energy Tech 13, 2401280. https://doi.org/10.1002/ente.202401280.
[21] H. Bristow, X. Li, M. Babics, S. Kosar, A.R. Pininti, S. Zhang, B. Vishal, S. Sarwade, A. Razzaq, A.A. Said, G. Lubineau, S. de Wolf, Mitigating Delamination in Perovskite/Silicon Tandem Solar Modules, Solar RRL 8 (2024) 2400289. https://doi.org/10.1002/solr.202400289.
[22] Magnus Herz, Gabi Friesen, Ulrike Jahn, Marc Köntges, Sascha Lindig, David Moser, Quantification of Quantification of Technical Risks in PV Power Systems: IEA PVPS Task 13, Report IEA-PVPS T13-23:2021, 2021.
[23] Sheng Yen Lee, Thermomechanical properties of polymeric materials and related stresses, United States, 1990.
[24] V. Bourg, P. Ienny, A.S. Caro-Bretelle, N. Le Moigne, V. Guillard, A. Bergeret, Modeling of internal residual stress in linear and branched polyethylene films during cast film extrusion: Towards a prediction of heat-shrinkability, J. Mater. Process. Technol. 271 (2019) 599–608. https://doi.org/10.1016/j.jmatprotec.2019.04.002.
[25] T.-I. Lee, M.S. Kim, T.-S. Kim, Contact-free thermal expansion measurement of very soft elastomers using digital image correlation, Polym. Test. 51 (2016) 181–189. https://doi.org/10.1016/j.polymertesting.2016.03.014.
[26] T.W. Womer, Optimizing Sheet Extrusion Conditions to Minimize Internal Stresses in Thermoformed Sheet, J. Plast. Film Sheeting 8 (1992) 26–36. https://doi.org/10.1177/875608799200800104.
[27] N. Saba, M. Jawaid, A review on thermomechanical properties of polymers and fibers reinforced polymer composites, J. Ind. Eng. Chem. 67 (2018) 1–11. https://doi.org/10.1016/j.jiec.2018.06.018.
[28] L. Eyann, M.A. Fatah Muhamed Mukhtar, A.A. Saad, M. Jaafar, Epoxy molding compounds for high-performance electronic packaging: A review on recent studies, Mater. Sci. Semicond. Process. 197 (2025) 109665. https://doi.org/10.1016/j.mssp.2025.109665.
[29] T. Tetsuya, Y. Hashimoto, U.S. Ishiaku, M. Mizoguchi, Y.W. Leong, H. Hamada, Effect of heat-sealing temperature on the properties of OPP/CPP heat seals. Part II. Crystallinity and

thermomechanical properties, J Appl Polym Sci 99 (2006) 513–519. https://doi.org/10.1002/app.22443.
[30] S. Pisani, I. Genta, T. Modena, R. Dorati, M. Benazzo, B. Conti, Shape-Memory Polymers Hallmarks and Their Biomedical Applications in the Form of Nanofibers, Int. J. Mol. Sci. 23 (2022). https://doi.org/10.3390/ijms23031290.
[31] J.-H. Park, E. Lee, I.-D. Kim, H. Jung, J. Kim, J. Cho, J. Kim, T.-I. Lee, S.-K. Kang, E.-H. Lee, A review of the thermo-mechanical analysis framework for microelectronics packaging: Mechanics, material property determination, and structural considerations, Mater. Sci. Semicond. Process. 205 (2026) 110321. https://doi.org/10.1016/j.mssp.2025.110321.
[32] A.G. Khina, D.P. Bulkatov, I.P. Storozhuk, A.P. Sokolov, Coefficient of Linear Thermal Expansion of Polymers and Polymer Composites: A Comprehensive Review, Polymers 17 (2025). https://doi.org/10.3390/polym17233097.
[33] M. Knausz, G. Oreski, M. Schmidt, P. Guttmann, K.A. Berger, Y. Voronko, G. Eder, T. Koch, G. Pinter, Thermal expansion behavior of solar cell encapsulation materials, Polym. Test. 44 (2015) 160–167. https://doi.org/10.1016/j.polymertesting.2015.04.009.
[34] G. Oreski, A. Rauschenbach, C. Hirschl, M. Kraft, G.C. Eder, G. Pinter, Crosslinking and post-crosslinking of ethylene vinyl acetate in photovoltaic modules, J. Appl. Polym. Sci. 134 (2017) 101. https://doi.org/10.1002/app.44912.
[35] P. Romer, G. Oreski, A.J. Beinert, H. Neuhaus, M. Mittag, More realistic considerations of backsheets coefficient of themal expansion on thermomechanics of PV modules, in: 37th European Photovoltaic Solar Energy Conference and Exhibition, pp. 772–776.
[36] N. Bosco, M. Springer, X. He, Viscoelastic Material Characterization and Modeling of Photovoltaic Module Packaging Materials for Direct Finite-Element Method Input, IEEE J. Photovoltaics 10 (2020) 1424–1440. https://doi.org/10.1109/JPHOTOV.2020.3005086.
[37] V. Meslier, B. Chambion, P.-O. Bouchard, J.-L. Bouvard, Thermal Expansion Behavior of a Thermoplastic Polyolefin for Photovoltaic Application Over Hygrothermal Aging, IEEE J. Photovoltaics (2024) 1–10. https://doi.org/10.1109/JPHOTOV.2024.3463950.
[38] V. Meslier, J.-L. Bouvard, P.-O. Bouchard, B. Chambion, A. Derrier, Measurement of Encapsulant Thermal Expansion (CTE): Impact of Residual Stresses, in: 41st European Photovoltaic Solar Energy Conference and Exhibition, 3AV.1.13.
[39] P. Nivelle, J.A. Tsanakas, J. Poortmans, M. Daenen, Stress and strain within photovoltaic modules using the finite element method: A critical review, RENEW SUST ENERG REV 145 (2021) 111022. https://doi.org/10.1016/j.rser.2021.111022.
[40] A.J. Beinert, P. Romer, A. Büchler, V. Haueisen, J. Aktaa, U. Eitner, Thermomechanical stress analysis of PV module production processes by Raman spectroscopy and FEM simulation, Energy Procedia 124 (2017) 464–469. https://doi.org/10.1016/j.egypro.2017.09.282.
[41] S.K. Tippabhotla, W. Song, A.A. Tay, A.S. Budiman, Effect of encapsulants on the thermomechanical residual stress in the back-contact silicon solar cells of photovoltaic modules – A constrained local curvature model, J. Sol. Energy 182 (2019) 134–147. https://doi.org/10.1016/j.solener.2019.02.028.
[42] U. Eitner, S. Kajari-Schröder, M. Köntges, H. Altenbach, Thermal Stress and Strain of Solar Cells in Photovoltaic Modules, in: H. Altenbach, V.A. Eremeyev (Eds.), Shell-like Structures, Springer Berlin Heidelberg, Berlin, Heidelberg, 2011, pp. 453–468.
[43] M. Paggi, S. Kajari-Schröder, U. Eitner, Thermomechanical deformations in photovoltaic laminates, The Journal of Strain Analysis for Engineering Design 46 (2011) 772–782. https://doi.org/10.1177/0309324711421722.

[44] N. Klasen, F. Heinz, A. de Rose, T. Roessler, A. Kraft, M. Kamlah, Root cause analysis of solar cell cracks at shingle joints, Sol. Energy Mater. Sol. Cells 238 (2022) 111590. https://doi.org/10.1016/j.solmat.2022.111590.
[45] A.J. Beinert, P. Romer, M. Heinrich, M. Mittag, J. Aktaa, D.H. Neuhaus, The Effect of Cell and Module Dimensions on Thermomechanical Stress in PV Modules, IEEE J. Photovoltaics 10 (2020) 70–77. https://doi.org/10.1109/JPHOTOV.2019.2949875.
[46] L. Papargyri, P. Papanastasiou, G.E. Georghiou, Sequential thermomechanical stress and cracking analysis of photovoltaic modules with full and half-cut cells, Sol. Energy Mater. Sol. Cells 278 (2024) 113166. https://doi.org/10.1016/j.solmat.2024.113166.
[47] M. Pander, S. Dietrich, S.-H. Schulze, U. Eitner, M. Ebert, Thermo-mechanical assessment of solar cell displacement with respect to the viscoelastic behaviour of the encapsulant, in: 12th International Thermal, Mechanical and Multi-Physics Simulation and Experiments in Microelectronics and Microsystems, pp. 433–438.
[48] D.C. Miller, X. Gu, L. Ji, G. Kelly, N. Nickel, P. Norum, T. Shioda, G. TamizhMani, J.H. Wohlgemuth, Examination of a size-change test for photovoltaic encapsulation materials, in: Reliability of Photovoltaic Cells, Modules, Components, and Systems V, San Diego, California, USA, SPIE, 2012, 84720T.
[49] Breyer GmbH, Green EVA extrusion line for encapsulation film: Advanced technology combines low shrinkage encapsulation film and high production speed – no energy consuming annealing necessary, no interlayer necessary., 2012 (accessed 18 February 2026.).
[50] H.-Y. Li, L.-E. Perret-Aebi, V. Chapuis, C. Ballif, Y. Luo, The effect of cooling press on the encapsulation properties of crystalline photovoltaic modules: residual stress and adhesion, Prog. Photovolt. 23 (2015) 160–169. https://doi.org/10.1002/pip.2409.
[51] C. Hirschl, M. Biebl–Rydlo, M. DeBiasio, W. Mühleisen, L. Neumaier, W. Scherf, G. Oreski, G. Eder, B. Chernev, W. Schwab, M. Kraft, Determining the degree of crosslinking of ethylene vinyl acetate photovoltaic module encapsulants—A comparative study, Sol. Energy Mater. Sol. Cells 116 (2013) 203–218. https://doi.org/10.1016/j.solmat.2013.04.022.
[52] G. Oreski, M. Bredacs, S. Feldbacher, P. Christöfl, J. Geier, C. Barretta, C. Camus, E. Malguth, Adrian, New rapid method for optical non-destructive determination of the degree of crosslinking of PV module encapsulants, in: 2025 IEEE 53rd Photovoltaic Specialists Conference (PVSC), Montreal, QC, Canada, IEEE, 2025, pp. 90–93.
[53] J.C. Schlothauer, C. Peter, C. Hirschl, G. Oreski, B. Röder, Non-destructive monitoring of ethylene vinyl acetate crosslinking in PV-modules by luminescence spectroscopy, J. Polym. Res. 24 (2017) 203. https://doi.org/10.1007/s10965-017-1409-y.
[54] G.M. Wallner, B. Adothu, R. Pugstaller, F.R. Costa, S. Mallick, Comparison of Crosslinking Kinetics of UV-Transparent Ethylene-Vinyl Acetate Copolymer and Polyolefin Elastomer Encapsulants, Polymers 14 (2022). https://doi.org/10.3390/polym14071441.
[55] R. Meier, I.M. Slauch, M.I. Bertoni, Ultrasonic Characterization of Ethylene Vinyl Acetate (EVA) Crosslinking for Quality Assurance and Lamination Process Control, in: 2023 IEEE 50th Photovoltaic Specialists Conference (PVSC), San Juan, PR, USA, IEEE, 2023, pp. 1–5.
[56] K. Agroui, G. Collins, G. Oreski, M. Boehning, A. Hadj Arab, D. Ouadjaout, Effect of crosslinking on EVA-based encapsulant properties during photovoltaic module fabrication process, J. Ren. Energies 18 (2023). https://doi.org/10.54966/jreen.v18i2.508.
[57] M. Jaunich, M. Böhning, U. Braun, G. Teteris, W. Stark, Investigation of the curing state of ethylene/vinyl acetate copolymer (EVA) for photovoltaic applications by gel content determination, rheology, DSC and FTIR, Polym. Test. 52 (2016) 133–140. https://doi.org/10.1016/j.polymertesting.2016.03.013.

[58] Ch. Hirschl, L. Neumaier, W. Mühleisen, M. Zauner, G. Oreski, G.C. Eder, S. Seufzer, Ch. Berge, E. Rüland, M. Kraft, In-line determination of the degree of crosslinking of ethylene vinyl acetate in PV modules by Raman spectroscopy, Sol. Energy Mater. Sol. Cells 152 (2016) 10–20. https://doi.org/10.1016/j.solmat.2016.03.019.
[59] S. Lust, T. Weber, S.R. Kuntamukkula, A. Mordvinkin, M. Wendt, Update of quality control tests for new PV encapsulation materials, EPJ Photovoltaics 15 (2024) 5. https://doi.org/10.1051/epjpv/2024006.
[60] A. Trefzer, A.K. Öz, J. Forster, C. Wellens, M. Çalışkan Arslan, C. Düz, Optimization of Soxhlet Extraction Parameters for Gel Content Determination of Co-Extruded EPE. WIP-Munich, 42nd European Photovoltaic Solar Energy Conference and Exhibition (2025). https://doi.org/10.4229/EUPVSEC2025/3AV.1.18.
[61] K. Liu, D.C. Miller, N. Bosco, R.H. Dauskardt, Determining the Crosslinking and Degradation Reaction Kinetics in Photovoltaic Encapsulants Using Accelerated Aging, in: 2024 IEEE 52nd Photovoltaic Specialist Conference (PVSC), Seattle, WA, USA, IEEE, 2024, pp. 909–914.
[62] M. Landa-Pliquet, T. Béjat, M. Serasset, A. Descormes, E. Mofakhami, E. Voroshazi, Enhancing photovoltaic modules encapsulation: Optimizing lamination processes for Polyolefin Elastomers (POE) through crosslinking behavior analysis, Sol. Energy Mater. Sol. Cells 267 (2024) 112725. https://doi.org/10.1016/j.solmat.2024.112725.
[63] A.K. Öz, C. Herzog, C. Wellens, D.E. Mansour, M. Heinrich, A. Kraft, The Impact of the Lamination Process on the Adhesion Properties at the Glass-Encapsulant Interface and Damp Heat Stability of PV Modules, in: 38th European Photovoltaic Solar Energy Conference and Exhibition, pp. 708–714.
[64] D. Wu, P. Wessel, J. Zhu, D. Montiel-Chicharro, T.R. Betts, A. Mordvinkin, R. GOttschalg, Influence of Lamination Conditions of EVA Encapsulation on Photovoltaic Module Durability, Materials (Basel) 16 (2023). https://doi.org/10.3390/ma16216945.
[65] S. Jonai, K. Hara, Y. Tsutsui, H. Nakahama, A. Masuda, Relationship between cross-linking conditions of ethylene vinyl acetate and potential induced degradation for crystalline silicon photovoltaic modules, Jpn. J. Appl. Phys. 54 (2015) 08KG01. https://doi.org/10.7567/JJAP.54.08KG01.
[66] J. Zhu, D. Montiel-Chicharro, T.R. Betts, R. Gottschalg, Correlation of Degree of EVA Crosslinking with Formation and Discharge of Acetic Acid in PV Modules, in: 33rd European Photovoltaic Solar Energy Conference and Exhibition; 1795-1798 / 33rd European Photovoltaic Solar Energy Conference and Exhibition, pp. 1795–1798.
[67] Kuan Liu, David C. Miller, Nick Bosco, Jimmy M. Newkirk, Reinhold H. Dauskardt (Eds.), Advancing Steady-State and Sequenced Accelerated Aging for Assessing the Adhesion Degradation of Contemporary Encapsulants, 2025.
[68] G. Oreski, A. Rauschenbach, C. Hirschl, L. Neumaier, M. Kraft, G. Pinter, Challenges in Measuring the Degree of Crosslinking of Ethylene Vinyl Acetate. 5 pages / 29th European Photovoltaic Solar Energy Conference and Exhibition; 2457-2461 (2014). https://doi.org/10.4229/EUPVSEC20142014-5DO.10.2.
[69] IEC, Measurement procedures for materials used in photovoltaic modules - Part 1-6: Encapsulants - Test methods for determining the degree of cure in Ethylene-Vinyl Acetate, 1st ed. 27.160 - Solar energy engineering, 2017. https://webstore.iec.ch/publication/33050 (accessed 21 January 2020).
[70] Gareth James, Daniela Witten, Trevor Hastie, Robert Tibshirani, Jonathan Taylor, An Introduction to Statistical Learning.

[71] Joseph F. Hair Jr, William C. Black, Barry J. Babin, Rolph E. Anderson, Multivariate Data Analysis, seventhth, Pearson, 2009.
[72] S. Ogier, C. Vidal, D. Chapron, P. Bourson, I. Royaud, M. Ponçot, M. Vite, M. Hidalgo, A comparative study of calorimetric methods to determine the crosslinking degree of the ethylene-co-vinyl acetate polymer used as a photovoltaic encapsulant, J. Polym. Sci., Part B: Polym. Phys. 55 (2017) 866–876. https://doi.org/10.1002/polb.24335.
[73] M. Wendt, P. Wessel, R. GOttschalg, A. Mordvinkin, R. Heidrich, 2024. Crosslinking Behavior of Ethylene-Vinyl Acetate Copolymer Encapsulants in Dependence of the Additive Composition. Prog. Photovoltaics Res. Appl., pip.3849. https://doi.org/10.1002/pip.3849.
[74] M. Hidalgo, F. Medlege, M. Vite, C. Corfias-Zuccalli, P. Voarino, J. González-León, A new DSC method for the quality control of PV modules: Simple and quick determination of the degree of crosslinking of EVA encapsulants, Photovoltaics International (2011) 131–137.
[75] K. Brecl, C. Barretta, G. Oreski, B. Malic, M. Topic, The Influence of the EVA Film Aging on the Degradation Behavior of PV Modules Under High Voltage Bias in Wet Conditions Followed by Electroluminescence, IEEE J. Photovoltaics 9 (2019) 259–265. https://doi.org/10.1109/JPHOTOV.2018.2875196.
[76] G. Oreski, M. Knausz, G. Pinter, C. Hirschl, G.C. Eder, Advanced methods for discovering PV module process optimization potentials and quality control of encapsulation materials, in: 28th European Photovoltaic Solar Energy Conference and Exhibition, Paris, France, 2013.
[77] Sraisth, D.E. Mansour, A.K. Öz, P. Gebhardt, D. Klaus, C. Wellens, Reducing process time of PV module lamination by using double-side heating system, EPJ Photovolt. 16 (2025) 26. https://doi.org/10.1051/epjpv/2025014.
[78] P. Gebhardt, S. Marletti, J. Markert, U. Kräling, M. Tu, I. Haedrich, D. Philipp, Comparison of Commercial TOPCon PV Modules in Accelerated Aging Tests, IEEE J. Photovoltaics 15 (2025) 24–29. https://doi.org/10.1109/JPHOTOV.2024.3483317.
[79] Eric Schneller, Alex Morgan, Neil Wiens, Hong Xiang Xuan, Tyler Frank, Andrey Zelenskiy (Eds.), Effects of Encapsulation Combinations on the Performance and Reliability of TOPCon Modules, 2024.
[80] Yuqiu Ye, Yanfang Zhou, Ye Wang, Bram Hoex, Xiaogang Zhu, Daoyuan Chen, Wenjuan Xue, Tiantian Wei, Bin Chen, Meng Cheng, Jiayan Lu, Haipeng Yin, Zi Ouyang, Damp-heat stability investigation of glass-backsheet modules based on TOPCon solar cells, Solar Energy Materials and Solar Cells 292 (2025). https://doi.org/10.1016/j.solmat.2025.113764.
[81] J. Tracy, D.R. D'hooge, N. Bosco, C. Delgado, R. Dauskardt, Evaluating and predicting molecular mechanisms of adhesive degradation during field and accelerated aging of photovoltaic modules, Prog. Photovolt. 26 (2018) 981–993. https://doi.org/10.1002/pip.3045.
[82] J.Y. Hartley, D.C. Miller, S. Uličná, N. Bosco, P. Hacke, Characterization, Accelerated Life Testing, and Finite Element Modeling of Low Temperature Solder Wire Interconnect Degradation Mechanisms, Prog. Photovolt. 33 (2025) 1139–1153. https://doi.org/10.1002/pip.70011.
[83] T. J. Silverman, M. Bliss, A. Abbas, T. Betts, M. Walls, and I. Repins, Movement of Cracked Silicon Solar Cells During Module Temperature Changes, in: 46th IEEE PVSC.
[84] M. Springer, T.J. Silverman, N. Bosco, J. Joe, I. Repins, Residual Stresses Affect Cell Fragment Movement, IEEE J. Photovoltaics 13 (2023) 547–551. https://doi.org/10.1109/JPHOTOV.2023.3269118.
[85] Sascha Dietrich, Matthias Pander, Martin Sander, Rico Meier, Matthias Ebert, Photovoltaics International (10 November 2014.) 89–97.
[86] I.M. Slauch, S. Vishwakarma, J. Tracy, W. Gambogi, R. Meier, F. Rahman, J.Y. Hartley, M.I. Bertoni, Manufacturing Induced Bending Stresses: Glass-Glass vs. Glass-Backsheet, in: 2021 IEEE

48th Photovoltaic Specialists Conference (PVSC), Fort Lauderdale, FL, USA, IEEE, 6202021, pp. 1943–1948.
[87] E. Özkalay, A. Virtuani, G. Eder, Y. Voronko, P. Bonomo, M. Caccivio, C. Ballif, G. Friesen, Correlating long-term performance and aging behaviour of building integrated PV modules, Energy Build. 316 (2024) 114252. https://doi.org/10.1016/j.enbuild.2024.114252.

5.6 Publication V

Title: Is EPE the Future of PV Encapsulation? A Comprehensive Material-Level Assessment

Journal: Solar Energy Materials and Solar Cells,

https://doi.org/10.1016/j.solmat.2026.114258

Date of publication: 20th of February 2026 (online), 15th of June 2026 (in print)

	Share in %							Total
	Author	Co-authors						
	PhD Student	1	2	3	4	5	6	
Conceptualization	70	15					15	100
Methodology	80	10					10	100
Formal analysis	70	10	10	5	5			100
Investigation	70	20		5	5			100
Visualization	95	5						100
Data curation	80	10	5	5				100
Writing - original draft	80	20						100
Writing - review & editing		25	10	5	5	5	50	100
Resources		20	10	10	10	10	40	100
Supervision							100	100
Project administration							100	100
Funding acquisition							100	100

Author, PhD Student: Nikolina Pervan

Co-author 1: Gabriele Eder

Co-author 2: Yuliya Voronko

Co-author 3: Astrid Macher

Co-author 4: Kamil Novotny

Co-author 5: Katharina Resch-Fauster

Co-author 6: Gernot Oreski

Solar Energy Materials & Solar Cells 300 (2026) 114258

Contents lists available at ScienceDirect

Solar Energy Materials and Solar Cells

journal homepage: www.elsevier.com/locate/solmat

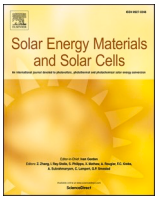

Is EPE the future of PV encapsulation? A comprehensive material-level assessment

Nikolina Pervan [a,b,*], Gabriele Eder [c], Yuliya Voronko [c], Astrid Macher [a], Kamil Novotny [b], Katharina Resch-Fauster [b], Gernot Oreski [a,b]

[a] Polymer Competence Center Leoben GmbH (PCCL), Sauraugasse 1, Leoben, 8700, Austria
[b] Material Science and Testing of Polymers, Montanuniversität Leoben, Franz Josef-Street 18, Leoben, 8700, Austria
[c] Österreichisches Forschungsinstitut für Chemie und Technik (OFI), Franz-Grill-Straße 5, Objekt 213, Vienna, 1030, Austria

ARTICLE INFO

Keywords:
n-type solar cell
Tandems
Encapsulants
EPE
Reliability
Material properties

ABSTRACT

Coextruded ethylene vinyl acetate - polyolefin - ethylene vinyl acetate (EPE) encapsulant films were developed in response to industrial demand and to support the technological transition in photovoltaic modules (PV) towards higher-efficiency solar cells that are more sensitive to moisture than previous generations. EPE was designed to combine cost-effectiveness and processability of ethylene vinyl acetate (EVA) with the superior electrical insulation and moisture barrier properties of polyolefin. This study systematically investigates the chemical, optical, thermal, and thermo-mechanical properties of commercially available EPE encapsulants.

The outer EVA layers of all EPE encapsulants were comparable, showing only slight differences in vinyl acetate content. The main difference between the four EPE encapsulants was found in the inner polyolefin layer. EPE-1 has an ethylene acrylate copolymer, whereas EPE-2; −3; −4 have ethylene α-olefin copolymer core layers, but with different side groups and/or varying comonomer contents. The water vapor transmission rate (WVTR) of all EPE films is significantly lower than that of EVA.

Differences in the crosslinking behaviour were evident from thermal analysis. EPE-1 was the only sample with a non-crosslinking inner polyolefin layer, whose high crystallinity reduced visible-light transmission but also enhanced barrier to water vapor. The co-extrusion process appeared to improve the dimensional stability of EPE-2; −3; −4, compared to standard EVA.

Overall, EPE encapsulants fulfil their intended purpose of reducing WVTR. However, the long-term impact of the EVA layer at the cell interface under environmental exposure remains to be evaluated.

1. Introduction

Environmental, economic, and social challenges are driving the development of photovoltaic (PV) technology towards more energy-efficient and cost-effective PV modules [1]. In practice, achieving cost reductions often requires removing, replacing, or reducing material thickness, as has already been observed for several module components such as solar cells, interconnections, and solar glass [1–6]. Such changes can cause various issues, including reduced mechanical stability and resistance to environmental influences, delamination of the intermediate layers, corrosion, glass breakage, encapsulant yellowing and cracks in the backsheet [5,7–10]. All of these can negatively impact the performance and lifespan of PV modules.

The technologies and materials on which the PV industry has relied in recent years are already being gradually replaced. Passivated Emitter and Rear Cell (PERC) solar cells are being replaced by n-type technologies such as Tunnel Oxide Passivated Contact (TOPCon) and Silicon Heterojunction (SHJ) cells, as these offer higher efficiency. Furthermore, bifacial modules are increasingly being manufactured using glass/glass (G/G) construction, while the use of polymer backsheets is declining [1,11]. Consequently, the requirements for the polymer encapsulation material, the binding element in the PV module layers, are also changing.

Ethylene vinyl acetate (EVA) has long dominated the encapsulation materials market due to its low cost, ease of processing, and widespread use in the PV industry [1]. However, the increased use of less robust n-type cells (TOPCon, SHJ) and tandem cells disfavours EVA as the encapsulant of choice, since it provides limited barrier against water

* Corresponding author. Polymer Competence Center Leoben GmbH (PCCL), Sauraugasse 1, Leoben, 8700, Austria
E-mail address: nikolina.pervan@pccl.at (N. Pervan).

https://doi.org/10.1016/j.solmat.2026.114258
Received 18 December 2025; Received in revised form 17 February 2026; Accepted 17 February 2026
Available online 20 February 2026

vapor and decomposes in the presence of moisture, forming corrosive acetic acid. Both moisture and an acidic environment can lead to corrosion of the front metallization of n-type solar cells, resulting in a reduction of the fill factor and overall electrical performance [7,12–15]. In glass/backsheet (G/BS) modules, acetic acid can diffuse outwards through the permeable polymer backside film, however, moisture penetration into the module is an undesirable side effect of non-diffusion-tight materials [16]. While moisture penetration is severely restricted in G/G modules (it can only occur via the side edges), if moisture does penetrate, both the moisture and the resulting acetic acid are retained within the module, promoting corrosion processes. These limitations have driven the development of new encapsulant formulations, including EVA with reduced VA content, polyolefin (POE) with improved glass adhesion, thermoplastic polyolefins (TPO), and coextruded EVA–polyolefin–EVA (EPE) encapsulants. The latter was developed to combine and balance the cost-effectiveness and processability of EVA with the superior electrical insulation and moisture barrier properties of POE [11,17].

Highly efficient and thinner silicon wafers of n-type solar cells will completely replace the PERC solar cell by 2030, according to market forecasts in the International Technology Roadmap for Photovoltaic (ITRPV) 2025 [1]. This leaves researchers and industry with only a few years to find the optimal material combinations and thus avoid premature failures and long-term reliability problems in these PV modules. However, PV modules with n-type solar cells and novel EPE encapsulation technology are already in use, even though the entire spectrum of their reliability challenges and degradation phenomena has not yet been fully explored. While the three primary degradation modes (humidity sensitivity, potential-induced degradation (PID) and ultraviolet-induced degradation (UVID)) for n-type technology are already widely known, far less is known about the properties and behaviour of EPE and its interaction with novel solar cell architectures. EPE has been used in several studies for encapsulating n-type cells in both G/G and G/BS module designs, where the focus has largely been on its impact on module efficiency. Although incorporating EPE in the module stacks has shown beneficial effects, including reduced cell degradation rates, limited data are available regarding its fundamental material properties, structure and composition [18].

To bridge the knowledge gap between material understanding and module performance, this study systematically investigates the chemical, optical, thermal, and thermo-mechanical properties of commercially available EPE encapsulants. The motivation arises from the many unknowns surrounding EPE that extend beyond the general claim that it combines the advantages of both EVA and polyolefin. Specifically, this study seeks to answer the following questions:

- Which EVA and polyolefin types are used in the co-extruded encapsulant?
- What are the thicknesses of the individual EPE layers, and how uniform are they?
- What happens to the layers during lamination regarding distribution, mixing, thickness changes, or bubble formation?
- How does the water vapor transmission rate/permeability (WVTR) of EPE compare to that of single layer EVA or polyolefin?
- What is the thermal behaviour of EPE and which layers crosslink?

Understanding the types of EVA and polyolefin in the co-extruded encapsulant is essential, as they influence both processability and long-term module stability. Therefore, in this study we aim to address these open questions through a comprehensive comparative study of four commercial EPE encapsulants with EVA and POE as reference materials.

2. Experimental: Materials and characterisation methods

Four different types of commercially available EVA–polyolefin–EVA (EPE) encapsulants were selected for this study. However, to avoid creating a bias or brand-specific interpretation, the encapsulants are referred to anonymously throughout the text.

The properties of these encapsulants were investigated in both their uncured and cured (laminated) states. Lamination of single encapsulant sheets was performed by placing encapsulant between two glass plates, using a non-stick mat made of Teflon between the glass and encapsulant layers. Thickness control spacers were employed to prevent edge pinching effects. The lamination parameters are summarized in Table 1.

For reference, EVA and crosslinking polyolefin encapsulants supplied by one of the EPE manufacturers (well known in the PV industry) were also included in the study. These materials were laminated under the same conditions and used for comparison of selected properties.

To facilitate certain analyses such as Fourier Transform Infrared Spectroscopy - Attenuated Total Reflectance (FTIR–ATR) and optical microscopy, the samples were embedded in epoxy resin. Additionally, mini-PV modules with dimensions of 10 × 10 cm^2 were laminated for cross-sectional microscopy in the regions of the solar cells and interconnections. The purpose of these mini modules was to evaluate encapsulant wetting behaviour, layer distribution, and variations in layer thickness. The same lamination conditions as for the single-sheet samples were applied.

2.1. FTIR-ATR spectroscopy

The surfaces of the uncured and cured encapsulants were analysed using a Fourier transform infrared (FTIR) spectrometer from PerkinElmer model Spectrum One, equipped with a deuterated triglycine sulphate (DTGS) detector. The measurements were performed on a universal attenuated total reflection (ATR) unit equipped with a diamond ATR-crystal having a contact area of ~1.5 mm in diameter. As it is not possible to investigate the polyolefin core layers of the EPE encapsulants with such a device, epoxy embedded cross-sections of the EPE were analysed by FTIR ATR imaging setup placed in the optical focus of a FTIR-Microscope. This device includes a germanium crystal with a round contact area with a diameter of ~750 µm. For the investigations, a FTIR spectrometer (PerkinElmer model Spectrum One) combined with an AutoImage microscope (PerkinElmer Spotlight 400) equipped with a liquid nitrogen-cooled mercury-cadmium-telluride (MCT) detector was used.

2.2. UV-vis-NIR spectroscopy

Hemispherical transmittance of the laminated encapsulants was recorded over the wavelength range between 250 and 1100 nm with a Lambda 950 Ultraviolet-Visible-Near Infrared (UV-Vis-NIR) Spectrophotometer from PerkinElmer Inc. Three samples were measured per laminated encapsulant sheet.

2.3. Water vapor transmission rate (WVTR)

The water vapor transmission rate (WVTR) of all samples was measured using a Mocon Permatran-W 3/34H. The measurements were performed at 85% relative humidity (RH) and 23 °C. The sample area was 5 cm^2 and two to three measurements were performed on multiple

Table 1
Encapsulant materials and lamination conditions.

Encapsulant	Lamination conditions
EPE-1	Evacuation step at 135 °C for 240 s
EPE-2	Lamination step at 150 °C (155 °C for EVA) for 900 s
EPE-3	Stack for single layer encapsulant lamination: glass/Teflon/
EPE-4	encapsulant/Teflon/encapsulant/Teflon/glass
POE	
EVA	

(2 to 4) independent sample specimen for each material. The thickness of the foils was determined according to DIN ISO 4593:2019, 5 points were measured and averaged. For better comparability, the measured WVTR of the encapsulant foils, [g m^{-2} day^{-1}], was also calculated/normalized for a foil thickness of 100 μm.

2.4. Light microscopy

The microscopic images of the embedded cross-sections of uncured and cured encapsulants were performed with an Olympus reflected-light microscope (bi-ocular) with 40x magnification. Light microscopic images of the cross-section of the laminated mini-PV modules were taken with Alicona InfiniteFocus Microscope IFM G4 from Alicona Imaging GmbH, implemented magnification of 5× was used in the bright field mode.

2.5. Differential Scanning Calorimetry (DSC)

Differential Scanning Calorimetry (DSC) was performed using a DSC 6000 from PerkinElmer Inc. to measure thermograms of encapsulants. Approximately 7 mg of each material was placed in an aluminium pan with perforated lid; measurements were done in the three repetitions and averages from all measurements were used for the calculations. Measurements were done following the IEC 62788-1-6:2017 standard for combined enthalpy and melt/freeze method [19]. Initial temperature was always set to 25 °C, first heating was done up to 100 °C, this step is done to melt the specimen and erase structure-related effects, but under the temperature of peroxide activation. Next step was first cooling, down to −20 °C to obtain crystallization peak of uncured encapsulants. The specimen was then heated up to 225 °C in the second heating step for the curing reaction to take place. Additional cooling down to −20 °C was done to obtain a “maximum cured” crystallization peak. The same heating steps were measured for the laminated samples. There was no dwell time between the steps; the heating rates were set to 10 °C min^{-1} and a nitrogen flow of 50 mL min^{-1} was imposed. Following this method, the degree of curing of EVA-based encapsulants can be calculated from residual enthalpy and from the crystallization peak.

2.6. Thermogravimetric analysis (TGA)

Thermogravimetric analysis (TGA) was done using a Thermogravimetric System TGA/DSC 1 of Mettler Toledo GmbH. The weight loss of approximately 10 mg of material was monitored while heating the sample in a nitrogen atmosphere (50 mL min^{-1}) from 35 to 700 °C, with a heating rate of 10 °C min^{-1}. The temperature at which the weight loss is equal to 5% with respect to the initial value ($T_{5\%}$) is considered an indicator for the beginning of the material's decomposition process.

2.7. Digital image correlation (DIC)

The dimensional stability of the uncured samples and coefficient of thermal expansion (CTE) of the laminated samples were measured using a Dantec Q400 TCT Digital Image Correlation (DIC) system from Dantec Dynamics. The device consists of two cameras, and a heating/cooling concealed chamber equipped with a thermal plate. Time series of images of the measured sample are taken during the thermal stages, which are then compared to the initial picture. During analysis, the evaluation software Istra 4D, Dantec Dynamics, calculates the relative displacement between the reference and each image of the acquired time series. Sample preparation is important as the software follows a speckle pattern that is applied on the surface of the rectangular sample of 4x4 cm^2. The speckle pattern was applied on the encapsulants in 2 layers; the first white coating serves as a primer and substrate cover and is followed by a second layer (black coating) which creates the speckle pattern. Achieving good contrast and independent speckles is necessary to guarantee a measurable surface area. The measurements were done in the temperature range from 25 to 140 °C, with a heating rate of 2 °C min^{-1}.

2.8. Dynamic mechanical analysis (DMA)

The experiments were conducted on a DMA 8000 instrument (PerkinElmer Inc.) in shear mode. Circular samples (9 mm in diameter) were prepared and measured at a sample displacement of 20 μm and a test frequency of 1 Hz. The sample temperature was varied from 50 to 200 °C at a heating rate of 3 °C min^{-1}, two measurement repetitions were done.

2.9. 180° peel test – adhesion strength

The 180° peel tests were performed using a 2.5 kN Zwicki from Zwick/Roell, equipped with a load cell of 1 kN capacity, at room temperature, with a test speed of 5 mm s^{-1}. Sample coupons, consisting of solar glass, a single layer of encapsulant, and a backsheet with an Al inner layer, were laminated under the conditions specified in Table 1. Samples measuring 20 cm in width, with an adhered length of 10 cm between the glass/encapsulant/backsheet layers and a non-adhered backsheet length of 20 cm were prepared according to ASTM D3330. Multiple strips of 1 cm width were cut with a scalpel and a minimum of five repetitions per encapsulant type were tested.

3. Results and discussion

3.1. Qualitative and quantitative material identification

3.1.1. Infrared spectroscopy

The IR-Spectra of the outer layers of all EPE foils (EPE-1 to 4) were comparable and showed the main absorptions of the polyethylene (PE) chain in the CH-stretching (ν) vibration region (maxima at 2918 and 2851 cm^{-1}) and the CH_2-deformation vibration region (at 1468 and 720 cm^{-1}). An additional absorption was observed at 1371 cm^{-1} and attributed to the deformation vibration of the methyl (CH_3) group. The bands at 1738 (ν C=O), 1240 (ν CO(=O)) and 1020 cm^{-1} (ν O-C) were assigned to vibrations of an acetate group. All observed IR absorptions are typical for EVA and in good agreement with literature on crosslinked EVA encapsulant films for PV applications [20–22]. The vinyl acetate (VA) content of the EVA films was then calculated from the absorption ratio of the ν C=O band (at 1738 cm^{-1}) and the n CH band at 2918 cm^{-1} according to Ref. [22]. For all 4 EPE types, the VA-content of the EVA-layers was between 25.3 and 29.4 % (see Table 2.).

However, the IR spectra of the polyolefin core layers showed some spectral differences (see Fig. 1.). The main features were identical for all polyolefin types and were observed in the CH-stretching and deformation region (maxima at 2918, 2850, 1467 and 720 cm^{-1}), typical for the PE molecular chain. The polyolefin layer of samples EPE-2, EPE-3 and EPE-4 showed small additional absorptions at 2954 (shoulder) and at 1377 cm^{-1}, which were assigned to CH_3 stretching and deformation vibrations, respectively. These two absorptions show increased intensity for sample EPE-3 indicating a higher relative concentration of methyl groups, thus branched side chains. Furthermore, only the polyolefin layer of EPE-2 has additional weak bands and 1092 and 770 cm^{-1}. The band at 770 cm^{-1} can be assigned to CH_2 rocking vibration characteristic of ethyl-type short-chain branches (evidence of α-olefin comonomer

Table 2
VA content of the EVA calculated from the IR intensity ratios of the EVA layers of the different EPE types and converted to the entire EPE film.

Sample	A_{1738}/A_{2918}	VA-content in EVA (%)	VA-content in EPE (%)
EPE-1	0.99	26.7	15
EPE-2	1.10	29.4	19
EPE-3	0.94	25.3	13.4
EPE-4	1.03	27.7	11.6

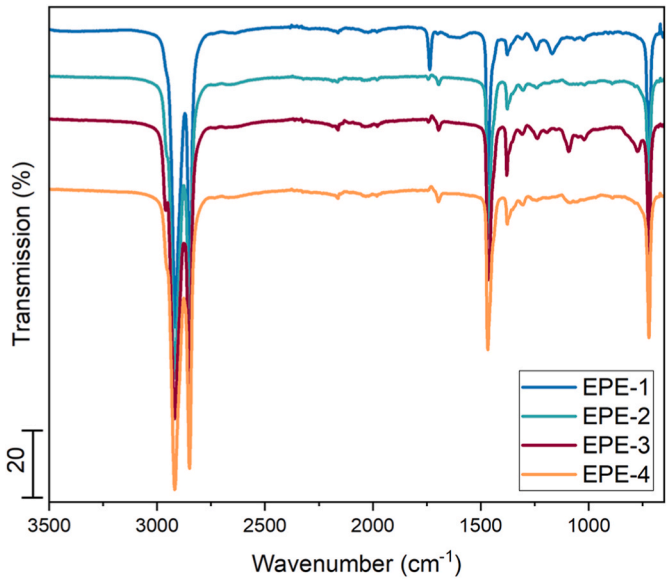

Fig. 1. FTIR-ATR spectra of the inner polyolefin layer of EPE encapsulants.

incorporation) [23,24]. In PE and related long-chain alkanes, a weak band around 1090–1095 cm^{-1} is commonly assigned to CH_2 twisting/skeletal C–C stretching in the polyethylene backbone, sensitive to chain conformation and crystallinity. Only if the material had been silane-grafted or contained siloxy additives, the absorption at 1092 cm^{-1} could be plausibly assigned to Si–O–C/Si–OCH_3 stretching [25]. Siloxane groups in encapsulants are either incorporated as adhesion promoters or, in certain thermoplastic polyolefin formulations, introduced by grafting to enable latent curing of the encapsulant [17,26].

In contrast, in the IR spectra of the core layer of EPE-1 hardly any absorptions characteristic for methyl groups were detected, but carbonyl absorptions at 1736 and 1242 cm^{-1} indicating the presence of a carboxylic acid ester. In addition, a low intensity absorption at 1170 cm^{-1} is observed and can be attributed to a secondary ester C–O stretching vibration (O–C–C) of an acrylate unit, possibly coupled with backbone C–C and CH wagging modes [27]. Consequently, the inner layer of EPE-1 can be identified as an ethylene acrylate–based material, which clearly distinguishes it from the other EPE types that lack ester-related absorptions and exhibit more typical polyolefin spectra.

3.1.2. *UV-vis-NIR spectroscopy*

One of the key roles of encapsulant in a PV module is optical coupling, for which high transmittance is essential. For the EPE encapsulants studied here, transmittance was measured after lamination, the corresponding UV-Vis-NIR spectra are shown in Fig. 2. EPE-2, EPE-3, and EPE-4 exhibited average transmittance values in the visible range between 90.5% and 93%. In contrast, a lower transmittance of 86.5% in the visible light region was observed for EPE-1, which can be attributed to a hazy appearance after lamination. A similar effect has been reported previously in the literature, where hazing of the polyolefin encapsulant was associated with material crystallization in dependence on the cooling rate after the lamination [17,28–30]. In addition to the haziness, some laminated samples form EPE-1 had a “marble effect,” characterized by white curved lines that likely resulted from uneven material distribution and high crystallinity of the polyolefin component. Interestingly, the UV-Vis-NIR curves shown in Fig. 2 show that all four EPE encapsulants under test were formulated without UV absorbers. The absorption at 275 nm for EPE-1 suggests the presence of light stabilizers and antioxidants [31]. However, because additive analysis tools were not used in this study, neither the identification of these compounds nor the determination of the EPE layer in which they are located was possible.

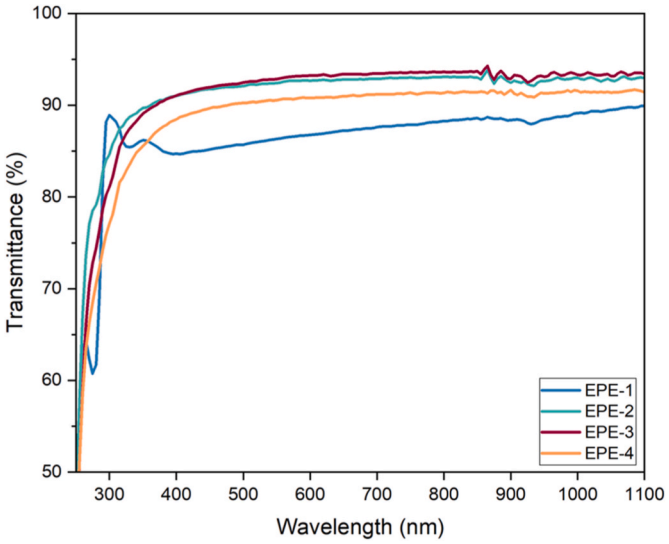

Fig. 2. UV-vis-NIR spectra of the EPE encapsulants.

3.1.3. *Light microscopy on cross sections of the foils and mini-PV modules*

After qualitative identification of the individual layers, the relative proportions were determined based on the thickness distribution data of the microscopic images of the cross-sections of the coextruded encapsulants after lamination (shown in Fig. 3.). The thickness of the individual layers and the relative proportion of polyolefin are given in Table 3. The relative fraction of polyolefin is ranging from 36% for EPE-2 to 58% for EPE-4.

As a next step, the encapsulant thickness and layer distribution in the laminated mini-PV modules, containing solar cells with 250 μm-high busbars, were examined. Mini-PV modules were cut through the middle, with a water jet saw, to expose the area containing the solar cell and interconnections. All encapsulants had good wetting of the interconnections. Despite the use of thickness controls during the lamination, some encapsulants were squeezed out, the reduction in total thickness of 20 and 30% was observed for EPE-1 and EPE-3, respectively. Adjustment of lamination parameters, such as applied pressure, may therefore be necessary to minimize this effect. Interestingly, the polyolefin layer was the one predominantly squeezed by the solar cell and busbars. A reason for this likely comes from the lower viscosity and slower curing process of the polyolefin component. The thickness reduction of the polyolefin layer was up to 75%, especially in the region above the interconnections. Thickness reduction of EPE-2, shown in Fig. 4., happened in all three layers. The inner EVA layer filled in the region around the interconnections and experienced the highest thickness reduction above the busbar, while the outer layer of EVA in contact with glass had the least thickness reduction of all three layers. In the case of EPE-4 the outer EVA layer maintained the same thickness throughout the entire cross-section, while the thickness of the inner EVA layer above the busbar was reduced to less than 20% of thickness above the solar cell. In addition to these observations, in some samples interlayer diffusion and flow of the polyolefin component into the EVA layer were observed in the surrounding of the interconnections and around the cell edges (see supporting information for corresponding figure).

3.2. *Permeation characteristics: Water vapor transmission rate (WVTR)*

The water vapor transmittance (WVTR) of all EPE types, as well as of EVA and POE for comparison, was determined in the laminated state. The measurements were performed at 23 °C and 80% relative humidity. For better comparability, the WVTR results were normalized to a sample thickness of 100 μm (shown in Fig. 5.).

EVA showed by far the highest WVTR of 35 g m^{-2} day^{-1} per 100 μm,

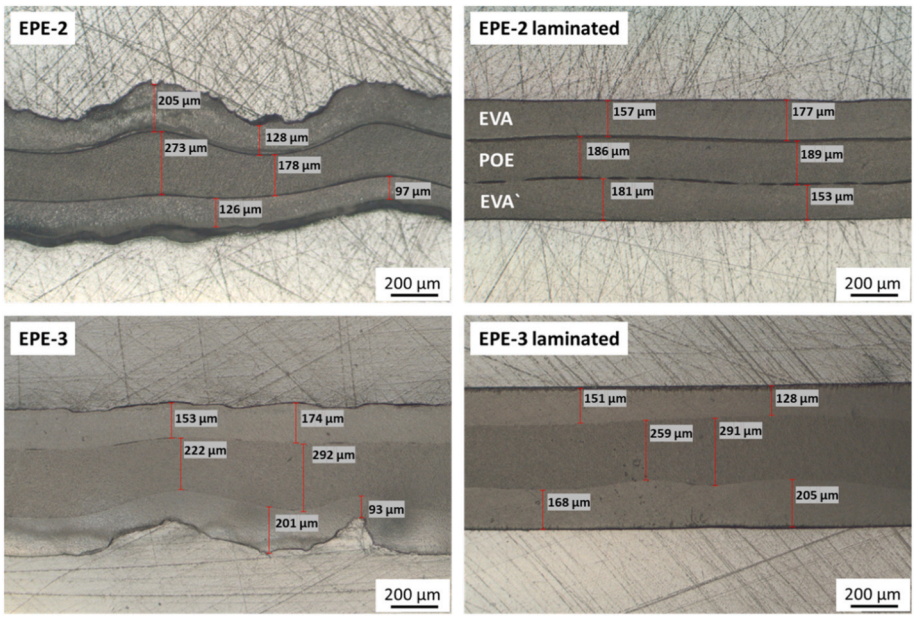

Fig. 3. Light microscopic images of the cross-sections of EPE-2 and EPE-3 before (left) and after (right) lamination.

Table 3
Thickness and relative contribution of the individual layers (after lamination) as derived from the light microscopic images (10 measuring points per value, standard deviation ± 10 µm).

Laminated sample	Layer thickness (µm)				Relative contribution per layer (%)			
	EVA	POE	EVA'	total	EVA	POE	EVA'	EVA + EVA'
EPE-1	132	210	133	475	28	44	28	56
EPE-2	178	187	159	523	34	36	30	64
EPE-3	155	293	171	619	25	47	28	53
EPE-4	101	283	107	490	20	58	22	42

*EVA and EVA' each present one side of the EVA layer in the coextruded encapsulant.

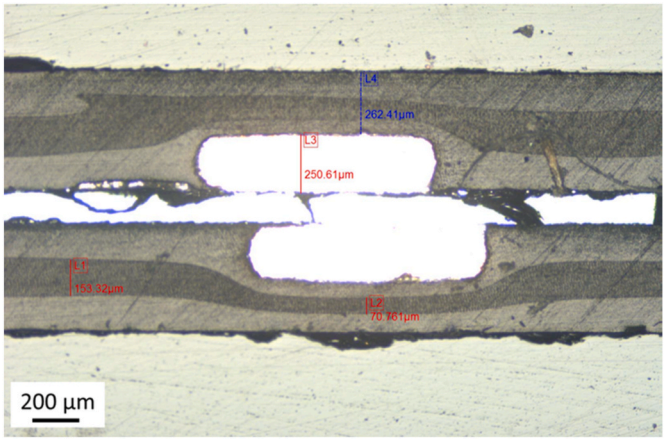

Fig. 4. Cross-section of a laminated mini-PV module with EPE-2 encapsulant.

while for the POE foil a low value of 5.4 was determined. The EPE films EPE-1 to EPE-4 gave normalized WVTRs between 3.1 and 11.7 g m^{-2} day^{-1} per 100 µm with EPE-1 having superior water vapor barrier properties, surprisingly even better than the single POE foil. This low value of the WVTR for EPE-1 confirms observation from the UV-Vis-NIR spectra, that the crystallinity of this polyolefin is higher compared to the others.

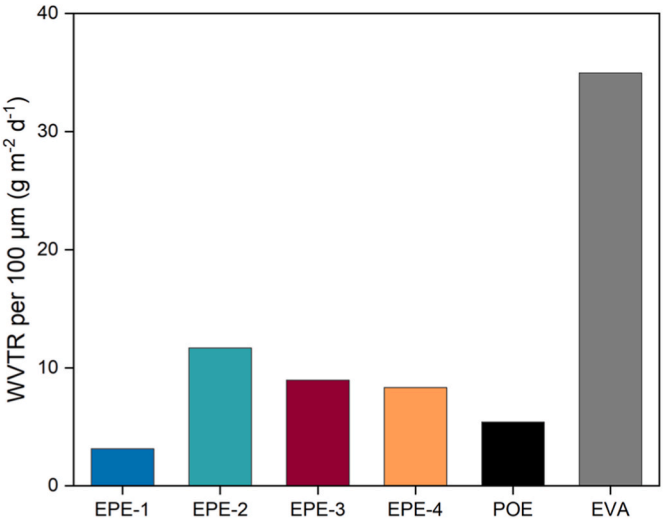

Fig. 5. WVTR of the cured EPE-1 to 4, POE and EVA encapsulants normalized to a sample thickness of 100 µm.

Since for a multi-material foil the layer with the lowest WVTR determines the overall WVTR, normalizing the WVTR to the polyolefin layer thickness can provide additional insights into the differences in barrier performance. Despite having the second thinnest polyolefin layer, EPE-1 exhibits the best barrier properties at 1.4 g m^{-2} d^{-1} per 100 µm of polyolefin layer, followed by EPE-2 at 4.2 g m^{-2} d^{-1}. In contrast, EPE-3 and EPE-4, both of which have a thicker polyolefin layer, show higher per 100 µm polyolefin normalized WVTR values of 4.3 and 4.8 g m^{-2} d^{-1}, respectively. This result underscores the influence of the respective polyolefin type on the barrier performance of the EPE.

3.3. *Thermal & thermo-mechanical properties*

3.3.1. *Differential scanning calorimetry (DSC)*

Thermal properties, including melting temperature (T_m), cross-linking reaction initiated by peroxide decomposition, and crystallization temperature (T_c), of encapsulants can be obtained from DSC curves using the combined enthalpy and melt/freeze method described in IEC

62788-1-6:2017. All results are summarized in Table 4., and it is important to note that the reported values were extracted after removal of the thermal history (i.e., after the first heating cycle to 100 °C). The values for uncured and 15 min laminated encapsulants are obtained from the 1st cooling and 2nd heating curves, and the max. cured values are obtained from the 2nd cooling curve, after heating up to 225 °C.

The second heating curves of uncured and laminated samples for EPE encapsulants are shown in Fig. 6., represented by solid line and dotted line, respectively. It is evident that EPE-3 and EPE-4 contain two different types of peroxides, most likely one intended for crosslinking the EVA component and the other for the polyolefin component, although a definitive conclusion cannot be drawn without additive analysis. The relatively flat curve above 120 °C for the laminated encapsulants indicates that most of the peroxides have reacted and that crosslinking process has likely reached its maximum. In addition to the crosslinking reaction, a second melting peak is present at 105 °C for the EPE-1. The melting peak value does not change after lamination, suggesting that it corresponds to the polyolefin component and that this layer is a non-crosslinking polyolefin type. This interpretation is consistent with the information provided in the manufacturer's technical data sheet (TDS). For the EPE-2, EPE-3 and EPE-4, only a single melting peak is observed, suggesting that the melting process of both EVA and polyolefin component overlaps.

The melting peak values of the cross-linkable components in the EPE encapsulants shift to lower temperatures, after crosslinking following the same trend as the corresponding shift of the crystallization peak. This behaviour arises from the reduced chain mobility after crosslinking, which limits the ability of the polymer chains to align and form well-ordered crystals. As a result, crystallization requires more energy (lower temperature), and the crystals that form are less perfect due to the restricted space available for their growth, making them easier to melt. Consequently, both the crystallization temperature and the melting temperature decrease, as shown in Fig. 6 and 7., and in Table 4.

The cooling curves provide more insights into the differences between the EPE encapsulants, particularly in respect to the crosslinking process. Fig. 7 shows only the temperature range where changes in material behaviour are present, i.e. 25 to 70 °C. The T_c at 90 °C observed for EPE-1, belongs to the non-crosslinking polyolefin component, remains unchanged after lamination (see the complete DSC cooling curve in the supporting information). The solid line represents the 1st cooling step of the uncured samples, while the dotted line corresponds to the 1st cooling curve of samples laminated for 15 min. The curve of the maximally cured sample (dashed line) was obtained from the second cooling after heating the laminated sample to 225 °C. Interestingly, EPE-2 and EPE-4 exhibit two crystallization peaks after lamination despite showing only a single melting peak. This behaviour can be explained by differences in crystallization kinetics between the two polymer components. Based on in-house DSC measurements of pure EVA and pure polyolefin encapsulants, the polyolefin crystallizes at higher temperatures, whereas EVA crystallizes at lower temperatures. Therefore, the first (higher-temperature) crystallization peak can be attributed to the polyolefin, while the second (lower-temperature) peak corresponds to the EVA component. Moreover, the 15 min lamination appears insufficient to achieve a high degree of cure in the polyolefin component of EPE-2 and EPE-4. This conclusion is supported by the shape and intensity of the crystallization peak, which differ from those of the maximally cured samples. In contrast, the crystallization peak in EPE-1 originates solely from the EVA component, and in EPE-3 the crystallization of both components overlaps due to the similar crystallization kinetics, resulting in a single crystallization peak.

Table 4
Thermal properties of uncured, 15 min laminated and maximally cured EPE encapsulants.

	Uncured				15 min laminated				Max. cured	
Sample	T_m (°C)		T_c (°C)		T_m (°C)		T_c (°C)		T_c (°C)	
EPE-1	72	105	51	91	64	104	42	91	43	91
EPE-2	70		48		62		39	50	39	48
EPE-3	68		50		63		40		40	
EPE-4	72		49		64		40	51	40	50

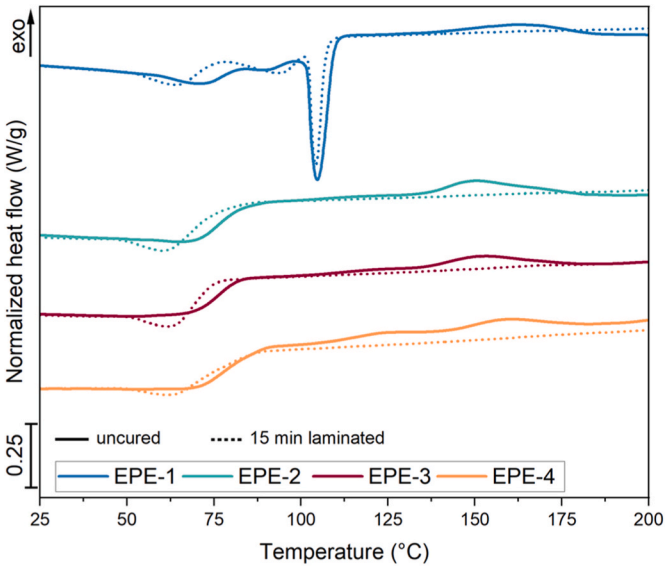

Fig. 6. The 2nd heating curves of uncured (solid line) and 15 min laminated (dotted line) EPE encapsulants.

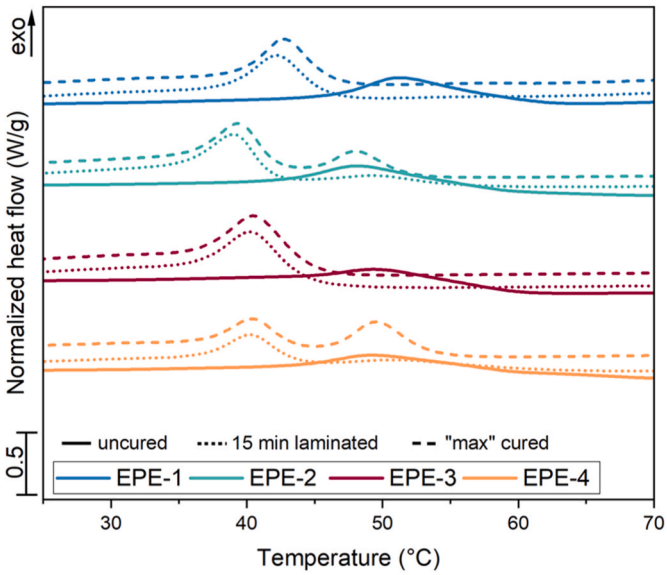

Fig. 7. The cooling curves of uncured (solid line), 15 min laminated (dotted line) and max. cured (dashed line) EPE encapsulants.

3.3.2. *Thermogravimetric analysis (TGA)*

Thermogravimetric analysis (TGA) provides information about the thermal decomposition of polymeric material. The temperature at which the sample has lost 5% of its initial weight ($T_{5\%}$) is commonly used as an indicator of the onset of decomposition. This technique has also been applied to estimate the vinyl acetate (VA) content in EVA-based encapsulants [18,32–34]. In principle, the weight loss occurring around 350 °C corresponds to the thermal degradation of VA units, while the ethylene backbone remains stable at this temperature. Therefore, by assuming that only the VA component decomposes in this temperature range, the observed mass loss can provide an approximate

quantitative measure of the VA fraction within the encapsulant. However, several factors must be considered: other components in the encapsulant, such as polyolefin layers, additives, or stabilizers, may also degrade at similar temperatures. Since additive analysis was not performed in this study, and the onset of degradation for the specific polyolefin component present in the EPE encapsulant is unknown, calculating weight loss at 350 °C may significantly overestimate the VA content. Nevertheless, the TGA curves shown in Fig. 8 indicate that EPE-1 and EPE-2 exhibit similar weight loss, as do EPE-3 and EPE-4, with all four encapsulants falling between the degradation curves of the pure POE and EVA reference materials. The presence of the POE layer appears to improve the thermal stability of the encapsulants, as evidenced by the higher $T_{5\%}$ values, i.e. 5 and 12 °C, compared to pure EVA.

3.3.3. Dimensional stability and coefficient of thermal expansion (CTE)

The dimensional stability of encapsulants is strongly influenced by their thermal and processing history during production. In the first step, the polymer is melted and mixed with additives through extrusion. In the second step, the foil is formed by flat-die extrusion or calendering, which introduces polymer orientation, industrially known as the machine direction (MD). Processing parameters such as melt temperature, calendering pressure, and cooling rate must be carefully optimized to minimize residual stress that could lead to shrinkage during the lamination process.

Dimensional stability was evaluated using digital image correlation (DIC), which enables the measurement of non-constrained, uncured encapsulant films on a heated plate to detect dimensional changes such as shrinkage, expansion, or warping. With greater dimensional change, the higher the thermo-mechanical stress that may be introduced during PV module lamination that can cause issues such as solar cell displacement, interconnection delamination, wrinkles in the polymeric frontsheet or backsheet [35]. Fig. 9 shows the dimensional (length) change in both MD and transversal to MD for the four EPE encapsulants. Among them, EPE-4 exhibited the smallest dimensional change, followed by EPE-3, EPE-2, and EPE-1 which showed the largest shrinkage in MD and is the only encapsulant with high expansion in the transversal to MD. Shrinkage begins once the onset of the melting temperature is reached. For EPE-2, EPE-3, EPE-4, and the POE encapsulant, shrinkage largely ceases above 80 - 90 °C. In contrast, for EPE-1, the highest shrinkage occurs when the polyolefin component begins to melt, causing the material to shrink to the extent that the speckle pattern above 105 °C can no longer be recognized by the software. EVA continues to shrink above 80 °C, but at a lower rate. Furthermore, comparing EPE-3 with the POE and EVA encapsulants from the same manufacturer shows that EPE-3 exhibits the lowest overall length change. These observations suggest that the co-extrusion process seems to reduce residual stress in the encapsulant films.

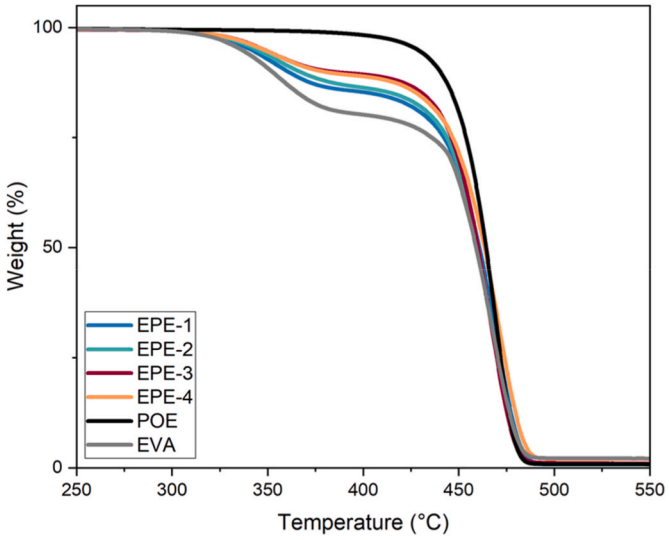

Fig. 8. TGA curves of the cured EPE-1 to 4, POE and EVA encapsulants.

The coefficient of thermal expansion (CTE) is a critical property within the PV module stack. CTE mismatches, high CTE values, and anisotropic thermal expansion can generate thermomechanical stresses during temperature fluctuations. Over time, these stresses may cause reliability issues such as solar cell displacement, microcracking, or interfacial delamination between the cells, interconnections, and the backsheet and frontsheet layers. In general, encapsulants with lower CTE improve PV module reliability, reduce residual stress, and help the material act effectively as a damping layer. The CTE values of the four EPE, as well as the POE and EVA reference materials, in the relevant PV module service temperature range (20 to 85 °C) are shown in Fig. 10. Although lamination reorients the initial molecular chain orientation introduced during film extrusion and crosslinking "locks in" the polymer network, encapsulant films generally remain anisotropic, exhibiting different CTE values and dimensional changes in the MD and transversal direction. Interestingly, although EPE-1 exhibited the highest shrinkage and expansion in the uncured state, lamination reduced its CTE, resulting in a lower range values compared to the other EPE encapsulants. With a heat stabilization process or prelamination step (below crosslinking onset) this encapsulant would introduce the lowest mismatch among the components of the PV module, within the tested temperature range.

3.3.4. Dynamic mechanical analysis (DMA)

Next to the DSC technique, the crosslinking behaviour of the encapsulants can be assessed by dynamic mechanical analysis (DMA) [20,36]. Fig. 11 shows the temperature-dependent storage viscosity (η') of the uncured encapsulant films and illustrates the progression of the thermal curing process. Upon heating, the storage viscosity initially decreases as the materials soften and transition toward a molten, more flowable state. A change in the slope of the curve in the mid-temperature range indicates that melting is essentially complete and the polymers are fully molten. With further heating, the storage viscosity continues to decrease until the curing reaction is thermally activated at temperatures above ~120 °C. At this point, the viscosity reaches a minimum and then begins to increase, reflecting the onset of crosslinking. This rise corresponds to the formation of a growing three-dimensional polymer network that restricts molecular mobility and increases resistance to flow. At higher temperatures, the storage viscosity levels off and becomes largely temperature-independent, indicating that the crosslinking reaction has reached completion and a stable network structure has formed in the encapsulant films. The crosslinking onset temperatures of the EPE encapsulants fall between those of the pure EVA and POE reference encapsulants, with only a few degrees difference in both onset and offset temperatures.

Additional information on material behaviour can be obtained from the storage viscosity values of all encapsulants before crosslinking (at 120 °C) and after crosslinking (at 150 °C), as presented in Table 5. Before the crosslinking reaction takes place all encapsulants exhibit similar storage viscosity values. A lower viscosity at this stage is beneficial, as it improves wetting of the PV module components, particularly of the interconnections. As crosslinking progresses, the storage viscosity increases, and at 150 °C differences between the encapsulation materials become noticeable. The strong influence of the non-crosslinking polyolefin component in EPE-1 on its storage viscosity is evident, as its viscosity does not change significantly after EVA crosslinking. The relatively low viscosity of the polyolefin also explains the thickness reduction of the EPE encapsulant observed in the mini-PV module. Due to its higher flowability, the polyolefin layer is more prone to squeeze-out during lamination, whereas the EVA layer crosslinks earlier and exhibits an increase in viscosity.

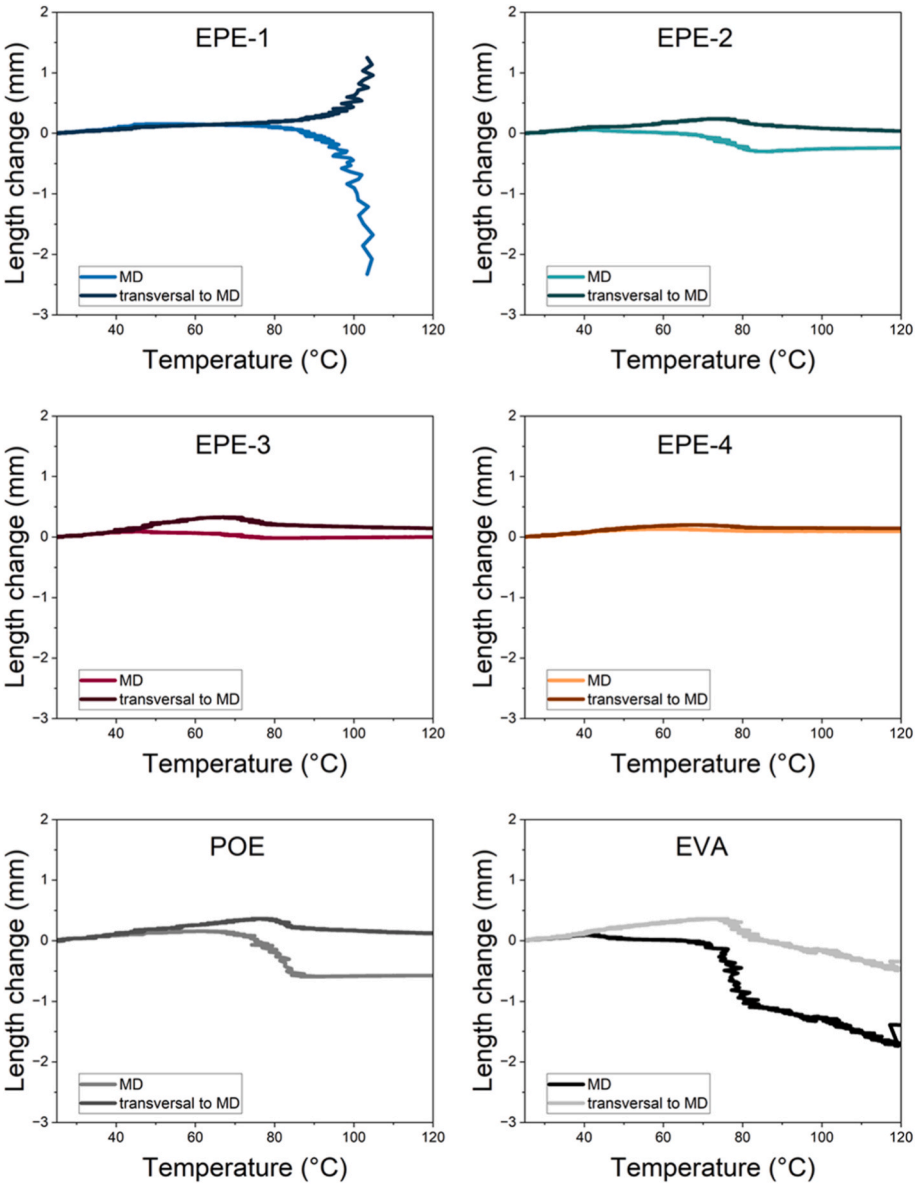

Fig. 9. Length change with temperature of uncured EPE-1 to 4, POE and EVA encapsulants in both MD and transversal to MD.

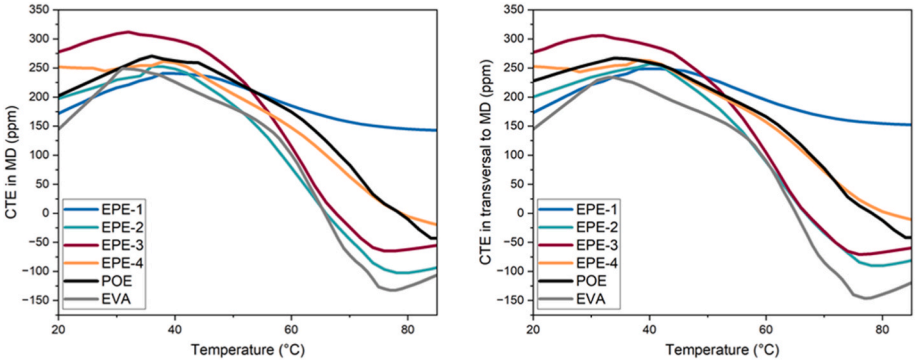

Fig. 10. CTE values from laminated EPE-1 to 4, POE and EVA from 20 to 85 °C in both MD and transversal to MD.

The POE encapsulants generally have lower storage viscosity than EVA as they crosslink more "lightly" [37]. Consequently, the influence of the polyolefin inner layer is also visible for EPE-2 and EPE-4, which show storage viscosity of one-half and one-fifth of the EVA. In contrast, EPE-3 shows the highest storage viscosity among the EPE samples and the closest value to EVA. Nevertheless, EPE-3 was the most strongly squeezed encapsulant in the mini-PV module tests, indicating that this behaviour was not related to viscosity but rather to the fact that EPE-3

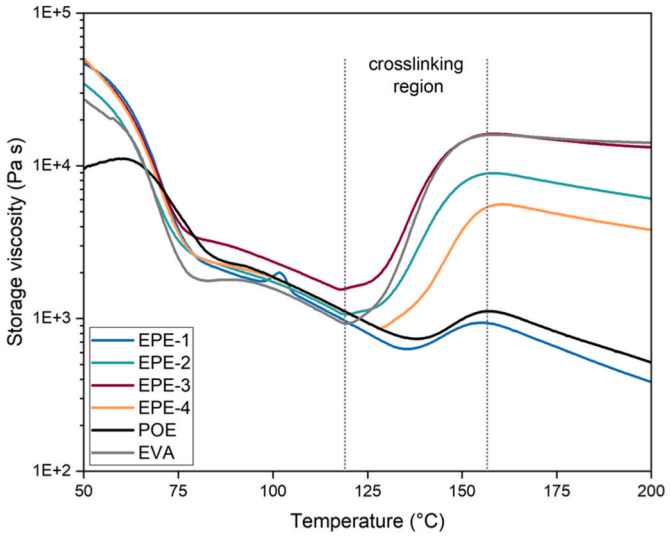

Fig. 11. Storage viscosity curves of uncured EPE-1 to 4, POE and EVA encapsulants.

Table 5
Storage viscosity values of four uncured EPEs, POE and EVA encapsulants at 120 °C and 150 °C.

Sample	η′ (Pa s) at 120 °C	η′ (Pa s) at 150 °C
EPE-1	935	890
EPE-2	1070	7770
EPE-3	1598	14435
EPE-4	1082	3775
POE	1071	998
EVA	926	14346

was the thickest EPE material examined, and thickness control and lamination pressure need to be optimized.

The storage viscosity values of the laminated encapsulants hold importance for the material behaviour during the service life, as it provides higher mechanical stability (graph and table is provided in supporting information). EPE-1 at 85 °C has the highest storage viscosity due to the non-crosslinking polyolefin inner layer that is in a solid state, the same positive impact as on the CTE values. However, above melting onset of the polyolefin the storage viscosity values decrease. Post curing was present for EPE-1 and EPE-2 which confirms that lamination time of 15 min is not long enough to reach maximal degree of cure. Since the EPE-4 has the highest amount of the polyolefin, the influence on its storage viscosity is high and is observed from decrease in the values as the material is heated, and eventually reach the same values as the pure POE.

3.4. Adhesion strength: 180° peel test

Multiple adhesion test methods are used to evaluate the adhesion between the various PV module components, and several have been proposed by various research institutes. These include the 90°, 180° and T-peel tests (measuring adhesion strength, N cm^{-1}), the width-tapered single cantilever beam test (measuring adhesion energy, J m^{-2}) and the compressive shear test (measuring shear stress, MPa) [38–42]. To be able to compare adhesion strength values presented in the manufacturer's TDS, based on 180° peel angle, we conducted measurements following ASTM D3330. To test adhesion strength between encapsulant and solar glass, a peel arm of backsheet with an aluminium inner layer was used, due to its strong adhesion to all types of encapsulants and minimal plastic deformation during the peel test.

The measured adhesion strength between EVA and glass was consistent with the values reported in the TDS, while the adhesion strength of POE exceeded the TDS values. In contrast, all EPE encapsulants exhibited adhesion strength below the range specified in the TDS. This deviation is most likely attributed to improper storage conditions of the EPE encapsulants prior to peel testing and coupon preparation and relates to the loss of silane adhesion promoters [43].

Since comparison and discussion on adhesion strength results obtained in this study is not possible and enhanced adhesion of EPE compared to POE, but comparable to EVA is expected, a literature review was conducted and observations from similar studies were integrated to evaluate whether EVA and EPE indeed provide better adhesion than POE encapsulant. The development of polyolefin encapsulants with improved adhesion to other components of PV modules has been widely researched, and the addition of various adhesion promoters has shown to be beneficial [44–46]. Comparing the TDS values of commercially available EPE, EVA, and POE, it appears that all of them exhibit adhesion in a similar range of $\geq$ 60 N cm^{-1} [11]. In various studies, POE and EVA show similar adhesion strengths; furthermore, accelerated aging tests suggest that POE experiences a lower reduction in adhesion strength compared to EVA [18,42,43,47]. Based on this and the results we observed between EVA and POE, it can be concluded that current POE formulations achieve adhesion strength similar or equal to EVA, although it remains a question how this material will compare to EVA in the long run under outdoor conditions.

4. Is EPE the future of PV encapsulation? Comparison between EPE, EVA and POE encapsulants

As mentioned in the introduction, EPE encapsulant was developed in response to industrial demand and to support the technological transition from PERC to TOPCON, HJT and tandem solar cells. It was designed to combine and balance the cost-effectiveness and processability of EVA with the superior electrical insulation and moisture barrier properties of POE. However, some questions and uncertainties regarding EPE were still unanswered, and were touched upon in this study. All observations are gathered in Table 6 with short comparison of EPE with POE and EVA.

- Which EVA and polyolefin types are used in the co-extruded encapsulant?

The IR-Spectra of the outer EVA layers of all EPE foils (EPE-1 to 4) were comparable, showing only slight differences in VA content. However, the main difference among the four EPE encapsulants was found in the inner polyolefin layer. Based on the IR-Spectra data, EPE-1 has an ethylene acrylate copolymer inner layer, whereas EPE-2; −3; −4 have ethylene α-olefin copolymer core layers, but with different side groups and/or varying comonomer contents. In addition, EPE-1 is a non-crosslinking type, while the others undergo crosslinking, as evidenced by the thermal transitions observed in the DSC curves. Since EPE-1 does not crosslink, it shows higher crystallinity, as seen in the DSC results. This higher crystallinity was also reflected in the UV–Vis–NIR spectra, where EPE-1 exhibited lower transmittance in the visible range, which can lead to reduced electricity yield.

- What are the thicknesses of the individual EPE layers, and how uniform are they?

The total encapsulant thickness and the thickness of each layer varied among the four EPE types. EPE-3 had the thickest polyolefin layer, accounting for about half of the total volume. It was followed by EPE-4, which had the second-thickest inner layer; however, its outer EVA layers were thinner than those of the other types, resulting in the lowest overall EVA content. EPE-2 had the thinnest polyolefin layer and the highest EVA content, comprising about two-thirds of the total encapsulant. EPE-1 was the thinnest overall, with just over half of the stack consisting of EVA. Layer distribution and uniformity were

Table 6
Summary and comparison of EPE, EVA and POE encapsulants properties.

Property	EPE	EVA	POE	EPE vs. EVA/POE
VA content (per total sample weight) (%)	11.6 - 19	~ 28	0	Less acetic acid formation per total weight compared to EVA.
Transmission (%)	86.5 - 93	>90 [11]	>90 [11]	Influenced by the crystallinity of the polyolefin component.
WVTR ($g\ m^{-2}\ d^{-1}$ per 100 μm)	3.1 - 11.7	35	5.4	Improved compared to the EVA.
Crosslinking	Yes, and partially	Yes	Yes	More complex – temperature and lamination duration must be optimized for both EVA and POE in case both are crosslinking.
Dimensional stability; length change in MD at 105 °C (%)	0.5 to 10%	7%	3%	Co-extrusion process seems to result in lower shrinkage.
DMA, storage viscosity during lamination (Pa s)	Low – high	High	Low	Applied pressure during the lamination needs to be optimized to minimize thinning of the encapsulant layer especially above interconnections
Adhesion strength	Similar to EVA according to [11]	High [11]	Good [11]	Complex – depends on the adhesion additives present in the POE – initial adhesion lower than for the pure EVA
Price	Between EVA and POE [1,11]	Cheap [1,11]	Expensive [1,11]	Economical solution for expensive POE.

consistent on the tested cross-sections.

- What happens to the layers during lamination regarding distribution, mixing, thickness changes, or bubble formation?

For lamination, the parameters recommended by the manufacturers were followed, with adaptations for the one-sided heating laminator available in-house. After lamination, all mini-PV module samples appeared defect-free, with no visible bubbles. Despite using thickness controls during lamination, some encapsulant material was squeezed out, predominantly from the polyolefin layer, due to its lower viscosity and slower curing process. A reduction in the POE layer thickness is expected to increase the WVTR and the probability of PID. Reducing lamination pressure could mitigate this issue, but may increase the risk of bubble formation, which is more common when laminating with POE [48]. In some samples, interlayer diffusion and flow of the polyolefin into the EVA layer were observed around the interconnections and cell edges; however, these effects were localized. Previous studies have reported insufficient wetting of the interconnections when laminating with EPE, identifying this as a weak spot for delamination propagation [7,12]. In contrast, in this study, complete wetting of the interconnections was observed for all four EPE encapsulants.

- How does the water vapor transmission rate/permeability (WVTR) of EPE compare to that of single layer EVA or polyolefin?

The WVTR of EPE is significantly lower than that of single-layer EVA, demonstrating the effectiveness of the multilayer structure. Among the EPE foils, EPE-1, despite having the thinnest polyolefin layer, exhibits the best barrier properties, even surpassing those of a single POE layer. his behaviour is attributed to its higher crystallinity. These results confirm that EPE fulfils its intended purpose of reducing water vapor permeation in PV modules.

- What is the thermal behaviour of EPE and which layers crosslink?

From DSC thermograms it was observed for EPE-1 that the 2nd melting peak and the 1st crystallization peak do not change after the lamination process, and that they belong to the non-crosslinking polyolefin component. On the other hand, in other three EPE materials both components were crosslinking. From the heating curves a single melting peak was observed, suggesting that the melting process of both EVA and polyolefin component overlaps, and after lamination it is translating to the lower temperature, following the same trend as the corresponding shift of the crystallization peak. The cooling curves provided more insights into the differences between the EPE encapsulants, particularly in respect to the crosslinking process. EPE-2 and EPE-4 exhibited two crystallization peaks after lamination despite showing only a single melting peak. The first (higher-temperature) crystallization peak is attributed to the polyolefin, while the second (lower-temperature) peak corresponds to the EVA component. Moreover, the 15 min lamination appears insufficient to achieve a high degree of cure in the polyolefin component of EPE-2 and EPE-4. This conclusion is supported by the shape and intensity of the crystallization peak, which differ from those of the maximally cured samples. In contrast, for EPE-3 the crystallization process overlaps for both components due to the similar crystallization kinetics, resulting in a single crystallization peak. Calculations of the degree of cure were out of the scope of this paper, as the calculations and measurement techniques are quantitative and were developed for single layer encapsulants, their adaptation would be necessary, therefore this will be part of the future work.

The presence of a polyolefin layer improved thermal resistance of the encapsulant. The co-extrusion process appeared to improve the dimensional stability of EPE-2; −3; −4, whereas the non-crosslinking polyolefin in EPE-1 led to higher shrinkage and expansion. This behaviour could result in high residual stress within the PV module. Contrary, if EPE-1 would be thermally stabilized so that residual stress from the co-extrusion process would be removed, its dimensional stability would be improved, and the CTE mismatch would be reduced compared to other tested encapsulants.

Besides the degree of curing, several issues remain unresolved. If EVA has a shorter processing window and polyolefin a longer one, it is unclear whether the polyolefin component in the EPE needs to be fully crosslinked or if partial crosslinking is sufficient. The long-term stability of this encapsulant also remains uncertain, including the potential for additive migration or other unexpected negative effects. Similar to "POE" encapsulants, datasheets do not reveal differences between the material type, which makes it difficult to compare different EPE encapsulants. Each EPE type can be expected to result in different levels of cell corrosion and PID behaviour, depending not only on WVTR but also on the absolute content of VA groups, which may degrade into acetic acid over time, ultimately affecting the long-term performance and reliability of PV modules.

In this context, providing a final conclusion on whether EPE is the future of PV encapsulation is challenging. EPE offers several advantages, including improved dimensional stability, lower WVTR, and reduced overall VA content. However, whether this will be sufficient for high humidity sensitive solar cells such as e.g. n-type and tandem solar cells contained in glass/glass PV modules remains to be seen after environmental exposure. As shown in the results, all four tested EPE variants differ from each other. Which of them will deliver the best long-term performance and how they will interact with the cells over time is still uncertain. Therefore, the next study will focus on additive analysis and artificial aging, after which we will perform material characterization to

provide further clarity. An additional perspective for avoiding direct EVA contact with the solar cell is a potential alternative encapsulant design involving a coextruded EVA–polyolefin structure, where a single thin EVA layer is combined with POE directly contacting the solar cells. If EVA and POE with similar material behaviour can be combined, this could eliminate stack asymmetry, something that EPE currently addresses with its two outer EVA layers.

5. Conclusions

The four studied EPE encapsulants from different manufacturers varied in their chemical composition, thermal and optical properties.

The IR-Spectra of the outer EVA layers of all EPE encapsulants were comparable, showing only slight differences in VA content. The main difference between the four EPE encapsulants was found in the inner polyolefin layer. Based on the IR-Spectra data, EPE-1 has an ethylene acrylate copolymer inner layer, whereas EPE-2; −3; −4 consists of ethylene α-olefin copolymer core layers, but with different side groups and/or varying comonomer contents.

The water vapor transmission rate (WVTR) of EPE is significantly lower than that of single-layer EVA, demonstrating the effectiveness of the multilayer structure in optimizing the barrier properties. The layer distribution and uniformity of the tested EPE films, as determined from the light microscopic images of the cross-sections were found to be comparable, and complete wetting of the interconnections could be achieved with all four EPE encapsulants.

Difference in the crosslinking behaviour were evident from the DSC analysis, EPE-1 was the only sample with a non-crosslinking inner polyolefin layer, whose high crystallinity reduced visible-light transmission but also enhanced barrier to water vapor. The presence of a polyolefin layer improved the thermal resistance of the encapsulant. The co-extrusion process appeared to improve the dimensional stability of EPE-2; −3; −4 compared to pure EVA film, whereas the non-crosslinking polyolefin in EPE-1 led to higher shrinkage and expansion.

Overall, EPE encapsulants fulfil their intended purpose of improving the barrier properties of the encapsulant to better protect the newly developed humidity sensitive solar cell types. However, the long-term impact of the EVA layer in direct contact with the cell, particularly under environmental exposure, has yet to be fully evaluated. This is especially relevant considering that the EVA content of EPE film ranges between 42% and 64% by volume, and the polyolefin core layer thins more during lamination than the EVA layer. Therefore, the formation of acetic acid is to be expected. In this context, a potential alternative approach for encapsulant design could involve a coextruded EVA-polyolefin material, with a single thin EVA layer and POE in direct contact with the solar cells.

In summary, EPE does not constitute a single-material solution but rather represents a materials design concept. Its performance and durability are determined by formulation parameters, additive chemistry, and processing conditions, which collectively impact long-term stability. Without systematic understanding and control of these factors, reliable device operation cannot be ensured. Future research should therefore aim to establish clear structure–property–stability relationships to support predictive formulation strategies and sustained long-term performance.

CRediT authorship contribution statement

Nikolina Pervan: Writing – original draft, Visualization, Validation, Methodology, Investigation, Formal analysis, Data curation, Conceptualization. **Gabriele Eder:** Writing – review & editing, Writing – original draft, Investigation, Formal analysis, Data curation. **Yuliya Voronko:** Investigation, Data curation. **Astrid Macher:** Investigation, Data curation. **Kamil Novotny:** Investigation, Formal analysis. **Katharina Resch-Fauster:** Investigation, Data curation. **Gernot Oreski:** Writing – review & editing, Writing – original draft, Visualization, Validation, Supervision, Resources, Project administration, Methodology, Funding acquisition, Conceptualization.

Data availability statement

The data that support the findings of this study are available on request from the corresponding author. The data are not publicly available due to privacy or ethical restrictions.

Declaration of competing interest

The authors declare no conflicts of interest.

Acknowledgements

The research work of this paper was performed at the Polymer Competence Center Leoben GmbH (PCCL, Austria) as part of the Solar Era Net Project “DELIGHT,” which is supported under the umbrella of SOLAR-ERA.NET co-fund by the Austrian Research Promotion Agency (FFG, contract number FO999897443) and the Swiss Federal Office of Energy (SFOE, contract number SI/502501-01). SOLAR-ERA.NET is supported by the European Commission within the EU Framework Programme for Research and Innovation HORIZON 2020 (co-fund ERA-NET Action, No. 691664).

Appendix A. Supplementary data

Supplementary data to this article can be found online at https://doi.org/10.1016/j.solmat.2026.114258.

Data availability

Data will be made available on request.

References

[1] e.V. Vdma, Photovoltaics equipment. International Technology Roadmap for Photovoltaics (ITRPV), sixteenth ed., 2025, 2025.
[2] Jarret Zuboy, Martin Springer, Elizabeth C. Palmiotti, Joseph Karas, Brittany L. Smith, Michael Woodhouse, Teresa M. Barnes, Getting ahead of the curve: assessment of new photovoltaic module reliability risks associated with projected technological changes, IEEE Journal of Photovoltacis 14 (2024) 4–22.
[3] Intersolar, Solar technology is undergoing great changes: market trend – january 28, 2025. https://www.intersolar.de/market-trends/solar-cell-development, 2025. (Accessed 10 December 2025).
[4] Emiliano Bellini, Amount of Silver Needed in Solar Cells to be More than Halved by 2028, Silver Institute says, 2018. (Accessed 10 December 2025).
[5] Timothy J. Silverman, Elizabeth C. Palmiotti, Martin Springer, Nick Bosco, Mike Deceglie, Ingrid Repins, Ashley Gaulding, Tough Break: Many Factors Make Glass Breakage More Likely, 2024.
[6] Fraunhofer Institute for Solar Energy Systems, Silicon heterojunction solar cells realized with record savings in silver. https://www.ise.fraunhofer.de/en/press-media/news/2025/silicon-heterojunction-solar-cells-realized-with-record-savings-in-silver.html, 2025. (Accessed 10 December 2025).
[7] Maulid Kivambe, Amir Abdallah, Benjamin Figgis, Abdelrahim Mohamed, Mohamed Elgaili, Dhanup Pillai, Brahim Aissa, Comprehensive assessment of performance and reliability of PERC, TOPCon and SHJ modules in desert climates, Sol. Energy 295 (2025), https://doi.org/10.1016/j.solener.2025.113555.
[8] A. Omazic, G. Oreski, M. Halwachs, G.C. Eder, C. Hirschl, L. Neumaier, G. Pinter, M. Erceg, Relation between degradation of polymeric components in crystalline silicon PV module and climatic conditions: a literature review, Sol. Energy Mater. Sol. Cells 192 (2019) 123–133, https://doi.org/10.1016/j.solmat.2018.12.027.
[9] J.H. Wohlgemuth, P. Hacke, N. Bosco, D.C. Miller, M.D. Kempe, S.R. Kurtz, Assessing the causes of encapsulant delamination in PV modules, in: Proceedings of the 2016 IEEE 43rd Photovoltaic Specialists Conference (PVSC), June 2016, pp. 5–10. Portland, Oregon.
[10] John H. Wohlgemuth, Michael D. Kempe, David C. Miller (Eds.), Discoloration of PV Encapsulants, 2014.
[11] Shravan K. Chunduri, Michael Schmela, TaiyangNews Solar Backsheets & Encapsulants Market Survey 2024/25, 2025.
[12] Yuqiu Ye, Yanfang Zhou, Ye Wang, Bram Hoex, Xiaogang Zhu, Daoyuan Chen, Wenjuan Xue, Tiantian Wei, Bin Chen, Meng Cheng, Jiayan Lu, Haipeng Yin, Zi Ouyang, Damp-heat stability investigation of glass-backsheet modules based on TOPCon solar cells, Sol. Energy Mater. Sol. Cell. 292 (2025), https://doi.org/10.1016/j.solmat.2025.113764.

[13] Paul M. Sommeling, Ji Liu, Jan M. Kroon, Corrosion effects in bifacial crystalline silicon PV modules; interactions between metallization and encapsulation, Sol. Energy Mater. Sol. Cell. 256 (2023), https://doi.org/10.1016/j.solmat.2023.112321.
[14] Eric Schneller, Alex Morgan, Neil Wiens, Hong Xiang Xuan, Tyler Frank, Andrey Zelenskiy (Eds.), Effects of Encapsulation Combinations on the Performance and Reliability of Topcon Modules, 2024.
[15] Chandany Sen, Haoran Wang, Muhammad Umair Khan, Jiexi Fu, Xinyuan Wu, Xutao Wang, Bram Hoex, Buyer aware: three new failure modes in TOPCon modules absent from PERC technology, Sol. Energy Mater. Sol. Cell. 272 (2024), https://doi.org/10.1016/j.solmat.2024.112877.
[16] G. Oreski, G.C. Eder, Y. Voronko, A. Omazic, L. Neumaier, W. Mühleisen, G. Ujvari, R. Ebner, M. Edler, Performance of PV modules using co-extruded backsheets based on polypropylene, Sol. Energy Mater. Sol. Cells 223 (2021) 110976, https://doi.org/10.1016/j.solmat.2021.110976.
[17] G. Oreski, C. Barretta, P. Christöfl, P. Gebhardt, K.-A. Weiß, D.C. Miller, S. Uličná, M. Kempe, L.S. Bruckman, A. Virtuani, H. Li, B. Habersberger, J. Munro, K. Proost, M. Kühne, What is a polyolefin? A critical overview of ethylene copolymers used as solar photovoltaic module encapsulants, Prog. Photovolt., pip. 70038 (2025), https://doi.org/10.1002/pip.70038.
[18] Kuan Liu, David C. Miller, Nick Bosco, Jimmy M. Newkirk, Tomoko Sakamoto, Reinhold H. Dauskardt, Investigating the crosslinking, degradation, and adhesion behavior of photovoltaic encapsulants under thermal accelerated aging, IEEE Journal of Photovoltacis 15 (2024) 303–319, https://doi.org/10.1109/JPHOTOV.2024.3496512.
[19] IEC, Measurement procedures for materials used in photovoltaic modules - part 1-6: encapsulants - test methods for determining the degree of cure in ethylene-vinyl acetate, Solar energy engineering (2017) 160, 1st ed. 27, https://webstore.iec.ch/publication/33050.
[20] C. Hirschl, M. Biebl–Rydlo, M. DeBiasio, W. Mühleisen, L. Neumaier, W. Scherf, G. Oreski, G. Eder, B. Chernev, W. Schwab, M. Kraft, Determining the degree of crosslinking of ethylene vinyl acetate photovoltaic module encapsulants—A comparative study, Sol. Energy Mater. Sol. Cells 116 (2013) 203–218, https://doi.org/10.1016/j.solmat.2013.04.022.
[21] G. Oreski, A. Omazic, G.C. Eder, Y. Voronko, L. Neumaier, W. Mühleisen, C. Hirschl, G. Ujvari, R. Ebner, M. Edler, Properties and degradation behaviour of polyolefin encapsulants for photovoltaic modules, Prog. Photovoltaics Res. Appl. 28 (2020) 1277–1288, https://doi.org/10.1002/pip.3323.
[22] Gary Säckl, Gernot M. Wallner, Jiri Duchoslav, Martin Tiefenthaler, David Stifter, Advanced analysis of ethylene vinyl acetate copolymer materials for photovoltaic modules, Polym. Test. 132 (2024), https://doi.org/10.1016/j.polymertesting.2024.108381.
[23] Ester Caro, Enric Comas, Polyethylene comonomer characterization by using FTIR and a multivariate classification technique, Talanta 163 (2017) 48–53, https://doi.org/10.1016/j.talanta.2016.10.082.
[24] Jonathan P. Blitz, Douglas C. McFaddin, The characterization of short chain branching in polyethylene using fourier transform infrared spectroscopy, J. Appl. Polym. Sci. 51 (1994) 13–20, https://doi.org/10.1002/app.1994.070510102.
[25] Ali Sharif-Pakdaman, Jalil Morshedian, Yousef Jahani, Effect of organoclay and silane grafting of polyethylene on morphology, barrierity, and rheological properties of HDPE/PA6 blends, J. Appl. Polym. Sci. 127 (2013) 1211–1220, https://doi.org/10.1002/app.37974.
[26] B. Adothu, F.R. Costa, S. Mallick, UV resilient thermoplastic polyolefin encapsulant for photovoltaic module encapsulation, Polym. Degrad. Stabil. 201 (2022) 109972, https://doi.org/10.1016/j.polymdegradstab.2022.109972.
[27] Brian C. Smith, Infrared spectroscopy of polymers, IX: pendant ester polymers and polycarbonates, Spectroscopy 37 (2022) 16–19, https://doi.org/10.56530/spectroscopy.xn9369p8.
[28] G. Oreski, J.S. Stein, G.C. Eder, K. Berger, L. Bruckman, R. French, J. Vedde, K. A. Weiß, Motivation, benefits, and challenges for new photovoltaic material & module developments, Prog. Energy 4 (2022) 32003, https://doi.org/10.1088/2516-1083/ac6f3f.
[29] J. Morse, M. Thuis, D. Holsapple, R. Willis, M.D. Kempe, D.C. Miller, Degradation in photovoltaic encapsulant transmittance: results of the second PVQAT TG5 artificial weathering study, Prog. Photovoltaics Res. Appl. 30 (2022) 763–783, https://doi.org/10.1002/pip.3551.
[30] H.-Y. Li, Y. Luo, C. Ballif, L.-E. Perret-Aebi, Effect of cooling press on the optical transmission through photovoltaic encapsulants, Polym.-Plast. Technol. Eng. 54 (2015) 416–424, https://doi.org/10.1080/03602559.2014.958778.
[31] V. Fiandra, L. Sannino, C. Andreozzi, G. Flaminio, M. Pellegrino, New PV encapsulants: assessment of change in optical and thermal properties and chemical degradation after UV aging, Polym. Degrad. Stabil. 220 (2024) 110643, https://doi.org/10.1016/j.polymdegradstab.2023.110643.
[32] J. Jin, S. Chen, J. Zhang, UV aging behaviour of ethylene-vinyl acetate copolymers (EVA) with different vinyl acetate contents, Polym. Degrad. Stabil. 95 (2010) 725–732, https://doi.org/10.1016/j.polymdegradstab.2010.02.020.
[33] S.-S. Choi, C.E. Son, Novel analytical method for determination of contents of backbone and terminal/branch vinyl acetate groups of poly(ethylene-co-vinyl acetate) using deacetylation reaction, Polym. Test. 56 (2016) 214–219, https://doi.org/10.1016/j.polymertesting.2016.10.012.
[34] C. Barretta, G. Oreski, S. Feldbacher, K. Resch-Fauster, R. Pantani, Comparison of degradation behavior of newly developed encapsulation materials for photovoltaic applications under different artificial ageing tests, Polymers 13 (2021), https://doi.org/10.3390/polym13020271.
[35] M. Knausz, G. Oreski, M. Schmidt, P. Guttmann, K.A. Berger, Y. Voronko, G. Eder, T. Koch, G. Pinter, Thermal expansion behavior of solar cell encapsulation materials, Polym. Test. 44 (2015) 160–167, https://doi.org/10.1016/j.polymertesting.2015.04.009.
[36] G. Oreski, A. Rauschenbach, C. Hirschl, M. Kraft, G.C. Eder, G. Pinter, Crosslinking and post-crosslinking of ethylene vinyl acetate in photovoltaic modules, J. Appl. Polym. Sci. 134 (2017) 101, https://doi.org/10.1002/app.44912.
[37] M. Landa-Pliquet, T. Béjat, M. Serasset, A. Descormes, E. Mofakhami, E. Voroshazi, Enhancing photovoltaic modules encapsulation: optimizing lamination processes for polyolefin elastomers (POE) through crosslinking behavior analysis, Sol. Energy Mater. Sol. Cells 267 (2024) 112725, https://doi.org/10.1016/j.solmat.2024.112725.
[38] F.J. Pern and S.H. Glick: NREL, Adhesion Strength Study of EVA Encapsulants on Glass Substrates.
[39] Steffen Bornemann, Sven Henning, Konstantin Naumenko, Matthias Pander, Nishanth Thavayogarajah, Mathias Würkner, Strength analysis of laminated glass/EVA interfaces: microstructure, peel force and energy of adhesion, Compos. Struct. 297 (2022), https://doi.org/10.1016/j.compstruct.2022.115940.
[40] J. Zhu, D. Wu, D. Montiel-Chicharro, T.R. Betts, R. Gottschalg, Realistic adhesion test for photovoltaic modules qualification, IEEE J. Photovoltaics 8 (2018) 218–223, https://doi.org/10.1109/JPHOTOV.2017.2775149.
[41] M. Tiefenthaler, G.M. Wallner, R. Pugstaller, The effects of global damp heat ageing on debonding of polyolefin glass laminates, in: 2023 IEEE 50th Photovoltaic Specialists Conference (PVSC), IEEE, San Juan, PR, USA, 2023, pp. 1–3.
[42] M. Tiefenthaler, G.M. Wallner, R. Pugstaller, Effect of global damp heat ageing on debonding of crosslinked EVA- and POE-glass laminates, Sol. Energy Mater. Sol. Cells 264 (2024) 112602, https://doi.org/10.1016/j.solmat.2023.112602.
[43] Kuan Liu, David C. Miller, Nick Bosco, Jimmy M. Newkirk, Reinhold H. Dauskardt (Eds.), Advancing Steady-State and Sequenced Accelerated Aging for Assessing the Adhesion Degradation of Contemporary Encapsulants, 2025.
[44] J.H. Park, S.-H. Hwang, A polyolefin elastomer encapsulant modified by an ethylene-propylene-diene terpolymer for photovoltaic applications, ACS Omega 9 (2024) 3858–3865, https://doi.org/10.1021/acsomega.3c07969.
[45] J.H. Park, S.-H. Hwang, Construction and characterization of polyolefin elastomer blends with chemically modified hydrocarbon resin as a photovoltaic module encapsulant, Polymers 14 (2022), https://doi.org/10.3390/polym14214620.
[46] Jishnu Ramachandran Nair, Nishant Pradhan, Paul Schenk, Matthias Pander, Steffen Bornemann, Mohammad Abdus Salam (Eds.), Formulation Studies of Polyolefin Elastomer Encapsulants with Adhesion Promoters: Impacts on Adhesion Strength and Crosslinking Behavior, 2025.
[47] Martin Tiefenthaler, Gernot M. Wallner, Gary Säckl, Francis Costa, Effect of UV ageing on debonding of double glass laminates based on different crosslinking and thermoplastic PV encapsulants, Sol. Energy Mater. Sol. Cell. 273 (2024).
[48] S. Sraisth, A.K. Öz, D. Klaus, C. Wellens, M. Heinrich, Influence of the lamination pressure on the adhesion, degree of cross-linking, and bubble formation of PV modules. 7 pages/8th world conference on photovoltaic energy conversion; 823-829, in: 8th World Conference on Photovoltaic Energy Conversion, 823-829.

6 Summary and Conclusions

The global expansion of PV has reached a point where land availability, particularly in densely populated or mountainous regions, constrains large-scale field-deployed installations. This has created space for alternative deployment strategies that integrate electricity generation into the existing built environment without competing for land. The integration of PV spans from BIPV, VIPV, and consumer products, representing a key development in the transition toward net-zero-energy environments.

While early IPV solutions were mainly restricted to simple two-dimensional roof attachments, modern requirements demand specialized, application-specific designs. However, a hurdle remains: conventional glass-glass modules are often too heavy for lightweight infrastructures, such as industrial complexes and heritage buildings. To overcome these limitations development of the solutions for glass-free PV modules based on polymer materials to enable flexible geometries, adaptable architectures, and reduced weight is ongoing.

Transitioning from glass-based to glass-free PV fundamentally redefines the requirements for the polymeric components within the module stack. In traditional designs, glass provides the primary mechanical stiffness and environmental barrier. In glass-free configurations, these functions are transferred to the polymer layers, which must then provide structural integrity, thermal stability, and long-term protection.

This thesis investigated how various design paths and roles of the polymer materials can be adapted to meet these shifted requirements. A central challenge lies in aligning material selection with the specific demands of the application. For building-integrated systems, the focus is on maintaining interfacial adhesion and dimensional stability under environmental loads. Conversely, for integrated consumer electronics, the objective shifts toward price and process efficiency, where standard industrial solutions may lead to over-engineering. By characterizing the physical, chemical, thermal, thermomechanical and mechanical behavior of materials, such as polymeric based honeycombs, co-extruded encapsulants and specialized coatings, this work established a scientific framework for developing application-specific, glass-free PV designs.

The initial focus of this thesis was to address the loss of structural rigidity in glass-free architectures via the characterization of thermoplastic honeycomb sandwich composites as functional backside materials. A key scientific finding was that these composites exhibit CTE only slightly higher than that of solar glass and significantly lower than typical polymeric backsheets. This alignment is essential for minimizing internal stresses and preventing cell-cracking during thermal cycling. However, their integration required a redefinition of standard

lamination conditions. The low thermal conductivity of the honeycomb sandwich composites will hinder heat transfer during the lamination process, extending the required duration, while the low melting point of the PP variants necessitates the use of low-temperature crosslinking or non-crosslinking encapsulants to preserve structural integrity. Long-term reliability testing further differentiated the material candidates: while PP-based honeycombs remained stable, PET-based structures proved unsuitable for hot and humid environments due to significant polymer chain-scission and embrittlement. The findings indicate that while PET remains a potential candidate if hydrolysis resistance is improved, PP-based HSCs are the more viable choice, as long as the material stack and lamination parameters are specifically tailored to their thermal constraints.

To facilitate the integration of PV modules into large-scale infrastructure, such as the 12-meter steel façade elements investigated in the PV Industriefassade project, the second part of this thesis evaluated the adhesion between polymeric backsheets and hot dip galvanized steel. In these glass-free architectures, the backsheet must function as a dielectric barrier against the conductive steel substrate, making the long-term integrity of the polymer-metal bond a primary safety and structural requirement. While three distinct bonding strategies achieved robust initial adhesion, the approach C (developed by the industrial partner) emerged as the most promising adhesion path. Results ultimately demonstrated that transitioning toward monolithic backsheets is necessary to minimize the number of internal interfaces and ensure a service life of at least 25 years for steel-integrated BIPV.

To expand the application of flexible CIGS solar cells beyond rigid glass encapsulation, the third study of this thesis established a screening methodology for identifying coating solutions capable of adhering to complex substrates with significant surface tension variations. Fourteen materials across four chemical families, acrylate, epoxy, silicone, and PU, were evaluated for compatibility with high-throughput roll-to-roll processing while maintaining optical transmittance and mechanical flexibility. Specific PU formulations demonstrated the most robust equilibrium of uniform coverage and interfacial stability. The results demonstrated that the PCT serves as an effective method for the rapid identification of weak interfacial adhesion. On the other hand, the standard 1000 h DH exposure was found to be an excessive stressor for these thin-film materials, highlighting the need to adapt aging conditions to avoid overestimating environmental degradation for products with shorter intended service lives, thereby preventing costly over-engineering.

The fourth study of this thesis investigated the impact of manufacturing history and lamination duration on the thermomechanical properties of six different encapsulant types (EVA, POE, TPO, and EPE). While the thermomechanical role of the encapsulant has often been simplified in numerical FEM simulations, this research demonstrated that its dimensional

stability and CTE values are fundamental to the module's long-term integrity. In glass-free designs, the lack of a rigid glass constraint means that even minor variations in the encapsulant's expansion or contraction can lead to significant warping and mechanical stress. Experimental measurements revealed that unlaminated encapsulants retain significant internal stresses and molecular orientations from the extrusion process, which are released as shrinkage during the first stages of heating. This dimensional instability is particularly relevant for mechanically sensitive technologies, such as perovskite solar cells, where such movements can trigger premature failure. The findings show that a lamination duration of 5–10 minutes is required for the materials to reach stable CTE values. Notably, non-crosslinking polyolefins (TPO and EPE) exhibited the highest initial shrinkage but ultimately achieved the lowest final CTE range, suggesting that with optimized processing, these materials can better minimize thermomechanical mismatch within the PV stack. This work established that using post-lamination material properties is essential for accurate thermomechanical modelling, especially in glass-free designs where the rigid locking effect of glass is absent. Furthermore, the study highlighted that even within the same polymer categories, particularly with co-extruded EPE, material behavior is more complex and challenges the current understanding of these materials.

Motivated by the complexities identified in the fourth study, the fifth study performed a systematic characterization of four commercially available co-extruded EPE encapsulants to investigate the factors driving their inconsistent behavior. While EPE was developed to combine the processability of EVA with the superior barrier properties of polyolefins for humidity-sensitive cells, this research demonstrated that EPE is not a single-material solution but a variable materials design concept. A comparative analysis of four EPEs revealed that while the outer EVA layers were similar, the core layers differed significantly, ranging from non-crosslinking ethylene acrylate copolymers to various ethylene α-olefin copolymer core layers, with different side groups and/or varying comonomer contents. These chemical differences directly impacted performance: the non-crosslinking core in EPE-1 provided a superior water vapor barrier due to high crystallinity but resulted in reduced visible light transmission. Crucially, the study revealed that EVA still constitutes between 42% and 64% of the total EPE volume. Cross-sectional analysis demonstrated that the polyolefin core thins more significantly than the EVA layers during lamination, meaning the final stack remains dominated by EVA. This volumetric majority, combined with the EVA's direct contact at the cell interface, suggests that the potential for acetic acid formation is not eliminated. By uncovering these structural and chemical variables, this work establishes that without a systematic understanding of EPE formulations, the long-term reliability of next-generation PV modules cannot be ensured.

The findings of this thesis demonstrate that glass-free designs allow for greater creativity in module architecture; yet this flexibility requires a shift from standardized manufacturing processes toward targeted optimization. Furthermore, the success of these designs depends on matching the material stack to the actual operational environment of the final product, rather than adhering to generalized industrial standards that may lead to over-engineering.

This research proves that diverse pathways, ranging from honeycomb reinforcements to specialized thin-film coatings, are feasible, provided the interactions between materials are thoroughly understood. A key finding in this regard is that current industrial classifications for PV products are often insufficient for predicting performance. For instance, encapsulants sharing the same nomenclature, such as POE or EPE, can exhibit significantly different material properties which can lead to unpredictable behavior in both glass-glass and glass-free stacks. Ultimately, integrating any commercial product is not a plug-and-play process. Whether dealing with new architectural components or standard encapsulants, even accredited materials require a three-stage integration strategy: first, a characterization phase to investigate fundamental properties; second, an adaptation of the lamination process; and finally, targeted material optimization (e.g., enhancing hydrolysis resistance) to ensure durability under PV-specific conditions.

The practical viability of the findings presented in this thesis is further evidenced by their implementation across three European research projects. While the specific field data falls outside the scope of the work presented here, these collaborations have already culminated in the production of functional PV modules that utilize the design principles established in this study. For instance, lightweight PP-based honeycomb modules, incorporating colored, low-temperature encapsulants and glass-free frontsheets, are currently being monitored in a rooftop installation in Neuchâtel, Switzerland. Similarly, coated thin-film CIGS mini-modules are undergoing outdoor performance observation at Sunplugged in Austria. Finally, a third project regarding integration into steel façades is still ongoing, focusing on the reformulation of adhesive layers and the development of monolithic polymeric insulating layers. In addition, the full material stack is being validated through outdoor aging of trial mini-modules at the Technical University of Leoben, alongside parallel sequential testing under accelerated laboratory conditions.

7 Outlook

While this thesis establishes a scientific framework for the design and integration of glass-free PV modules, several areas remain for future investigation to ensure the long-term success and adoption of these technologies.

Looking ahead, enhancing the fire retardancy of polymer-rich PV modules represents a clear direction for future work. Although this topic was not part of the scope of the present thesis, investigations into strategies for improving fire performance were carried out and viable approaches were identified. These results provided the basis for a new funding project dedicated to further developing such solutions in line with future safety and regulatory demands.

Another aspect for future development is the adaptation of existing IEC standards toward application-specific testing procedures for integrated PV devices. Current standards are often based on conventional module designs and can lead to over-stressing during qualification testing, resulting in unnecessary over-engineering. The need for tailored standards is increasingly recognized and has emerged as a recurring topic of discussion at recent conferences and industry meetings.

Finally, further research is required to better understand the thermomechanical behaviour of different module material stacks. Detailed experimental investigation of interfacial displacement and layer interaction in polymer-based, glass-glass, glass-polymer, glass-metal, and polymer-metal configurations is required for the development of reliable predictive FEM simulations. Bridging this knowledge gap is a prerequisite for addressing challenges such as delamination in perovskite and tandem solar cells, which currently limits the broader deployment of these next-generation technologies.

Addressing these remaining challenges will ensure that glass-free modules meet the reliability requirements necessary for large-scale industrial application.

8 AI Based Tools

Table 1. Declaration of the use of AI-based tools.

Reason	Share [%]	AI Tool	Prompts
Correction of grammar and improvement of the writing style	10%	ChatGPT (GPT-4o and GPT-5.5)	Identify and correct grammatical mistakes, and provide synonyms that align with an academic writing style.
Correction of grammar, improvement of the writing style and help with summarizing	10%	Gemini (Gemini 3 Flash)	Identify and correct grammatical mistakes, and provide synonyms that align with an academic writing style. Summarize these paragraphs to one-third of their original length.
Translation of abstract to German and Dutch languages	100%	Deep L	n/a

9 References

[1] D.C. Fessler, The Energy Disruption Triangle, Wiley, 2019.

[2] Gary Cook, Lynn Billman, Rick Adcock, Photovoltaic Fundamentals, 1995. https://docs.nlr.gov/docs/legosti/old/16319.pdf (accessed 3 May 2026).

[3] Emiliano Bellini, Longi announces world record efficiency of 28.13% for silicon solar cell, 2026. https://www.pv-magazine.com/2026/04/28/longi-announces-world-record-efficiency-of-28-13-for-silicon-solar-cell/ (accessed 3 May 2026).

[4] H.W. Seo, S. Rudra, S. Khanam, S. Sarker, D.M. Kim, Revisiting the Shockley-Queisser Limit: Understanding Solar Cell Efficiency in One Sun and Indoor Environments, J. Phys. Chem. Lett. 16 (2025) 11795–11812. https://doi.org/10.1021/acs.jpclett.5c01792.

[5] U.S. Department of Energy, The History of Solar. https://www1.eere.energy.gov/solar/pdfs/solar_timeline.pdf (accessed 3 May 2026).

[6] A.O. Ali, A.T. Elgohr, M.H. El-Mahdy, H.M. Zohir, A.Z. Emam, M.G. Mostafa, M. Al-Razgan, H.M. Kasem, M.S. Elhadidy, Advancements in photovoltaic technology: A comprehensive review of recent advances and future prospects, Energy Convers. Manage.: X 26 (2025) 100952. https://doi.org/10.1016/j.ecmx.2025.100952.

[7] H. Cao, W. He, Y. Mao, X. Lin, K. Ishikawa, J.H. Dickerson, W.P. Hess, Recent progress in degradation and stabilization of organic solar cells, Journal of Power Sources 264 (2014) 168–183. https://doi.org/10.1016/j.jpowsour.2014.04.080.

[8] VDMA e.V. Photovoltaics Equipment (Ed.), International Technology Roadmap for Photovoltaics (ITRPV): 16th Edition 2025, 2025.

[9] G. Masson, A. Van Rechem, M. de l'Epine, A. Jäger-Waldau, Snapshot of Global PV Markets 2025, International Energy Agency Photovoltaic Power Systems Programme, 2025.

[10] Markus A.W. Hoehner, Daniel Fuchs, PV Magazine (12 January 2026).

[11] J.M. Kiesecker, J.S. Evans, J.R. Oakleaf, K.Z. Dropuljić, I. Vejnović, C. Rosslowe, E. Cremona, A.L. Bhattacharjee, S.K. Nagaraju, A. Ortiz, C. Robinson, J.L. Ferres, M. Zec, K. Sochi, 2024. Land use and Europe's renewable energy transition: identifying low-conflict areas for wind and solar development. Front. Environ. Sci. 12, 1355508. https://doi.org/10.3389/fenvs.2024.1355508.

[12] M. Deshaies, Problèmes géographiques des transitions énergétiques quelles perspectives pour l'évolution du système énergétique ?, Transition énergétique et développement (2020) 25–44.

[13] G. Kakoulaki, R. Kenny, N. Taylor, A.M. Gracia-Amillo, S. Szabo, A.M. Martínez, C. Thiel, A. Jäger-Waldau, Mapping Europe's rooftop photovoltaic potential with a building-level database, Nat Energy 11 (2026) 324–333. https://doi.org/10.1038/s41560-025-01947-x.

[14] M. Trommsdorff, P.E. Campana, J. Macknick, A. Fernández Solas, S. Gorjian, I. Tsanakas, Dual Land Use for Agriculture and Solar Power Production: Overview and Performance of Agrivoltaic Systems, International Energy Agency Photovoltaic Power Systems Programme, 2025.

[15] J. Selj, S. Wieland, I. Tsanakas, Floating Photovoltaic Power Plants: A Review of Energy Yield, Reliability, and Maintenance, International Energy Agency Photovoltaic Power Systems Programme, 2025.

[16] IEA PVPS, Successful Building Integration of Photovoltaics – A Collection of International Projects, 2021.

[17] K. Araki, A.J. Carr, F. Chabuel, B. Commault, R. Derks, K. Ding, T. Duigou, N.J. Ekins-Daukes, J. Gaume, T. Hirota, O. Kanz, K. Komoto, B.K. Newman, R. Peibst, A. Reinders, E. Roman Medina, M. Sechilariu, L. Serra, A. Sierra, A. Valverde, D. Zurfluh, State-of-the-Art and Expected Benefits of PV-Powered Vehicles: Report IEA-PVPS T17-01 2021, 2021.

[18] N.M. Chivelet, C. Kapsis, F. Frontini, Building-Integrated Photovoltaics: A Technical Guidebook, firstst, Routledge, New York, 2024.

[19] The European Parliament and the Council of the European Union, DIRECTIVE (EU) 2024/1275 OF THE EUROPEAN PARLIAMENT AND OF THE COUNCIL of 24 April 2024 on the energy performance of buildings, 2024.

[20] M. van Noord, N.M. Chivelet, N. Weerasinghe, J. Halme, F. Tilli, A. Baggini, M. Tabakovic, O. Bernsen, R. Yang, E. Daun, Analysis of Technological Innovation Systems for BIPV in Different IEA Countries, International Energy Agency Photovoltaic Power Systems Programme, 2025.

[21] Philippe Macé, Caroline Plaza, Lightweight PV modules could unlock more than 85 GW of untapped rooftop potential in Europe, 2026. https://www.pv-magazine.com/2026/03/11/lightweight-pv-modules-could-unlock-more-than-85-gw-of-untapped-rooftop-potential-in-europe/ (accessed 9 May 2026).

[22] Dyaqua srls, What is Invisible Solar. https://www.invisiblesolar.it/EN/technology/ (accessed 3 May 2026).

[23] SolarXplorers SA, SolarStratos: A stratospheric odyssey for cleaner skies. https://www.solarstratos.com/en/challenge/ (accessed 3 May 2026).

[24] Wattway, PHOTOVOLTAIC COVERING FOR TRAFFIC-BEARING SURFACES. https://www.wattwaybycolas.com/en/wattway-technology.html (accessed 3 May 2026).

[25] Soleva, A 100% Solar Powered Van. https://soleva.org/en/electric-conversion-van (accessed 3 May 2026).

[26] N. Martín Chivelet, C. Kapsis, F. Frontini (Eds.), Building-Integrated Photovoltaics, Routledge, New York, 2024.

[27] G. Oreski, J. Stein, G. Eder, K. Berger, L. Bruckman, J. Vedde, K.-A. Weiss, T. Tanahashi, R. French, S. Ranta, Designing New Materials for Photovoltaics: Opportunities for Lowering Cost and Increasing Performance through Advanced Material Innovations: Report IEA-PVPS T13-13:2021, 2021.

[28] M. Köntges, J. Lin, L. Bruckman, Degradation and Failure Modes in New Photovoltaic Cell and Module Technologies, International Energy Agency Photovoltaic Power Systems Programme, 2025.

[29] Shravan Chunduri, Designing Solar Modules With Polymers And Composites, 2025. https://taiyangnews.info/technology/designing-solar-modules-with-polymers-and-composites (accessed 6 May 2026).

[30] F. Lisco, F. Bukhari, L. Jones, A. Law, J.M. Walls, C. Ballif, ETFE and its role in the fabrication of lightweight c-Si solar modules, in: 2022 IEEE 49th Photovoltaics Specialists Conference (PVSC), Philadelphia, PA, USA, IEEE, 2022, p. 604.

[31] Y. Voronko, G.C. Eder, E. Reiser, M. Babin, G. Oreski, Development of Novel Frontsheets With Protective Coatings to Increase the Durability and Reliability of

Glass-Free Lightweight PV Modules, Prog. Photovolt. 33 (2025) 1352–1364. https://doi.org/10.1002/pip.3871.

[32] A. Backes, N. Adamovic, U. Schmid, New Light Management Concepts for Standard Si Solar Cells Fabricated by Embossing of Polycarbonate Front & Back Sheets, in: 28th European Photovoltaic Solar Energy Conference and Exhibition, pp. 3096–3098.

[33] M. Marengo, M. Abdullah, K. Kotsovos, S. Aqeel, M. Heeney, M. Salvador, S. de Wolf, 2025. Lightweight Photovoltaics Enabled by Polycarbonate-Based Sheets. Adv. Eng. Mater. 27, e202500958. https://doi.org/10.1002/adem.202500958.

[34] N. Kim, S. Lee, X.G. Zhao, D. Kim, C. Oh, H. Kang, Reflection and durability study of different types of backsheets and their impact on c-Si PV module performance, Sol. Energy Mater. Sol. Cells 146 (2016) 91–98. https://doi.org/10.1016/j.solmat.2015.11.038.

[35] Shravan K. Chunduri, Michael Schmela, TaiyangNews Solar Backsheets & Encapsulants Market Survey 2024/25, 2025.

[36] A. Gassner, G.C. Eder, J. Anger, V.-M. Archodoulaki, Evolution of the fluorine content in photovoltaic module backsheets, Sol. Energy Mater. Sol. Cells 304 (2026) 114393. https://doi.org/10.1016/j.solmat.2026.114393.

[37] Chandany Sen, Haoran Wang, Muhammad Umair Khan, Jiexi Fu, Xinyuan Wu, Xutao Wang, Bram Hoex, Buyer aware: Three new failure modes in TOPCon modules absent from PERC technology, Solar Energy Materials and Solar Cells 272 (2024). https://doi.org/10.1016/j.solmat.2024.112877.

[38] Eric Schneller, Alex Morgan, Neil Wiens, Hong Xiang Xuan, Tyler Frank, Andrey Zelenskiy (Eds.), Effects of Encapsulation Combinations on the Performance and Reliability of TOPCon Modules, 2024.

[39] Sebastian Gatz, Rethinking the next wave of TOPCon production, 2026. https://www.pv-tech.org/rethinking-the-next-wave-of-topcon-production/ (accessed 6 May 2026).

[40] J. Gong, L. Schneider, Y. Liu, 2026. Review on Perovskite Solar Cells: From Single-Junction Devices to Tandem Deployment in Space. Adv. Sustainable Syst. 10, e01343. https://doi.org/10.1002/adsu.202501343.

[41] A. Gerthoffer, F. Roux, F. Emieux, P. Faucherand, H. Fournier, L. Grenet, S. Perraud, CIGS solar cells on flexible ultra-thin glass substrates: Characterization and bending test, Thin Solid Films 592 (2015) 99–104. https://doi.org/10.1016/j.tsf.2015.09.006.

[42] Y.-C. Wang, T.-T. Wu, Y.-L. Chueh, A critical review on flexible Cu(In, Ga)Se2 (CIGS) solar cells, Mater. Chem. Phys. 234 (2019) 329–344. https://doi.org/10.1016/j.matchemphys.2019.04.066.

[43] P. Gebhardt, U. Kräling, E. Fokuhl, I. Hädrich, D. Philipp, 2024. Reliability of Commercial TOPCon PV Modules—An Extensive Comparative Study. Prog. Photovolt., pip.3868. https://doi.org/10.1002/pip.3868.

[44] M.R.M. Neves, A.M.C. Silveira, J.F.S. de Paula, H. Franca Santos, T. Crestani, L. S. Costa, R.M. Garcia, M. Gradella Villalva, Barros, Tárcio Andre dos Santos, Analysis of the Effects of Leakage Current Produced by Potential Induced Degradation (PID) in Photovoltaic Modules with PERC and TOPCon Technology. WIP-Munich, in: 40th European Photovoltaic Solar Energy Conference, 020184-001 - 020184-005.

[45] C. Sen, H. Wang, M.U. Khan, J. Fu, X. Wu, X. Wang, B. Hoex, Buyer aware: Three new failure modes in TOPCon modules absent from PERC technology, Sol. Energy Mater. Sol. Cells 272 (2024) 112877. https://doi.org/10.1016/j.solmat.2024.112877.

[46] Yuqiu Ye, Yanfang Zhou, Ye Wang, Bram Hoex, Xiaogang Zhu, Daoyuan Chen, Wenjuan Xue, Tiantian Wei, Bin Chen, Meng Cheng, Jiayan Lu, Haipeng Yin, Zi Ouyang, Damp-heat stability investigation of glass-backsheet modules based on TOPCon solar cells, Solar Energy Materials and Solar Cells 292 (2025). https://doi.org/10.1016/j.solmat.2025.113764.

[47] G. Oreski, C. Barretta, P. Christöfl, P. Gebhardt, K.-A. Weiß, D.C. Miller, S. Uličná, M. Kempe, L.S. Bruckman, A. Virtuani, H. Li, B. Habersberger, J. Munro, K. Proost, M. Kühne, What Is a Polyolefin? A Critical Overview of Ethylene Copolymers Used as Solar Photovoltaic Module Encapsulants, Prog. Photovolt. (2026) 367–395. https://doi.org/10.1002/pip.70038.

[48] Nikolina Pervan, Jutta Geier, Christian Veas, Gernot Oreski, Festina Lente! The Impact of Lamination Duration on Encapsulant Stability, 2025.

[49] A. Bennett, S.J. Bennison, C.H. Butler, A.V. Hester, T.L. Nutter, S. Schleidt, C.A. Smith, Next Generation Ionomer Encapsulants for Low Cost Processing in the Photovoltaic

Industry, in: 26th European Photovoltaic Solar Energy Conference and Exhibition, pp. 3045–3051.

[50] Y. Yue, Y. Zhang, Y. Zheng, Y. Shao, B. Wei, W. Shi, 2025. Moisture-Resistant Thermoplastic Polyurethane Encapsulation for Flexible Perovskite Solar Cells. Energy Tech 13, 2402310. https://doi.org/10.1002/ente.202402310.

[51] N. Ronayette, O. Poncelet, S. Sousa Nobre, S. Barthélémy, D. Bellet, R. Monna, Reduction of silver content in Electrically Conductive Adhesives for low-temperature interconnection of solar cells, Sol. Energy Mater. Sol. Cells 292 (2025) 113762. https://doi.org/10.1016/j.solmat.2025.113762.

[52] A. de Rose, A. Kahane, D. Güldali, P. Molina, B. Grübel, C. Reichel, Lead-free solder alloys for PV modules: Life cycle assessment for environmental impact and toxicity, J. Sol. Energy 303 (2026) 114181. https://doi.org/10.1016/j.solener.2025.114181.

[53] A. Elsafi, B. Aïssa, K. Ilse, A. Abdallah, Performance and durability of anti-soiling and anti-reflective coatings for photovoltaic systems in desert climates, J. Sol. Energy 293 (2025) 113446. https://doi.org/10.1016/j.solener.2025.113446.

[54] U. Desai, K. Nicolet, S. Prabhudesai, G. Cattaneo, J. Robin, C. Cunha, J. Silva, L. Jacques, F. Mujovi, J. Levrat, M. Despeisse, A. Hessler-Wyser, A. Faes, C. Ballif, Stress tolerance of lightweight glass-free PV modules for vehicle integration, EPJ Photovolt. 15 (2024) 10. https://doi.org/10.1051/epjpv/2024003.

[55] Shravan Chunduri, Coveme's Non-Fluoropolymer Backsheets With Barrier & Transparent Variants: Italian supplier lists 26 non-fluoropolymer models in the TaiyangNews 2024/25 survey, including high-barrier, rPET, and glass-replacement frontsheets, 2025. https://taiyangnews.info/technology/covemes-non-fluoropolymer-backsheets-with-barrier-transparent-variants (accessed 6 May 2026).

[56] L.C. Olsen, M.E. Gross, G.L. Graff, S.N. Kundu, X. Chu, S. Lin, Approaches to encapsulation of flexible CIGS cells, in: Reliability of Photovoltaic Cells, Modules, Components, and Systems, San Diego, CA, SPIE, 2008, 70480O.

[57] S. Shital, C. Fanara, M.H. Saw, P. Hart, A. Nairi, L. Wang, Status of UV-induced degradation in state-of-the-art solar cells and its mitigation through encapsulants, Sol. Energy Mater. Sol. Cells 304 (2026) 114407. https://doi.org/10.1016/j.solmat.2026.114407.

[58] M. Babics, V. Barth, Y. Roujol, T. Béjat, M. Sérasset, A. Boulanger, A. Descormes, J. Aime, D. Boyer, G. Bianca, S. Caccamo, M. Leonardi, F. Rametta, A. Ragonesi, C. Gerardi, E. Voroshazi, 2026. Performance and Reliability of PV Modules Made With Novel Co-Extruded Encapsulant Containing UV Downshifting Compound. Prog. Photovolt., pip.70086. https://doi.org/10.1002/pip.70086.

[59] H.-Y. Li, Y. Luo, C. Ballif, L.-E. Perret-Aebi, Effect of Cooling Press on the Optical Transmission Through Photovoltaic Encapsulants, Polymer-Plastics Technology and Engineering 54 (2015) 416–424. https://doi.org/10.1080/03602559.2014.958778.

[60] S. Smith, S. Mitterhofer, S.L. Moffitt, S.-S. Jhang, S.S. Watson, L.-P. Sung, X. Gu, Long-term durability of transparent backsheets for bifacial photovoltaics: An in-depth degradation analysis, Sol. Energy Mater. Sol. Cells 256 (2023) 112309. https://doi.org/10.1016/j.solmat.2023.112309.

[61] A. Omazic, G. Oreski, M. Edler, G.C. Eder, C. Hirschl, G. Pinter, M. Erceg, Increased reliability of modified polyolefin backsheet over commonly used polyester backsheets for crystalline PV modules, J. Appl. Polym. Sci. 2020 48899. https://doi.org/10.1002/app.48899.

[62] G.C. Eder, Y. Voronko, G. Oreski, W. Mühleisen, M. Knausz, A. Omazic, A. Rainer, C. Hirschl, H. Sonnleitner, Error analysis of aged modules with cracked polyamide backsheets, Sol. Energy Mater. Sol. Cells 203 (2019) 110194. https://doi.org/10.1016/j.solmat.2019.110194.

[63] G.C. Eder, Y. Voronko, W. Muehleisen, C. Hirschl, G. Oreski, K. Knoebl (Eds.), Aging induced cracking of polymeric backsheets: Analytical approach to identify the drivers, Institute of Electrical and Electronics Engineers Inc, 2019.

[64] W. Gambogi, Reliability of transparent polymeric backsheets under accelerated aging for bifacial modules, in: NREL PVRW.

[65] S. Smith, L. Perry, S. Watson, S.L. Moffitt, S.-J. Shen, S. Mitterhofer, L.-P. Sung, D. Jacobs, X. Gu, 2021. Transparent backsheets for bifacial photovoltaic (PV) modules: Material characterization and accelerated laboratory testing. Prog. Photovoltaics Res. Appl., pip.3494. https://doi.org/10.1002/pip.3494.

[66] G. Eder, G. Peharz, R. Trattnig, P. Bonom, E. Saretta, F. Frontini, C. Polo Lopez, H.R. Wilson, J. Eisenlohr, N.M. Chivelet, S. Karlson, N. Jakica, A. Zanelli, COLOURED BIPV - Market, Research and Development: Report IEA-PVPS T15-07: 2019, 2019.

[67] J. Eymard, R. Clerc, V. Duveiller, B. Commault, M. Hebert, Characterization of UV–Vis–NIR optical constants of encapsulant for accurate determination of absorption and backscattering losses in photovoltaics modules, Sol. Energy Mater. Sol. Cells 240 (2022) 111717. https://doi.org/10.1016/j.solmat.2022.111717.

[68] C. Barretta, G. Oreski, S. Feldbacher, K. Resch-Fauster, R. Pantani, Comparison of Degradation Behavior of Newly Developed Encapsulation Materials for Photovoltaic Applications under Different Artificial Ageing Tests, Polymers 13 (2021). https://doi.org/10.3390/polym13020271.

[69] R. Heidrich, C. Barretta, A. Mordvinkin, G. Pinter, G. Oreski, R. GOttschalg, UV lamp spectral effects on the aging behavior of encapsulants for photovoltaic modules, Sol. Energy Mater. Sol. Cells 266 (2024) 112674. https://doi.org/10.1016/j.solmat.2023.112674.

[70] M. Aghaei (Ed.), Solar Radiation - Measurement, Modeling and Forecasting Techniques for Photovoltaic Solar Energy Applications, IntechOpen, 2022.

[71] M. Aminul Islam, N. M. Kassim, A. Ahmed Alkahtani, N. Amin, Assessing the Impact of Spectral Irradiance on the Performance of Different Photovoltaic Technologies, in: M. Aghaei (Ed.), Solar Radiation - Measurement, Modeling and Forecasting Techniques for Photovoltaic Solar Energy Applications, IntechOpen, 2022.

[72] F.T. Thome, P. Meßmer, S. Mack, E. Schnabel, F. Schindler, W. Kwapil, M.C. Schubert, 2024. UV-Induced Degradation of Industrial PERC, TOPCon, and HJT Solar Cells: The Next Big Reliability Challenge? Solar RRL 8, 2400628. https://doi.org/10.1002/solr.202400628.

[73] F.J. Pern, S.H. Glick, Photothermal stability of encapsulated Si solar cells and encapsulation materials upon accelerated exposures, Sol. Energy Mater. Sol. Cells 61 (2000) 153–188. https://doi.org/10.1016/S0927-0248(99)00108-7.

[74] F. PERN, Factors that affect the EVA encapsulant discoloration rate upon accelerated exposure, Sol. Energy Mater. Sol. Cells 41-42 (1996) 587–615. https://doi.org/10.1016/0927-0248(95)00128-X.

[75] S. Uličná, R.L. Arnold, J.M. Newkirk, A. Sinha, K. Terwilliger, L.T. Schelhas, P. Pasmans, C. Thellen, D.C. Miller, 2024. Material characterization of seven photovoltaic backsheets using seven accelerated test conditions. Solar Energy Materials and Solar Cells 267, 112726.

[76] A. Kraft, L. Labusch, T. Ensslen, I. Durr, J. Bartsch, M. Glatthaar, S. Glunz, H. Reinecke, Investigation of Acetic Acid Corrosion Impact on Printed Solar Cell Contacts, Photovoltaics, IEEE Journal of 5 (2015) 736–743. https://doi.org/10.1109/JPHOTOV.2015.2395146.

[77] J. Li, Y.-C. Shen, P. Hacke, M. Kempe, Electrochemical mechanisms of leakage-current-enhanced delamination and corrosion in Si photovoltaic modules, Sol. Energy Mater. Sol. Cells 188 (2018) 273–279. https://doi.org/10.1016/j.solmat.2018.09.010.

[78] G.J. Jorgensen, K. M. Terwilliger, J. A. DelCueto, S. H. Glick, M. D. Kempe, J. W. Pankow, F. J. Pern, T. J. McMahon, Moisture transport, adhesion, and corrosion protection of PV module packaging materials, Sol. Energy Mater. Sol. Cells 90 (2006) 2739–2775.

[79] M. Babin, G.C. Eder, Y. Voronko, G. Oreski, Water vapor permeability of polymeric packaging materials for novel glass-free photovoltaic applications, J. Appl. Polym. Sci. 141 (2024) e55733. https://doi.org/10.1002/app.55733.

[80] Z. Pan, M. Bora, R. Gee, R.H. Dauskardt, Water vapor transmission rate measurement for moisture barriers using infrared imaging, Mater. Chem. Phys. 308 (2023) 128289. https://doi.org/10.1016/j.matchemphys.2023.128289.

[81] M. D. Kempe, M. O. Reese, A. A. Dameron, Evaluation of the sensitivity limits of water vapor transmission rate measurements using electrical calcium test, Rev. Sci. Instrum. 84 (2013) 1–10.

[82] R.R. Cordero, A. Damiani, D. Laroze, S. MacDonell, J. Jorquera, E. Sepúlveda, S. Feron, P. Llanillo, F. Labbe, J. Carrasco, J. Ferrer, G. Torres, Effects of soiling on photovoltaic (PV) modules in the Atacama Desert, Sci. Rep. 8 (2018) 13943. https://doi.org/10.1038/s41598-018-32291-8.

[83] G.P. Smestad, T.A. Germer, H. Alrashidi, E.F. Fernández, S. Dey, H. Brahma, N. Sarmah, A. Ghosh, N. Sellami, I.A.I. Hassan, M. Desouky, A. Kasry, B. Pesala, S. Sundaram, F. Almonacid, K.S. Reddy, T.K. Mallick, L. Micheli, Modelling photovoltaic soiling losses

through optical characterization, Sci. Rep. 10 (2020) 58. https://doi.org/10.1038/s41598-019-56868-z.

[84] N. Martin, M.A. Ariza, D. Neumann, M.-O. Prast, M.C. Alonso-Garc■a, F. Chenlo, M. Angulo, E. Mejuto, P. Mazn, W.A. Nositschka (Eds.), Surface Soiling Losses Measurement in PV Modules under Real Operation, 2011.

[85] K.A.M. Ali, Y.K.O.T. Osman, G.G.A. El-Wahhab, T.A.M. Abdelwahab, A.E.M. Fodah, Improving solar PV performance under bird-dropping conditions with a dual-cooling approach, Sci Rep 15 (2025) 8211. https://doi.org/10.1038/s41598-024-84932-w.

[86] M. Springer, T.J. Silverman, N. Bosco, J. Joe, I. Repins, Residual Stresses Affect Cell Fragment Movement, IEEE J. Photovoltaics 13 (2023) 547–551. https://doi.org/10.1109/JPHOTOV.2023.3269118.

[87] F. Rahman, I.M. Slauch, R. Meier, J. Tracy, E.C. Palmiotti, M.I. Bertoni, J.Y. Hartley, Lamination Process Induced Residual Stress in Glass-Glass vs. Glass-Backsheet Modules, in: 2022 IEEE 49th Photovoltaics Specialists Conference (PVSC), Philadelphia, PA, USA, IEEE, 2022, p. 199.

[88] A. Beinert, M. Ebert, U. Eitner, J. Aktaa, Influence of Photovoltaic Module Mounting Systems on the Thermo-Mechanical Stresses in Solar Cells by FEM Modelling, Fraunhofer-Gesellschaft, 2016.

[89] A.R. Wittwer, J.M. Podestá, H.G. Castro, J.L. Mroginski, J.O. Marighetti, M.E. de Bortoli, R.R. Paz, F. Mateo, Wind loading and its effects on photovoltaic modules: An experimental–Computational study to assess the stress on structures, J. Sol. Energy 240 (2022) 315–328. https://doi.org/10.1016/j.solener.2022.04.061.

[90] P. Romer, A.J. Beinert, Effects of Inhomogeneous Snow Load on the Mechanics of a PV Module, in: 38th European Photovoltaic Solar Energy Conference and Exhibition, pp. 602–606.

[91] A. Gassner, G.C. Eder, E. Özkalay, G. Friesen, M. Feichtner, V.-M. Archodoulaki, Enhanced mechanical load testing of photovoltaic modules for cold and snowy climates, EES Sol. 2 (2026) 161–173. https://doi.org/10.1039/D5EL00125K.

[92] A. C. Oliveira Martins, V. Chapuis, A. Virtuani, L.-E. Perret-Aebi, and C. Ballif, Hail Resistance of Composite-Based Glass-Free Lightweight Modules for Building Integrated Photovoltaics Applications, in:

[93] W. Muehleisen, G.C. Eder, Y. Voronko, M. Spielberger, H. Sonnleitner, K. Knoebl, R. Ebner, G. Ujvari, C. Hirschl, Outdoor detection and visualization of hailstorm damages of photovoltaic plants, Renewable Energy 118 (2018) 138–145. https://doi.org/10.1016/j.renene.2017.11.010.

[94] J. Govaerts, P. Dufke, B. Luo, M. Bonnart, R. van Dyck, T. Borgers, J. Poortmans, A. Derluyn, J. Saelens, W. Winant, C.M. Arslan, U. Desai, F. Lisco, A. Faes, C. Ballif, G. Oreski, N. Pervan, G. Eder (Eds.), Light as Heaven, Strong as Hell(?): Testing Honeycomb-Based Laminates for Light-Weight c-Si PV Applications, 2023.

[95] J. Hum, K. Hollands, J. Wright, Analytical model for the thermal conductance of double-compound honeycomb transparent insulation, with validation, Sol. Energy 76 (2004) 85–91. https://doi.org/10.1016/j.solener.2003.07.034.

[96] A.C. Martins, V. Chapuis, F. Sculati-Meillaud, A. Virtuani, C. Ballif, Light and durable: Composite structures for building-integrated photovoltaic modules, Prog. Photovoltaics Res. Appl. 26 (2018) 718–729. https://doi.org/10.1002/pip.3009.

[97] A. Virtuani, A. Martins, E. Annigoni, C. Ballif, Glass-free lightweight PV modules made to last, Halle an der Saale, 2018.

[98] J. Govaerts, B. Luo, T. Borgers, R. van Dyck, A. van der Heide, L. Tous, A. Morlier, F. Lisco, L. Cerasti, M. Galiazzo, J. Poortmans, Development and testing of light-weight PV modules based on glass-fibre reinforcement, EPJ Photovolt. 13 (2022) 13. https://doi.org/10.1051/epjpv/2022007.

[99] U. Desai, M. Courtant, G. Eder, G. Oreski, A. Faes, C. Ballif, Novel mechanically robust and environmentally stable light-weight colored photovoltaic modules based on composite polymer backsheets, Solar RRL (2025).

[100] H. Nussbaumer, M. Klenk, N. Keller, P. Ammann, and J. Thurnheer, Record-Light Weight c-Si Modules Based on the Small Unit Compound Approach – Mechanical Load Tests and General Results, in: 33rd European Photovoltaic Solar Energy Conference and Exhibition.

[101] C. Schubbert, T. Bachmann, S. Dietrich, M. Ebert (Eds.), Exemplary results of temperature-dependent mechanical load tests under variation of glass and foil parameters and investigation of different load types.

[102] IEC, Terrestrial photovoltaic (PV) modules - Design qualification and type approval - Part 2: Test procedures: Terrestrial photovoltaic (PV) modules - Design qualification and type approval - Part 2: Test procedures 27.160 - Solar energy engineering, 2016. https://webstore.iec.ch/publication/24311.

[103] A.J. Beinert, P. Romer, A. Büchler, V. Haueisen, J. Aktaa, U. Eitner, Thermomechanical stress analysis of PV module production processes by Raman spectroscopy and FEM simulation, Energy Procedia 124 (2017) 464–469. https://doi.org/10.1016/j.egypro.2017.09.282.

[104] N. Bosco, T.J. Silverman, S. Kurtz, Climate specific thermomechanical fatigue of flat plate photovoltaic module solder joints, Microelectron. Reliab. 62 (2016) 124–129. https://doi.org/10.1016/j.microrel.2016.03.024.

[105] T. Geipel, L.C. Rendler, M. Stompe, U. Eitner, L. Rissing, Reduction of Thermomechanical Stress Using Electrically Conductive Adhesives, Energy Procedia 77 (2015) 346–355. https://doi.org/10.1016/j.egypro.2015.07.049.

[106] A. Badiee, I.A. Ashcroft, R.D. Wildman, The thermo-mechanical degradation of ethylene vinyl acetate used as a solar panel adhesive and encapsulant, Int. J. Adhes. Adhes. 68 (2016) 212–218. https://doi.org/10.1016/j.ijadhadh.2016.03.008.

[107] M.T. Zarmai, N.N. Ekere, C.F. Oduoza, E.H. Amalu, Evaluation of thermo-mechanical damage and fatigue life of solar cell solder interconnections, Rob. Comput. Integr. Manuf. 47 (2017) 37–43. https://doi.org/10.1016/j.rcim.2016.12.008.

[108] H. Jiao, M. Hegde, N. Li, M. Owen-Bellini, L. Schelhas, T.J. Dingemans, J. Huang, Metal Halide Perovskite Solar Module Encapsulation Using Polyolefin Elastomers: The Role of Morphology in Preventing Delamination, PRX Energy 3 (2024). https://doi.org/10.1103/PRXEnergy.3.023013.

[109] M. Köntges, G. Oreski, U. Jahn, P. Hacke, K. Weiss, G. Razzongles, M. Paggi, D. Parleviet, T. Tanahashi, R. French, M. Richter, A. Morlier, C. Tjengdrawira, H. Li, K.A. Berger, G. Makrides, W. Herrmann, Assessment of Photovoltaic Module Failures in the Field: Report IEA-PVPS T13-09:2017, 2017.

[110] U. Erdil, M. Khenkin, W.M. Bernardes de Araujo, Q. Emery, I. Lauermann, V. Paraskeva, M. Norton, S. Vediappan, D.K. Kumar, R.K. Gupta, I. Visoly-Fisher, M. Hadjipanayi, G.E. Georghiou, R. Schlatmann, A. Abate, E.A. Katz, C. Ulbrich, 2025. Delamination of

Perovskite Solar Cells in Thermal Cycling and Outdoor Tests. Energy Tech 13, 2401280. https://doi.org/10.1002/ente.202401280.

[111] P. Romer, G. Oreski, A.J. Beinert, H. Neuhaus, M. Mittag, More realistic considerations of backsheets coefficient of themal expansion on thermomechanics of PV modules, in: 37th European Photovoltaic Solar Energy Conference and Exhibition, pp. 772–776.

[112] V. Meslier, J.-L. Bouvard, P.-O. Bouchard, B. Chambion, A. Derrier, Measurement of Encapsulant Thermal Expansion (CTE): Impact of Residual Stresses, in: 41st European Photovoltaic Solar Energy Conference and Exhibition, 3AV.1.13.

[113] V. Meslier, B. Chambion, P.-O. Bouchard, J.-L. Bouvard, Thermal Expansion Behavior of a Thermoplastic Polyolefin for Photovoltaic Application Over Hygrothermal Aging, IEEE J. Photovoltaics (2024) 1–10. https://doi.org/10.1109/JPHOTOV.2024.3463950.

[114] M. Barucci, G. Bianchini, T. Del Rosso, E. Gottardi, I. Peroni, G. Ventura, Thermal expansion and thermal conductivity of glass-fibre reinforced nylon at low temperature, Cryogenics 40 (2000) 465–467. https://doi.org/10.1016/S0011-2275(00)00067-9.

[115] W.A. MacDonald, M.K. Looney, D. MacKerron, R. Eveson, R. Adam, K. Hashimoto, K. Rakos, Latest advances in substrates for flexible electronics, J. Soc. Inf. Disp. 15 (2007) 1075–1083. https://doi.org/10.1889/1.2825093.

[116] I. Shakir Abbood, S.a. Odaa, K.F. Hasan, M.A. Jasim, Properties evaluation of fiber reinforced polymers and their constituent materials used in structures – A review, Materials Today: Proceedings 43 (2021) 1003–1008. https://doi.org/10.1016/j.matpr.2020.07.636.

[117] C. Peike, I. Häldrich, K.-A. Weiß, I. Dürr, Overview of PV module encapsulation materials, Photovoltaics International (2013) 85–92.

[118] P. Nivelle, J.A. Tsanakas, J. Poortmans, M. Daenen, Stress and strain within photovoltaic modules using the finite element method: A critical review, RENEW SUST ENERG REV 145 (2021) 111022. https://doi.org/10.1016/j.rser.2021.111022.

[119] M. Knausz, G. Oreski, M. Schmidt, P. Guttmann, K.A. Berger, Y. Voronko, G. Eder, T. Koch, G. Pinter, Thermal expansion behavior of solar cell encapsulation materials, Polym. Test. 44 (2015) 160–167. https://doi.org/10.1016/j.polymertesting.2015.04.009.

[120] G. Oreski, A. Rauschenbach, C. Hirschl, M. Kraft, G.C. Eder, G. Pinter, Crosslinking and post-crosslinking of ethylene vinyl acetate in photovoltaic modules, J. Appl. Polym. Sci. 134 (2017) 101. https://doi.org/10.1002/app.44912.

[121] N. Bosco, M. Springer, X. He, Viscoelastic Material Characterization and Modeling of Photovoltaic Module Packaging Materials for Direct Finite-Element Method Input, IEEE J. Photovoltaics 10 (2020) 1424–1440. https://doi.org/10.1109/JPHOTOV.2020.3005086.

[122] U. Eitner, S. Kajari-Schröder, M. Köntges, H. Altenbach, Thermal Stress and Strain of Solar Cells in Photovoltaic Modules, in: H. Altenbach, V.A. Eremeyev (Eds.), Shell-like Structures, Springer Berlin Heidelberg, Berlin, Heidelberg, 2011, pp. 453–468.

[123] M. Paggi, S. Kajari-Schröder, U. Eitner, Thermomechanical deformations in photovoltaic laminates, The Journal of Strain Analysis for Engineering Design 46 (2011) 772–782. https://doi.org/10.1177/0309324711421722.

[124] Schott, TIE-31: Mechanical and thermal properties of optical glass, 2004. https://www.schott.com/shop/medias/schott-tie-31-mechanical-and-thermal-properties-of-optical-eng.pdf?context=bWFzdGVyfHJvb3R8MjIxODU3fGFwcGxpY2F0aW9uL3BkZnxoYjkvaGI0Lzg4MjAyMzc5MjY0MzAucGRmfGJmMzI4ZjE5ZTEyNzdiMjRkYWQ5Y2QyOWFiNmU1MTU5ZDdmMWJjZDFlODEwZTllMjlkMjk1ZWEzN2JlNjY5MjI (accessed 31 March 2025.).

[125] thyssenkrupp Materials (UK) Ltd, Stainless Steel 430 1.4016. https://www.thyssenkrupp-materials.co.uk/stainless-steel-430-14016.html (accessed 7 May 2026).

[126] Nikolina Pervan, Christian Veas, Sonja Feldbacher, Lukas Geymayer, Gregor Kitzberger, Martin Fleischanderl, Hannes Kurz, Friedrich Füreder-Kitzmüller, Gernot Oreski, Transforming Industrial Facades with Integrated Photovoltaics. 3AV.1.20, in: EU PVSEC 2025.

[127] M. Pander, S. Dietrich, S.-H. Schulze, U. Eitner, M. Ebert, Thermo-mechanical assessment of solar cell displacement with respect to the viscoelastic behaviour of the encapsulant, in: 12th International Thermal, Mechanical and Multi-Physics Simulation and Experiments in Microelectronics and Microsystems, pp. 433–438.

[128] E. Özkalay, G. Friesen, M. Caccivio, P. Bonomo, A. Fairbrother, C. Ballif, A. Virtuani, Operating Temperatures and Diurnal Temperature Operating Temperatures and Diurnal Temperature Variations of Modules Installed in Open-Rack and Typical BIPV Configurations, IEEE Journal of Photovoltacis 12 (2022) 133–140.

[129] H. Quest, A. Fairbrother, C. Ballif, A. Virtuani, Towards a quantification of thermal and thermomechanical stress for modules in building-integrated photovoltaics configurations, Prog. Photovolt. 33 (2025) 64–75. https://doi.org/10.1002/pip.3762.

[130] ASTM, Standard Test Method for Evaluating the Resistance to Thermal Transmission of Materials by Guarded Heat Flow Meter Technique.

[131] Netzsch, Thermal Characterization of Photovoltaic Materials: Analyzing & Testing. https://analyzing-testing.netzsch.com/_Resources/Persistent/0/1/f/5/01f50b477e260deece93eee263918af24059421c/Photovoltaic_E.pdf (accessed 7 May 2026).

[132] R. Sadeghi, S. Memme, S. Morchio, M. Fossa, M. Parenti, Infrared Thermography in Photovoltaic Systems: A Review for Maximizing Energy Yield and Long-Term Reliability, Energies 19 (2026) 1570. https://doi.org/10.3390/en19061570.

[133] S.E. Julien, J.H. Kim, Y. Lyu, D.C. Miller, X. Gu, K. Wan, Cohesive and adhesive degradation in PET-based photovoltaic backsheets subjected to ultraviolet accelerated weathering, J. Sol. Energy 224 (2021) 637–649. https://doi.org/10.1016/j.solener.2021.04.065.

[134] S. Jahreis, B. Jaeckel, R. Koepge, J. Fröbel, P. Schenk, M. Pander, R. Castro, Design, manufacturing, and performance of innovative aluminium-backed BIPV facade modules: a case-study in Germany, Energy and Buildings 344 (2025) 116047. https://doi.org/10.1016/j.enbuild.2025.116047.

[135] Y.-S. Kim, A.-R. Kim, S.J. Tark, C.-B. Mo, S. Hwang, Y. Kang, Analysis of adhesion characteristics of steel back plates and encapsulants for fire-proof BIPV modules, Results Eng. 21 (2024) 101649. https://doi.org/10.1016/j.rineng.2023.101649.

[136] J. Friedrich, Tailoring of Interface/Interphase to Promote Metal-Polymer Adhesion, in: K.L. Mittal, T. Ahsan (Eds.), Adhesion in Microelectronics, Wiley, 2014, pp. 65–135.

[137] H. Moon, J.E. Park, W. Cho, J. Jeon, J.J. Wie, Curing Kinetics and Structure-Property Relationship of Moisture-Cured One-Component Polyurethane Adhesives, Eur. Polym. J. 201 (2023) 112579. https://doi.org/10.1016/j.eurpolymj.2023.112579.

[138] Jishnu Ramachandran Nair, Nishant Pradhan, Paul Schenk, Matthias Pander, Steffen Bornemann, Mohammad Abdus Salam (Eds.), Formulation Studies of Polyolefin Elastomer Encapsulants with Adhesion Promoters: Impacts on Adhesion Strength and Crosslinking Behavior, 2025.

[139] G. Primc, M. Mozetič, Surface Modification of Polymers by Plasma Treatment for Appropriate Adhesion of Coatings, Materials (Basel) 17 (2024). https://doi.org/10.3390/ma17071494.

[140] Kuan Liu, David C. Miller, Nick Bosco, Jimmy M. Newkirk, Reinhold H. Dauskardt (Eds.), Advancing Steady-State and Sequenced Accelerated Aging for Assessing the Adhesion Degradation of Contemporary Encapsulants, 2025.

[141] A. Omazic, G. Oreski, M. Halwachs, G.C. Eder, C. Hirschl, L. Neumaier, G. Pinter, M. Erceg, Relation between degradation of polymeric components in crystalline silicon PV module and climatic conditions: A literature review, Sol. Energy Mater. Sol. Cells 192 (2019) 123–133. https://doi.org/10.1016/j.solmat.2018.12.027.

[142] N. Bosco, J. Eafanti, S. Kurtz, J. Tracy, R. Dauskardt, Defining Threshold Values of Encapsulant and Backsheet Adhesion for PV Module Reliability, IEEE J. Photovoltaics 7 (2017) 1536–1540. https://doi.org/10.1109/JPHOTOV.2017.2746682.

[143] G. Oreski, G. Pinter, Peeling of Flexible Laminates-Determination of Interlayer Adhesion of Backsheet Laminates Used for Photovoltaic Modules, Materials (Basel) 15 (2022). https://doi.org/10.3390/ma15093294.

[144] D. Wu, J. Zhu, T.R. Betts, R. GOttschalg, Degradation of interfacial adhesion strength within photovoltaic mini-modules during damp-heat exposure, Prog. Photovoltaics Res. Appl. 22 (2014) 796–809. https://doi.org/10.1002/pip.2460.

[145] M. Tiefenthaler, G.M. Wallner, R. Pugstaller, Effect of global damp heat ageing on debonding of crosslinked EVA- and POE-glass laminates, Sol. Energy Mater. Sol. Cells 264 (2024) 112602. https://doi.org/10.1016/j.solmat.2023.112602.

[146] Casey C. Grant, Fire Fighter Safety and Emergency Response for Solar Power Systems, 2013. https://sustainable-fire-engineering.sustainable-design.ie/wp-

content/uploads/2015/08/NFPA-FPRF_Firefighter-Tactics-Solar-Power_2013.pdf (accessed 12 May 2026).

[147] P. Cancelliere, PV electrical plants fire risk assessment and mitigation according to the Italian national fire services guidelines, Fire Mater. 40 (2016) 355–367. https://doi.org/10.1002/fam.2290.

[148] Nikolina Pervan, Sonja Feldbacher, Umang Desai, Antonin Faes, Christophe Ballif, Gernot Oreski, Tackling the Fire Safety in Glass Free PV Modules. 3AV.2.17, in: EU PVSEC 2024, 020185-001 - 020185-001.

[149] F. Ollagnon, O. Aurrekoetxea-Arratibel, E. Gottis, H.-Y. Li, X. Olano-Azkune, M. Despeisse, A. Faes, C. Ballif, 2026. Advanced Flame Retardant Strategies and Fire Performance Assessment for Safer Photovoltaics in Buildings: A Two-Part Review. Advanced Functional Materials 36, e09194. https://doi.org/10.1002/adfm.202509194.

[150] BVS - Brandverhütungsstelle für Oö. reg. Genossenschaft m.b.H., Photovoltaic systems: Fire protection requirements for the installation of photovoltaic systems on hall roofs with areas larger than 1,800 m2 or for objects equipped with automatic fire suppression systems or with oxygen reduction systems. https://www.bvs-ooe.at/wp-content/uploads/2023/04/MVB-036-2022_Photovoltaic-systems_eng.pdf (accessed 7 May 2026).

[151] K.T.Q. Nguyen, P. Weerasinghe, P. Mendis, T. Ngo, Performance of modern building façades in fire: a comprehensive review, EJSE 16 (2016) 69–87. https://doi.org/10.56748/ejse.16212.

[152] U. Desai, J. Govaerts, B. Luo, Y. Voronko, G. Eder, J. Saelens, W. Winant, N. Pervan, G. Oreski, A. Faes, C. Ballif, Novel Lightweight PV Modules Based on Polymeric Honeycomb for Building Integration, in: 2024 IEEE 52nd Photovoltaic Specialist Conference (PVSC), Seattle, WA, USA, IEEE, 2024, pp. 89–91.

[153] J. Kettle, M. Aghaei, S. Ahmad, A. Fairbrother, S. Irvine, J.J. Jacobsson, S. Kazim, V. Kazukauskas, D. Lamb, K. Lobato, G.A. Mousdis, G. Oreski, A. Reinders, J. Schmitz, P. Yilmaz, M.J. Theelen, Review of technology specific degradation in crystalline silicon, cadmium telluride, copper indium gallium selenide, dye sensitised, organic and perovskite solar cells in photovoltaic modules: Understanding how reliability

improvements in mature technologies can enhance emerging technologies, Prog. Photovoltaics Res. Appl. 30 (2022) 1365–1392. https://doi.org/10.1002/pip.3577.

[154] A. Omazic, G. Oreski, M. Halwachs, G.C. Eder, C. Hirschl, L. Neumaier, G. Pinter, M. Erceg, Relation between degradation of polymeric components in crystalline silicon PV module and climatic conditions: A literature review, Sol. Energy Mater. Sol. Cells 192 (2019) 123–133. https://doi.org/10.1016/j.solmat.2018.12.027.

[155] S. Mitterhofer, C. Barretta, L. F. Castillon, G. Oreski, M. Topič, M. Jankovec, A Dual-Transport Model of Moisture Diffusion in PV Encapsulants for Finite-Element Simulations, IEEE J. Photovoltaics 10 (2020) 94–102. https://doi.org/10.1109/JPHOTOV.2019.2955182.

[156] H. A Kim, J.H. Baeg, J. Shin, J. Park, S. Lee, Effect of Damp Heat on the Performance Degradation of Flexible CIGS Photovoltaic Modules, Int J Adv Tech 09 (2018). https://doi.org/10.4172/0976-4860.1000200.

[157] B. Chen, N. Ren, Y. Li, L. Yan, S. Mazumdar, Y. Zhao, X. Zhang, Insights into the Development of Monolithic Perovskite/Silicon Tandem Solar Cells, Advanced Energy Materials 12 (2022) 2003628. https://doi.org/10.1002/aenm.202003628.

[158] F. Toniolo, H. Bristow, M. Babics, L.M.D. Loiola, J. Liu, A.A. Said, L. Xu, E. Aydin, T.G. Allen, M. Meneghetti, S.P. Nunes, M. de Bastiani, S. de Wolf, Efficient and reliable encapsulation for perovskite/silicon tandem solar modules, Nanoscale 15 (2023) 16984–16991. https://doi.org/10.1039/d2nr06873g.

[159] C. Barretta, A.E. Macher, M. Köntges, J. Ascencio-Vásquez, M. Topič, G. Oreski, Effect of Encapsulant Degradation on Photovoltaic Modules Performances Installed in Different Climates, IEEE J. Photovoltaics (2025) 1–7. https://doi.org/10.1109/JPHOTOV.2024.3523546.

[160] IEC, Photovoltaic (PV) modules - Cyclic (dynamic) mechanical load testing 27.160 - Solar energy engineering, 2016. https://webstore.iec.ch/publication/24310.

[161] IEC, Photovoltaics in buildings - Part 1: Requirements for building-integrated photovoltaic modules, Intertnational Electrotechnical Commission 27.160 - Solar energy engineering, 2020. https://webstore.iec.ch/publication/32158 (accessed 1 October 2020).

[162] IEC, Terrestrial photovoltaic (PV) modules - Design qualification and type approval - Part 1: Test requirements: Terrestrial photovoltaic (PV) modules - Design qualification and type approval - Part 1: Test requirements, 2021. https://webstore.iec.ch/publication/61345.

[163] IEC, Extended thermal cycling of PV modules - Test procedure 27.160 - Solar energy engineering. https://webstore.iec.ch/publication/29329.

[164] IEC, Guidelines for qualifying PV modules, components and materials for operation at high temperatures 27.160 - Solar energy engineering. https://webstore.iec.ch/publication/59551.

[165] IEC, Photovoltaic (PV) modules - Type approval, design and safety qualification - Retesting 27.160 - Solar energy engineering. https://webstore.iec.ch/publication/31110.

[166] P. Hacke, M. Owen-Bellini, M.D. Kempe, D.B. Sulas-Kern, D.C. Miller, M. Jankovec, S. Mitterhofer, M. Topič, S. Spataru, W. Gambogi, T. Tanahashi, 2023. Acceleration Factors for Combined-Accelerated Stress Testing of Photovoltaic Modules. Solar RRL 7, 2300068. https://doi.org/10.1002/solr.202300068.

[167] G. Oreski, J.S. Stein, G.C. Eder, K. Berger, L. Bruckman, R. French, J. Vedde, K.A. Weiß, Motivation, benefits, and challenges for new photovoltaic material & module developments, Prog. Energy 4 (2022) 32003. https://doi.org/10.1088/2516-1083/ac6f3f.

[168] C. Sen, H. Wang, R. Heidrich, M. Lüdemann, M.U. Khan, B. Hoex, The dark side of certain POE encapsulant: Chemical pathways to metallisation corrosion in TOPCon modules, Solar Energy Materials and Solar Cells 298 (2026) 114164. https://doi.org/10.1016/j.solmat.2026.114164.

[169] N. Adamovic, A. Zimmermann, A. Caviasca, R. Harboe, F. Ibanez, 2017. Custom designed photovoltaic modules for PIPV and BIPV applications. J. Renewable Sustainable Energy 9, 021202. https://doi.org/10.1063/1.4979820.

[170] M. Cheikh Sow, Y. Jouane, M. Zghal, BI 2 PV simulator for optimized BIPV design in industrial buildings, Energy and Buildings 350 (2026) 116576. https://doi.org/10.1016/j.enbuild.2025.116576.

[171] I. Del Hierro López, L. Olivieri, Comprehensive review of building-integrated photovoltaics in the renovation of heritage buildings, J. Build. Eng. 108 (2025) 112883. https://doi.org/10.1016/j.jobe.2025.112883.

[172] Z. Li, P. Xue, J. Xiong, Fabrication and mechanical properties of CFRP honeycomb cylinder based on the transforming from the flat honeycombs, Composites Science and Technology 259 (2025) 110948. https://doi.org/10.1016/j.compscitech.2024.110948.

[173] A.C. Martins, V. Chapuis, A. Virtuani, C. Ballif, Robust Glass-Free Lightweight Photovoltaic Modules with Improved Resistance to Mechanical Loads and Impact, IEEE J. Photovoltaics 9 (2019) 245–251. https://doi.org/10.1109/JPHOTOV.2018.2876934.

[174] C. Kutter, F. Basler, L.E. Alanis, J. Markert, M. Heinrich, D.H. Neuhaus (Eds.), INTEGRATED LIGHTWEIGHT, GLASS-FREE PV MODULE TECHNOLOGY FOR BOX BODIES OF COMMERCIAL TRUCKS, 2020.

[175] L.E. Alanis, A. Velte-Schäfer, N. Jajoo, M.-A. Schüler, L.C. Rendler, D.H. Neuhaus, M. Heinrich, Thermal effect of VIPV modules in refrigerated trucks, Solar Energy Materials and Solar Cells 275 (2024).

[176] S. Jahreis, B. Jaeckel, R. Koepge, J. Froebel, P. Schenk, M. Pander, Design, Manufacturing and Analysis of Aluminium-backed BIPV Facade Modules: Electrical Performance and Outdoor Tests. WIP-Munich, 42nd European Photovoltaic Solar Energy Conference and Exhibition (2025). https://doi.org/10.4229/EUPVSEC2025/3AV.3.24.

[177] Fraunhofer CSP, Modular aluminum elements with integrated photovoltaic modules for solar facades, 2024. https://www.imws.fraunhofer.de/en/presse/pressemitteilungen/2024/solar-facade-building-integrated-module-aluminum.html (accessed 4 May 2026).

[178] F. Kessler, D. Rudmann, Technological aspects of flexible CIGS solar cells and modules, J. Sol. Energy 77 (2004) 685–695. https://doi.org/10.1016/j.solener.2004.04.010.

[179] M. Powalla, W. Witte, P. Jackson, S. Paetel, E. Lotter, R. Wuerz, F. Kessler, C. Tschamber, W. Hempel, D. Hariskos, R. Menner, A. Bauer, S. Spiering, E. Ahlswede, T.M. Friedlmeier, D. Blazquez-Sanchez, I. Klugius, W. Wischmann, CIGS Cells and Modules With High Efficiency on Glass and Flexible Substrates, IEEE J. Photovoltaics 4 (2014) 440–446. https://doi.org/10.1109/JPHOTOV.2013.2280468.

[180] C. Han, Analysis of moisture-induced degradation of thin-film photovoltaic module, Sol. Energy Mater. Sol. Cells 210 (2020) 110488. https://doi.org/10.1016/j.solmat.2020.110488.

[181] G. Griffini, S. Turri, Polymeric materials for long-term durability of photovoltaic systems, J. Appl. Polym. Sci. 133 (2016). https://doi.org/10.1002/app.43080.

[182] K. Aitola, G. Gava Sonai, M. Markkanen, J. Jaqueline Kaschuk, X. Hou, K. Miettunen, P.D. Lund, Encapsulation of commercial and emerging solar cells with focus on perovskite solar cells, Sol. Energy 237 (2022) 264–283. https://doi.org/10.1016/j.solener.2022.03.060.

[183] E.Y. Choi, J. Kim, S. Lim, E. Han, A.W. Ho-Baillie, N. Park, Enhancing stability for organic-inorganic perovskite solar cells by atomic layer deposited Al2O3 encapsulation, Sol. Energy Mater. Sol. Cells 188 (2018) 37–45. https://doi.org/10.1016/j.solmat.2018.08.016.

[184] S.-T. Zhang, M. Guc, O. Salomon, R. Wuerz, V. Izquierdo-Roca, A. Pérez-Rodríguez, F. Kessler, W. Hempel, T. Hildebrandt, N. Schneider, Effective module level encapsulation of CIGS solar cells with Al2O3 thin film grown by atomic layer deposition, Sol. Energy Mater. Sol. Cells 222 (2021) 110914. https://doi.org/10.1016/j.solmat.2020.110914.

[185] S.K. Tippabhotla, W. Song, A.A. Tay, A.S. Budiman, Effect of encapsulants on the thermomechanical residual stress in the back-contact silicon solar cells of photovoltaic modules – A constrained local curvature model, J. Sol. Energy 182 (2019) 134–147. https://doi.org/10.1016/j.solener.2019.02.028.

[186] A.J. Beinert, P. Romer, M. Heinrich, M. Mittag, J. Aktaa, D.H. Neuhaus, The Effect of Cell and Module Dimensions on Thermomechanical Stress in PV Modules, IEEE J. Photovoltaics 10 (2020) 70–77. https://doi.org/10.1109/JPHOTOV.2019.2949875.

[187] L. Papargyri, P. Papanastasiou, G.E. Georghiou, Sequential thermomechanical stress and cracking analysis of photovoltaic modules with full and half-cut cells, Sol. Energy Mater. Sol. Cells 278 (2024) 113166. https://doi.org/10.1016/j.solmat.2024.113166.

[188] M. de Bastiani, G. Armaroli, R. Jalmood, L. Ferlauto, X. Li, R. Tao, G.T. Harrison, M.K. Eswaran, R. Azmi, M. Babics, A.S. Subbiah, E. Aydin, T.G. Allen, C. Combe, T. Cramer, D. Baran, U. Schwingenschlögl, G. Lubineau, D. Cavalcoli, S. de Wolf, Mechanical Reliability of Fullerene/Tin Oxide Interfaces in Monolithic Perovskite/Silicon Tandem

Cells, ACS Energy Lett. 7 (2022) 827–833. https://doi.org/10.1021/acsenergylett.1c02148.

[189] J.-H. Park, E. Lee, I.-D. Kim, H. Jung, J. Kim, J. Cho, J. Kim, T.-I. Lee, S.-K. Kang, E.-H. Lee, A review of the thermo-mechanical analysis framework for microelectronics packaging: Mechanics, material property determination, and structural considerations, Mater. Sci. Semicond. Process. 205 (2026) 110321. https://doi.org/10.1016/j.mssp.2025.110321.

[190] A.G. Khina, D.P. Bulkatov, I.P. Storozhuk, A.P. Sokolov, Coefficient of Linear Thermal Expansion of Polymers and Polymer Composites: A Comprehensive Review, Polymers 17 (2025). https://doi.org/10.3390/polym17233097.

[191] V. Bourg, P. Ienny, A.S. Caro-Bretelle, N. Le Moigne, V. Guillard, A. Bergeret, Modeling of internal residual stress in linear and branched polyethylene films during cast film extrusion: Towards a prediction of heat-shrinkability, J. Mater. Process. Technol. 271 (2019) 599–608. https://doi.org/10.1016/j.jmatprotec.2019.04.002.

[192] T.W. Womer, Optimizing Sheet Extrusion Conditions to Minimize Internal Stresses in Thermoformed Sheet, J. Plast. Film Sheeting 8 (1992) 26–36. https://doi.org/10.1177/875608799200800104.

[193] L. Eyann, M.A. Fatah Muhamed Mukhtar, A.A. Saad, M. Jaafar, Epoxy molding compounds for high-performance electronic packaging: A review on recent studies, Mater. Sci. Semicond. Process. 197 (2025) 109665. https://doi.org/10.1016/j.mssp.2025.109665.

[194] P. Gebhardt, S. Marletti, J. Markert, U. Kräling, M. Tu, I. Haedrich, D. Philipp, Comparison of Commercial TOPCon PV Modules in Accelerated Aging Tests, IEEE J. Photovoltaics 15 (2025) 24–29. https://doi.org/10.1109/JPHOTOV.2024.3483317.

10 Appendix

10.1 Supplementary material

10.1.1 Publication IV: Supporting information

Title: Effects of Manufacturing Process History and the Lamination Duration on Thermomechanical Properties of PV Encapsulants

Journal: Advanced Energy and Sustainability Research

Date of submission: 5th of May 2026

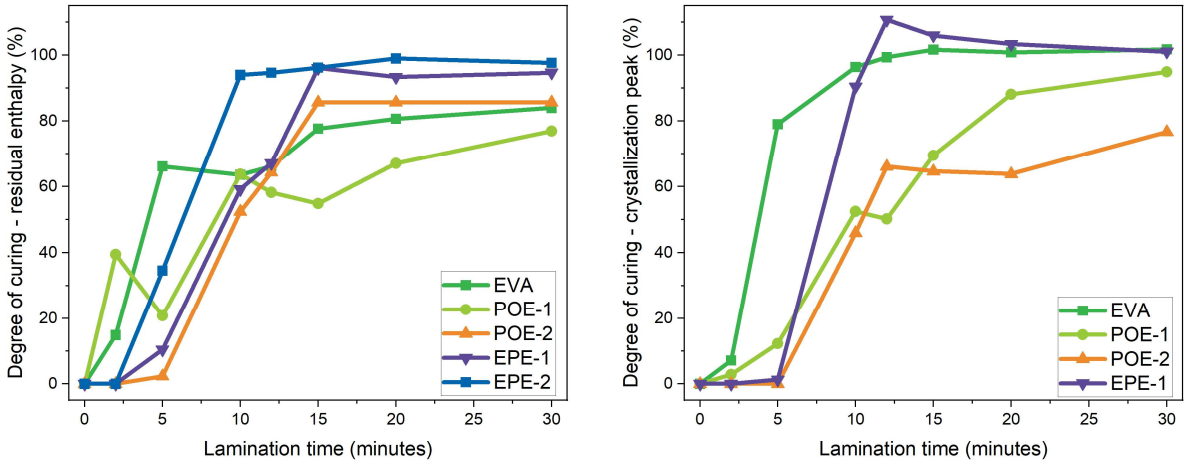

Figure 1. Curing degrees calculated according to residual enthalpy and melt/freeze method.

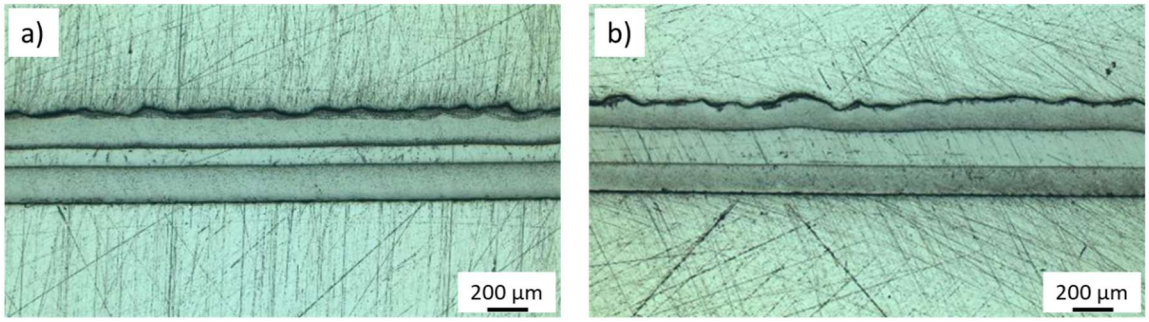

Figure 2. Microscope images of the cross-section of EPE-1 encapsulant samples with a) lower amount and b) higher amount of the polyolefin core layer.

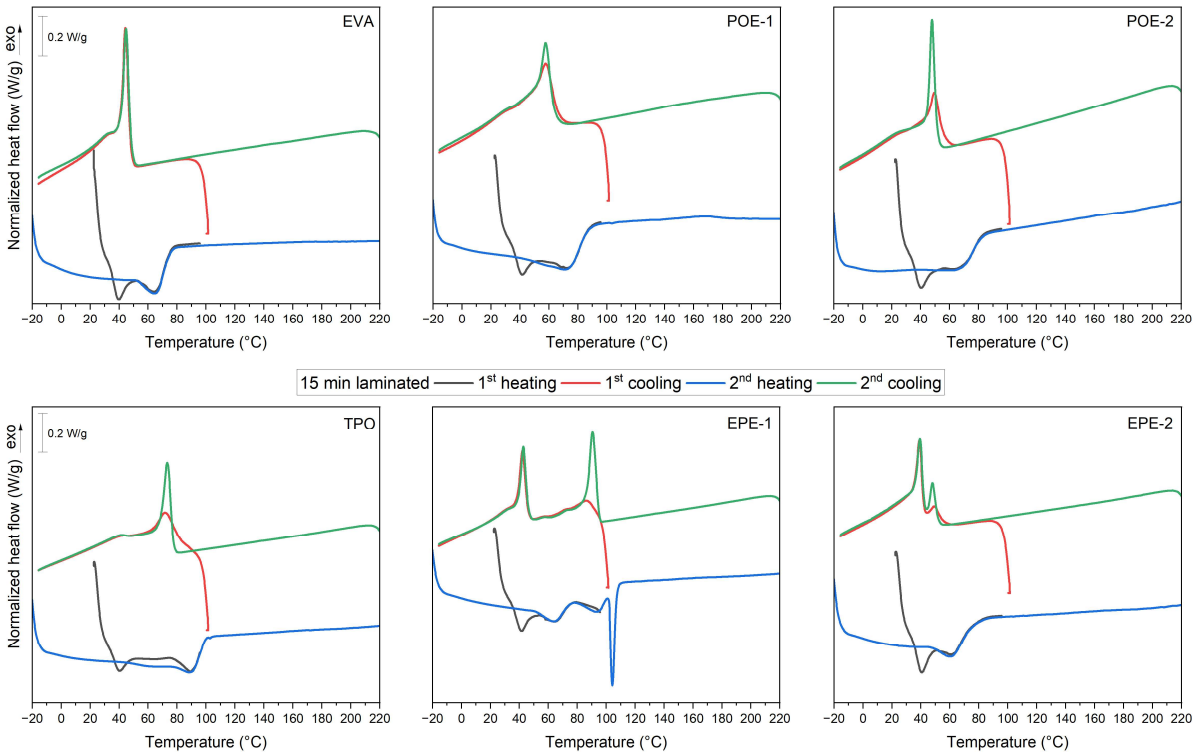

Figure 3. DSC 1st and 2nd heating and cooling thermograms from 15 min laminated encapsulants.

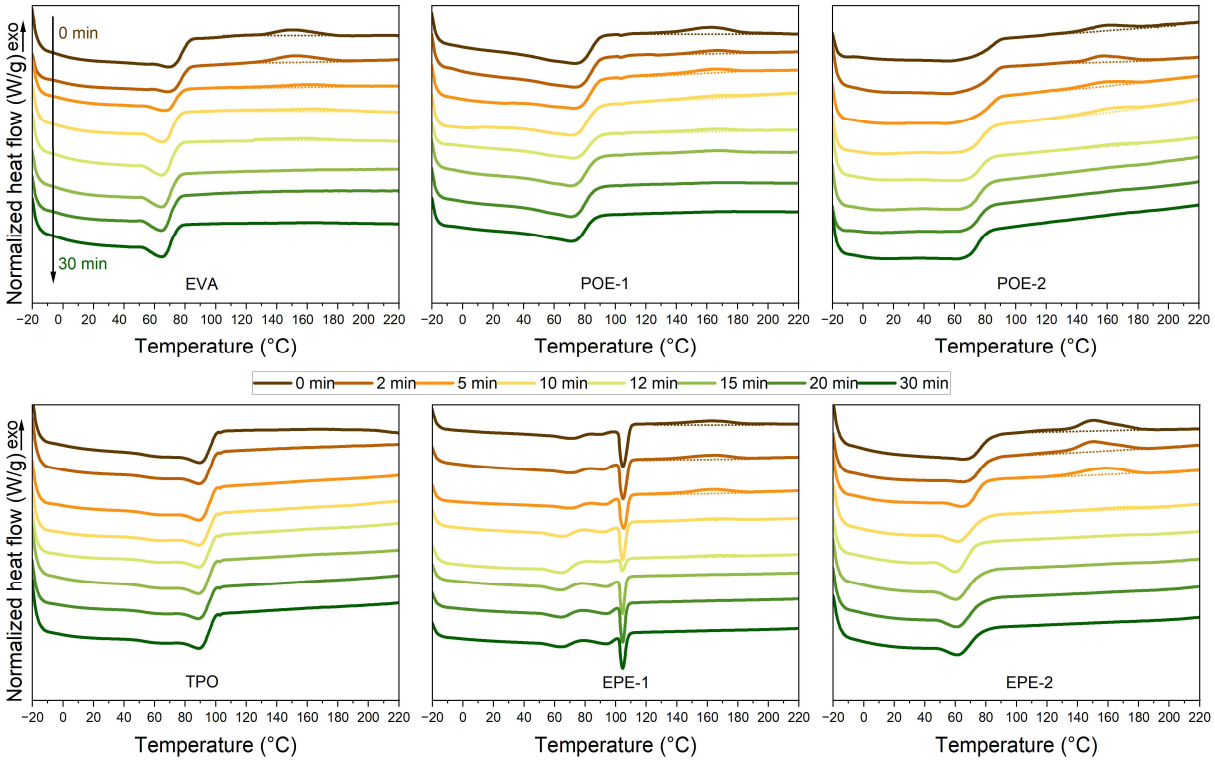

Figure 4. DSC – 2nd heating curves for all lamination times and encapsulants.

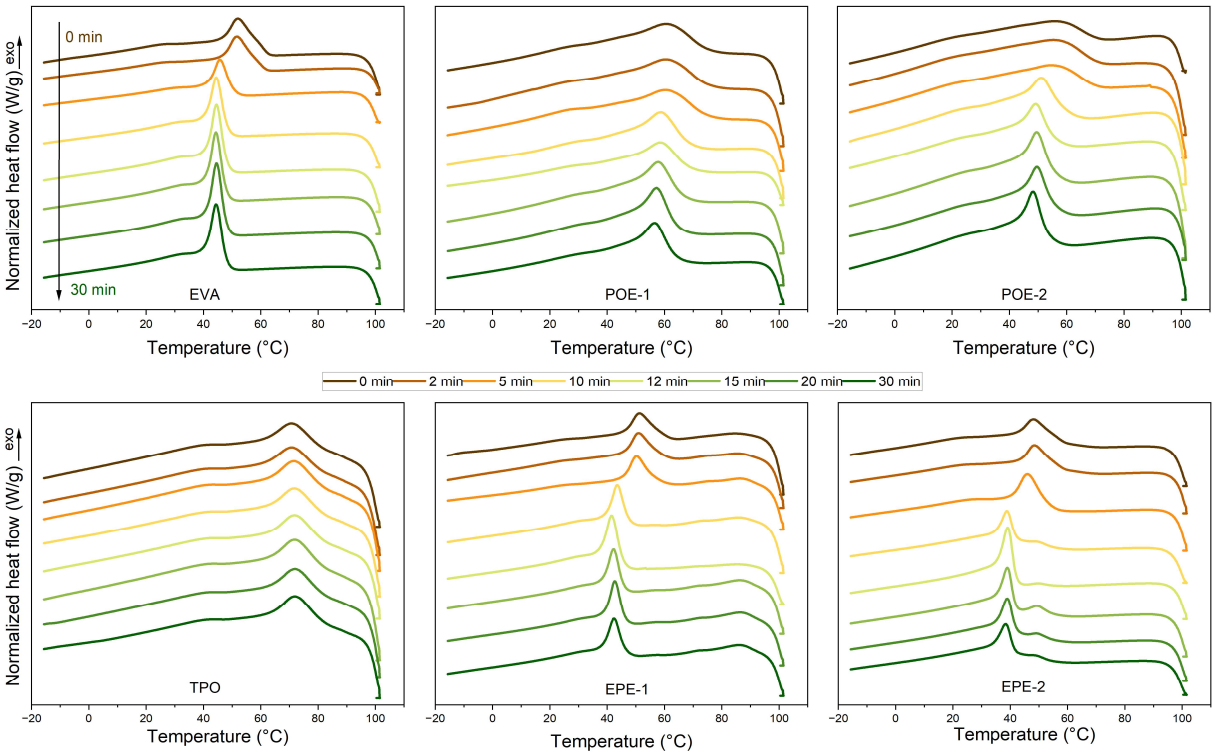

Figure 5. DSC - 1st cooling curves for all lamination times and encapsulants.

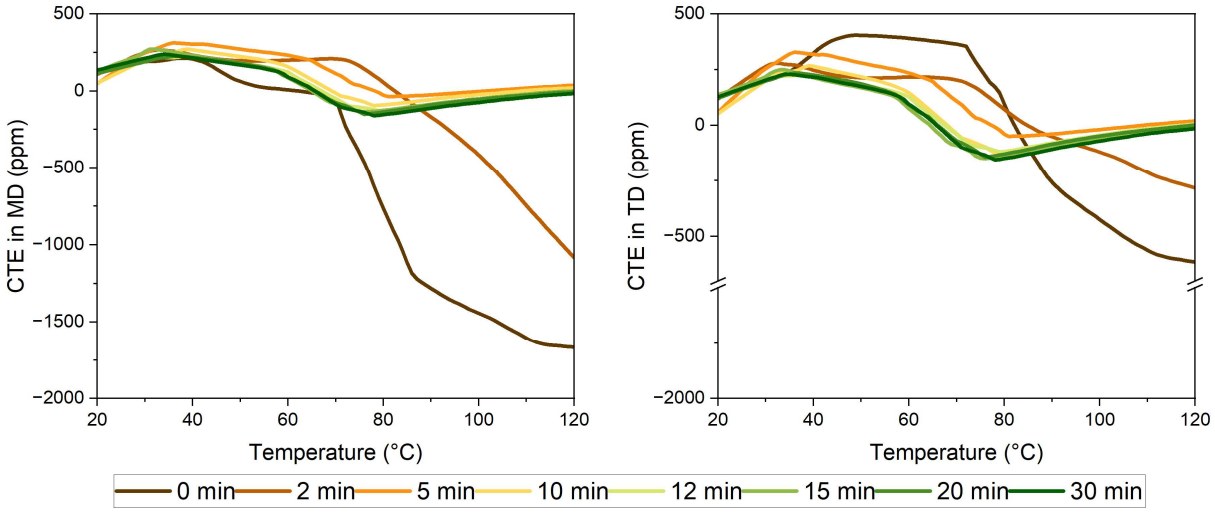

Figure 6. CTE curves of EVA for all lamination times.

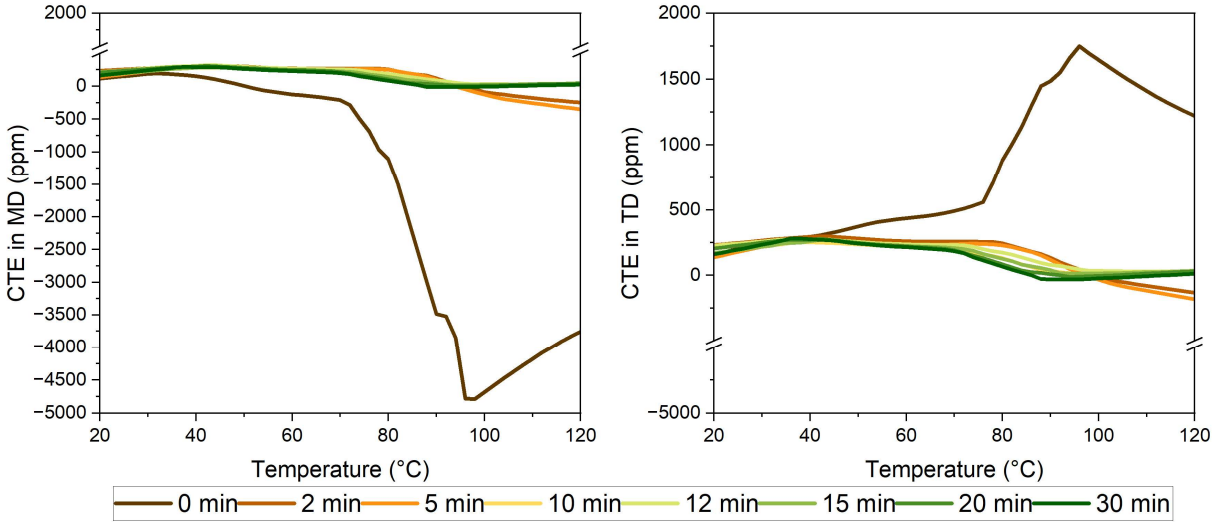

Figure 7. CTE curves of POE-1 for all lamination times.

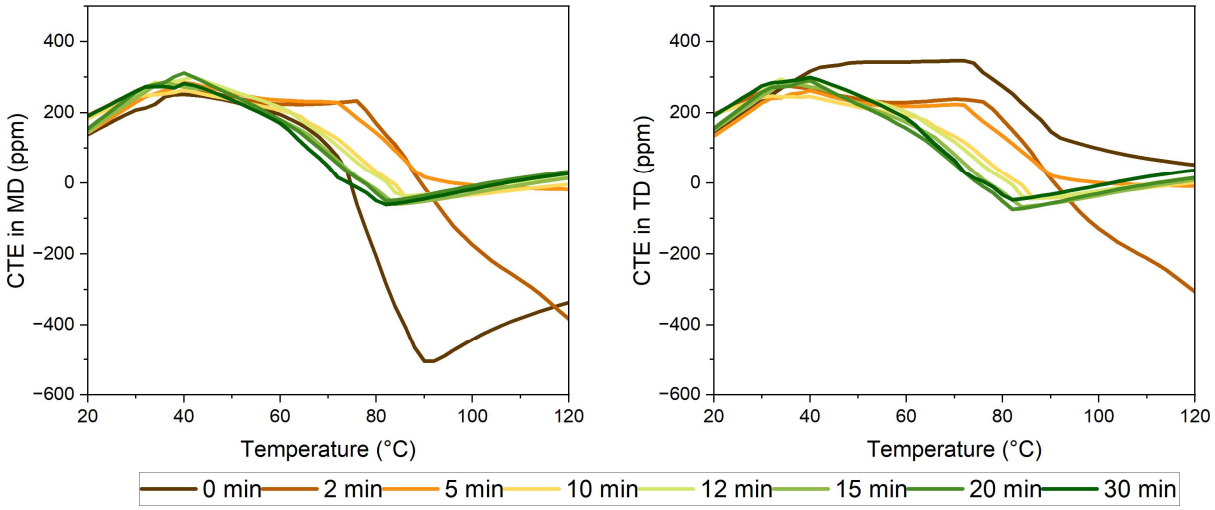

Figure 8. CTE curves of POE-2 for all lamination times.

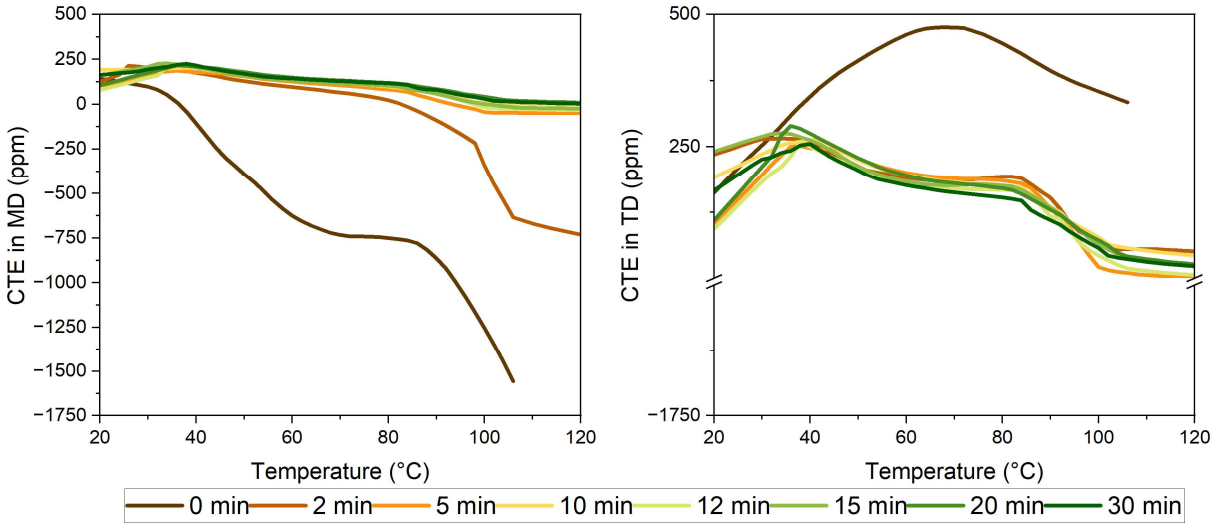

Figure 9. CTE curves of TPO for all lamination times.

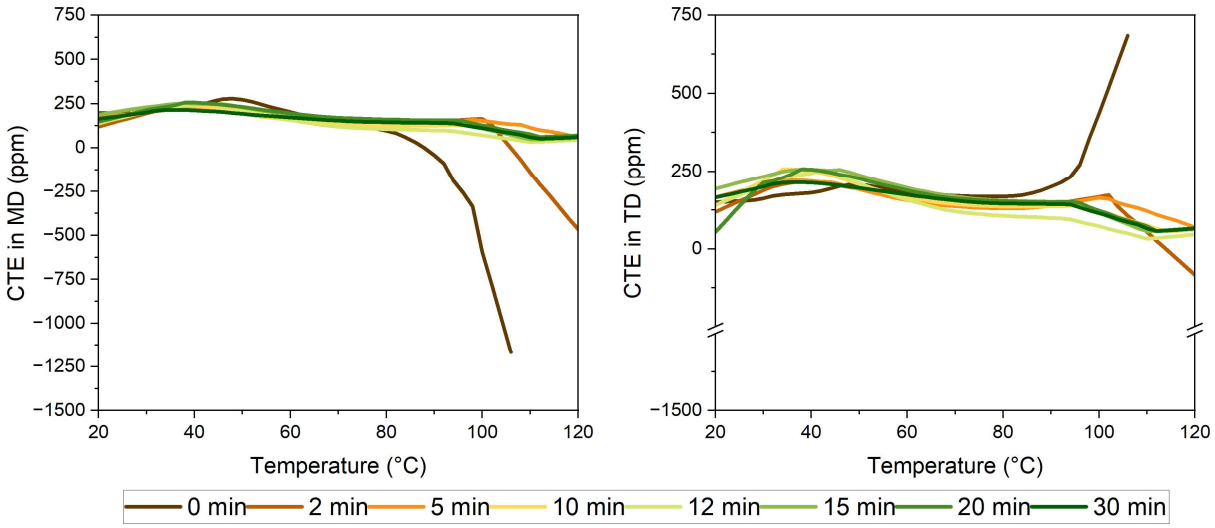

Figure 10. CTE curves of EPE-1 for all lamination times.

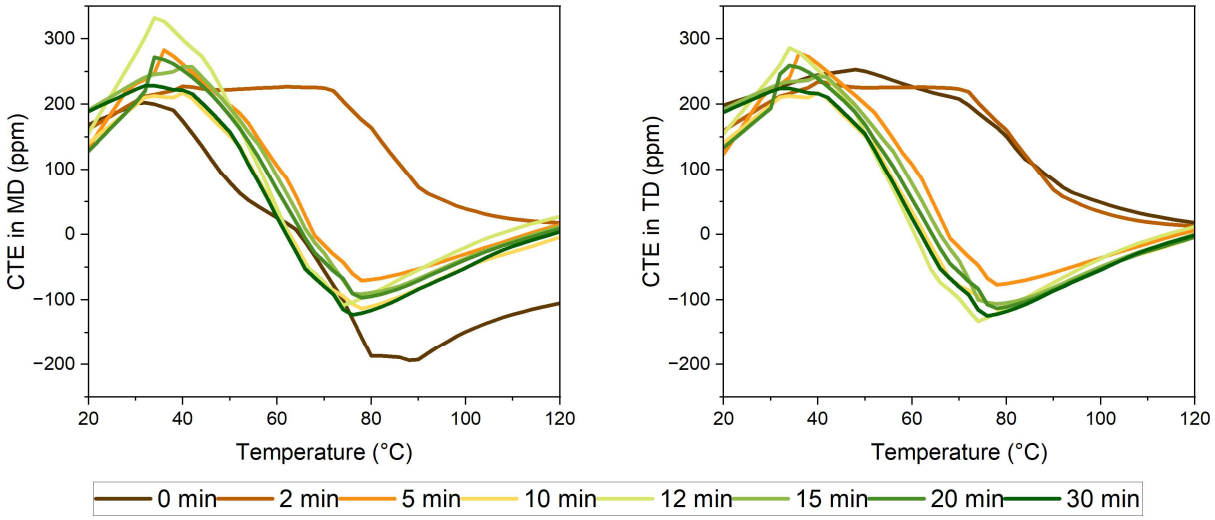

Figure 11. CTE curves of EPE-2 for all lamination times.

10.1.2 Publication V: Supporting information

Title: Is EPE the Future of PV Encapsulation? A Comprehensive Material-Level Assessment

Journal: Solar Energy Materials and Solar Cells,

https://doi.org/10.1016/j.solmat.2026.114258

Date of publication: 20th of February 2026 (online), 15th of June 2026 (in print)

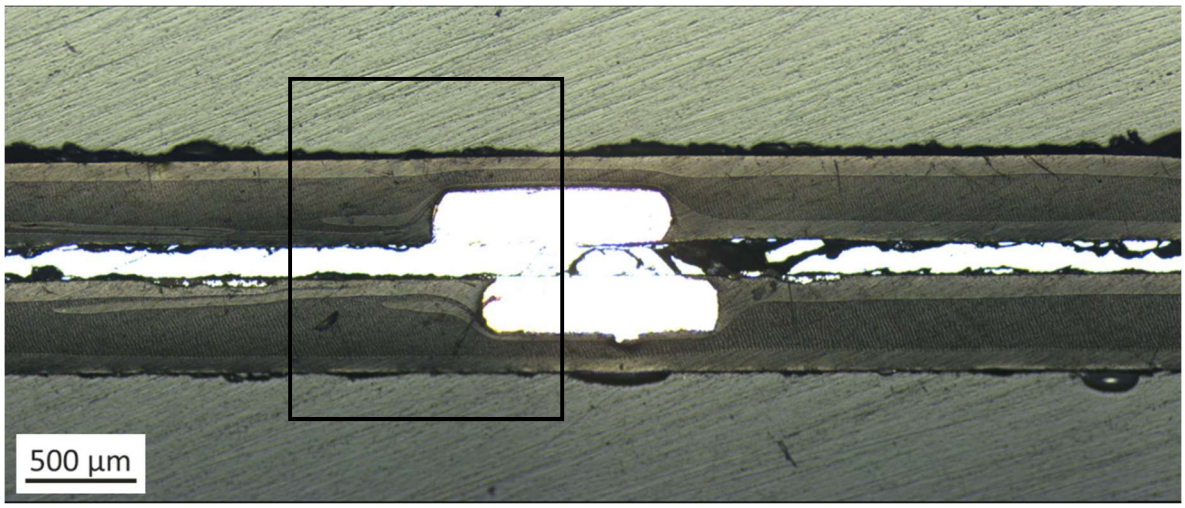

Figure 1. Microscope image of the cross-section of mixing between EVA and POE around the interconnections.

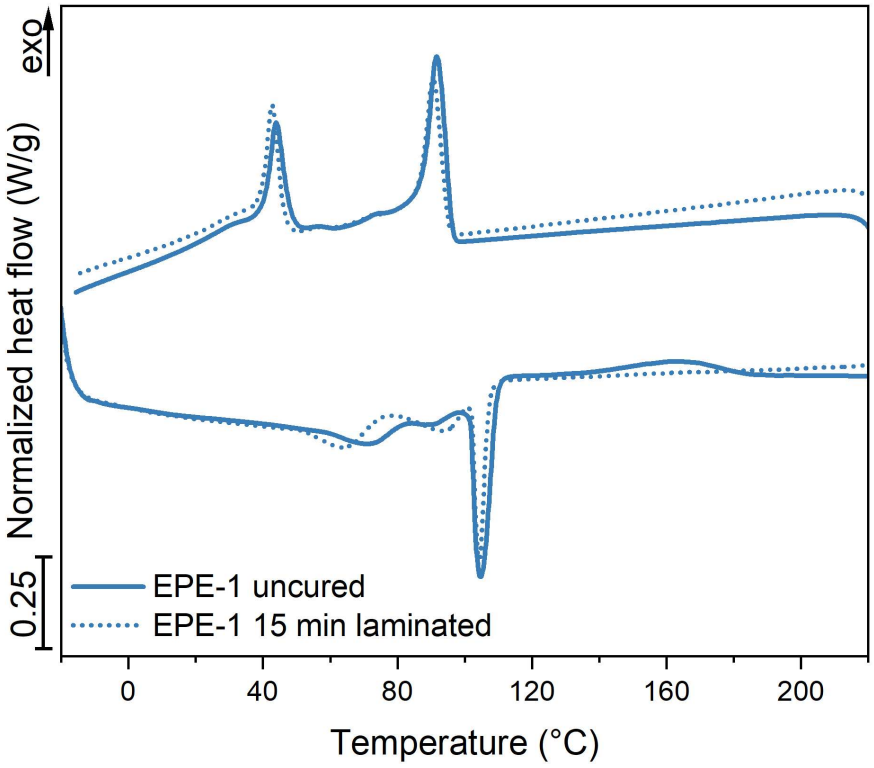

Figure 2. 2nd heating and 2nd cooling DSC thermograms of uncured (solid line) and 15 min laminated (dotted line) EPE-1 in full scale.

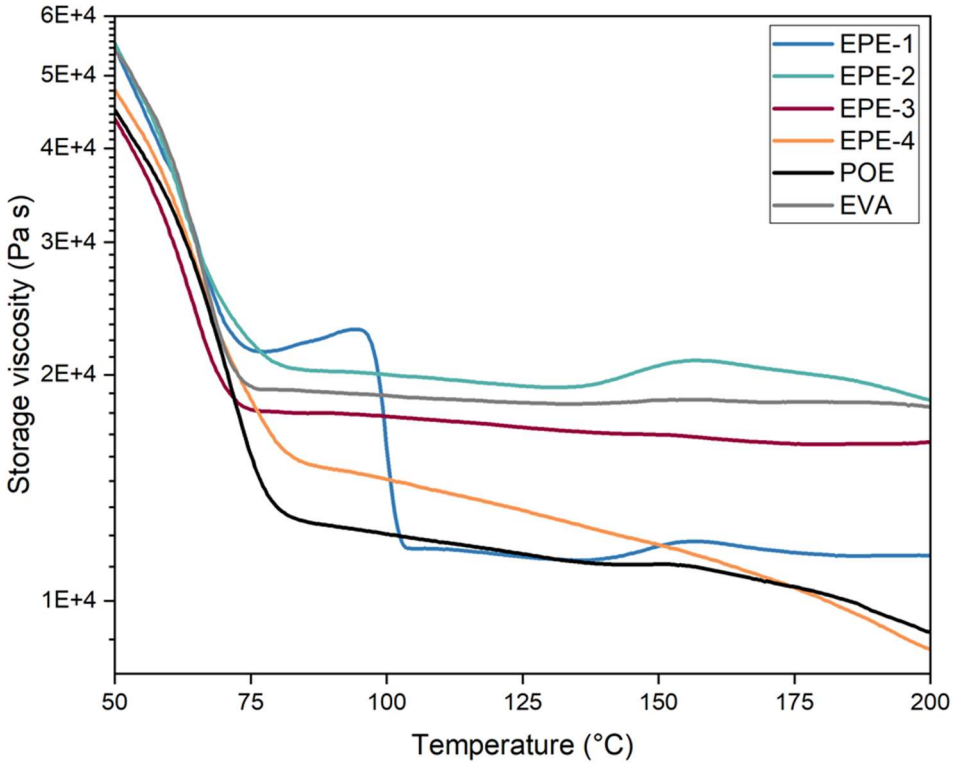

Figure 3. Storage viscosity curves of laminated EPE-1 to 4, POE and EVA encapsulants.

Table 1. Storage viscosity values of four laminated EPEs, POE and EVA encapsulants at 85 °C and 105 °C.

Sample	η' (Pa s) at 85 °C	η' (Pa s) at 105 °C
EPE-1	22 080	11 740
EPE-2	20 295	19 860
EPE-3	17 780	17 472
EPE-4	15 260	14 200
POE	12 755	12 100
EVA	19 026	18 700

10.2 Scientific and Professional Activities

10.2.1 Publications

- U. Desai, J. Govaerts, B. Luo, Y. Voronko, G. Eder, J. Saelens, W. Winant, N. Pervan, G. Oreski, A. Faes, C. Ballif, Novel Lightweight PV Modules Based on Polymeric Honeycomb for Building Integration, 2024 IEEE 52nd Photovoltaic Specialist Conference (PVSC), Seattle, WA, USA, 2024, pp. 0089-0091, https://doi.org/10.1109/PVSC57443.2024.10749199
- N. Pervan, U. Desai, G. C. Eder, J. Govaerts, A. Derluyn, W. Winant, A. Faes, C. Ballif, G. Oreski, Characterization of Lightweight Polymeric Honeycomb Structures for Use as Backsides in Glass-Free PV Modules, Journal of Applied Polymer Science 142, no. 48 (2025): e57892, https://doi.org/10.1002/app.57892.
- N. Pervan, S. Feldbacher, C. Barretta, L. Geymayer, G. Kitzberger, M. Fleischanderl, H. Kurz, F. Füreder-Kitzmüller, G. Oreski, Integration of Photovoltaics in Steel Facade Panels, 2025 IEEE 53rd Photovoltaic Specialists Conference (PVSC), Montreal, QC, Canada, 2025, pp. 0597-0597, https://doi.org/10.1109/PVSC59419.2025.11132397
- M. Casasola, N. Pervan, T. Engelen, N. Kyranaki, J. Govaerts, G. Oreski, J. Poortmans, M. Daenen, Strain monitoring within photovoltaic laminates: A fibre Bragg grating sensor proof-of-concept and comparison with digital image correlation, Solar Energy Materials and Solar Cells, Volume 299, 2026, 114203, ISSN 0927-0248, https://doi.org/10.1016/j.solmat.2026.114203.
- N. Pervan, G. Eder, Y. Voronko, A. Macher, K. Novotny, K. Resch-Fauster, G. Oreski, Is EPE the future of PV encapsulation? A comprehensive material-level assessment, Solar Energy Materials and Solar Cells, Volume 300, 2026, 114258, ISSN 0927-0248, https://doi.org/10.1016/j.solmat.2026.114258.
- M. Casasola, N. Pervan, B. Luo, N. Kyranaki, J. Govaerts, G. Oreski, J. Poortmans, M. Daenen, Thermomechanical Simulation and Influence of Constitutive Material Models for a Thermoplastic Polyolefin Encapsulant in a Photovoltaic Module, Solar Energy, 2026 (under revision SEJ-D-25-04725R1)
- N. Pervan, S. Feldbacher, M. Harnisch, A. Zimmermann, G. Oreski, Systematic study of barrier layer coatings for encapsulation of flexible CIGS PV modules, Results in Engineering, 2026 (under revision, RINENG-D-26-06508)
- N. Pervan, L. Geymayer, M. Fleischanderl, H. Kurz, G. Kitzberger, F. Füreder-Kitzmüller, G. Oreski, Backsheet-Galvanized Steel Adhesion Approaches for Integrated Photovoltaic Façades: A Comparative Study, 2026 IEEE 54th Photovoltaic Specialists Conference (PVSC), New Orleans, LA, USA, 2026 (accepted)

- N. Pervan, J. Geier, M. Daenen, G. Oreski, Effects of Manufacturing Process History and the Lamination Duration on Thermomechanical Properties of PV Encapsulants, Advanced Energy and Sustainability Research, 2026 (submitted)

10.2.2 Conferences

- First author, poster, Honeycomb Structures as Backsheets for Light Weight PV Modules, 40th European Photovoltaic Solar Energy Conference (EUPVSEC) 2023, Lisbon, Portugal
- Co-author, presentation, Light as Heaven, Strong as Hell(?): Testing Honeycomb-Based Laminates for Light-Weight c-Si PV Applications, 40th EUPVSEC 2023, Lisbon, Portugal
- Co-author, poster, Flexible Transparent Polymeric Front Encapsulation as Finish Layer for CIGS PV Cells Using Additive Manufacturing, 40th EUPVSEC 2023, Lisbon, Portugal
- Co-author, presentation, Novel Lightweight PV Modules Based on Polymeric Honeycomb for Building Integration, 2024 IEEE 52nd Photovoltaic Specialist Conference (PVSC), Seattle, WA, USA
- First author, presentation, Enabling glass-free light weight PV modules via honeycomb structures, 5th EUROREG-PV 2024, Ljubljana, Slovenia
- Co-author, presentation, Mechanically Robust and Environmentally Stable Novel Lightweight PV Modules for Building Integration Based on Polymeric Honeycomb, 41st EUPVSEC 2024, Vienna, Austria
- First author, poster, Ultra-Thin Flexible Glass as Environmental Shield for CIGS Photovoltaic Modules, 41st EUPVSEC 2024, Vienna, Austria
- First author, poster, Tackling the Fire Safety in Glass Free PV Modules, 41st EUPVSEC 2024, Vienna, Austria
- Co-author, poster, DIC as a Thermo-Mechanical Characterisation Method for the Inner Layers in a Multi-Layer PV Module Structure, 41st EUPVSEC 2024, Vienna, Austria
- First author, presentation, Ultra-Thin Glass Integration in CIGS PV Modules: Boosting Durability and Performance, 15th SOPHIA Workshop on Solar PV Module Reliability, 2025, DTU Risø Campus, Denmark
- First author, poster, Integration of Photovoltaics in Steel Facade Panels, 2025 IEEE 53rd PVSC, Montreal, QC, Canada
- Co-author, presentation, Near Infrared Spectroscopy for Rapid, Inline Quantification of Encapsulant Crosslinking in PV Modules, 42nd EUPVSEC 2025, Bilbao, Spain
- First author, poster, Transforming Industrial Facades with Integrated Photovoltaics, 42nd EUPVSEC 2025, Bilbao, Spain

- First author, presentation, Festina Lente! The Impact of Lamination Duration on Encapsulant Stability, 42nd EUPVSEC 2025, Bilbao, Spain
- Co-author, poster, Façade Application of Light-Weight Glass-Free Colored PV Modules: Reliability Testing of the Large-Format Modules and Monitoring of the Demonstration Site, 42nd EUPVSEC 2025, Bilbao, Spain
- Co-author, poster, Sonnenschutzlamellen mit photovoltaischer Beschichtung für klimaneutrale, energieeffiziente Strukturen, Österreichische Fachtagung für Photovoltaik und Stromspeicherung, 2025, Vienna, Austria
- Co-author, poster, Adhesion Mechanics of Steel Polymer Laminates for BIPV A Theoretical Insight, 33rd Leoben-Conference on Polymer Engineering and Science, 2025, Leoben, Austria
- First author, presentation, Insights into the material properties of EPE encapsulants for PV application, 2026 IEEE 54th PVSC, New Orleans, LA, USA
- First author, poster, Backsheet-Galvanized Steel Adhesion Approaches for Integrated Photovoltaic Façades: A Comparative Study, 2026 IEEE 54th PVSC, New Orleans, LA, USA
- First author, poster, Flexible Lamination Concepts for Durable CIGS Photovoltaic Modules, 43rd EUPVSEC 2026, Rotterdam, Netherlands
- First author, presentation, Material Matters: Understanding EPE Encapsulants, 43rd EUPVSEC 2026, Rotterdam, Netherlands
- First author, poster, Integrated Photovoltaic Façades for Industrial Buildings: Adhesion Approaches between Backsheet and Galvanized Steel, 43rd EUPVSEC 2026, Rotterdam, Netherlands

10.2.3 Collaborations and mentorships

- PhD Peer Mentorship: provided technical guidance and collaborative support to Bin Luo and Marta Casasola during their research stays at PCCL, 2024.
- Master's Thesis Co-supervision: Christian Veas, "Interfacial adhesion of polymeric components in a steel façade integrated PV module" (2025).
- Graduate Research Supervision: managed and mentored Master's students Christian Veas, Maja Knezovic, and Marissa Maier during their research internships at PCCL (2024–2026).

10.2.4 EurecaPro activities

- PhD Journey workshop participation at University of Hasselt, Belgium 2024
- PhD Journey workshop participation at University of Leon, Spain 2025
- Three months research stay at University of Hasselt with collaborations at imec and EnergyVille (Belgium), and TNO (Netherlands), Belgium 2025

10.2.5 Awards

- Best poster award at 40th European Photovoltaic Solar Energy Conference (EUPVSEC) 2023, Lisbon, Portugal
- Best poster award at 41st European Photovoltaic Solar Energy Conference (EUPVSEC) 2024, Vienna, Austria
- Student award at 42nd European Photovoltaic Solar Energy Conference (EUPVSEC) 2025, Bilbao, Spain